



**HAL**  
open science

# Novel function of the ER stress transducer IRE1 $\alpha$ in cell migration and invasion of metastatic melanoma cells

Celia María Limia León

## ► To cite this version:

Celia María Limia León. Novel function of the ER stress transducer IRE1 $\alpha$  in cell migration and invasion of metastatic melanoma cells. Human health and pathology. Université de Rennes, 2021. English. NNT : 2021REN1B015 . tel-03585530

**HAL Id: tel-03585530**

**<https://theses.hal.science/tel-03585530v1>**

Submitted on 23 Feb 2022

**HAL** is a multi-disciplinary open access archive for the deposit and dissemination of scientific research documents, whether they are published or not. The documents may come from teaching and research institutions in France or abroad, or from public or private research centers.

L'archive ouverte pluridisciplinaire **HAL**, est destinée au dépôt et à la diffusion de documents scientifiques de niveau recherche, publiés ou non, émanant des établissements d'enseignement et de recherche français ou étrangers, des laboratoires publics ou privés.

# THESE DE DOCTORAT DE

L'UNIVERSITE DE RENNES 1

ECOLE DOCTORALE N° 605  
*Biologie Santé*  
Spécialité : Cancérologie

Par

**Celia María LIMIA-LEÓN**

**Novel function of the ER stress transducer IRE1 $\alpha$  in cell migration and invasion of metastatic melanoma cells.**

Thèse présentée et soutenue à Rennes, le 8 juin 2021  
Unité de recherche : INSERM U1242

## Rapporteurs avant soutenance :

Jacky Goetz    Directeur de Recherches, Inserm, Strasbourg  
Elif Karagöz    Group leader, Max Perutz Lab, Vienne

## Composition du Jury :

Président :	Nathalie Théret	Directeur de Recherches, Inserm
Examineurs :	Jacky Goetz	Directeur de Recherches, Inserm, Strasbourg
	Elif Karagöz	Group leader, Max Perutz Lab, Vienne
	Lise Boussemart	PUPH, Univ. Nantes, Nantes
Dir. de thèse :	Eric Chevet	Directeur de Recherches, Inserm
Co-dir. de thèse :	Claudio Hetz	Professeur, Univ. Chili

*To my family*

## 1. INDEX.

1. INDEX.	1
2. TABLE OF FIGURES.	4
3. ABBREVIATIONS.	6
4. INTRODUCTION.	10
4.1. Cancer: a public health problem.	10
4.2. Tumorigenesis and metastasis.	11
4.3. Mechanisms and molecular actors of tumor cell migration, invasion and metastasis.	13
4.3.1. Different steps of the migration/invasion process at the cellular and molecular levels.	15
4.4. Endoplasmic Reticulum Stress in Cancer.	19
4.5. Unfolded Protein Response.	21
4.5.1. PERK and ATF6 signaling.	21
4.5.2. IRE1 signaling, stress sensing and activation mechanism.	22
4.6. Connections between IRE1 signaling and cancer progression.	26
4.7. IRE1 in cell migration and metastasis.	28
4.8. FLNA function in cell migration and metastasis.	31
4.9. Melanoma signaling and the UPR.	33
5. HYPOTHESIS.	36
6. GENERAL AIM.	36
7. SPECIFIC AIMS.	36
8. MATERIALS AND METHODS.	37
8.1. Reagents.	37
8.2. Cell culture and generation of the IRE1 Knockout cell lines.	37
8.3. NIH-conditioned medium.	38
8.4. RNA isolation and RT-PCR.	39
8.5. Immunoprecipitations.	39
8.6. Western blot analysis.	40
8.7. Knockdown of IRE1 and FLNA.	41

8.8.	Cell proliferation assay.	41
8.9.	Transwell Migration Assay.	42
8.10.	Adhesion Assay.	42
8.11.	Actin cytoskeleton analysis.	42
8.12.	Cell invasion assay.	43
8.13.	Experimental metastasis assay.	44
8.14.	Bioinformatic analysis.	46
8.15.	Statistical analysis.	48
9.	RESULTS.	49
9.1.	Activation status of IRE1 during metastasis in melanoma.	49
9.2.	Role of IRE1 in migration and invasion of melanoma cells.	54
9.2.1.	Role of IRE1 in melanoma cell migration.	55
9.2.2.	Regulation of actin cytoskeleton organization by IRE1 in metastatic melanoma cells.	66
9.2.3.	Regulation of cell adhesion by IRE1 in metastatic melanoma cells.	70
9.2.4.	Effect of IRE1 deficiency in cell invasion of human metastatic melanoma cells.	72
9.3.	Role of the IRE1/FLNA pathway in the regulation of cell migration and invasion in melanoma.	75
9.3.1.	Role of the IRE1 RNase-RIDD dependent activity in the suppression of melanoma cell migration.	81
9.4.	Correlation of IRE1 activity and metastasis in melanoma in vivo.	88
10.	DISCUSSION.	94
11.	CONCLUSIONS.	109
12.	SUPPLEMENTARY FIGURES.	110
13.	PUBLICATIONS	119
13.1.	IRE1 $\alpha$ controls cytoskeleton remodeling and cell migration through a direct interaction with Filamin A.	119
	Nat Cell Biol. 2018 Aug;20(8):942-953.	119
13.1.1.	Foreword	119
13.1.2.	Contribution	119
13.2.	Emerging Roles of the Endoplasmic Reticulum Associated Unfolded Protein Response in Cancer Cell Migration and Invasion.	121

Cancers (Basel). 2019 May 6;11(5).	121
13.2.1. Foreword	121
13.2.2. Contribution	121
14. CONGRESSES AND FUNDING	123
14.1. Congresses	123
14.2. Funding	123
15. REFERENCES.	124

## 2. TABLE OF FIGURES.

Figure 1. Metastatic cascade.	15
Figure 2. The cellular processes and molecular actors involved in cell migration/invasion.	18
Figure 3. Secretory protein demand and disruption of endoplasmic reticulum homeostasis in cancer cells.	20
Figure 4. Unfolded protein response and the hallmarks of cancer.	21
Figure 5. Unfolded protein response.	25
Figure 6. Filamin a structure and regulation.	33
Figure 7. Workflow of the generation of ire1 knockout (ko) human melanoma cells.	38
Figure 8. Lung metastasis using an experimental tail vein injection model in immunosuppressed mice.	45
Figure 9. Lung metastasis using an experimental tail vein injection model in immunocompetent mice.	45
Figure 10. Ire1 activation in mouse melanoma metastasis.	51
Figure 11. Ire1 signaling in human melanoma tumors.	53
Figure 12. Ire1 activation status in human melanoma metastasis.	54
Figure 13. Characterization of human melanoma cell lines.	58
Figure 14. Standardization of the transmigration assay.	59
Figure 15. Ire1 deficiency increases cell migration in human metastatic melanoma cells.	60
Figure 16. Validation of the generation of ire1 ko in a375-ma2 cells.	62
Figure 17. Characterization the of ire1 ko a375-ma2 clones selected.	63
Figure 18. Ire1 deficiency increases cell migration in human metastatic melanoma cells.	65
Figure 19. Actin cytoskeleton is not affected by ire1 deficiency in ma2-a375 cells.	67

Figure 20. Filopodia formation is independent of ire1 expression.	69
Figure 21. Cell adhesion capacity to fibronectin and matrigel is independent of ire1 expression in a375-ma2 cells.	71
Figure 22. Silencing of ire1 increases cell invasion in human metastatic melanoma cells.	72
Figure 23. Ire1 deficiency increases cell invasion in human metastatic melanoma cells.	74
Figure 24. Silencing of flna expression do not influence cell migration of metastatic cells.	76
Figure 25. Flna phosphorylation is independent of ire1 expression under promigratory stimuli.	78
Figure 26. Flna phosphorylation is independent of ire1 expression under er stress.	80
Figure 27. The mkc-8866 ire1 rnase inhibitor increases cell migration in human metastatic melanoma cells.	82
Figure 28. Forced xbp1s expression does not influence cell migration of metastatic melanoma cells.	83
Figure 29. Pipeline of the analysis to identify pro-metastatic genes and putative ridd-targets in melanoma.	86
Figure 30. Pro-metastatic genes and putative ridd-targets in melanoma.	87
Figure 31. Standardization of a375-ma2 lung metastatic model by tail vein injection.	89
Figure 32. Lung metastasis is independent of ire1 expression in an experimental metastatic melanoma model.	91
Figure 33. Frequency distribution of metastatic foci size.	92
Figure 34. Regulation of melanoma cell movement by the ire1 and ridd axis: proposed model.	108



### 3. ABBREVIATIONS.

ABD	:	Actin-binding domain
ATF4	:	Activating transcription factor 4
ATF6	:	Activating transcription factor 6 $\alpha$
ATF6f	:	Fragment of ATF6
Bcl-2	:	B-cell lymphoma 2
Bcl-xL	:	B-cell lymphoma-extra large
BiP	:	Immunoglobulin binding protein
BRAF	:	B-Raf Proto-Oncogene
Cdc42	:	Cell division control protein 42 homolog
CHOP	:	C/EBP homologous protein
CTC	:	Circulating tumor cells
DCC	:	Disseminated cancer cells
DMEM	:	Dulbecco's Modified Eagle's
eIF2 $\alpha$	:	Eukaryotic translation initiation factor 2 alpha
EMC	:	Extracellular matrix
EMEM	:	Eagle's Minimum Essential Medium
EMT	:	Epithelial-mesenchymal transition
ER	:	Endoplasmic reticulum
ERAD	:	ER-associated degradation system
F-actin	:	Actin filaments
FAK	:	Focal adhesion kinase
FBS	:	Fetal bovine serum
FGF	:	Fibroblast growth factor
FGFR	:	Fibroblast growth factor receptor
FLNA	:	Filamin A

GADD34	:	Growth Arrest and DNA Damage-Inducible Protein
GBM	:	Glioblastoma multiforme
Grp94	:	Glucose -regulated protein 94
H&E	:	Hematoxylin & Eosin
HERPUD1	:	Homocysteine-responsive endoplasmic reticulum-resident ubiquitin-like domain member 1
HIF1 $\alpha$	:	Hypoxia-inducible factor 1-alpha
IL-6	:	Interleukin-6
IL2 $\gamma$ null	:	Null allele of the IL2 receptor common gamma chain
IP	:	Immunoprecipitations
IRE1 $\alpha$	:	Inositol-requiring protein 1 $\alpha$
KO	:	Knockout
MAPK	:	Mitogen-activated protein kinases
MCM7	:	Minichromosome maintenance complex component 7
MLC	:	Myosin light chain
MLKC	:	Myosin light-chain kinase
MMP	:	Metalloproteinases
MT1-MMP	:	Membrane type 1-matrix metalloproteinase
MTHFD2	:	Methylenetetrahydrofolate dehydrogenase (NADP+ Dependent) 2, methenyltetrahydrofolate cyclohydrolase
NIH-CM	:	NIH- conditioned medium
NNT	:	NAD(P) transhydrogenase
NSG	:	NOD/SCID/IL2 $\gamma$ <sup>null</sup> mice
PBST	:	PBS, 0.1% Tween20
PERK	:	PKR-like ER kinase
PFA	:	Paraformaldehyde
PI3Ks	:	Phosphoinositide 3-kinases
PKC $\alpha$	:	Protein kinase C alpha

PP1	:	Protein phosphatase-1
Rac1	:	Ras-related C3 botulinum toxin substrate 1
Rb	:	Retinoblastoma protein
RIDD	:	IRE1-dependent decay
RNase	:	Endoribonuclease
ROBO1	:	Roundabout guidance receptor 1
ROCK	:	Rho-associated serine/threonine kinase
SCID	:	Severe combined immune deficiency
sgRNAs	:	Single guide RNAs
siRNA	:	Small-interfering RNA
SKCM	:	Skin cutaneous melanoma
SKIV2L2	:	Mtr4 exosome RNA helicase
SMC4	:	Structural maintenance of chromosomes protein 4
Snail1	:	Snail family transcriptional repressor 1
Snail2	:	Snail family transcriptional repressor 2
SPARC	:	Secreted protein acidic and cysteine rich
SPCS3	:	Signal peptidase complex subunit 3
Src	:	Proto-oncogene tyrosine-protein kinase
TARDBP	:	TAR DNA binding protein
TCF3	:	Transcription Factor 3
TM	:	Tunicamycin
TNBC	:	Triple-negative breast cancer
TRAF2	:	TNFR-associated factor 2
uPA	:	urokinase-type plasminogen activator
UPR	:	Unfolded protein response
VEGF-A	:	Vascular endothelial growth factor A
WASP	:	Wiskott-Aldrich syndrome protein

WAVE : WASP-family verprolin-homologous protein  
XBP1 : X-box binding protein-1  
XBP1s : Spliced form of XBP1  
ZEB2 : Zinc Finger E-Box Binding Homeobox 2

## 4. INTRODUCTION.

### 4.1. *Cancer: a public health problem.*

Cancer is a disease characterized by the uncontrolled growth of abnormal cells that can originate from most of the human body's cells and organs. The most accepted theory is that a set of genetic mutations in normal cells allows them to proliferate, invade tissue, and metastasize autonomously (1). This disease is one of the leading causes of morbidity and mortality worldwide and is the second leading cause of death globally. Currently, it causes millions of deaths a year, generating high economic and social costs (2).

In Chile, malignancies are the second cause of mortality, accounting for 21.8% of deaths, with approximately 35,000 new cancer cases per year and a rate of 143 per 100,000 inhabitants in 2015 (3, 4). In comparison with other causes of death, cancer shows an upward trend with increasing mortality. In Chile, the most frequent tumor locations are stomach, lung and prostate among men and breast, lung and cervix in women (5). On the other hand, cancer is the leading cause of death in France, accounting for 185621 deaths, with 467965 new cases in 2020 (6). The most frequent tumors are prostate, lung and colorectum among men and breast, colorectum and lungs among women (7).

Importantly, the leading cause of death in patients with cancer is the dissemination of the tumor cells from the primary site of the tumor to different organs (8). One of the most metastatic tumors is cutaneous malignant melanoma, in which incidence and mortality have increased over the past several decades in Chile (9). Melanoma constitutes between 1 and 4% of skin cancers; however, it is responsible for most of the deaths related to skin cancer (10). This type of tumor presents a high

rate of early metastasis in the disease progression, which can occur even from thin primary tumors (11). Although substantial progress has been made to understand the complexity of melanoma metastasis, the identification of new targets is essential to restrain tumor dissemination from the primary lesion to distant organs.

#### 4.2. ***Tumorigenesis and metastasis.***

Tumorigenesis involves (i) the acquisition of genetic alterations by individual cells and (ii) the subsequent action of natural selection upon this phenotypic diversity that allows tumor cells to acquire fundamental characteristics that drive the development of the tumor (12). These distinctive features of tumor cells –collectively known as the **hallmarks of cancer**– include sustained proliferative signals, evasion of cell proliferation control mechanisms, resistance to programmed cell death, unlimited replicative potential, angiogenesis, reprogrammed energy metabolism, immune system evasion and tissue invasion and metastasis (12, 13).

The most fundamental traits of tumor cells involves the autocrine stimulation of cancer cell proliferation and is mediated by: an increased secretion of growth factors, the induction of the production of these growth factors in the stromal cells (14, 15) and the negative control of anti-proliferative signals mediated by tumor suppressor genes such as p53 and retinoblastoma protein (pRb) (16, 17). Importantly, another relevant feature in tumor cells is the capacity to **resist to the induction of cell death**. Tumor cells that have increased expression of anti-apoptotic regulators, such as B-cell lymphoma 2 (Bcl-2), B-cell lymphoma-extra-large (Bcl-xL), or enhancing survival signals, through a decrease in the expression of proapoptotic factors, are positively selected (18). Also, tumor cells have capacity to induce a process of **neo-angiogenesis** adding new vessels associated with the

tumor to sustain the neoplastic growth (19) through the regulation of vascular endothelial growth factor A (VEGF-A) and thrombospondin-1 (20, 21). The generation of new vessels, which give access to the circulation, and the acquisition of invasive capacities allow tumor cells to migrate from the primary tumor to other organs and initiate a process known as **metastasis**.

**Metastasis is defined as the movement of tumor cells from a primary site to progressively colonize distant organs, representing a major contributor to the death of cancer patients.** This ability of tumor cells to metastasize is one of the most concerning problems in cancer research (22). Indeed, despite the substantial effort dedicated to the early detection and diagnosis of cancer, most patients present metastasis at the time of medical care, and approximately 90% die from metastatic lesions (23, 24). Tumor metastasis generates three major medical problems: (i) resistance to conventional therapeutic treatments, (ii) high invasive and proliferation rates and (iii) failure of vital organs (25). Metastasis treatment with drugs such as bevacizumab (VEGF blocking antibody) and dasatinib/saracatenib (Proto-oncogene tyrosine-protein kinase (Src) kinase inhibitors) have been tested in cellular and animal models with positive outcomes; however, all efforts to specifically target metastasis have failed in preclinical models and clinical trials (25); therefore, a deep understanding of the key molecular pathways involved in this malignant event is required to design future therapeutic options.

As mentioned, the capacity of tumor cells to invade adjacent tissues and form distant metastases is one of the most aggressive features of cancer. Most solid cancers progress to disseminated metastatic disease, leading to secondary tumors and the invasion of tumor cells from the primary tumor to distant tissues is one of the early steps in the metastatic cascade (26). **One of the best characterized**

**metastatic processes is the metastasis in melanoma, known to exhibit high migration/invasion properties through a metastatic infiltration process.**

Melanoma is developed by the transformation of melanocytes, cells specialized in the production of melanin, and accounts for approximately 80% of skin cancer-related deaths (27). The classical model describing melanoma progression consists in a series of steps, beginning for the formation of a benign precursor (melanocytic nevus), followed by the generation of a dysplastic nevus, progression through radial and vertical growth phases, and finally the metastasis (28, 29). The radial growth phase represents an early stage in the disease, and it is determined by a horizontal growth in the epidermis. The second phase (vertical growth phase) represents the first stage of melanoma dissemination, and it is characterized by a vertical growth that allows the invasion into deeper skin layers. To progress through all these stages, metastatic cells exhibit common cellular and molecular features including increased reorganization of actin cytoskeleton, uncontrolled cellular migration, and an increased capacity of degradation of extracellular matrix and invasion (30). In the next section, we will provide a brief overview of the molecular mechanism and actors that regulate cell migration, invasion, and metastasis in cancer.

#### ***4.3. Mechanisms and molecular actors of tumor cell migration, invasion and metastasis.***

The process of metastasis has been schematized as a sequence of steps involving (i) local invasion and intravasation of tumor cells to neighboring blood and lymphatic vessels, (ii) transit of tumor cells through the lymphatic and blood system, (iii) extravasation or escape from the vessels to the parenchyma of distant tissues,



(iv) the formation of small nodules of tumor cells, denominated micro-metastasis, and (v) the growth of these lesions into macroscopic tumors (31). A series of alterations in critical molecular and cellular processes allow tumor cells to rapidly and effectively complete all these steps (Reviewed in (32)) (**Figure 1**).

Cell migration is required for multiple biological processes, such as tissue repair, immune system responses, and organogenesis during development (33). However, aberrant cell migration promotes the progression of many diseases, including metastasis (reviewed in (30)). During migration, cells polarize through the leading edge triggering the formation of focal adhesions and protrusions. Once adhesions are formed, the rear retracts, allowing the cell body to move forward. **These steps are spatiotemporally regulated by different proteins involved in signaling pathways that ultimately lead to increased actin and microtubule dynamics** (34, 35). Meanwhile, the invasion occurs when tumor cells acquire the ability to penetrate the surrounding tissues through the degradation of the extracellular matrix (ECM) and pass through the basement membrane. An essential process for tumor cell invasion is the epithelial-mesenchymal transition (EMT), a cellular process through which epithelial cells undergo morphological and biochemical changes leading to a more mesenchymal phenotype with enhanced invasive capabilities (36).

Invasion of tumor cells is initiated by different signaling pathways that control actin cytoskeleton dynamics, the turnover of cell-cell and cell-matrix junctions, and remodeling of the tumor environment (30). The remodeling of the tumor microenvironment can guide tumor cells and induce several types of movement (13). Moreover, the tumor microenvironment is also involved in the activation of

several signaling pathways and cellular processes that lead to the metastatic process (37).

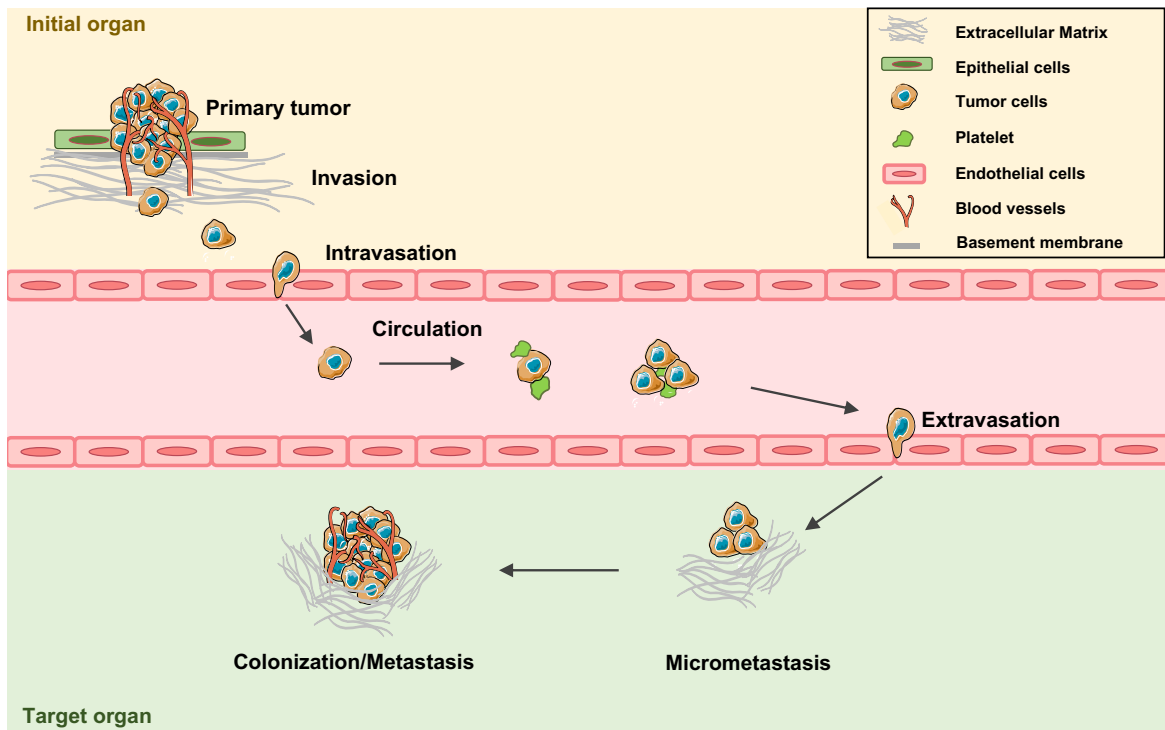


**Figure 1. Metastatic cascade.**

Metastasis is a multistep process that has been schematized as a sequence of steps, firstly involving primary tumor detachment and invasion to the surrounding extracellular matrix. This process allows tumor cells to intravasate to blood and lymphatic vessels and enters in the circulation. Tumor cells then attach to endothelial cells, a process that facilitates the extravasation from the blood vessels to the parenchyma of the target organ. The next step is forming small nodules of cancer cells, denominated micro-metastasis, where tumoral cells can remain dormant for a long time before the growth of these lesions into macroscopic tumors. This last step is known as colonization. **(Figure modified from: Gómez-Cuadrado, L. et al., 2017).**

#### 4.3.1. *Different steps of the migration/invasion process at the cellular and molecular levels.*

Tumor cells use similar migration mechanisms to spread within tissues that the ones used by non-tumor cells during physiological processes. Cell migration through tissues can be described as a cycle of the five-steps process **(Figure 2)**

(38, 39). **In the first step**, the moving cells become polarized and elongate with the generation of protrusions at the leading edge, where little adhesion to the ECM is required (**Figure 2.1**). These protrusions are formed by parallel and crosslinked actin filaments and a group of scaffolding and signaling proteins that allow signal exchange with the ECM substrates. Cell protrusions during the migratory process can take several forms, including lamellipodia, filopodia, pseudopods, and invadopodia (40). The formation of these structures is regulated by the activation of Rho GTPase family members (35, 41). Of these GTPases, Ras-related C3 botulinum toxin substrate 1 (Rac1) and Cell division control protein 42 homolog (Cdc42) are required for lamellipodia and filopodia formation. Cdc42 interacts with the Wiskott-Aldrich syndrome protein (WASP) proteins to induce filopodia formation, while Rac1 enhances lamellipodia generation by the activation of WASP-family verprolin-homologous protein (WAVE) proteins (42).

**In the second step**, cells form focal contacts with the ECM (**Figure 2.2**). These contacts are composed of clusters of adhesion proteins, mainly integrins, transmembrane receptors that recruit adaptor and signaling proteins to form an initial focal complex, which can grow and stabilize to form a focal contact. The integrin intracellular domains interact with signaling proteins such as the focal adhesion kinase (FAK), paxillin, and tensin that together with actin-binding proteins, like vinculin, paxillin, Filamin A (FLNA) and  $\alpha$ -actinin, lead to the activation of Rho GTPases family and Phosphoinositide 3-kinases (PI3Ks) (43-45).

**In a third step**, proteases are secreted near to the attachment sites leading to the degradation of the ECM components like collagen, fibronectin, and laminins (**Figure 2.3**). Among these proteases implicated in ECM degradation are surface

matrix metalloproteinases (MMP) such as Membrane type 1-matrix metalloproteinase (MT1-MMP) that cleaves native collagens, along with other macromolecules, into smaller fragments making them more accessible for secreted proteases like MMP2 and MMP9 or serine proteases (38, 46). This step is one of the major drivers of tumor cell invasion. The major structure that orchestrates this process is the invadopodium, being a hallmark of tumor cells favoring dissemination and metastasis (38). Invadopodia are dynamic actin-rich protrusions with proteolytic activities that degrade the ECM. These structures are composed by a complex network of integrins, signaling proteins, and a local deposition of membrane-bound or secreted MMPs (47, 48).

**The fourth stage of the migration cycle** is the cell contraction of actin filament provided by myosin II, which is the main motor protein in eukaryotic cells (**Figure 2.4**). Myosin II controls stress fibers assemble and contraction, and this process is regulated by the GTPase protein Rho and its downstream effector Rho-associated serine/threonine kinase (ROCK) (49). On the other side, myosin light-chain kinase (MLCK) phosphorylates myosin light chain (MLC) and activates myosin II regulating cortical actin network (50). These two signaling allows cells to control separately, the contraction in cortical actin dynamic and inner regions.

**In the last step**, by several mechanisms which are not fully understood, focal adhesions are disassembly preferentially in the trailing edge of the cells, whereas the leading edge remains attached allowing to move forward (**Figure 2.5**). The major mechanisms that regulate focal contact disassembly at the trailing edge are the actin filament turnover, the cleavage of focal contact components by the protease calpain, and focal contact disassembly by FAK (51-53).

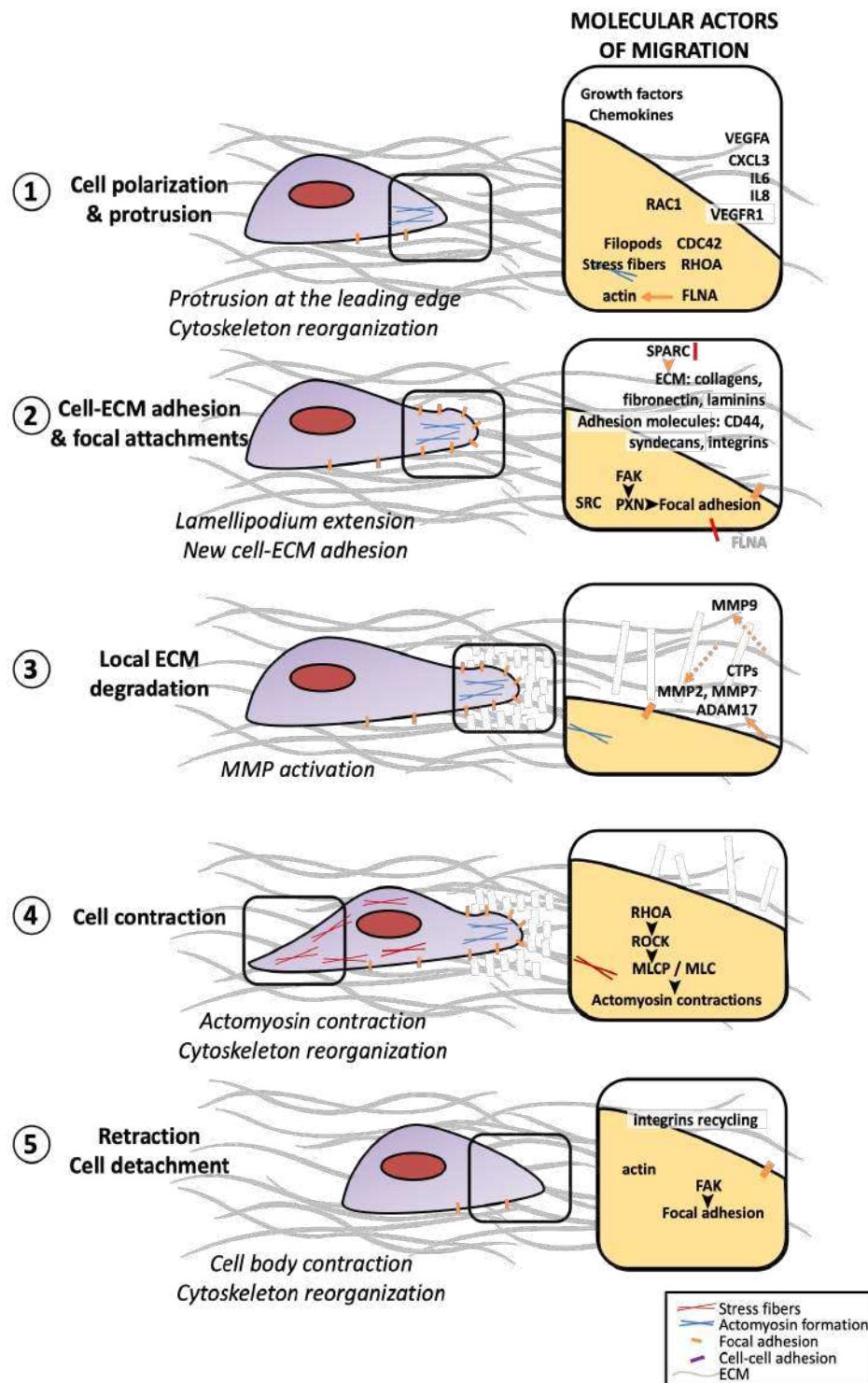


**Figure 2. The cellular processes and molecular actors involved in cell migration/invasion.**

During cell migration, cells start the cycle with polarization at the leading edge through the reorganization of the actin cytoskeleton (1) and the generation of new contacts with the extracellular matrix (ECM), known as focal contacts (2). The ECM surrounding the leading edge is degraded by metalloproteinases (MMPs), a process that allows cell movement (3). Finally, cell contractions (4), synchronized with cell-matrix detachments (5), lead the cell body's movement. The molecular partners involved in the different cancer cell migration steps are presented in the associated boxes. (Modified from: Limia, CM et al., 2019).

#### 4.4. *Endoplasmic Reticulum Stress in Cancer.*

The cellular factors that drive malignant cell transformation are highly complex and depend on a combination of oncogenes overexpression, mutations and micro-environmental factors (54). Among them, alteration in protein homeostasis (also known as proteostasis) is an emerging feature of cancer cells that drive the adaptation to adverse and stressful conditions that challenge cancer cell survival (55).

The generation of a highly efficient secretory pathway, comprising by the endoplasmic reticulum (ER) and the Golgi apparatus, is one of the essential adaptive mechanism in tumor cells (55). The ER is the main intracellular compartment that mediates the synthesis and folding of proteins that traffic through the secretory pathway. Despite this elaborated system, under intrinsic and extrinsic perturbations, protein synthesis and folding demand can exceed the ER folding capacity and unfolded proteins accumulate in the ER lumen, generating a condition named as ER stress (**Figure 3**). **This condition engages an adaptive response termed as the unfolded protein response (UPR), an integrated signal transduction pathway that transmits information about protein folding status at the ER lumen to the cytoplasm and nucleus.** These signaling pathways regulate transcriptional programs of genes coding for proteins associated with ER protein folding capacity, quality control, and the ER-associated degradation system (ERAD) (56, 57). If ER homeostasis cannot be restored, the UPR switches its signaling toward a pro-apoptotic mode to eliminate irreversibly damaged cells (58). Tumor cells are exposed to several perturbations such as nutrient deprivation, hypoxia, low pH, oncogenic addiction and an exacerbated secretory demand,

inducing alterations in protein homeostasis in the ER and favoring cell transformation (**Figure 3**) (12, 59). During the last decade, this adaptive response has been described as a pro-oncogenic mechanism, not only because it is an adaptive pathway that supports tumor progression but has been directly related to the acquisition of almost all hallmarks of cancer (**Figure 4**) (60, 61). Interestingly, fingerprints of UPR activation have been found in several types of primary and metastatic tumors, including brain, breast, colon, liver, lung, hepatocellular carcinoma, and skin cancer (reviewed in (62)).

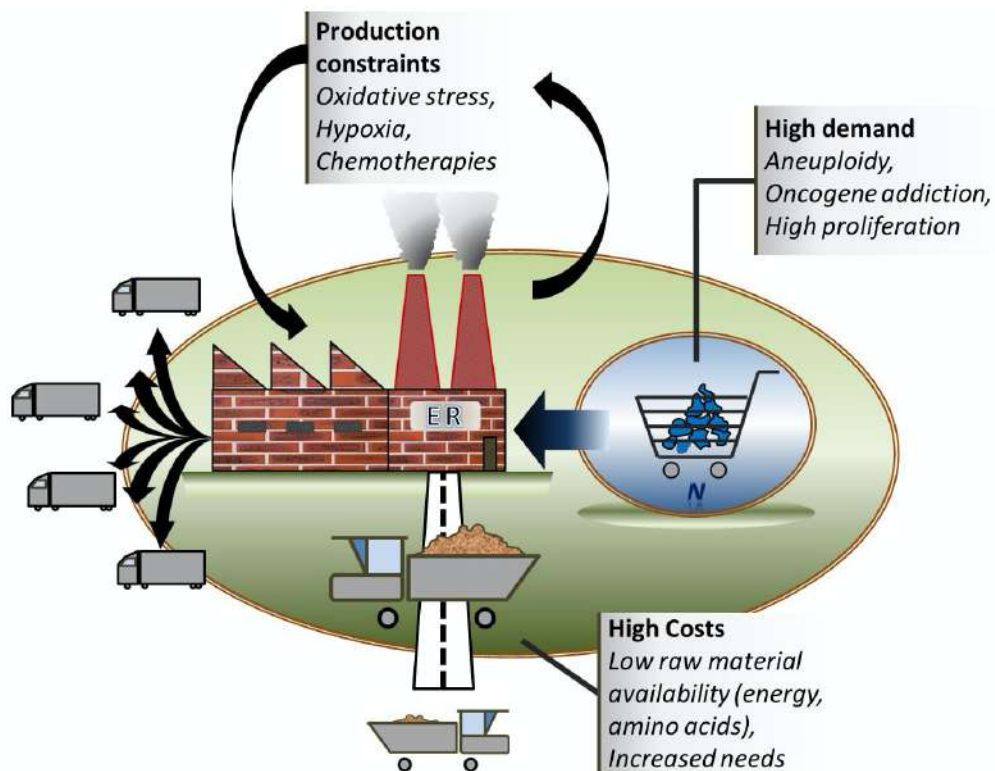


**Figure 3. Secretory protein demand and disruption of endoplasmic reticulum homeostasis in cancer cells.**

Tumor cells present a great variety of adaptive mechanisms and, among them, the generation of a highly efficient secretory pathway. The amount of secreted proteins is dependent on the demand and the availability of materials. In tumor cells, various intrinsic factors increase protein demand, and proteotoxic extrinsic factors that challenge the homeostasis in the ER by the accumulation of unfolded proteins in the ER lumen, generating a cellular condition known as ER stress. Tumor cells need to adapt to this condition to grow, and for that is activated an adaptive signaling named as Unfolded Protein Response. Abbreviations: N, nucleus; ER, endoplasmic reticulum. (**Figure from: Dejeans, N. et al., 2014**).



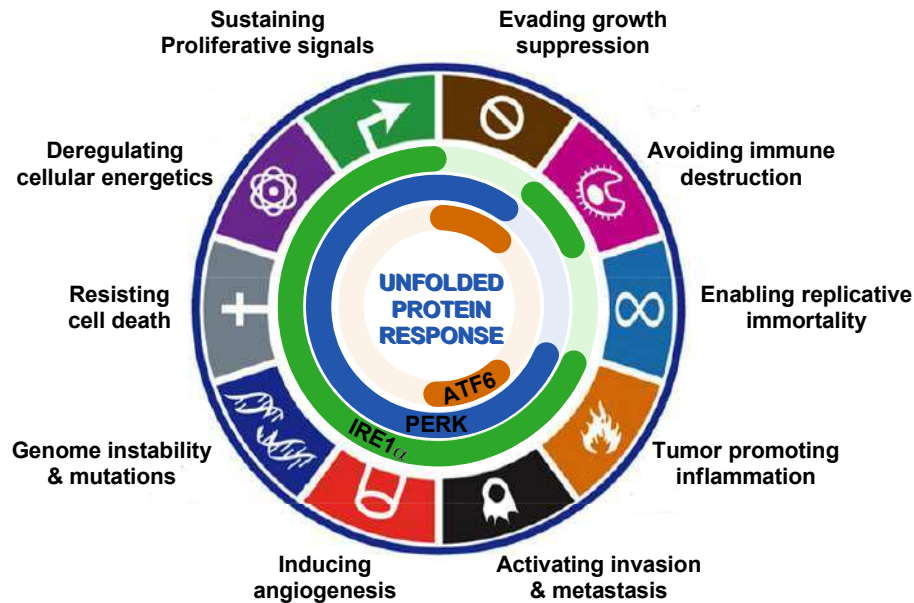


**Figure 4. Unfolded protein response and the hallmarks of cancer.**

The Unfolded Protein Response (UPR) activation has been described in different tumors and multiple cellular and animal models of cancer. In the last years, it has been proposed that UPR signaling can act as a pro-tumoral mechanism, favoring adaptation to stress factors and directly promoting the development of several Hallmark of Cancer. Abbreviations: IRE1 $\alpha$ , inositol-requiring enzyme 1 $\alpha$ ; PERK, PKR-like ER kinase; ATF6, activating transcription factor 6; ER, endoplasmic reticulum. (Figure from: Urrea, H. et al., 2016).

#### 4.5. *Unfolded Protein Response.*

The UPR is composed by three ER-resident transmembrane proteins including PKR-like ER kinase (PERK); Activating transcription factor 6 $\alpha$  (ATF6 $\alpha$ ) and Inositol-requiring protein 1 $\alpha$  (IRE1 $\alpha$ , referred to as IRE1 hereafter), that altogether aim to restore protein homeostasis (Figure 5) (55, 59, 63-65).

##### 4.5.1. *PERK and ATF6 signaling.*

Upon ER stress, PERK auto-transphosphorylation leads to its activation and phosphorylation of the eukaryotic translation initiation factor 2 alpha (eIF2 $\alpha$ ). Phosphorylation of eIF2 $\alpha$  leads to an inhibition of global protein translation, resulting in a reduction of ER load (66). Phosphorylated eIF2 $\alpha$ , also initiates the selective



translation of a group of mRNAs that harbors upstream reading frames (67, 68). One of these selective mRNAs encodes the activating transcription factor 4 (ATF4), which regulates genes involved in protein folding, antioxidant responses, autophagy, amino acid metabolism, and apoptosis (55, 59, 69, 70). ATF4 also regulate cell death through the induction of the C/EBP homologous protein (CHOP), a transcription factor that upregulates pro-apoptotic members of the Bcl-2 protein family (71). Growth Arrest and DNA Damage-Inducible Protein (GADD34), a protein activated downstream CHOP, forms a complex with the protein phosphatase-1 (PP1) to dephosphorylate eIF2 $\alpha$  and restore protein translation, resulting in a negative feedback loop for the PERK signaling pathway (72) (Figure 5).

On the other hand, ATF6 is a type II ER-resident transmembrane protein and can be found in two isoforms,  $\alpha$  and  $\beta$ , forming homo and heterodimers (73, 74). Under ER stress conditions, ATF6 is translocated through COPII vesicles to the Golgi compartment, where is cleaved by S1P and S2P proteases (75, 76). This proteolysis releases a cytosolic fragment of ATF6 (ATF6f), a potent transcription factor that regulates genes involved in the ERAD response and ER homeostasis maintenance (77, 78) (Figure 5).

#### **4.5.2. IRE1 signaling, stress sensing and activation mechanism.**

IRE1 is a type I ER-resident transmembrane protein and represents the most conserved branch of the UPR (66, 79, 80). The cytoplasmic region of IRE1 is composed of two domains with distinct enzymatic functions, including a serine/threonine kinase and an endoribonuclease (RNase) activity (Figure 5). Under ER stress, IRE1 dimerization and/or oligomerization leads to its auto-transphosphorylation that triggers a conformational change, resulting in the

activation of its RNase activity (59, 81). Together with the tRNA ligase RTCB, IRE1 catalyzes the unconventional splicing of X-box binding protein-1 (XBP1) mRNA, removing a 26-nucleotide intron, shifting its open reading frame and leading to the translation of a new protein and potent transcription factor termed XBP1s (spliced form) (82). XBP1s acts as a potent transcription factor and modulates the expression of several UPR target genes involved in protein folding, glycosylation, and ERAD (66). In addition, IRE1 RNase activity catalyzes the degradation of multiple ER-localized mRNAs and microRNAs through a process known as regulated IRE1-dependent decay (RIDD) that also attenuates the global mRNA translation (83, 84) (Figure 5). Of note, the molecular mechanism underlying the regulation of both RNase activities is still controversial and under debate. On the other hand, the IRE1 kinase domain interacts with the adaptor protein TNFR-associated factor 2 (TRAF2) and triggers a phosphorylation cascade that leads to c-Jun N-terminal protein kinase (JNK) and nuclear factor kappa-light-chain-enhancer of activated B cells (NF $\kappa$ B) pathways activation (85, 86).

The first model that explained IRE1 activation mechanism and ER stress sensing mechanism proposed that IRE1 is maintained in an inactive form in basal conditions due to its interaction with the chaperone BiP (Immunoglobulin binding protein, also known as GRP78) (92). Once unfolded proteins accumulate in the ER, BiP chaperone dissociates from IRE1 and allow its homodimerization, leading to the activation of the UPR branches (64, 93). However, this mechanism is still under debate, and new models to explain the fine-tuning of the ER stress sensors have been proposed more precisely in the last years. Some studies have strengthened the role of BiP in ER stress sensing, and the involvement of other molecular partners have been described. For instance, ERdj4 (also known as DNAJB9) was shown to

be necessary for BiP/IRE1 interaction. In this model, ERdj4 binds to IRE1 and facilitates BiP recruitment to the complex (94). Furthermore, based on an interactome screening and a functional validation, our lab recently identified the collagen chaperone HSP47 as a binding partner of IRE1 that promotes the dissociation of BiP and the subsequent activation of IRE1 signaling (95). Alternatively, the other two models describing the sensing mechanism of unfolded proteins in the ER lumen have been described. One suggests that BiP can act as a UPR sensor, binding to misfolded proteins through its substrate-binding domain and transduce the information to IRE1 by its ATPase domain, triggering a conformational change and UPR activation (96). Finally, the direct interaction of the IRE1-luminal domain with unfolded proteins has been proposed. The structure of the IRE1-luminal domain showed that yeast IRE1p present an MHC-like groove, and *in vitro* studies demonstrated that unfolded proteins can directly bind to IRE1 and induce its activation (96, 97). This observation leads to the possibility that the UPR components can act as direct sensors of ER stress. Altogether, this evidence indicates that the ER stress sensing mechanism is a complex network that comprises not just the UPR machinery, but also the protein folding system.

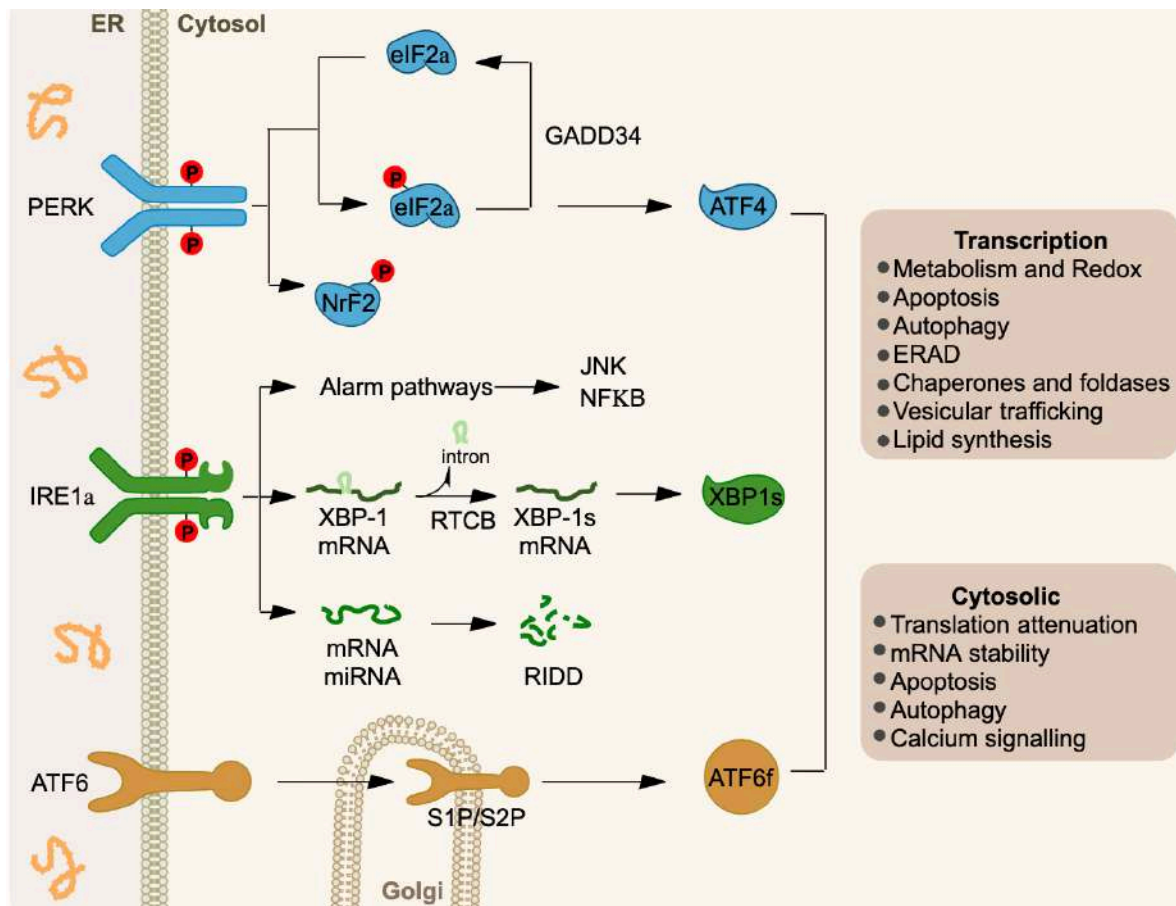


**Figure 5. Unfolded protein response.**

The UPR is mediated by three stress sensors localized at the endoplasmic reticulum (ER) membrane: activating transcription factor 6 (ATF6), the PKR-like ER kinase (PERK), and the inositol-requiring enzyme 1 $\alpha$  (IRE1). Under basal conditions, the luminal domains of these three sensors are constitutively bound to BiP (also known as GRP78), an essential ER chaperone. When unfolded or misfolded proteins accumulate in the ER, BiP dissociates from the UPR sensors leading to the activation of the UPR branches. PERK activation leads to inhibition of the global protein translation through the phosphorylation of the eukaryotic translation initiation factor (eIF2 $\alpha$ ), resulting in reduced ER load. Upon ER stress ATF6 is transported to the Golgi apparatus where is processed by S1P and S2P proteases releasing the cytosolic fragment (ATF6f). ATF6f is a potent transcription factor regulating the expression of genes related to ER-associated degradation (ERAD) response and other genes involved in reestablishing ER homeostasis. IRE1 is a kinase and endoribonuclease that catalyzes the unconventional splicing of X-box binding protein-1 (XBP1) mRNA removing a 26-nucleotide intron. This processing event changes the open reading frame of XBP1, leading to the translation of a new protein termed XBP1s (spliced form). XBP1s acts as a potent transcription factor and modulates the expression of several UPR target genes involved in ER folding, glycosylation, and ERAD. Besides, the IRE1 $\alpha$  endoribonuclease activity can target other mRNAs and microRNAs through a process termed regulated IRE1-dependent decay (RIDD). (Figure from: Hetz, C. and Papa, FR, 2017).

Remarkably, the IRE1 function is also regulated by a complex and dynamic signaling platform at the ER, termed as the UPRosome. The UPRosome involves many proteins that interact with IRE1 and assemble a signaling platform at the ER membrane that regulate IRE1 activity (reviewed in (87)). During the last years, novel UPRosome-related physiological functions of IRE1 have been described, such as regulation of apoptosis, autophagy, protein degradation pathway, and calcium homeostasis (88-92). Remarkably, we recently discovered a fundamental and new function of IRE1 in cell migration. Our lab described that **IRE1 can enhance cell migration and regulate actin cytoskeleton remodeling in non-tumor cells through its interaction with FLNA**, an essential protein involved in actin filament crosslinking (93). Nevertheless, the impact of this novel function of IRE1 in cell migration has not been tested in tumor cells yet.

#### 4.6. ***Connections between IRE1 signaling and cancer progression.***

The three pathways of the UPR have been related to cancer progression; in fact, fingerprints of UPR activation have been found in different types of primary tumors (reviewed in (61)). The signaling pathway of IRE1 is the most studied branch of the UPR in this context, and its association with cancer progression has increased in the last years (reviewed in (60)). Remarkably, **IRE1 has been described as the fifth human kinase more likely to carry at least one tumor driver mutation**, highlighting the importance of this ER stress sensor in cancer progression (94).

As mentioned, IRE1 has an endoribonuclease activity that leads to XBP1 splicing and RIDD, and both outputs have been associated with oncogenic processes (59, 62, 95). Several studies have linked IRE1/XBP1s signaling to cancer progression, enhancing tumor growth and cell survival (96, 97). **Importantly,**

**clinical studies in patients with glioblastoma multiforme (GBM) (98), triple-negative breast cancer (TNBC) (99), multiple myeloma (100), and pre-B acute lymphoblastic leukemia (101), have demonstrated an indirect association between XBP1s expression and patient prognosis.** Additionally, research in different tumor cell lines has connected XBP1s expression levels to chemotherapy resistance, angiogenesis, immune response modulation, invasion, and tumor survival (99, 102-105). Small molecules that inhibit IRE1 RNase activity have been evaluated *in vivo* multiple myeloma, TNBC and GBM showing beneficial effects (106-109). Some reports also associate the UPR signaling with early stages of melanoma carcinogenesis and progression, particularly with tumor growth, resistance to apoptosis and chemoresistance (reviewed in (110)). In addition, melanoma cells have a constitutive activation of the IRE1 branch, being largely associated to resistance to ER-stress-induced apoptosis (111-113). However, the direct impact of IRE1 during melanoma progression has not been fully investigated.

**Despite the growing evidence suggesting that IRE1 is an important regulator of tumor progression and others hallmarks of cancer, its implication in metastasis is still ambiguous.** An exacerbated cell migration capacity and invasion of surrounding tissues are essential features of cancer progression leading to tumor expansion and dissemination. As we mentioned before, growing evidence point UPR pathways as regulators of different hallmarks of cancer, including cell migration, invasion, and metastasis of tumor cells. Although the three ER stress sensors have been linked to cell mobility and EMT, the signaling associated to PERK activation has been recognized to play a critical role in tumor invasion and metastasis (60, 62, 114-116). On the other hand, the IRE1 axis has been the most extensively correlated with cancer progression due to the ability to regulate many

cancer cells functions, but its ability to regulate metastasis has not been addressed in depth. However, some studies suggest that IRE1 can regulate the ability of cancer cells to migrate and invade surrounding tissues (117). We will summarize the main discoveries about this association in the next section.

#### **4.7. *IRE1 in cell migration and metastasis.***

As previously mentioned, some reports correlate IRE1 activity with actin cytoskeleton dynamics, cell migration, invasion and metastasis. Currently, it is known that **IRE1 has two major mechanisms to control migration/invasion: the control of gene expression through its RNase activity (XBP1s and RIDD), and the modulation of signaling pathways through direct binding with proteins, such as FLNA.**

**IRE1/XBP1s axis has been the most extensively correlated with cancer progression and metastasis.** For instance, studies with tumor samples from patients with colorectal carcinoma, breast cancer, and oral squamous cell carcinoma, described the overexpression of IRE1 or XBP1 in metastatic samples compared to the primary tumors (118-121). Also, elevated levels of XBP1s at primary tumors are associated with the presence of distant metastasis in patients with esophageal carcinoma, hepatocellular carcinoma, and oral squamous cell carcinoma (122-124). A role for the IRE1/XBP1s axis in invasion and metastasis has been proposed (118, 121, 124). Indeed, some studies indicate that XBP1s increase the metastatic potential of tumor cells by the induction of the expression of several EMT transcription factors, including Snail family transcriptional repressor 1 (Snail1), Snail family transcriptional repressor 2 (SNAIL2), zinc finger E-box binding homeobox 2 (ZEB2) and transcription factor 3 (TCF3) (119, 123, 125, 126). Another

important process in metastasis is the invasion and degradation of the ECM through the expression of MMPs (127). In a model of esophageal squamous cell carcinoma, XBP1s overexpression promoted cell invasion through the upregulation of MMP-9, one of the MMP most widely associated with cancer progression, and correlated with increased lymph nodes metastasis (122). Similarly, XBP1 deficiency in oral squamous cell carcinoma cells impairs cell invasion and leads to a decrease in the expression of invasion-associated genes: MMP1, MMP3 and urokinase-type plasminogen activator (uPA) (120). Interestingly, high levels of XBP1s have been linked to TNBC tumorigenesis, where XBP1s interact with Hypoxia-inducible factor 1-alpha (HIF1 $\alpha$ ) and enhance the expression of HIF1 $\alpha$ -regulated genes. Of note, this study showed that the silencing of XBP1 decreased the formation of lung metastases (99).

Interestingly, another study showed that single disseminated cancer cells (DCC) that develop latent liver metastasis in pancreatic cancer, presented a decreased IRE1 activity leading to the escape from the immune system response by inhibiting MHC class I molecules expression. However, restoration of the IRE1 signaling branch or overexpression of XBP1s in DCC, leads to the outgrowth of liver macro-metastatic lesions (128). These findings suggest that IRE1 activation might be important for the initial and final steps in metastasis, like tumor cell dissemination and the formation of macro-metastasis, with a temporary downregulation of IRE1 activity to avoid anti-tumor immune response. Together, these studies suggest that IRE1/XBP1s signaling contributes to cancer metastasis.

**Intriguingly, the IRE1/RIDD axis has been shown to negatively modulate cell migration and invasion** (98, 102, 129-132). In GBM cells, a gene expression profiling revealed that loss of the enzymatic activity of IRE1 resulted in an



upregulation of ECM proteins. In this study, **IRE1 signaling was found to negatively regulate cell migration and invasion of GBM cells through RIDD-mediated degradation of secreted protein acidic and cysteine rich (SPARC) mRNA** (130). SPARC is a glycoprotein present in the extracellular matrix and its function is correlated with changes in cell shape and synthesis of ECM promoting cell migration, invasion and metastasis in a several types of tumors, including melanoma (133-138). Dejeans *et al.*, found that impairment of IRE1 signaling with the subsequent increase in SPARC transcriptional expression, enhanced cell migration, stress fiber formation and focal adhesion number in GBM cells (130). Also, selective impairment of IRE1 RNase activity increases invasion, vessel co-option capacity, and mesenchymal features in U87 cells (131). Finally, a recent study demonstrated antagonistic roles of XBP1 mRNA splicing and RIDD regarding GBM outcomes. In this study, GBM patients were stratified into four mixed groups with high or low XBP1s and RIDD activity. XBP1s high/RIDD low tumors were associated with a more mesenchymal phenotype and invasive properties (139).

On the other hand, a study from our laboratory uncovered a novel mechanism of cell movement regulation underlying IRE1 function. Using an interactome screening, FLNA was identified as a major IRE1-binding partner. **We found that IRE1 acts as a scaffold to recruit FLNA and increases its phosphorylation at serine 2152, enhancing cell migration.** Deletion of IRE1 impaired actin cytoskeleton dynamics at the protruding and retracting areas. The function of FLNA in cytoskeleton dynamics depends on its phosphorylation at serine 2152 (140). Our results indicate that IRE1 facilitate FLNA phosphorylation to control actin cytoskeleton and cell migration. Importantly, the regulation of cytoskeleton dynamics by IRE1 is independent of its canonical RNase activity (XBP1 and RIDD).

Besides fibroblasts, these results were also observed in a panel of tumor cell lines and in various *in vivo* models such as zebra fish, drosophila and mouse models, suggesting a conserved mechanism in evolution (141). Considering this new function of IRE1 in cell migration of normal cells and that FLNA has been associated with cancer; we consider that the IRE1/FLNA axis could have an impact in cell migration and invasion of tumor cells, increasing metastasis.

These observations highlight the complexity of IRE1 signaling and the different pathways that can exert a regulation on tumor cell migration, invasion and metastasis. It is essential to understand the role of IRE1 activities in metastasis and how its arms (XBP1s, RIDD, and FLNA) can favor different outcomes depending on the type of tumor.

#### 4.8. ***FLNA function in cell migration and metastasis.***

FLNA is an actin cross-linking protein that also acts as scaffold for over 90 protein partners including ion channels, signaling proteins, receptors and transcription factors (142). FLNA (280 kDa) dimerize generating V shape structures that crosslink actin filaments. This protein has an N-terminal actin-binding domain (ABD) followed by two Rod domains composed of 24 immunoglobulin-like tandem repeats and by two hinge structures (**Figure 6**) (143). FLNA function is regulated mostly by phosphorylation at different residues mediated by different protein kinases (144-146). Particularly, serine 2152 phosphorylation is an important event in actin filaments (F-actin) crosslinking, impacting in various biological processes such as cell migration (140). FNLA is also regulated through the cleavage by calpains in the two hinge domains of the C-terminal region, generating a 200 kDa N-terminal and a 90 kDa C-terminal fragments (Figure 6) (147). This cleavage is inhibited by the

S2152 phosphorylation (148). It has been described that the 90kDa fragment translocate to the nucleus and interacts with transcription factors, such as the androgen receptor, and has been recently associated with novel functions like the regulation of gene expression (148).

FLNA has been widely related to cancer progression, particularly to cell invasion and metastasis (reviewed in (149)). Of note, this protein can act either as a tumor suppressor or an oncogene, depending on its subcellular localization and its binding partners (reviewed in (150)). **In clinical samples of hepatocellular carcinoma, breast cancer and pancreas adenocarcinoma, high levels of FLNA have been correlated with increased metastatic potential** (151-155). Furthermore, gain and loss of function approaches in tumor cell lines demonstrated the implication of FLNA in cancer cell spreading, migration and metastasis (152, 156, 157). For instance, knockdown of FLNA reduces metastasis of melanoma cells in a xenograft mouse models (152). These findings support the model that FLNA acts as an oncogene that promotes cancer cells invasion. However, controversial results suggest that the 90 kDa FLNA might also suppress metastasis (reviewed in (150)). Recent findings indicate that FLNA negatively regulates cancer cell invasion promoting MMP9 degradation (158, 159). On the other hand, was also found that overexpression of FLNA decrease cell invasion and migration through the regulation of focal adhesions via calpain-dependent mechanism in breast cancer models (160). Based on this evidence, some authors hypothesize that nuclear fragments of FLNA suppress cell migration, while cytoplasmic localization of full length FLNA promotes cancer metastasis. One might speculate that proteins that potentiate FLNA phosphorylation might also inhibit FLNA proteolysis and thus promote metastasis.

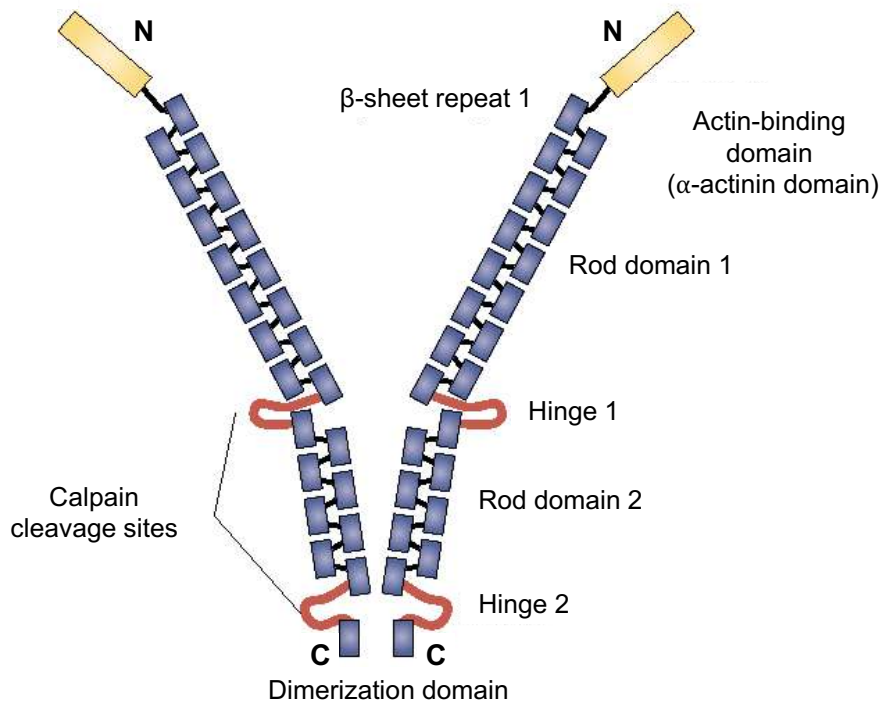


**Figure 6. Filamin A structure and regulation.**

FLNA is an actin crosslinking protein that can also act as a scaffold for over 90 proteins. FLNA is a 280 kDa protein that dimerizes generating V shape structures that crosslink actin filaments in the N-terminal domain denominated as an actin-binding domain (ABD). This ABD is followed by two Rod domains composed of 24 immunoglobulin-like tandem repeats of ~96 amino acids each and by two hinge structures. The two hinge domains allow a flexible form of FLNA and are susceptible to proteolysis by calpain. FLNA function is mostly regulated by phosphorylation, particularly at serine 2152. However, FNLA is also regulated through the cleavage by calpains in the two hinge domains. This process generates a 90 kDa C-terminal fragment that has been shown to translocate to the nucleus and regulate gene expression. (Figure from: Hartwig, Z. et al., 2010).

#### 4.9. *Melanoma signaling and the UPR.*

As we mentioned before, skin cutaneous melanoma is one of the deadliest metastatic tumors. At the molecular level, melanoma progression is regulated mainly by the activation of some signaling pathways, including mitogen-activated protein kinase (MAPK), PI3K, and Wnt/  $\beta$ -catenin (27, 161). Mutations in B-Raf Proto-Oncogene (BRAF) and NRAS genes have been found in the majority of melanoma tumors, leading to the activation of the MAPK pathway and increasing proliferation, survival and migration. **Interestingly, a link between oncogenic**

**BRAF activity and a basal UPR induction, mainly ATF6 and IRE1 branch, have been described in melanoma cells** (113, 162). This UPR activation enhances tumor growth and inhibits cell death induction, promoting tumor progression and chemoresistance. **ATF6 and IRE1 activation in melanoma cells have been associated with an increase of autophagy contributing to the desensitization of cells to apoptosis induction** (111, 113, 162). Also, inhibition of BRAF or MEK prevents IRE1 and ATF6 activation, which subsequently increases UPR-induced apoptosis (162).

Besides, increased levels of BiP have been positively correlated with progression and poor survival outcome in patients with melanoma (163). On one hand, high expression levels of BiP have been described as a potential biomarker for early diagnosis of melanoma (164). On the other hand, a study with different human melanoma cell lines concluded that chronic UPR activation promotes melanoma progression by the activation of the fibroblast growth factor (FGF) and fibroblast growth factor receptor (FGFR) pathways (165). Of note, in this study was found that activation of PERK and ATF6 pathways, but not IRE1, correlated with poor overall survival of melanoma patients. On the contrary, high expression of homocysteine-responsive endoplasmic reticulum-resident ubiquitin-like domain member 1 (HERPUD1), a downstream target of the IRE1 branch, was associated with a better prognosis, suggesting that the IRE1 pathway may be a tumor suppressor in this type of cancer (165).

All this evidence shows a correlation between UPR activation, including IRE1, and melanoma progression and chemotherapy resistance; however, **no evidence regarding the role of IRE1 in cell migration and invasion in melanoma has been published**. Taking in consideration the highly metastatic potential of

melanoma cells, the knowledge of the more relevant molecular pathways that regulate the transition from the primary tumor to disseminated disease, and the evidence that links the more common genetics alteration in this cancer to UPR activation, we decided to test in this tumor the possible role of IRE1 as a regulator of cell migration, invasion and metastasis and its relationship with FLNA signaling.

## **5. HYPOTHESIS.**

IRE1 regulates migration and invasion of melanoma cells by promoting FLNA phosphorylation and actin cytoskeleton remodeling.

## **6. GENERAL AIM.**

To determine the involvement of IRE1/Filamin A signaling in the migration and invasion capacity of melanoma cells.

## **7. SPECIFIC AIMS.**

**Specific aim 1.** To evaluate the activation status of IRE1 during metastasis in melanoma.

**Specific aim 2.** To study the contribution of IRE1 in migration and invasion in melanoma cells.

**Specific aim 3.** To investigate the possible participation of the IRE1/FLNA pathway in the regulation of cell migration and invasion in melanoma.

**Specific aim 4.** To correlate IRE1 function with metastasis in melanoma in vivo.

## **8. MATERIALS AND METHODS.**

### **8.1. *Reagents.***

Tunicamycin (TM) was purchased from Sigma®. Cell culture media, fetal bovine serum (FBS), and antibiotics were obtained from Gibco™ and ATCC. Phalloidin, Fluorescein Isothiocyanate Labeled peptide from Amanita phalloides P5282 was purchased from Sigma®. Corning Matrigel Basement Membrane Matrix Growth Factor Reduced LDEV-Free was obtained from Corning (cat n. 356230). The IRE1 RNase activity inhibitor MKC-8866, purity 98.13%, was order in Selleckchem®. Other reagents used here were Sigma or the highest grade available.

### **8.2. *Cell culture and generation of the IRE1 Knockout cell lines.***

The A375, A375-MA2 and A2058 human melanoma cell lines and the B16F10 mouse melanoma cell line, were maintained in Dulbecco's modified Eagle's Medium (DMEM), high glucose (Gibco™). The SK-MEL5 melanoma human cell line was maintained in ATCC-formulated Eagle's Minimum Essential Medium (EMEM). All the mediums were supplemented with 10% FBS, non-essential amino acids and grown at 37°C and 5% CO<sub>2</sub>.

Additionally, we generated A375-MA2 and B16F10 IRE1 Knockout (KO) cells using the double nickase method of CRISPR/CAS9 technology (Figure 7). For this purpose, we used a double nickase that was targeted to IRE1 or scrambled as a control (sc-400576-NIC and sc-437281); Santa Cruz). Melanoma cells were transfected, using Effectene protocol (Cat No./ID: 301425, Qiagen), with 1ug of plasmids DNA per well in a 6-well plate. After 48 hours of incubation, transfected



cells were selected with 2 ug/ml of puromycin for 72 hours and a pool of cells transfected with the IRE1KO plasmid or Control were obtained. We then proceeded to isolate individual clones from a pooled population of IRE1KO or Control cells by limiting dilutions, a protocol that requires a highly diluted cell suspension from which single cell-derived clones are isolated and further expanded. The pool of cells was diluted in density of 0.3, 3 or 30 cells per 100  $\mu$ L aliquots. This requires transferring 100uL aliquots into each well of 96 well plate. The wells with individual clones were identified and that clones were expanded and checked for IRE1 expression and activity.

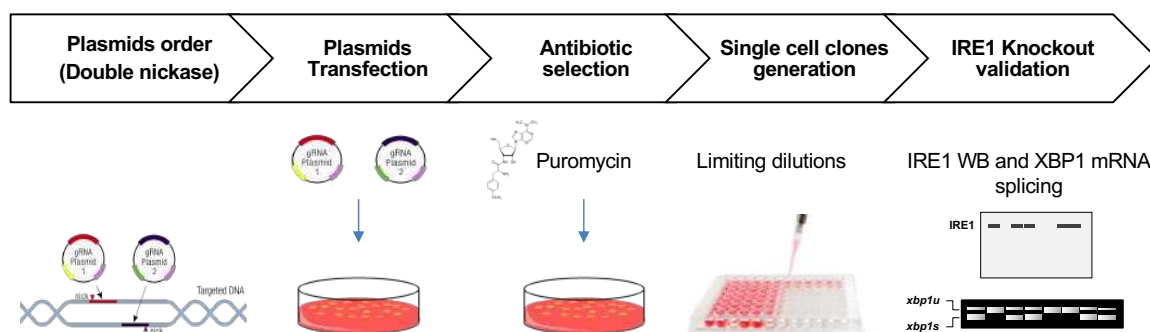


**Figure 7. Workflow of the generation of IRE1 knockout (KO) human melanoma cells.**

For the generation of A375-MA2 IRE1KO cells, we used the double nickase method of CRISPR/CAS9 technology with commercial plasmids (Santa Cruz Biotechnology). Plasmids containing sgRNAs Control or sgRNAs for IRE1 were transfected in A375-MA2 parental cells. After 48 h, cells transfected were selected with puromycin for 72h, and a pool of cells containing the plasmids was obtained. We then proceeded to isolated individual clonal IRE1KO and Control cells by limiting dilutions. The efficiency of the genetic approach and the identification of IRE1KO clones were evaluated by measuring the level expression of IRE1 protein by western blot and the IRE1 activity using XBP1 mRNA splicing under treatment with tunicamycin.

### 8.3. *NIH-conditioned medium.*

For the generation of the NIH 3T3- conditioned medium (NIH-CM)  $20 \times 10^6$  NIH-3T3 cells were seeded in a 100  $\text{cm}^2$  plate in 30 ml of complete growth medium. Conditioned medium was gently aspirated after 24 hours in culture. To remove any

remaining cells, the medium was centrifugated at 3000 rpm and the cell pellet, if any, discarded and the medium was then pass through a syringe filter of 0.45 µm. The media was used immediately or distributed in un 1 ml aliquots and frozen at -20°C.

#### **8.4. RNA isolation and RT-PCR.**

RNA isolation was performed using TRIzol™, a ready-to-use reagent, designed to isolate high-quality total RNA (as well as DNA and proteins) from cell and tissue samples. The isolation was used based in the protocol described according to the manufacturer's instructions (Invitrogene, Catalog Number 15596026). The cDNA was synthesized with SuperScript III reverse transcriptase (Life Technologies) using random primers p(dN)6 (Roche). PCR primers and methods for the XBP-1 mRNA splicing assay were previously described (166). XBP-1s mRNA was monitored by semi-quantitative time PCR using the following primers: 5'-AAGAAC ACGCTTGGGAATGG-3' and 5'-CTGCACCTGCTGCGGAC-3'.

#### **8.5. Immunoprecipitations.**

Endogenous immunoprecipitations (IP) were performed in SK-MEL5 and B16F10 cells using a protocol previously described (166). In brief, to immunoprecipitate IRE1, cells were plated in 10 cm dishes and protein extracts were lysed by using a lysis buffer (0.5% NP-40, 150–350mM NaCL, 150mM KCl, 50mM Tris pH7.6, 5% glycerol, 50mM NaF, 1mM Na3VO4, 250mM PMSF, and protease inhibitors) for 20 minutes at 4°C. Lysates were clarified by centrifugation at 13.200 rpm for 15 min. Protein extracts were incubated overnight at 4°C with 1µg of a high-affinity anti-IRE1 antibody (Cell signaling, 14C10) per 1mg of protein lysate. Next

day protein complexes were incubated for 1 hour at 4°C with 30uL of Protein A magnetic bead (10002D, Invitrogene), then washed 3 times with 1 ml of Lysis buffer and then one time in Lysis buffer with 500 mM NaCl. Beads were dried and resuspended in Sample Buffer 2x. Samples were heated for 5 min at 95°C and resolved by SDS-PAGE 8% followed by western blot analysis.

#### 8.6. **Western blot analysis.**

Cells were collected and homogenized in RIPA buffer (20 mM Tris pH 8.0, 150 mM NaCl, 0.1% SDS, 0.5% Triton X-100) containing a protease inhibitor cocktail (Roche, Basel, Switzerland) in presence of 50 mM NaF and 1 mM Na<sub>3</sub>VO<sub>4</sub>. After sonication, protein concentration was determined in all experiments by micro-BCA assay (Pierce, Rockford, IL), and 25-40 µg of total protein was loaded onto 8-12 % SDS-PAGE minigels (Bio-Rad Laboratories, Hercules, CA) prior transfer onto Amersham™ Protran® Premium Western blotting membranes, nitrocellulose pore size 0.2 µm. The membranes were blocked using PBS, 0.1% Tween20 (PBST) containing 5% Bovine Serum Albumin for 60 min at room temperature, then incubated overnight with primary antibodies. The following antibodies diluted in blocking solution were used: anti-HSP90 (1:1000, sc-69703 Santa Cruz Biotechnology), anti-filamin A (1:5000, rabbit mAb ab76289 abcam); anti-phospho S2152 filamin A (1:1000, rabbit mpAb ab51229 Abcam); anti-IRE1α (1:1000, rabbit mAb 14C10 Cell Signaling Technology); anti-calnexin (1:1000, Novus Biologicals); anti-GAPDH (1:1000, Santa Cruz Biotechnology). After the incubation with the primary antibodies the membranes were washed with PBST. Bound antibodies were detected with peroxidase-coupled secondary antibodies incubated for 1 h at room temperature and the ECL-Plus system (Thermofisher).

### **8.7. Knockdown of IRE1 and FLNA.**

We performed transient knockdown of IRE1 in the four human melanoma cell lines, using a small-interfering RNA (siRNA) targeting IRE1 or a scrambled siRNA as a control. siRNAs were obtained from Eurofins MWG Operon. Each siRNA (25 nM) was transfected using Lipofectamine RNAiMAX (Invitrogen). Transient transfections were performed following manufactured instructions. In brief,  $2 \times 10^5$  cells were seeded in 6 well plate. After 24 hours, 10 pmol or 30 pmol of siRNA targeting IRE1, FLNA or Control was transfected diluted in Opti-MEM medium and together with RNAiMAX reagent for 48 h.

### **8.8. Cell proliferation assay.**

Cell proliferation of A375-MA2 cells was evaluated using the WST-1 proliferation assay (Roche, ref: 1 644 807). The protocol was performed following manufacturer's instructions. Briefly, 2000 cells were seeded in triplicate in 96 well plates (200  $\mu$ L/well), one plate per day. For the quantification, 20  $\mu$ L of WST-1 was added per well and incubated for 4 hours at 37°C. The absorbance was readed using 450 and 595 wavelengths in a microplate reader (The Infinite® 200 PRO NanoQuant, Tecan). The number of cells was determined for four consecutive days.

On the other hand, the protocol to determine cell proliferation in B16F10 cells was based in automatic cell counting. Cells (2000 cells/well) were seeded in 96 well plates (200  $\mu$ L/well), one plate per day. For the quantification, cells were stained with Hoechst dye solution (10 mg/ mL, Invitrogen Hoechst 33342) diluted 1/5000 in complete medium. Cells were incubated with the staining for 15 minutes and counted on an ArrayScan XTI Live High Content Platform (Thermo Fisher) for 4 consecutive days.

### 8.9. ***Transwell Migration Assay.***

Assays were performed in Boyden Chambers (Millipore®, 12 mm diameter, 8 µm pore size) according to the manufacturer's instructions. Briefly, for the human cell lines, 50,000 cells resuspended in serum-free medium were plated onto the top of each chamber insert and NIH-CM was added to the bottom chamber. After 4 hours, inserts were removed, washed and cells that migrated to the bottom side of the inserts were stained with 0.1% crystal violet in 2% ethanol and counted in an inverted microscope using a 20X objective lens.

In addition, B16F10 were seeded onto the top of each chamber insert coated with 2 µg/ml fibronectin and allowed to migrate for 6 hours. Then, inserts were removed, washed and stained with 0.1% crystal violet in 2% ethanol and counted in an inverted microscope using a 20X objective lens.

### 8.10. ***Adhesion Assay.***

Cells (20,000) were suspended in serum-free medium and allowed to attach to fibronectin coated-24 well plates (2 µg/ml) or Matrigel (500 ng/mL) at different periods of time. Non-adherent cells were removed by washing gently in serum-free medium and adherent cells were stained with 0.1% crystal violet in 2% ethanol. Cell-bound dye was eluted with methanol, and the absorbance was measured at 600 nm in a microplate reader (Tecan® infinite 200Pro).

### 8.11. ***Actin cytoskeleton analysis.***

Cells (20,000) were seeded on non-coated 12-mm coverslips for 48 hours, fixed with Paraformaldehyde (PFA) 4% per 15 minutes and stained with phalloidin coupled to FITC, following manufacturer's instructions (Sigma). Images were taken

using a confocal microscope (Leica SP8) with a 40x/1.2 oil-immersion objective at room temperature. Fluorescence intensity of FITC was quantified from the border of the cell to the center using the ImageJ software. Stress fibers number and size were quantified automatically using the plugin Filament detector of the ImageJ software. Filopodia formation was determined using the software FiloQuant of the ImageJ software.

Moreover, B16F10 (100,000) cells were seeded onto fibronectin-coated 25-mm coverslips, transfected with EGFP-Lifeact using Lipofectamine 2000 Transfection Reagent and imaged in HBSS medium supplemented with HEPES using a confocal microscope (Zeiss LSM 710) with a  $\times 63/1.4$  NA oil-immersion objective lens at 37 °C. Images were acquired every 5s for 10 min using time-lapse confocal microscopy. To perform a protrusion and retraction analysis, images were segmented using maximum threshold. Then, subsequent images were merged assigning the first image as green and the second image as red. The total area of green (protrusions) and red (retractions) color of merged images was obtained using ImageJ software. In addition, cells were fixed and stained with phalloidin coupled to rhodamine and visualized by confocal microscopy. The number and size of stress fibers and filopodia per cell was determined using the ImageJ software as described previously (93).

#### 8.12. ***Cell invasion assay.***

Invasion assays were performed in Boyden Chambers (Millipore®, 12 mm diameter, 8  $\mu$ m pore size). The inside compartment of the chamber was coated with 200 ng/mL of Matrigel and incubated for 1h at 37°C. Cells (30,000) resuspended in 300  $\mu$ L serum-free medium were plated onto the top of each chamber and 500  $\mu$ L

of NIH-CM was added to the bottom chamber. After 24 hours, inserts were removed, washed carefully and cells that migrated to the bottom side of the inserts were stained with 0.1% crystal violet in 2% ethanol and counted in an inverted microscope using a 20X objective lens.

### 8.13. *Experimental metastasis assay.*

We evaluated lung metastasis using an experimental tail vein injection model. Human melanoma metastatic cells were injected through the tail vein in eight-weeks old NOD/SCID/IL2 $\gamma$ <sup>null</sup> (NSG) mice (Figure 8). NSG mice carry a severe combined immune deficiency (SCID) and a null allele of the IL2 receptor common gamma chain (IL2 $\gamma$ <sup>null</sup>). The severe immunodeficiency allows the mice to be humanized by engraftment of tumors with human origin (167).

The animals were placed in a beaker; the tail was heated in order to dilate the veins, and then with a syringe of 1 mL (26G), we performed an injection in one lateral vein of 25,000 cells in 200  $\mu$ L of PBS. Mice were clinically monitored for four weeks and sacrificed 28 days after injection. Next, lungs were collected and fixed with formaldehyde solution at 4%, paraffin-embedded and stained with Hematoxylin & Eosin (H&E). The number and the surface area of the metastatic nodules were determined through serial section of H&E staining of lungs through ImageJ software.

To evaluate metastasis using the mouse melanoma cell line B16F10 a similar protocol was performed (Figure 9). B16F10 cells (200,000) resuspended in 500  $\mu$ L of PBS were injected intravenously in the lateral tail vein of 8-12 weeks old C57BL/6 mice. At day 21 post-injection mice were sacrificed, lungs were collected and rinsed in PBS to remove excess blood. Next, the lungs were placed in a labeled vial containing 5 ml Fekete's solution and once the lungs were fixed and bleached to

and the B16F10 nodules showed up black, pictures of the lungs were taken, and dissection of the tumor mass was performed. Subsequently, the weight of the total mass of the metastatic nodules per lung was determined.

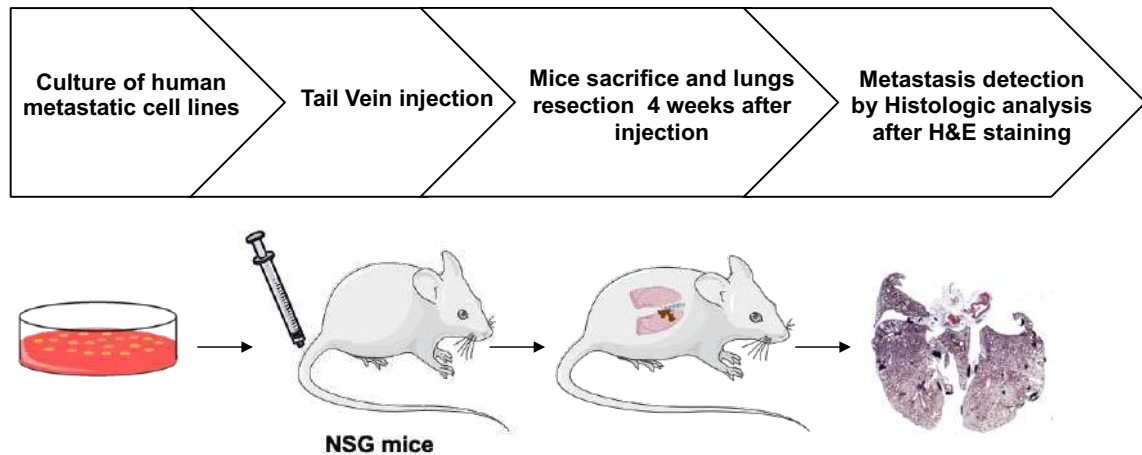


**Figure 8. Lung metastasis using an experimental tail vein injection model in immunosuppressed mice.**

Metastatic cells (15.000) were injected in the tail vein of eight-week-old male NSG mice. Mice were clinically monitored for four weeks and sacrificed 28 days after injection. Next, the lungs were collected, fixed in formaldehyde solution 4%, and paraffin-embedded for histologic analysis after hematoxylin and eosin (H&E) staining. The number of metastasis nodules and the size of the metastatic foci were determined using the ImageJ software and compared between the different conditions.

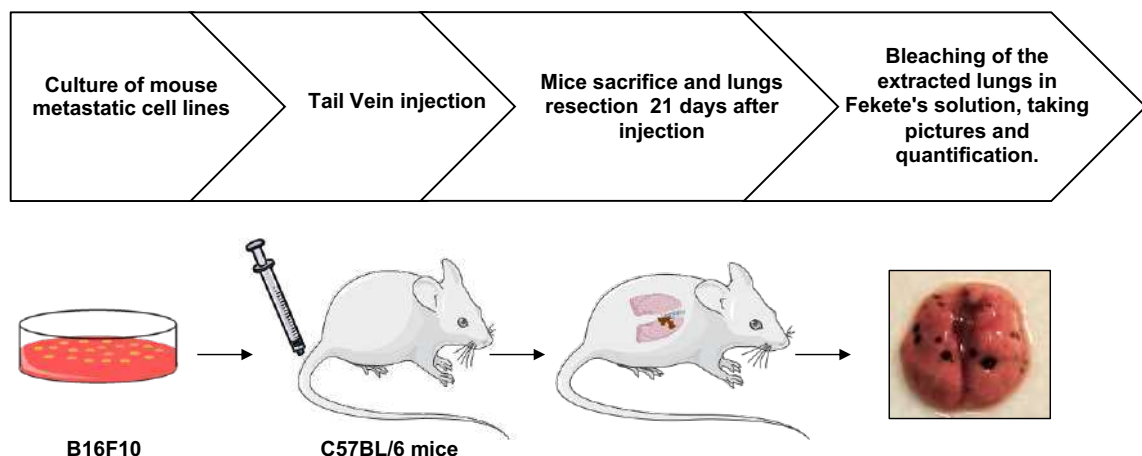


**Figure 9. Lung metastasis using an experimental tail vein injection model in immunocompetent mice.**

Mouse metastatic melanoma cells (200.000) were injected in eight-week-old male C57BL/6 mice. Mice were clinically monitored for three weeks and sacrificed 21 days after injection. Next, the lungs



were collected, fixed, and bleached in Fekete's solution, and pictures were taken to quantify the metastatic nodules.

#### 8.14. **Bioinformatic analysis.**

From the TCGA repository, we selected data from 469 tumors classified as primary or metastatic skin cutaneous melanoma (SKCM). Using this database, we first divided the samples into tumors presenting high or low IRE1 activity. To do this, we used an IRE1-dependent gene expression signature previously described by Lhomond et al. in 2018 (139). This signature was identified using IRE1 dominant-negative (DN)-expressing U87 cells, an approach that entirely blocks all RNase outputs of this ER stress sensor (139). The gene expression signature obtained using this approach was processed through a Bioinforminer pipeline to increase its functional relevance. This analysis led to the identification of 38 (19 upregulated and 19 downregulated) IRE1-dependent hub genes (139). We used this 38 gene signature to be confronted with the transcriptome data from the SKCM-TCGA database.

To evaluate the presence of two populations displaying either high or low IRE1 activity, gene signature scores were quantified, and a quartile scoring method was used (139). Each gene of the IRE1 signature was assigned to a quartile-oriented gene score for each patient, based on its complete expression distribution in the specific cohort. Each gene of the signature was rated with 1 when the z-score was  $\leq Q1$  (the first quartile; the 25th item of ordered data); with 2 when the z-score was  $>Q1$  AND  $\leq Q2$  (median); with 3 when the z-score was  $>Q2$  AND  $< Q3$  (the third quartile; the 75th item of ordered data) and with 4 when the z-score was  $\geq Q3$ . After quartile ranking, each patient was assigned an IRE1 score based on the

average of gene scores for all the genes included in the signature. Patients were ordered based on their signature scores, generated in the R environment (R version 3.4.1 for windows).

The same protocol was applied to classify tumors from the TCGA database with either high or low RIDD and XBP1s activities. XBP1s-dependent or RIDD-dependent signatures were described in the same study previously mentioned (139). To identify the XBP1s-dependent signature, a transcriptome profile of U87 cells overexpressing IRE1 WT, which is known to increase IRE1 activity, and two mutants (P336L and A414T) that were identified in the same study as variants that exhibited high IRE1 RNase activity, was performed (139). Based on this analysis, the authors identified 40 genes upregulated in the WT, P336L, and A414T cells and correlated this regulation with high XBP1s levels (139). On the other hand, they determined a potential RIDD signature based on the ability of IRE1 to cleave mRNAs. First, an *in vitro* cleavage assay was performed (139). A group of 1141 mRNAs susceptible to be cleaved *in vitro* by IRE1 was identified from this screening. These genes were then intersected with the set of genes upregulated in IRE1-DN U87 cells. We used these signatures to stratify melanoma primary and metastatic tumors in IRE1, XBP1s, and RIDD high or low activity.

To evaluate the correlation of the expression levels of pro-metastatic genes with XBP1s and RIDD activity, XBP1s and RIDD signatures scores were overlapped to generate four cohorts: High\_XBP1s\_High\_RIDD, High\_XBP1s\_Low\_RIDD, Low\_XBP1s\_High\_RIDD, Low\_XBP1s\_Low\_RIDD. Then, the relative expression of pro-metastatic genes between the four cohorts was compared, and a heatmap was generated.

### 8.15. ***Statistical analysis.***

Statistical analysis was performed using the GraphPad software. Mann-Whitney test and Kruskal-Wallis test with Dunn's multiple comparison tests were used for non-Gaussian distributed data. Student's t-test was performed for unpaired or paired groups. When pertinent, two-way ANOVA with Bonferroni's multiple comparison test was executed. A p value of  $< 0.05$  was considered significant. In all plots p values are show as indicated: \*  $p < 0.05$ , \*\*  $p < 0.01$ , and \*\*\*  $p < 0.001$  and were considered significant. n.s: non-significant.

## 9. RESULTS.

### 9.1. *Activation status of IRE1 during metastasis in melanoma.*

In this thesis, we decided to study the involvement of IRE1 signaling in metastasis and we used metastatic cutaneous melanoma as a model. Melanoma begins with the transformation of melanocytes, pigment-producing cells. Although this cancer present a low incidence representing about 1% of all malignant skin tumors, cutaneous melanoma is the most aggressive and deadliest form of skin cancer (168). Therefore, the identification of molecular targets that regulate the metastatic process of melanoma tumors is crucial for the development of future therapies. As mentioned before, IRE1 has been linked to melanoma progression (111, 162, 169); however, the link with metastasis has not been described yet.

IRE1 activation and XBP1s expression have been associated with cancer progression in different cancer models and with several hallmarks of cancer (60). Also, in a previous work from our laboratory we found that IRE1 dimerization, an indirect measure of activation, is important for the increase of FLNA phosphorylation and the increase of cell migration (93). Thus, as part of the aim 1 we decided to determine if IRE1 activation was observed during the metastatic process. With this aim, we performed an *in vivo* assay by injecting the C57BL/6-derived B16F10 cell line, a highly metastatic and well-established model for the study of melanoma metastasis in C57BL/6 mice. The cells were injected subcutaneously, to form a primary tumor (300,000 cells), or intravenously in the tail vein to form metastatic foci at the lungs (200,000 cells). Next, we compared the expression of XBP1s, as a measure of IRE1 activity, in primary tumor and metastatic nodules in the lungs. For comparative purpose, adjacent non-tumoral tissue was also incorporated to the

analysis. After 21 days, all tissues were dissected, and total RNA was extracted for PCR analysis. As shown in Figure 10, quantification of XBP1s relative to total XBP1 showed increased levels of XBP1s in metastatic nodules compared with the normal tissue, and a slight increase compared with the primary tumor (Figure 10, right panel). This result support that an increase of IRE1/XBP1s signaling could be important in the development of metastasis. However, a proper comparison between the level of IRE1 activation in primary tumors and metastasis was not possible, since just one primary tumor was obtained. Also, this approach had several limitations. First, the metastatic tumors were not spontaneously derived from the primary tumor. In addition, the comparison between a primary tumor and metastatic lesions with different size indicate that the level of hypoxia in each tumor could be different, and it is known that hypoxia can induce ER stress and UPR activation (170). Finally, we dissected a fragment of the tumor tissue that could contain a mixt of melanoma cells and other types of cells present in the tumoral microenvironment. Thus, tumor cells from metastatic lesions generated spontaneously from a primary tumor with a similar size and sorted by a melanoma marker, could be the best alternative to evaluate activation of IRE1 signaling in metastatic cells and primary tumors compared to normal tissue.

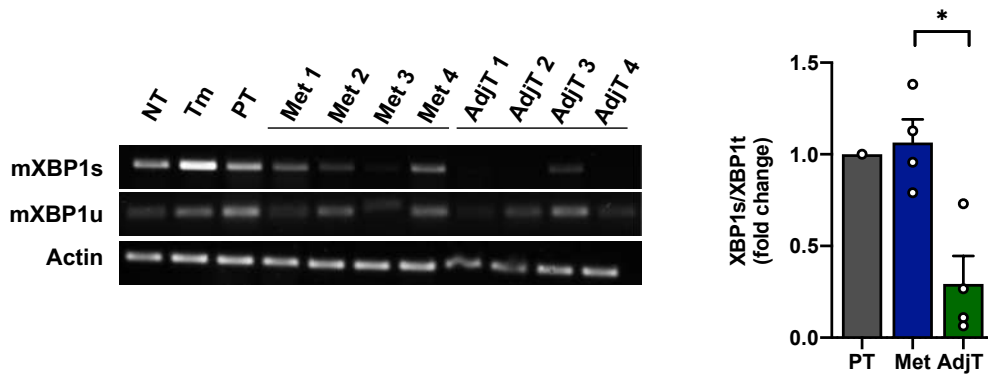


**Figure 10. IRE1 activation in mouse melanoma metastasis.**

For the formation of the primary tumor, B16F10 cells ( $3 \times 10^5$ ) were re-suspended in 100  $\mu$ L saline solution (0.9% NaCl) and injected subcutaneously into the flanks of C57BL/6 mice (8-12 weeks). The appearance of tumors was monitored by palpitation and tumor volume measurement, and at day 16 post-inoculation, the animals were sacrificed, and the tumor was extracted. For the generation of the metastatic nodules, B16F10 cells ( $2 \times 10^5$ ) were re-suspended in 300  $\mu$ L saline solution (0.9% NaCl) and injected intravenously into the tail vein of 8-12 weeks old C57BL/6 mice. On day 21, post-inoculation, lungs were collected. mRNA was extracted from primary tumor tissue, lung metastasis, and non-tumoral adjacent tissue, and IRE1 signaling was evaluated by measuring XBP1 mRNA splicing by PCR. Data represents 1 experiment and the average and standard error of four samples of metastatic tumors and four adjacent tissue samples. Results were statistically compared using two-tailed t-test. (\*:  $p < 0.05$ ). NT: non treated; Tm: treated with tunicamycin; PT: primary tumor; Met: metastatic tissue; AdjT: Tissue adjacent to the metastatic tumor.

Since metastatic cells located in the lungs presented an increased IRE1/XBP1s activity, we decided to evaluate the activation of IRE1 signaling in metastatic melanoma tumor by using transcriptome data from human tissues. A dataset of 469 tumors classified as primary or metastatic SKCM from the TCGA database was analyzed. Using this data, we first divided tumor samples into two groups presenting High or Low IRE1 activity. To do this, we used an IRE1 gene signature previously identified by Lhomond *et al.* in 2018 through the analysis of transcriptome data from U87 cells overexpressing a dominant-negative form of IRE1 (139). This signature is composed of 38 genes, which expression is either positively or negatively regulated by IRE1 activity. An IRE1 score was assigned for each patient, and patients were clustered according to IRE1 activity as IRE1\_High or IRE1\_Low (Figure 11A). To quantify gene signature scores, a z-scoring method was

used. Once we classified tumors as IRE1\_Low or IRE1\_High, we compared IRE1 activity between primary and metastatic tumors (Figure 12A). Interestingly, we observed a decreased activation of IRE1 signaling in metastatic samples compared to primary tumors (Figure 12A).

To further dissect the contribution of signals downstream of IRE1, we performed the same analysis using XBP1s (Figure 11B) and RIDD (Figure 11C) signatures previously published in 2018 (139). The authors determined a list of 40 genes as the hallmark of XBP1s expression by an approach previously explained in the material and methods section. On the other hand, in the same study, the RIDD signature was described by the intersection of the list of RNA cleaved by IRE1 in vitro and that of mRNA whose expression was upregulated in IRE1-DN cells under basal conditions (139).

Similar to the result observed with IRE1 activity, RIDD activity was significantly downregulated in human metastatic tumors compared to primary tumors (Figure 12B). Interestingly, the opposite result was observed for XBP1s dependent signature, where a small increase was observed in metastatic tumors compared to primary tumors (Figure 12C).

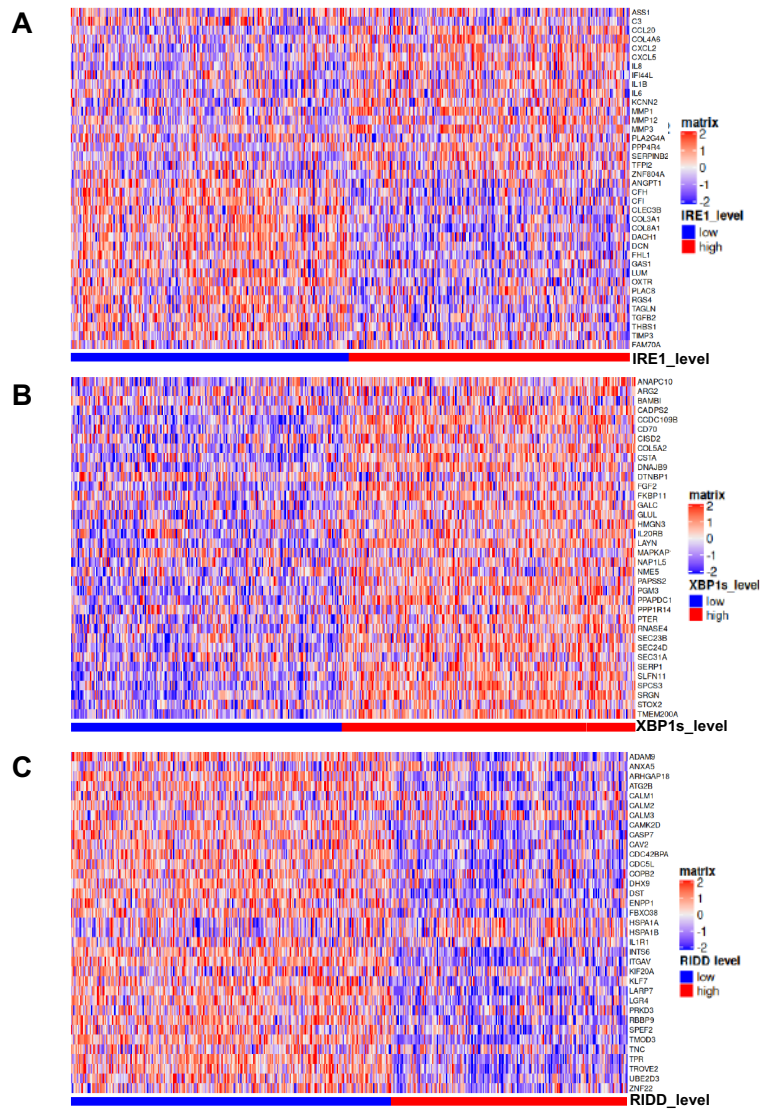


**Figure 11. IRE1 signaling in human melanoma tumors.**

Data from 469 melanoma tumors was evaluated in order to determine the IRE1 branch activation status. The clustering of patients using the dataset from the TCGA revealed the existence of two populations displaying either High or Low IRE1, RIDD, or XBP1s activity. IRE1 (A), XBP1s (B), and RIDD (C) activities were defined by a previously identified gene expression signature (139). To quantify gene signature scores in TCGA patient data, a quartile scoring method was used. Patients were ordered based on their signature scores generated in the R environment.



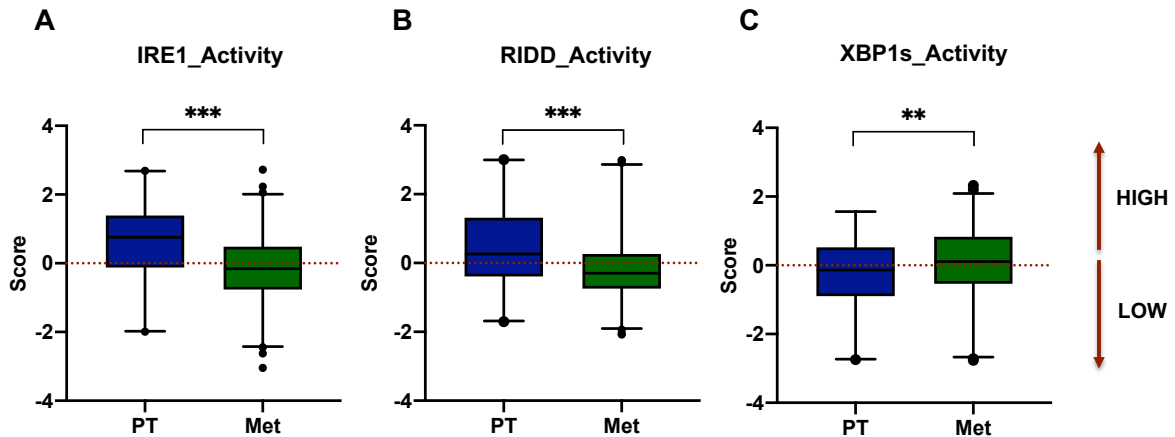


**Figure 12. IRE1 activation status in human melanoma metastasis.**

Data from 469 human melanoma tumors was evaluated to determine IRE1 branch activation status in metastatic tumors (N= 366) compared with primary tumors (N= 103). IRE1 (A), XBP1s (B), and RIDD (C) activities were defined by a previously identified gene expression signature (139). To quantify gene signature scores in TCGA patient data, a quartile scoring method was used. Each tumor sample was assigned an IRE1, XBP1s, or RIDD score based on the average of gene scores for all the genes included in the signature. Results were statistically compared using two-tailed t-test. (\*\*:  $p < 0.001$ , \*\*\*:  $p < 0.001$ ). PT: primary tumor; Met: metastasis.

IRE1 activity, particularly related to RIDD, appears to be decreased in the metastatic lesions, indicating that maybe the inhibition of this pathway could be a necessary process for developing melanoma metastasis. Considering that in highly metastatic cells, metastasis suppressors are usually downregulated in comparison with primary tumor cells, these results could suggest that IRE1 could be acting in melanoma as a suppressor of the metastatic process. Of note, this is contrary to what we initially hypothesized. Thus, a comprehensive analysis of all signaling outputs of IRE1 is necessary to understand the role of IRE1 signaling in the metastatic process.

## 9.2. *Role of IRE1 in migration and invasion of melanoma cells.*

As previously mentioned, IRE1 activity has been linked to cell migration and invasion of tumor cells; however, no evidence regarding its role in melanoma have been published. Previous work from our laboratory indicates that IRE1 can enhance

the migration of non-tumor cells through the specific regulation of the actin cytoskeleton remodeling (93). We found that IRE1 can act as a scaffold promoting FLNA phosphorylation at serine 2152 and potentiate cell migration, independently of its RNase activity. On the other hand, it is known that XBP1s can regulate the expression of genes associated with invasion and EMT and some reports indicate that RIDD may exhibit the opposite effect in certain tumors (102, 118, 119, 121, 130, 132, 139). Thus, the role of IRE1 activity in migration and invasion in cancer and its implication in the metastatic process is still controversial and more studies are needed. Based on our findings in non-tumor cells and the discovery of the IRE1/FLNA axis, we hypothesize that IRE1 could enhance cell migration of melanoma cells. Thus, as part of our specific aim 2, we decided to evaluate at different layers the possible contribution of IRE1 to the migration and invasion process in melanoma cell lines.

#### 9.2.1. ***Role of IRE1 in melanoma cell migration.***

As part of the specific aim 2, we explored the possible impact of IRE1 in melanoma cell migration. To address this question, we selected as cellular model one poorly metastatic and three highly metastatic human melanoma cell lines, described in Figure 10A. All the human cell lines selected contain the BRAF V600E mutation that is a common feature for melanoma (171, 172). For some complementary experiments we used the C57BL/6-derived B16F10 cell line, a highly metastatic and well-established model for the study of melanoma metastasis. Of note, this cell line does not contain BRAF mutation (Figure 10A) (173).

As part of the characterization of our cellular model, we determined the protein levels of IRE1 expression in the four human cell lines. We interestingly found that

the three metastatic cell lines A375-MA2, A2058, and SK-MEL5 expressed on average 3, 5, and 7 times more protein levels of IRE1 compare with the non-metastatic cell line A375, respectively (Figure 13B and 13C, left panel). Taking in consideration that one of the recently described IRE1 signaling that is associated to cell migration is through FLNA, we decided to also evaluate the levels of this protein in our model. We found that the expression levels of FLNA was increased in 1.7 and 2.6 times in the metastatic cell lines A375-MA2 and A2058, respectively, in comparison with the non-metastatic cell (A375) (Figure 13B and 13C, right panel). However, SK-MEL5, one of the metastatic cell lines and the one with the higher protein levels of IRE1, showed the lower expression of FLNA. These results suggest that the increase in FLNA expression in A375-MA2 and A2058, might not be related with the metastatic capacity.

Next, we evaluated IRE1 activity by measuring the percentage of XBP1 mRNA splicing by a PCR based assay under ER stress conditions induced with the N-Glycosylation inhibitor TM. We did not observe a basal activation of IRE1/XBP1s pathway in any of the cell lines. After ER stress, similar induction of XBP1 mRNA splicing was observed between all cell lines, with the exception of the SK-MEL5 that presented the lower percentage of XBP1 mRNA splicing (Figure 13D). The elevated levels of IRE1 might suggest that IRE1 signaling is relevant for the metastatic process; however, we were not able to corroborate differences in IRE1/XBP1s signaling, and probably a more sensitive method such as Real time-PCR is needed to detect basal activation of this signaling in adherent cells.

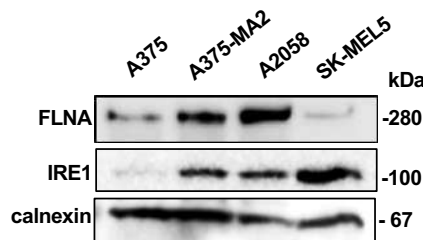
Once our model was characterized regarding IRE1 expression levels and activation status, we evaluated transmigration using Boyden chambers, a classical experiment to determine migratory cell capacity (174). These assays were performed in the four human melanoma cell lines previously described, and some complementary experiments were done with the B16F10 mouse cells.

The first step was to establish the best promigratory stimulus for these melanoma cell lines in the transmigration assays. We tested DMEM with 10% of FBS, a widely used stimulus for cell migration, and conditioned media from NIH 3T3 fibroblast cells grown in DMEM medium containing 10% FBS for 24 hours, as possible chemo-attractors (Figure 13, left panel) (175, 176). The number of cells seeded and the timing were selected based on previous works with these cell lines (177). As shown in Figure 14, right panel, there was an increase of 6 (A375-MA2), 3 (A2058), and 7 (SK-MEL5) times in the number of migrating cells towards the NIH-CM in comparison with the FBS migration stimulus. Remarkably, the non-metastatic cells (A375) had a similar number of migrating cells with both stimuli presenting a lower migratory capacity compared to metastatic cell lines. NIH-CM was also the best chemo-attractant for transmigration assays in the mouse metastatic cell line B16F10 (Supplementary Figure 1). Based on these results, we decided to use for further experiments the NIH-CM as the chemo-attractant for all the melanoma cell lines.

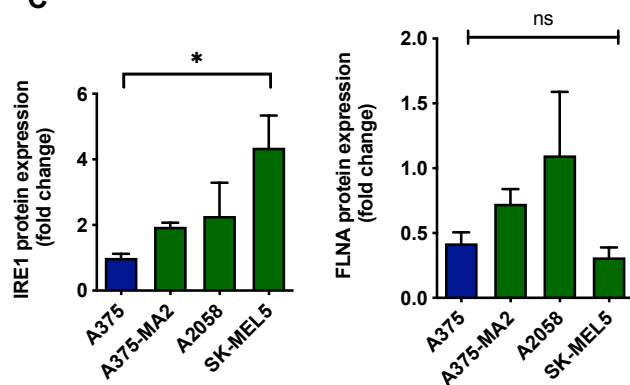
**A**

Cell line	Origin	Localization of the tumor	BRAF mutation status	Metastatic potential
A375	Human	Primary solid tumor.	V600E	Low
A375-MA2	Human	Metastatic cell line derived using an in vivo selection process of highly metastatic cells from a population of poorly metastatic tumor cells, A375.	V600E	High
A2058	Human	Derived from metastatic site: lymph node.	V600E	High
SK-MEL5	Human	Derived from metastatic site: axillary node.	V600E	High
B16F10	Mouse	Metastatic cell line derived using an in vivo selection process of highly metastatic cells from a population of poorly metastatic tumor cells, B16F0.	—	High

**B**



**C**



**D**

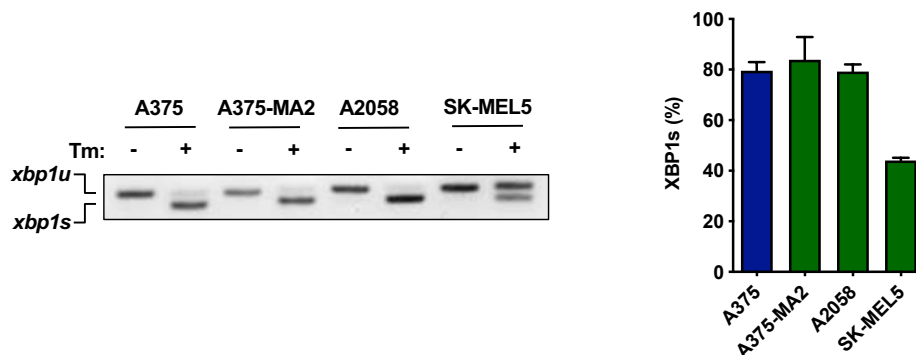


**Figure 13. Characterization of human melanoma cell lines.**

(A) Main characteristics of four human melanoma cell lines were described. (B) IRE1 and FLNA of A375, A375-MA2, A2058 and SK-MEL5 levels were evaluated by western blot using specific antibodies. (C) IRE1 (Left panel) and FLNA (Right panel) protein levels were quantified by scanning densitometry and normalized to the levels of the housekeeping gene. Data represent the mean  $\pm$  s.e.m. of 3 independent experiments. Results were statistically compared using a two-tailed t-test. (ns: not statistically significant, \*:  $p < 0.05$ ). (D) Left panel: A375, A375-MA2, A2058, and SK-MEL5 cells were treated with 1  $\mu$ g/mL of Tm for 6h, and then XBP1 mRNA splicing was evaluated by PCR. PCR fragments corresponding to the XBP1u or XBP1s forms of XBP1 mRNA are indicated. Right panel: the percentage of XBP1 mRNA splicing was calculated after densitometric analysis of the XBP1u and XBP1s-related PCR products to quantify the splicing percentage each time point.

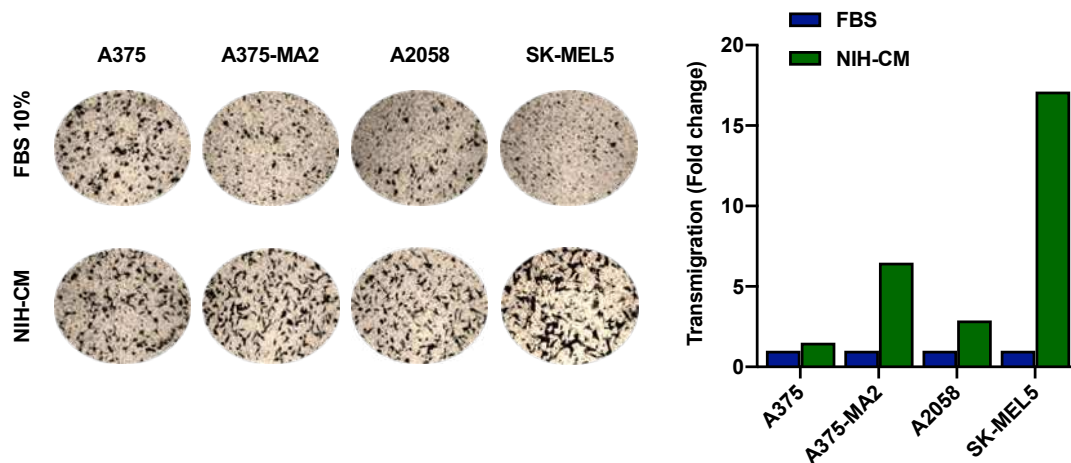


**Figure 14. Standardization of the transmigration assay.**

**Left panel:** Human melanoma cells ( $5 \times 10^4$ ) were plated on non-coated transwell plates. Transmigration was assessed in the presence of 10% of fetal bovine serum (FBS), or NIH 3T3 conditioned medium (NIH-CM). After 4h, cells that migrated to the lower side of the Boyden chamber were stained with crystal violet, and images were taken. **Right panel:** The number of cells that migrated was counted using the ImageJ software. Data represent 1 experiment.

Once the experimental conditions were established, we decided to use a siRNA to ablate IRE1 expression and evaluate the impact on cell migration in human melanoma cells. We validated our experimental approach transfecting siRNAs targeting IRE1 for 48 h and obtained a significant reduction in the protein levels of IRE1 in the four cell lines upon siRNA transfection (Figure 15A). We then evaluated the effect of the deficiency of IRE1 expression in the migratory capacity of the human melanoma cell lines. Unexpectedly, we observed that IRE1 silencing was associated with an increase in cell migration capacity compared with cells transfected with the control siRNA. Of note, this was only observed in the metastatic melanoma cells, since no changes in the migratory capacity was detected in the non-metastatic melanoma cell line A375 (Figure 15B). These results suggest that, IRE1 could be acting as a suppressor of migration in melanoma cells, specifically in cells with high metastatic capacity.

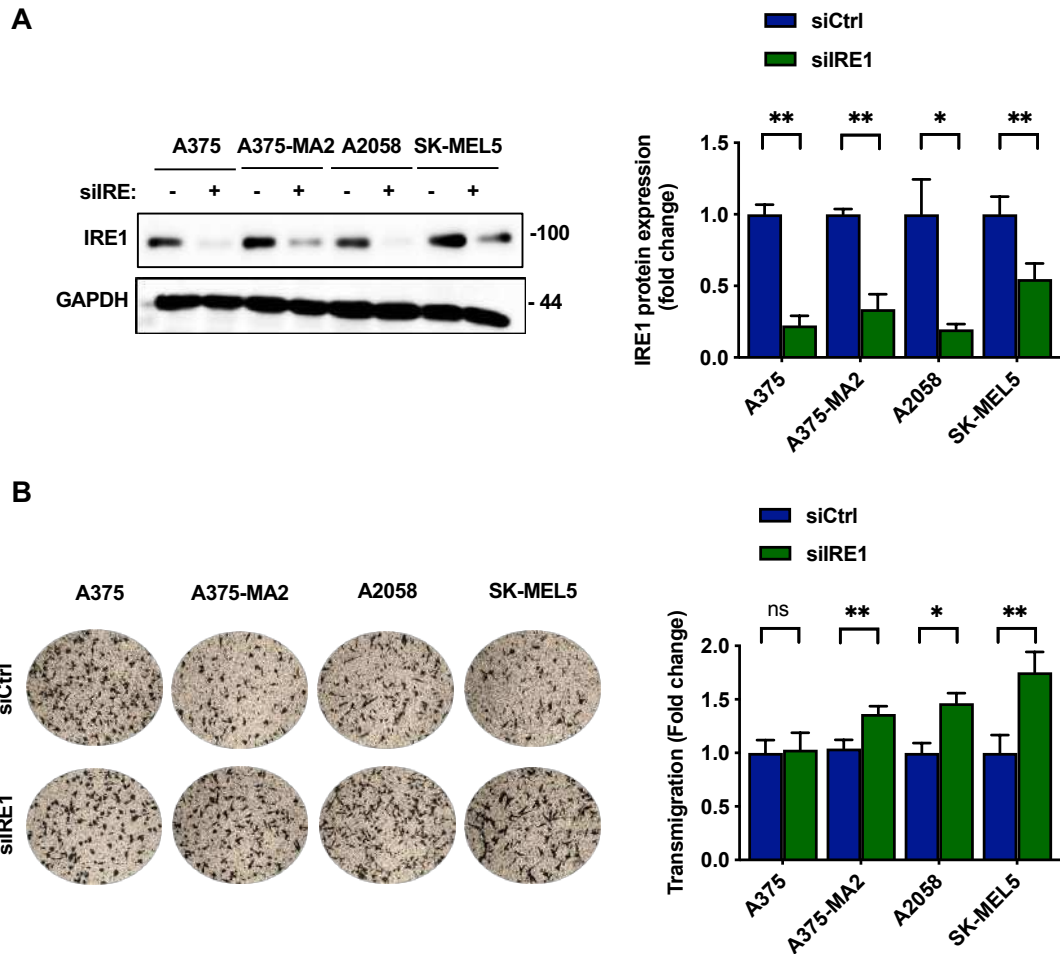


**Figure 15. IRE1 deficiency increases cell migration in human metastatic melanoma cells.**

**(A) Left panel:** Human melanoma cells were transiently transfected with 10 pmol of siRNA Control (siCtrl) or a siRNA against IRE1 (siIRE1). After 48h of the transfection, total protein extracts were analyzed by western blot using specific antibodies. **Right panel:** IRE1 protein levels were quantified by scanning densitometry and normalized to the levels of the housekeeping gene. Data represent the mean  $\pm$  s.e.m of 3 independent experiments. Results were statistically compared using a two-tailed t-test. **(B) Left panel:** After 48h,  $5 \times 10^4$  cells transfected with siCtrl or siIRE1 were seeded on transwell plates, and transmigration was assessed. Transmigration was performed in the presence of conditioned medium of NIH-3T3. After 4h, cells that migrated to the lower side were stained with crystal violet. Images of the lower side of the transwell were taken. **Right panel:** The number of cells that migrated was counted using the ImageJ software. Data represent the mean  $\pm$  s.e.m of at least 4 independent experiments. Results were statistically compared using a two-tailed t-test. (ns: not statistically significant, \*:  $p < 0.05$ , \*\*:  $p < 0.01$ ).

We then decided to use a genetic approach to ablate IRE1 gene with the aim to corroborate the impact of this ER stress sensor in cell migration of melanoma cells. For this purpose, we selected the human metastatic cell line A375-MA2 because (i) this cell line was obtained through an *in vivo* selection process from a

population of the poorly metastatic cell line A375, (ii) using an experimental metastasis approach with all metastatic cell lines we were only able to observe metastatic lesions with the injection of A375-MA2 cells (Supplementary figure 2) (178). Therefore, targeting IRE1 expression in A375-MA2 cells will allow us to evaluate the relevance of IRE1 expression in cell migration, invasion and metastasis *in vivo*.

The procedure to obtain IRE1KO cells is described in Figure 7, using the double nickase method of CRISPR/Cas9 technology. After plasmid transfections and the selection with puromycin, we obtained a pool of cells transfected with the IRE1KO plasmid or Control (Figure 7). In order to corroborate the efficiency of this genetic approach, we decided to evaluate IRE1 activity in these cells measuring the level of XBP1 mRNA splicing under ER stress induced with TM. We observed that the pool of cells transfected with the plasmids containing the single guide RNAs (sgRNAs) that target IRE1 gene showed a decrease of ~40% in the XBP1 mRNA splicing compared with the cells transfected with the Control, suggesting that a subpopulation of cells was deficient for IRE1 (Figure 16A). We decided to isolate individual clones of IRE1KO and Control cells using the limiting dilution approach. We were able to obtain eleven IRE1KO clones (Figure 16B) that were further validated using XBP1 mRNA splicing as a measurement of IRE1 activity. Seven clones obtained from the pool of cells transfected with the Control plasmid were also evaluated. Remarkably, six IRE1KO clones showed no IRE1 activity under the presence of TM (Figure 16C). We decided then to use two Control clones, C5 and C7 (renamed as C1 and C2, respectively) and three IRE1-deficient clones, KO4, KO5, and KO16 (renamed as KO1, KO2, and KO3, respectively) for the next experiments. To complement some experiments, we also generated IRE1-deficient



B16F10 cells using the same protocol. However, in this case, we did not isolate individual clones since the pool of IRE1KO cells showed a total reduction of IRE1 expression and activity (Supplementary Figure 3A).

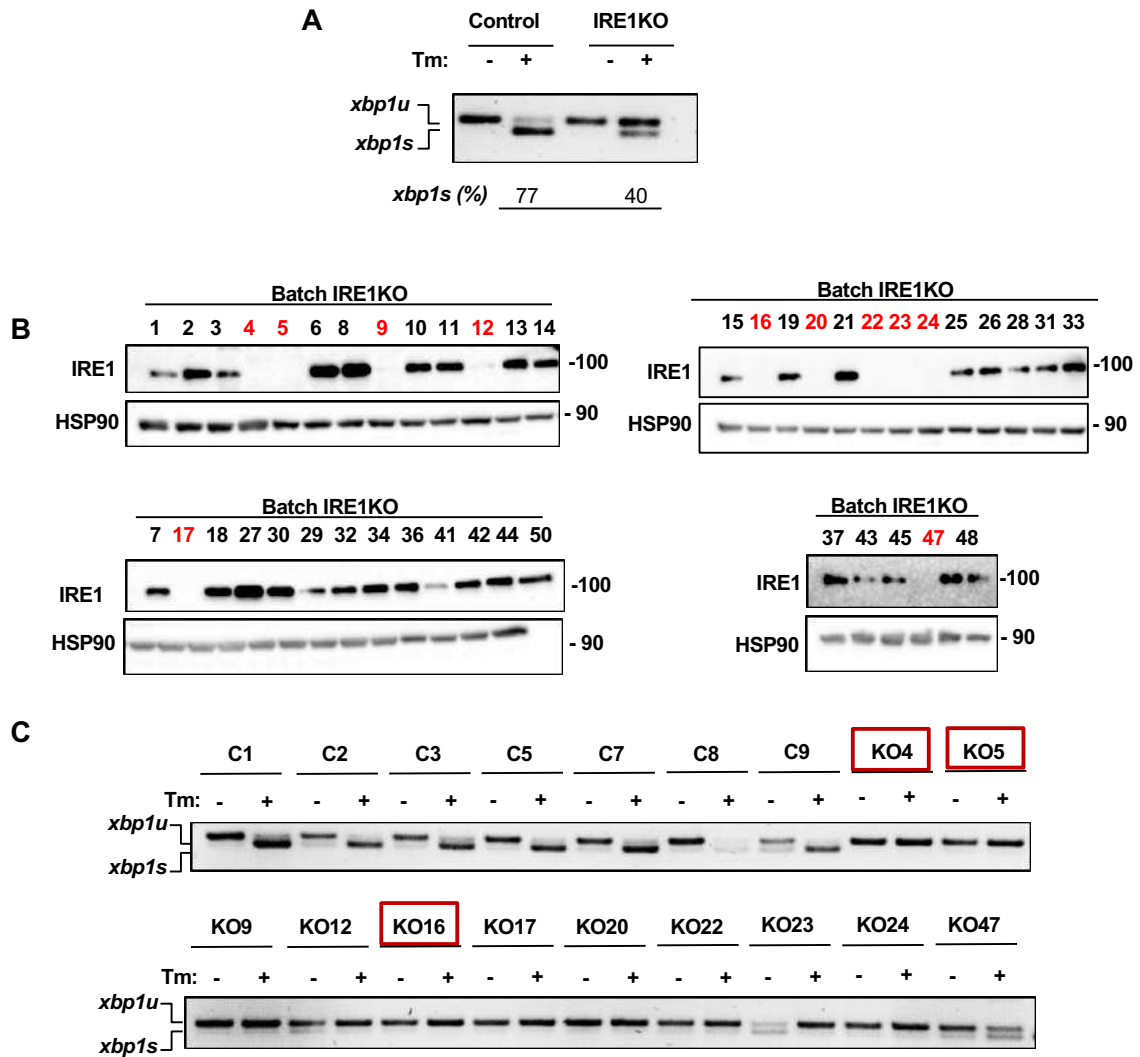


**Figure 16. Validation of the generation of IRE1 KO in A375-MA2 cells.**

(A) IRE1 activity was evaluated in the pool of cells obtained after transfection with plasmids containing sgRNAs Control or IRE1, and selection with puromycin. Cells were treated with 1  $\mu\text{g}/\text{mL}$  of Tm for 6 h, and then XBP1 mRNA splicing was evaluated by RT-PCR. PCR fragments corresponding to the XBP1u or XBP1s forms of XBP1 mRNA are indicated. The percentage of XBP1 mRNA splicing was calculated after the densitometric analysis of the XBP-1u and XBP1s-related PCR products to quantify the splicing percentage in each condition. (B) The level of IRE1 protein was determined in total protein extracts by western blot in the clones obtained after the limiting dilutions performed with the pool of cells IRE1KO mentioned in A. (C) IRE1 activity was determined in seven clones transfected with sgRNA Control, and clones transfected with sgRNAs for IRE1, and that did not present IRE1 expression in B. To evaluate the levels of XBP1 splicing, the same protocol described in A was used. Data represents 1 experiment.

As part of the characterization of the clones, we performed a WST-1 proliferation assay based on the cleavage of the tetrazolium salts to formazan by cellular mitochondrial dehydrogenase, that will indicate us the metabolic activity in live cells and indirectly the proliferation rate (179). For this purpose, we seeded 2000 cells in four 96 well plates and the number of cells was determined for four consecutive days in a microplate reader according to the manufacturer's instructions. Importantly, a similar proliferation capacity was observed between Control and IRE1 KO clones of A375-MA2 cells (Figure 17B). The same result was observed in B16F10 using a different protocol based on daily nuclei count the ArrayScan XTI Live High Content Platform (Supplementary Figure 3B). These results suggest that IRE1 does not promote proliferation of melanoma cells, contrary to what has been described for other types of cancer (96, 97).

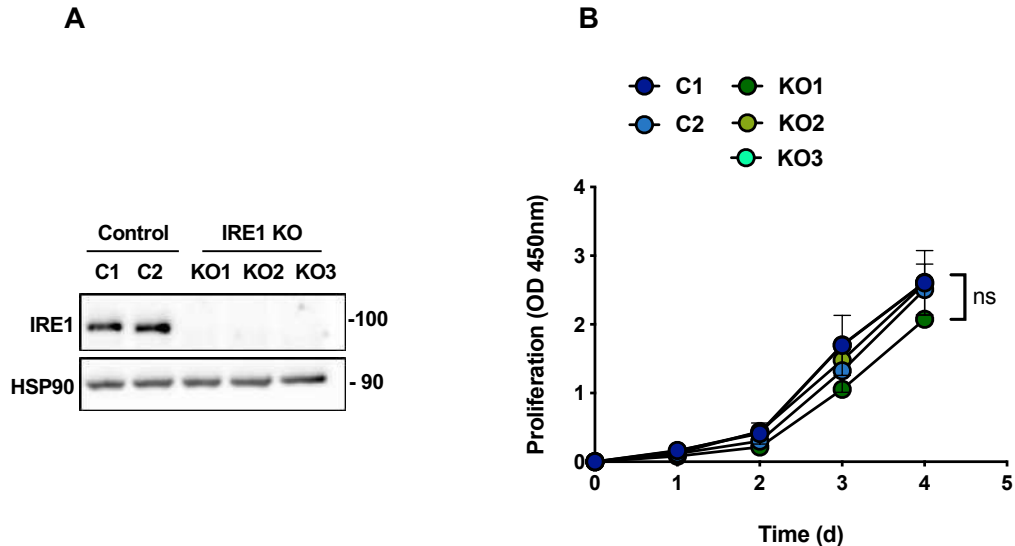


**Figure 17. Characterization the of IRE1 KO A375-MA2 clones selected.**

IRE1KO A375-MA2 clones were generated using CRISPR/Cas9 technology. **(A)** The levels of IRE1 in Control and IRE1KO clones were evaluated using total protein extracts by western blot. **(B)** The proliferation of Control and IRE1KO clones was evaluated by using the WST-1 assay. Two thousand cells were seeded in four 96 well plates, one for each day, and the number of cells was determined in four consecutive days in a microplate reader. The assay was performed according to the manufacturer's protocols instructions. Data represent the mean  $\pm$  s.e.m of 3 independent experiments. Results were statistically compared using two-way ANOVA followed by Bonferroni's multiple comparisons test. (ns: not statistically significant).

Once characterized the IREKO and Control clones, we decided to evaluate the effect of IRE1 deficiency in metastatic melanoma cell migration using the Boyden chamber assay. Control and IRE1KO A375-MA2 clones were seeded in the chambers and 4 hours later cells that transmigrated to the lower compartment of the chamber were fixed and counted. We observed an increased cell migration capacity in IRE1 deficient melanoma cells (Figure 18A), corroborating our previous results using siRNAs (Figure 15). Individual analysis of the migratory behavior of each clone showed that the three IRE1KO clones had an increased migratory capacity compared to Controls (Figure 18B, left panel). Also, when analyzing the Control clones and the IRE1KO clones as groups, we observed that IRE1 deficiency increased cell migration by an average of 40% (Figure 18B, right panel). Since the three IRE1KO clones had similar behavior, clones IRE1KO1 and KO2 were selected to further experiments. These experimental approaches showed us that IRE1 could be acting as a suppressor of cell migration in melanoma cell lines with high metastatic capacity, which is contrary to our initial hypothesis.

To test if this effects in cell migration could also be observed in mouse melanoma cells, we evaluated the effect of IRE1 deficiency in cell migration in B16F10 cells. After performing the transmigration assay, we found not significant differences in the cell migration of IRE1KO cells compared with Control (Supplementary Figure 4). Of note, the transmigration assays with the B16F10 cells were performed using Boyden chambers coated with fibronectin in the bottom, unlike the ones performed with the human cell lines. Remarkably, it was shown recently that fibronectin mRNA is enhanced by IRE1 through XBP1s (180). Thus, using fibronectin might not be the best ECM to perform *in vitro* experiments. Futures migration experiments with B16F10 need to be done using the same conditions that

the assays performed in human cell lines. Also, it is important to mention that the human and mouse melanoma cells used in this thesis differ in the presence of BRAF mutation, a common and relevant mutation in the progression of melanoma, a factor that was previously described as an inducer of ER stress in melanoma cells (113).

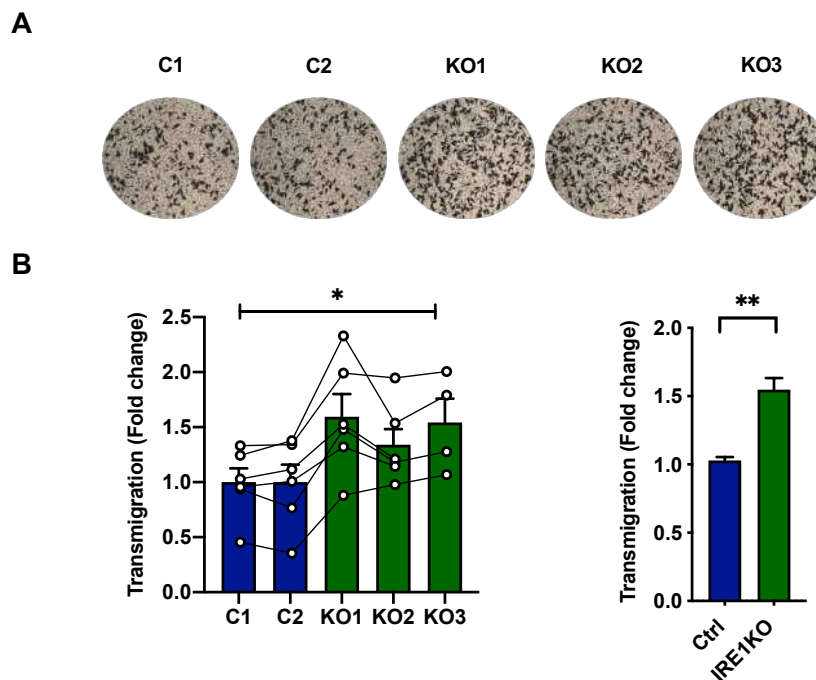


**Figure 18. IRE1 deficiency increases cell migration in human metastatic melanoma cells.**

**(A)** Cells from Control and IRE1KO A375-MA2 clones ( $5 \times 10^4$ ) were seeded on transwell plates, and transmigration was assessed. Transmigration was performed in the presence of NIH-CM. After 4h, cells that migrated to the lower side were stained with crystal violet. Images of the lower side of the transwell were taken. **(B)** The number of cells that migrated was counted using the ImageJ software. **Left panel:** Data is represented as fold change migration of individual clones using C1 as reference. Each connector line represents an experimental replica. **Right panel:** Data is represented as groups using the Control clone group as reference. Data represent the mean  $\pm$  s.e.m of at least 4 independent experiments. Results were statistically compared using one-way ANOVA using followed by Dunn's multiple comparison test (Left panel) or two-tailed t-test (Right panel). (\*:  $p < 0.05$ , \*\*:  $p < 0.01$ ).

Altogether, our results indicate that the ablation of IRE1 expression using siRNA or CRISPR/Cas9 approaches led to a significant increase in cell migratory capacity of human metastatic melanoma cell lines. This evidence suggests that IRE1 may be an important suppressor of cell migration in metastatic cells, since the migration of the non-metastatic cells A375 did not rely on IRE1 expression.

### 9.2.2. *Regulation of actin cytoskeleton organization by IRE1 in metastatic melanoma cells.*

Actin filaments are the primary cytoskeletal component involved in cell motility. During migration, F-actin reorganizes toward the cortical area and extends different protrusions, including membrane ruffling, lamellipodia, filopodia, and invadopodia (181). As mentioned before, we previously demonstrated that IRE1, through the engagement of FLNA signaling, enhance actin cytoskeleton remodeling and increases cell migration of fibroblasts (93). Thus, we decided to evaluate if the changes observed in IRE1-deficient melanoma cells can be associated to an alteration of the actin cytoskeleton dynamics. Control and IRE1KO A375-MA2 cells were plated on coverslips for 48 hours, fixed, stained with phalloidin-coupled to FITC and visualized using a Leica SP8 confocal microscope. Stained cells showed a strong signal of polymerized actin, showing structures resembling stress fibers, lamellipodia and filopodia (Figure 19A, left panel). We decided to analyze the effect in F-actin distribution upon deficiency of IRE1 expression using the ImageJ software to evaluate fluorescence intensity of FITC from the borders to the center of the cell. Using this approach, we did not observed changes associated to IRE1 deficiency in the distribution of the actin cytoskeleton in this human metastatic melanoma cells (Figure 19B), suggesting that at least in basal conditions IRE1 signaling could not play a relevant role in actin cytoskeleton dynamics during cell migration.

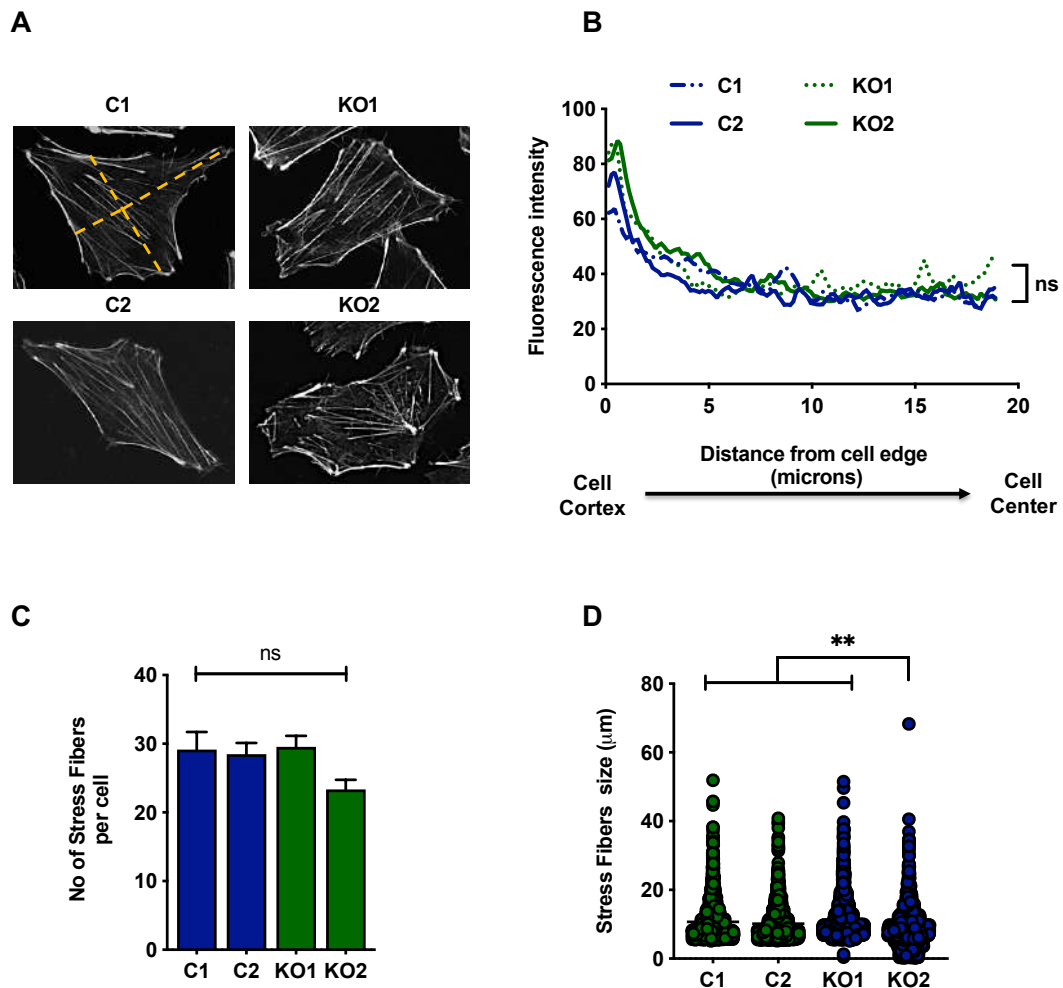


**Figure 19. Actin cytoskeleton is not affected by IRE1 deficiency in MA2-A375 cells.**

(A) Controls and IRE1KO A375-MA2 clones were plated onto non-coated slides. After 48 h, cells were fixed and stained with phalloidin coupled to FITC. Pictures were taken using confocal microscopy. (B) Using the ImageJ software, fluorescence intensity was determined from the border to the center of the cell to analyze actin cytoskeleton distribution. Representative lines of the analysis are shown in panel A. The number of Stress Fibers per cell (C) and the Stress fibers size (D) was determined using the plugin Filament detector of the ImageJ software. Data represent the mean  $\pm$  s.e.m of 3 independent experiments. Results were statistically compared using one-way ANOVA using followed by Dunn's multiple comparison test. (ns: not statistically significant, \*\*:  $p < 0.01$ ).

Visualization of actin cytoskeleton in human melanoma cells revealed a high amount of stress fibers, that constitute essential elements that act as a contractile apparatus, and together with focal adhesions, allow cell attachment to the extracellular matrix through the plasma membrane and promote cell migration (182). Using the plugin Filament detector of the ImageJ software, we determine the number of stress fibers and the stress fibers size. As observed in Figure 19C, targeting IRE1 expression did not present an effect on the number of stress fibers. However, we found a decrease in the stress fibers length in one of the IRE1KO clone (clone KO2) (Figure 19D). Of note, this clone showed less increase in cell migration in the Boyden chamber assays compared to the others IRE1KO clones (Figure 18B), evidencing some clonal effects of the selection process of CRISPR/Cas9. Based on this evidence, we hypothesize that this effect in the size of stress fibers is IRE1-independent and that can be due to a clonal effect. This result can explain why this clone has a lower migratory capacity compared with the other IRE1KO clones.

To further characterize the actin cytoskeleton dynamics, we evaluated the amount of Filopodia, the main protrusions formed during the migration cycle (183). Using the FiloQuant plugin of the ImageJ software, we were able to segment and analyze the number of filopodia per cell and filopodia size. This analysis revealed that IRE1-deficient human metastatic melanoma cells have an equivalent number and size of filopodia per cell compare with Controls (Figure 20A and 20B). This indicated that IRE1 do not impact in the regulation of actin cytoskeleton in human metastatic melanoma cells in basal conditions.

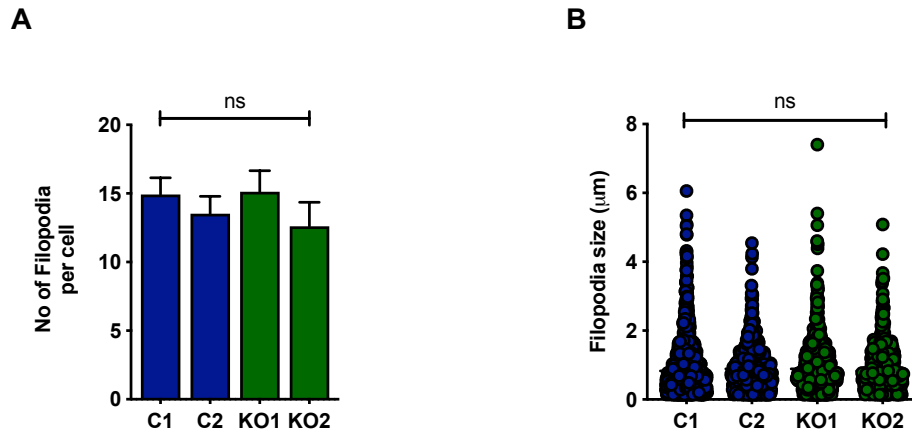


**Figure 20. Filopodia formation is independent of IRE1 expression.**

Controls and IRE1KO A375-MA2 clones were plated onto non-coated slides. After 48 h, cells were fixed and stained with phalloidin coupled to FITC. Pictures were taken using confocal microscopy. The number of Filopodia per cell (**A**) and Filopodia size (**B**) was determined using the plugin FiloQuant of the ImageJ software. Data represent the mean  $\pm$  s.e.m of 3 independent experiments. Results were statistically compared using one-way ANOVA followed by Dunn's multiple comparison test. (ns: not statistically significant).

In order to corroborate this phenotype, we also evaluated filopodia formation in the mouse metastatic melanoma cell line B16F10. When we compared WT and Control cells with IRE1KO B16F10 cells, we observed a tendency to increase the number filopodia per cell (Supplementary Figure 5A), with no changes in the size (Supplementary Figure 5B). We also evaluated actin dynamics using a fluorescent protein to visualize polymerized actin in real-time called Lifeact (184). We transiently transfected Lifeact in WT, Control and IRE1KO B16F10 cells, seeded on coverslips coated with 2  $\mu$ g/mL of fibronectin and recorded every 5 seconds for 10 min using time-lapse confocal microscopy. As observed in Supplementary Figure 6A, transfected cells showed structures resembling stress fibers, lamellipodia and filopodia. To analyze and quantify actin dynamics, we used ADAPT software to evaluate the changes in protrusion, and retraction velocities based on changes in cortical actin. We observed that B16F10 cells deficient of IRE1 presented a more dynamic formation of protrusions (Supplementary Figure 6B) and retractions



(Supplementary Figure 6D). Mean protrusion and retraction velocities indicate the same results (Supplementary Figure 6C and E). Of note, all the experiments with B16F10 cells were performed in fibronectin-coated plates that could affect the results based in our previous results (Supplementary Figure 4) and the fact that IRE1 can affect fibronectin expression (180).

Altogether, these results suggest that in human melanoma cell lines, actin cytoskeleton is not regulated by IRE1 and that the increased migratory capacity in IRE1-deficient cells can be independent of the capacity of actin reorganization. Nevertheless, in the mouse metastatic B16F10 cell line a possible contribution of IRE1 expression in the formation of protrusions can be observed, this will need further analysis.

### **9.2.3. Regulation of cell adhesion by IRE1 in metastatic melanoma cells.**

Cell adhesion is another essential cellular response involved in physiological processes like cell migration, as well as in the pathology of neoplastic transformation and metastasis (185, 186). Thus, once we determined that the regulation of cell migration by IRE1 in human melanoma cells was independent of the actin cytoskeleton at least in basal conditions, we decided to explore its possible role in cell adhesion. With this aim, we first performed cell adhesion assays in Control and IRE1KO A375-MA2 cells plated onto fibronectin-coated plates (2 $\mu$ g/ml) at different times, followed by staining with crystal violet. Using this approach, we observed that A375-MA2 IRE1KO cells had similar adhesion capacity that Control cells over fibronectin (Figure 21A). Next, we evaluate the effect of IRE1 expression in the adhesion of this metastatic melanoma cells onto Matrigel, a complex basement

membrane preparation rich in ECM proteins as collagen, laminin, heparan sulfate proteoglycans and some growth factors that resembles the extracellular matrix found in tumor microenvironment. Cell adhesion capacity of IRE1KO and Control cells were seeded onto Matrigel (500 ng/ml) coated plates was virtually the same regarding IRE1 deficiency. Nevertheless, we found significant differences in cell adhesion between the clones that were independent of IRE1 expression, since clones C2 and KO1 were the ones with the higher percentage of adhesion (Figure 21B). These results indicate that the regulation of cell migration by IRE1 in human metastatic melanoma cells appears to be independent of the capacity to attach to extracellular matrixes.

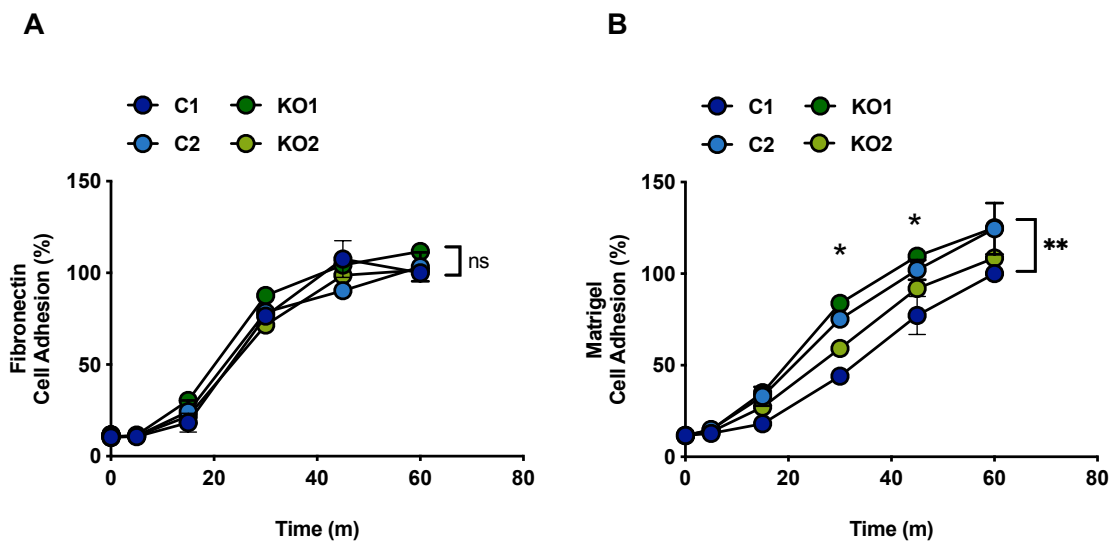


**Figure 21. Cell adhesion capacity to Fibronectin and Matrigel is independent of IRE1 expression in A375-MA2 cells.**

Control and IRE1 A375-MA2 clones were maintained in suspension and allowed to attach to fibronectin (2  $\mu\text{g/ml}$ ) (**A**) or matrigel (500 ng/ml) (**B**) coated plates for different times. Adherent cells were stained with crystal violet. Dye was extracted with methanol and the total absorbance was measured. Data represents the mean  $\pm$  s.e.m of 3 independent experiments. Results were statistically compared using two-way ANOVA followed by Bonferroni's multiple comparisons test. (ns: not statistically significant, \*\*:  $p < 0.01$ ).

#### 9.2.4. *Effect of IRE1 deficiency in cell invasion of human metastatic melanoma cells.*

Aberrant cell migration and invasion are two common cellular processes in metastatic cells (30). Particularly, invasion allows tumor cells to penetrate the surrounding tissues through the degradation of the extracellular matrix and pass through the basement membrane, enabling cell migration (187). Considering that IRE1 deficiency increase cell migration in human metastatic melanoma cells, we proposed to determine if IRE1 could also regulate cell invasion. To that end, we performed invasion experiments with the four human melanoma cell lines transfected with siRNAs targeting IRE1 expression and Control siRNA (Figure 13A). To perform the invasion assays, cells were seeded on Boyden chambers coated with Matrigel (200 ng/ml) in the upper compartment, and NIH-CM was used as a chemoattractant to allow cells to invade (Figure 22, left panel) (177).

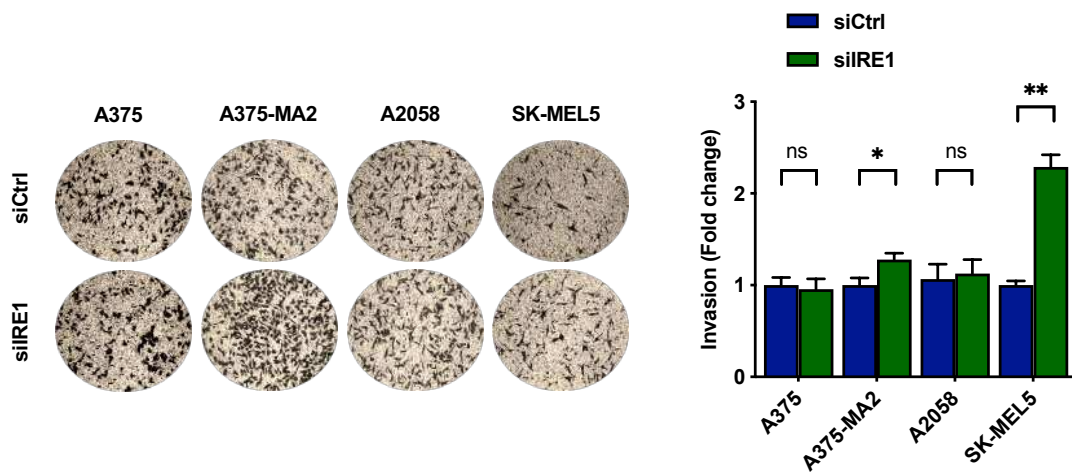


**Figure 22. Silencing of IRE1 increases cell invasion in human metastatic melanoma cells.**

Human melanoma cells were transiently transfected with siRNA Control (siCtrl) or siRNA against IRE1 (siIRE1). **Left panel:** After 48h,  $3 \times 10^4$  cells transfected with siCtrl or siIRE1 were seeded on Matrigel-coated (200 ng/ml) transwell plates, and invasion was assessed. The invasion was evaluated in the presence of NIH-CM. After 24 h, cells that invaded to the lower side were stained with crystal violet. Images of the lower side of the transwell were taken. **Right panel:** The number of cells that invaded was counted using the ImageJ software. Data represent the mean  $\pm$  s.e.m of at least 4 independent experiments. Results were statistically compared using a two-tailed t-test. (ns: not statistically significant, \*:  $p < 0.05$ , \*\*:  $p < 0.01$ ).

Similar to the phenotype observed in cell migration, silencing IRE1 expression in two metastatic cell lines, A375-MA2 and SK-MEL5, showed an increase in the number of cells that invaded to the lower compartment and no effect was observed in the non-metastatic cell line A375 nor the A2058 metastatic cell line (Figure 22, right panel)

We then corroborated these findings in A375-MA2 Control and IRE1KO clones. As observed in Figure 23, IRE1KO clones showed an increase in cell invasion compared with the controls (Figure 23A). However, analyzing cell invasion capacity between individual clones, a significant increase was only found in the KO1 clone compared with both controls. Nevertheless, in each biological replicate, a trend can be observed where IRE1-deficient cells presented higher cell migration in comparison with controls (Figure 23B, left panel). Analysis of control and IRE1KO clones as two independent groups showed a significant increase in the invasion capacity of cells deficient of IRE1 (Figure 23B, right panel).

These results indicate that IRE1 could be a regulator of melanoma cell invasion in metastatic cells. However, further experiments are needed to establish if IRE1 can directly regulate cell invasion through other mechanism such as invadopodia formation, a major invasive structure, and ECM degradation mechanism (48).

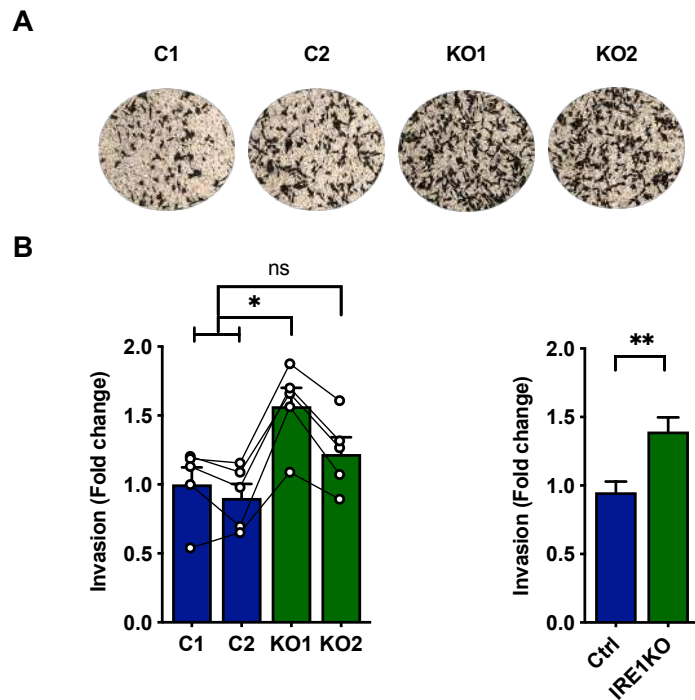


**Figure 23. IRE1 deficiency increases cell invasion in human metastatic melanoma cells.**

**(A)** Cells from Control and IRE1KO A375-MA2 clones ( $3 \times 10^4$ ) were seeded on Matrigel-coated (200 ng/ml) transwell plates, and invasion was assessed. The invasion was evaluated in the presence of NIH-CM. After 24 h, cells that invaded to the lower side were stained with crystal violet. Images of the lower side of the transwell were taken. **(B)** The number of cells that invaded was counted using the ImageJ software. Data are represented as fold change migration of individual clones using C1 as reference (**Left panel**) or groups using Control clones group as reference (**Right panel**). Data represent the mean  $\pm$  s.e.m of at least 4 independent experiments. Results were statistically compared using one-way ANOVA followed by Dunn's multiple comparison test (Left panel) or two-tailed t-test (Right panel). (ns: not statistically significant, \*:  $p < 0.05$ , \*\*:  $p < 0.01$ ).

### 9.3. ***Role of the IRE1/FLNA pathway in the regulation of cell migration and invasion in melanoma.***

The results described until now indicate that IRE1 could act as a suppressor of cell migration and invasion in melanoma cells with high metastatic capacities. Previous data from our laboratory revealed an interaction between IRE1 and FLNA that enhance FLNA phosphorylation in S2152 and promote actin cytoskeleton dynamics, enhancing migration in non-tumor cells (93). Although FLNA is a protein that has been extensively recognized as an enhancer of cell migration, some functions as a suppressor of cell invasion and metastasis have been described (160, 188) Then, as part of the specific aim 3 we explored the possibility that IRE1 could be suppressing cell migration in melanoma cells through FLNA regulation.

To that end, we first evaluated the effect of FLNA silencing in cell migration by transfecting with 10 pmol or 30 pmol of siRNA target for FLNA in A375-MA2 parental cells. Using, this strategy we observed a higher decrease in FLNA protein levels using the maximum concentration of siRNA (Figure 24A). Then, we evaluated transmigration capacity in parental A375-MA2 transfected with siRNA for FLNA or control siRNA (30 pmol). No significant differences were obtained between FLNA-deficient cells and the Control; nevertheless, a high variation of data was observed with a trend to increase the migratory capacity in the cells transfected with siFLNA (Figure 24B). These results suggest that at least in our model, regulation of cell migration by IRE1 could be independent of FLNA, since targeting this protein does not show significant effects on cell migration.

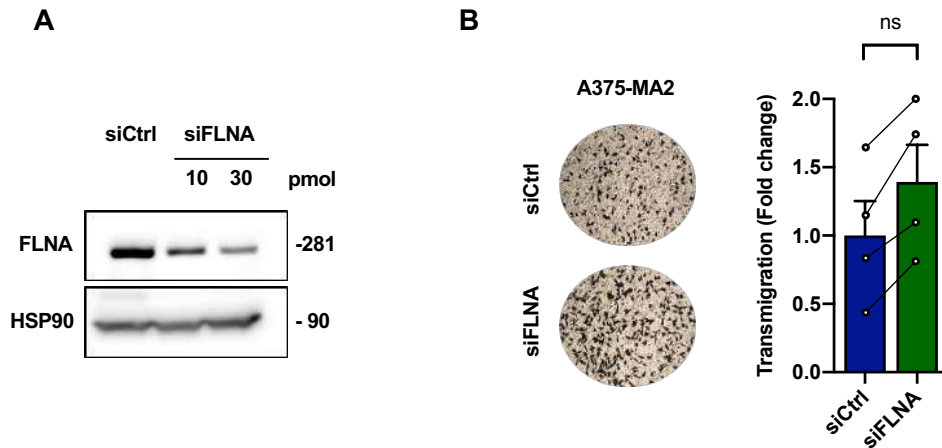


**Figure 24. Silencing of FLNA expression do not influence cell migration of metastatic cells.**

**(A)** A375-MA2 parental cells were transiently transfected with siRNA Control (siCtrl) or siRNA against FLNA (siFLNA) using 10 or 30 pmol. Total protein extracts were analyzed by western blot using specific antibodies. **(B) Left panel:** After 48h,  $5 \times 10^4$  cells transfected with 30 pmol of siCtrl or siFLNA were seeded on transwell plates, and transmigration was assessed. Transmigration was assessed in the presence of NIH-CM. After 4h, cells that migrated to the lower side were stained with crystal violet. Images of the lower side of the transwell were taken. **Right panel:** The number of cells that migrated was counted using the ImageJ software. Data represent the mean  $\pm$  s.e.m of 4 independent experiments. Results were statistically compared using a two-tailed t-test. (ns: not statistically significant).

Next, we decided to determine if the IRE1/FLNA signaling described before by our group in non-tumor cells was also present in melanoma. With this aim we assessed the endogenous interaction of these proteins in the human cell line SK-MEL5, since these cells express high protein levels of IRE1, and the mouse cell line B16F10. Using IP of IRE1 with a high-affinity anti-IRE1 antibody, we were not able to confirm the interaction between endogenous IRE1 and FLNA at basal levels (Supplementary Figure 7). Of course, this does not exclude the possibility that both proteins interact in melanoma cells, since this interaction could be weak or regulated by a promigratory stimulus. Other complementary studies need to be done to further explore this possibility.

Although we were not able to confirm an interaction between IRE1 and FLNA, we tested if IRE1 could affect the phosphorylation status of FLNA under promigratory stimuli. We previously described that in non-tumor cells under treatments with FBS there is an IRE1-dependent induction of FLNA phosphorylation in S2152, a critical phosphorylation site for activation of FLNA signaling through the actin cytoskeleton (93, 140). Thus, we treated melanoma cells with 20% FBS for 1 or 2 hours and analyzed the phosphorylation of FLNA by Western blot. As expected, an increase in FLNA phosphorylation after 1 hour of stimulation compared with non-treated parental A375-MA2 cells was observed (Figure 25A). When we performed the same experiment in Control clone C2 and IRE1KO clone KO2 treated with 20% of FBS, no significant differences were observed between both groups, suggesting that the induction of FLNA phosphorylation was independent of IRE1 (Figure 25B).

To validate this result, we treated cells with NIH-CM, a more efficient promigratory stimulus in melanoma cells. Interestingly, we did not observe a marked induction in phosphorylation of FLNA at any time of the treatment and no significant differences between the Control and IRE1KO clones were not obtained (Figure 25C). Since NIH-CM is a powerful promigratory stimulus in melanoma cells, this data suggests that FLNA phosphorylation may not be relevant during melanoma migration induced by NIH-CM. These results support our previous results showing that FLNA may not be relevant for the increase of cell migration in IRE1-deficient melanoma cells.



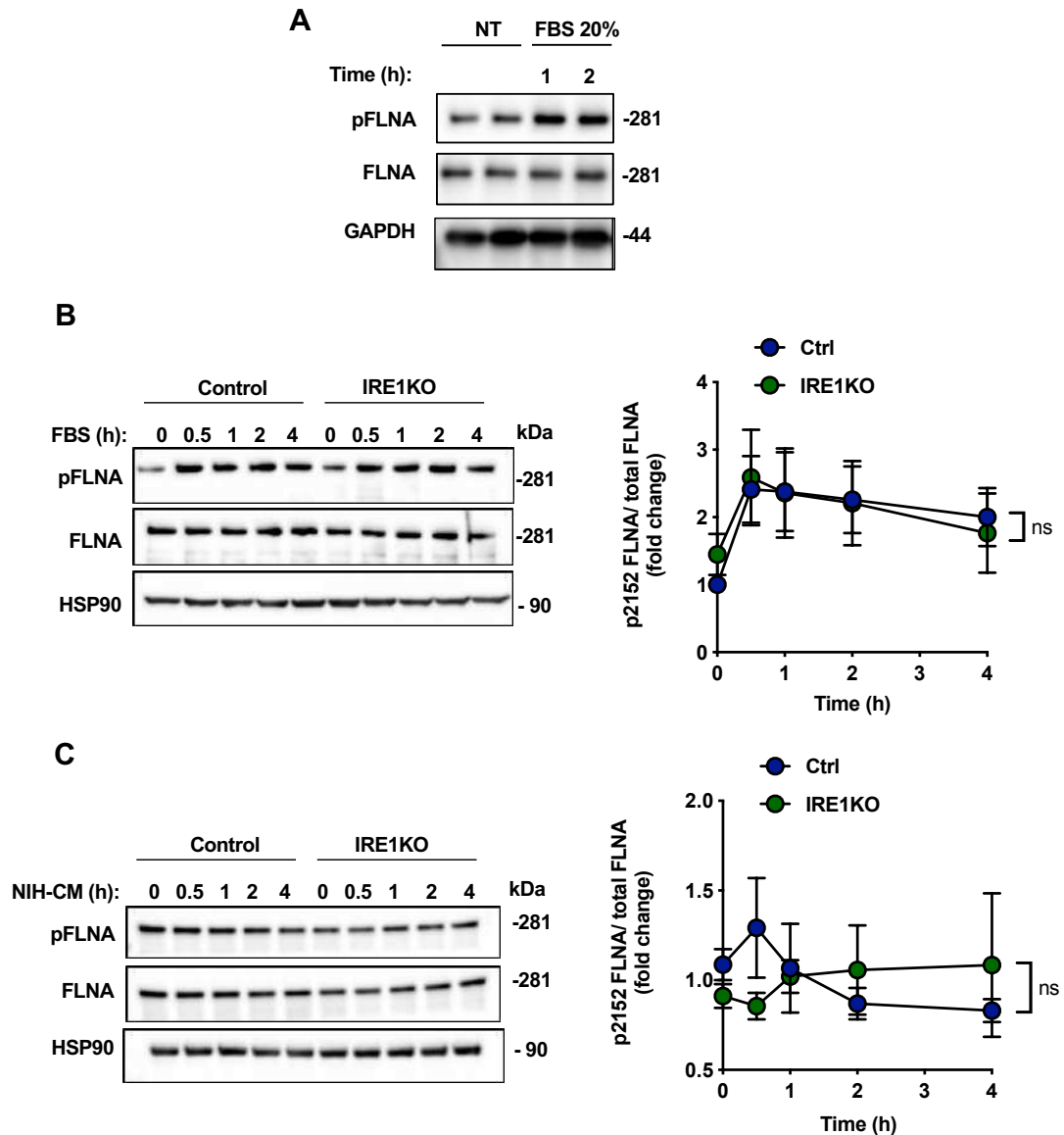


**Figure 25. FLNA phosphorylation is independent of IRE1 expression under promigratory stimuli.**

(A) Parental A375-MA2 cells were treated with 20% FSB for 1 and 2 hours. Total protein extracts were analyzed by western blot using specific antibodies for pS2152-Filamin A, Filamin A, and HSP90. (B) Left panel: Control C2 and IRE1KO KO2 were treated with 20% FSB (B) or 20% NIH-CM (C) for different time points. Total protein extracts were analyzed by western blot using specific antibodies for pS2152-Filamin A, Filamin A, and HSP90 (Left panels). Quantification of the levels of Filamin A phosphorylation in cells stimulated with promigratory stimuli was quantified by scanning densitometry and represented as fold change using non-treated control cells as reference (Right panels). Data represent the mean  $\pm$  s.e.m of 3 independent experiments. Results were statistically compared using two-way ANOVA followed by Bonferroni's multiple comparisons test. (ns: not statistically significant).

Finally, we treated cells with TM to activate IRE1 and measure the levels of FLNA phosphorylation under ER stress. To select the experimental conditions, we treated parental A375-MA2 cells with different TM concentrations for one or two hours and evaluated as readout of IRE1 activation the levels of XBP1 mRNA splicing. We selected 500 ng/mL of Tm since this concentration induced 80% of XBP1 splicing at two hours of treatments, the same induction that the one triggered by the higher concentration used (Figure 26A). Under these conditions, we treated for different times the Control clone C2 and IRE1KO clone KO2. Supporting the results obtained under promigratory stimuli, we found that IRE1 activation did not affected FLNA phosphorylation at S2152 in either of the two cell lines (Figure 26B). The induction of ER stress under TM treatment was verified with the induction of ATF4 translation (Figure 26B).

With these approaches, we demonstrated that in our model, activation of FLNA phosphorylation in S2152 is IRE1-independent. Also, we were unable to observe the interaction between these proteins in melanoma cells. Both results suggest that the modulation of FLNA signaling through IRE1 is not relevant in metastatic melanoma cells and that suppression of cell migration by IRE1 is a FLNA-independent mechanism.

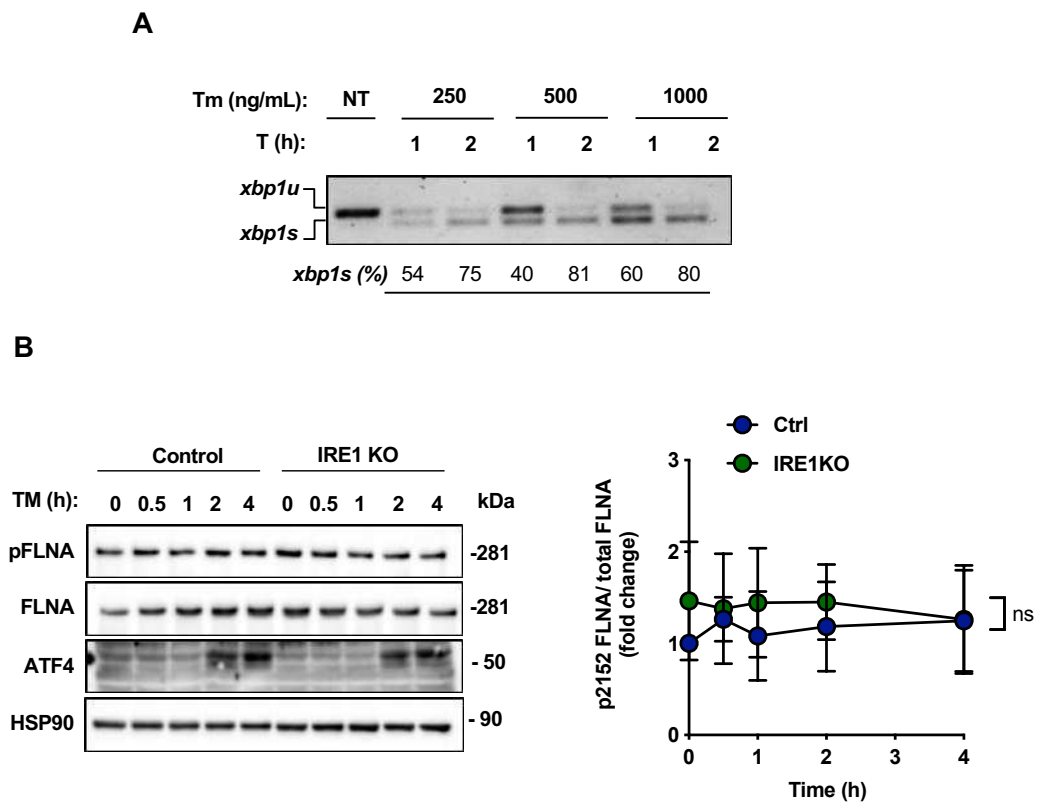


**Figure 26. FLNA phosphorylation is independent of IRE1 expression under ER stress.**

(A) IRE1 activity induced by different tunicamycin (TM) concentrations was evaluated in A375-MA2 parental cells. Cells were treated with different TM concentrations for 1 and 2 hours, and then XBP1 mRNA splicing was evaluated by RT-PCR. PCR fragments corresponding to the XBP1u or XBP1s forms of XBP1 mRNA are indicated. The percentage of XBP1 mRNA splicing was calculated after the densitometric analysis of the XBP-1u and XBP1s-related PCR products to quantify the splicing percentage in each condition. (B) **Left panel:** Control C2 and IRE1KO KO2 were treated with 500 ng/mL OF TM for different time points. Total protein extracts were analyzed by western blot using specific antibodies for pS2152-Filamin A, Filamin A, ATF4, and HSP90. **Right panel:** Quantification of the levels of Filamin A phosphorylation in cells stimulated with an ER stress inducer was quantified by scanning densitometry and represented as fold change using non-treated control cells as a reference. Data represent the mean  $\pm$  s.e.m of 3 independent experiments. Results were statistically compared using two-way ANOVA followed by Bonferroni's multiple comparisons test. (ns: not statistically significant).

### **9.3.1. Role of the IRE1 RNase-RIDD dependent activity in the suppression of melanoma cell migration.**

Another mechanism of IRE1 that has been linked to the regulation of cell migration in tumor cells is its RNase activity through the regulation of XBP1s or the degradation of multiple mRNAs through RIDD (117). A role for the IRE1/XBP1s axis enhancing invasion and metastasis has been proposed through the regulation of EMT-related genes (118, 121, 124). Nevertheless, some reports indicate that RIDD activity may exhibit the opposite role through a RIDD-mediated degradation of the mRNA of SPARC by RIDD (130). SPARC is a non-structural glycoprotein present in the extracellular matrix and that has been associated with aggressiveness, invasion and metastasis (133-138). Of note, there are no previous studies evaluating the role of IRE1 activity in migration and invasion in melanoma.

Thus, we decided to evaluate if the RNase activity of IRE1 could be involved in the suppression of metastatic melanoma cell migration using human cell lines as a model. With this aim we first tested MKC-8866, a salicylaldehyde analog, for a potent and selective pharmacological inhibition of IRE1 RNase activity (189). Dose-response of the IRE1 inhibitor showed that the treatment of cells with 20  $\mu$ M of MKC-8866 inhibits almost completely the activity of IRE1 upon ER stress based on the percentage of XBP1 mRNA splicing (Figure 27A). Then, A375-MA2 parental cells were seeded in a 6-well plate and pre-treated with 20 $\mu$ M of MKC-8866 for 48 hours before the experiment. Transmigration assays were performed using the same protocol previously described. Supporting our new hypothesis that the RNase activity of IRE1 could be involved in the regulation of cell migration in melanoma, we found that inhibition of IRE1 RNase activity with MKC-8866 significantly increased cell migration of A375-MA2 cells, same phenotype as the one observed

in cells deficient of IRE1 expression (Figure 27B). This result is in agreement with the fact that IRE1 acts as a suppressor of cell migration in metastatic melanoma cells and indicates that its enzymatic activity could be responsible.

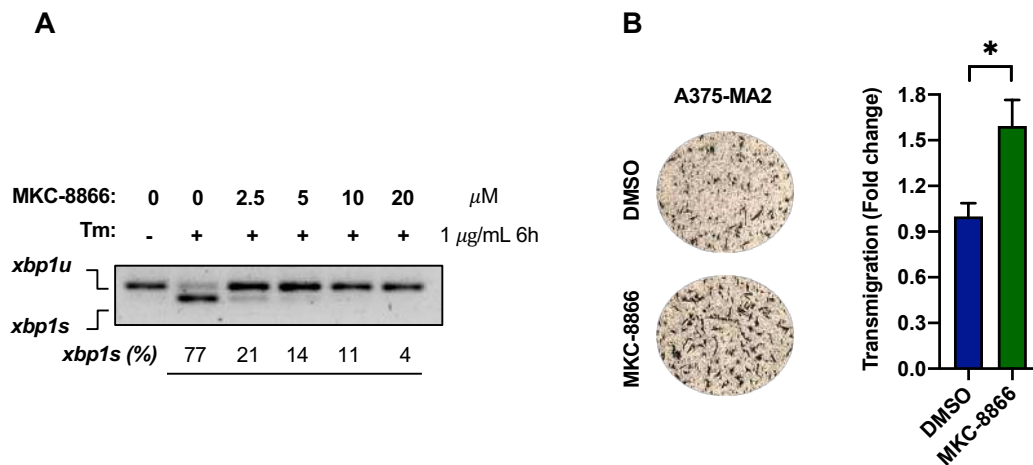


**Figure 27. The MKC-8866 IRE1 RNase inhibitor increases cell migration in human metastatic melanoma cells.**

(A) IRE1 RNase activity inhibition by different concentrations of MKC-8866 was evaluated in A375-MA2 parental cells co-treated with 1 μg/mL of TM for 6 h. XBP1 mRNA splicing was determined by RT-PCR. PCR fragments corresponding to the XBP1u or XBP1s forms of XBP1 mRNA are indicated. The percentage of XBP1 mRNA splicing was calculated after the densitometric analysis of the XBP1u and XBP1s-related PCR products to quantify the splicing percentage in each condition. (B) **Left panel:** After 48h,  $5 \times 10^4$  cells treated with 20 μM MKC-8866 were seeded on transwell plates, and transmigration was assessed. Transmigration was assessed in the presence of NIH-CM. After 4h, cells that migrated to the lower side were stained with crystal violet. Images of the lower side of the transwell were taken. **Right panel:** The number of cells that migrated was counted using the ImageJ software. Data represent the mean  $\pm$  s.e.m of 6 independent experiments. Results were statistically compared using a two-tailed t-test. (\*:  $p < 0.05$ ).

Based on the previously described function of IRE1 RNase activities, were XBP1s have been extensively described in a great variety of tumors as an enhancer of cell migration and invasion (118, 121, 124), we hypothesized that the effects of IRE1 as a suppressor of cell migration could be mediated by the degradation of a pro-metastatic gene through the RIDD. To further support this idea we first, performed gain-of-function assays by transiently transfecting plasmids coding for XBP1s-GFP or GFP (Mock) retroviral vectors followed by the Boyden chamber

assay. Total RNA extractions were analyzed to confirm overexpression of XBP1s by PCR (Figure 28A). Quantification of GFP positive cells that migrated to the lower chamber indicated that XBP1s overexpression did not affect cell migration compared with Mock cells (Figure 28B). The same phenotype was observed when we bypass IRE1 deficiency by the forced expression of XBP1s using the same experimental setting (Figure 28C). These results indicate that IRE1 negatively regulates cell migration in metastatic melanoma cell lines through a process independent of the XBP1s expression.

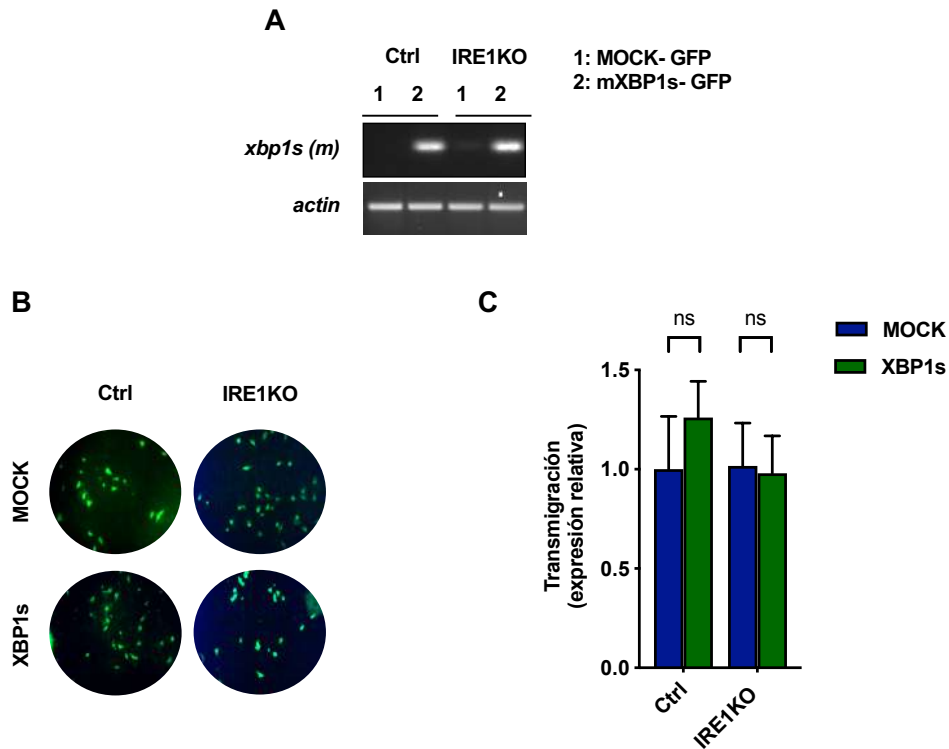


**Figure 28. Forced XBP1s expression does not influence cell migration of metastatic melanoma cells.**

(A) A375-MA2 parental cells were transiently transfected with Mock-GFP and mouse XBP1s-GFP plasmids. (A) The levels of XBP1s were evaluated by PCR using specific primers. After 72h transfected A375-MA2 clone Control C1 (B) and clone IRE1KO KO1 (C) were seeded on transwell plates, and transmigration was assessed. Transmigration was assessed in the presence of NIH-CM. After 4h, cells that migrated to the lower side were fixed with PFA 4%. Images of the lower side of the transwell were taken, and the number of cells GFP positive that migrated was counted using the ImageJ software. Data represent the mean  $\pm$  s.e.m of 3 independent experiments. Results were statistically compared using a two-tailed t-test. (ns: not statistically significant).

Next, we evaluated the possibility that IRE1 through RIDD could regulate some key mRNAs that affect cell migration. To this end, we decided to determine possible mRNAs of enhancers of cell migration/invasion and metastasis in melanoma that could be degraded by the IRE1/RIDD activity. Briefly, we selected two lists of genes that were previously identified as candidates associated with pro-metastatic capacities in melanoma (190, 191). These candidates were intersected, by using the program FunRich, with two dataset of genes that have been previously classified as potential RIDD-targets, by searching *in silico* the presence of CUGCAG-like sequences in all human transcriptome (192) or all mRNAs cleaved *in vitro* by IRE1 recombinant protein (139). This analysis revealed 39 putative RIDD targets with described pro-migratory and invasive roles in melanoma (Figure 29). Then, to narrow the list, we selected genes with a negative impact in survival in patients with melanoma according to the Human Protein Atlas (Figure 29). This analysis shown that 16 genes that are putative RIDD targets have an impact of melanoma patient survival.

To corroborate if some of these genes correlates with IRE1 activation status and RIDD activity, we evaluated the expression levels of these genes in four populations of melanoma patients displaying either High or Low RIDD activity, and High or Low XBP1s activity. This analysis was performed using the same database (TCGA) and protocol previously described in section 11.1.

Remarkably, tumors exhibiting high RIDD activity, independently of XBP1s, also correlated with a significant decrease in the expression level of nine pro-metastatic melanoma genes (Figure 30, left panel). A global effect in the expression levels of these genes mediated by RIDD activity can be more clearly observed in the heatmap represented in Figure 30, right panel. Between the genes possibly

regulated by RIDD we found: Minichromosome Maintenance Complex Component 7 (MCM7), Methylenetetrahydrofolate Dehydrogenase (NADP+ Dependent) 2, Methenyltetrahydrofolate Cyclohydrolase (MTHFD2), NAD(P) transhydrogenase (NNT), Nucleoporin 98 And 96 Precursor (NUP98), Protein Kinase C Alpha (PRKCA), Roundabout Guidance Receptor 1 (ROBO1), Mtr4 Exosome RNA Helicase (SKIV2L2, also known as MTREX), Structural maintenance of chromosomes protein 4 (SMC4), Signal Peptidase Complex Subunit 3 (SPCS3), and TAR DNA Binding Protein (TARDBP). After a gene ontology analysis, we found that these genes are associated to metabolic pathways, RNA transport, cell cycle, DNA replication, proteasome and secretory pathway. All of them have been found to be associated with the metastatic process in melanoma. Interestingly, among these genes, we found PRKCA that encodes for PKC $\alpha$ , an important mediator of the IRE1/FLNA signaling (93). The degradation of PKC $\alpha$  by RIDD could explain the lack of evidence of this signaling in our model.

This data supports the idea that these pro-metastatic genes could be putative RIDD-targets in melanoma and that the degradation of the mRNA of these genes could be mediating the suppression of cell migration and invasion in the metastatic melanoma cell lines. Nevertheless, further experiments are needed to corroborate this hypothesis in addition to functional test of the impact of this putative RIDD targets in melanoma cell migration.



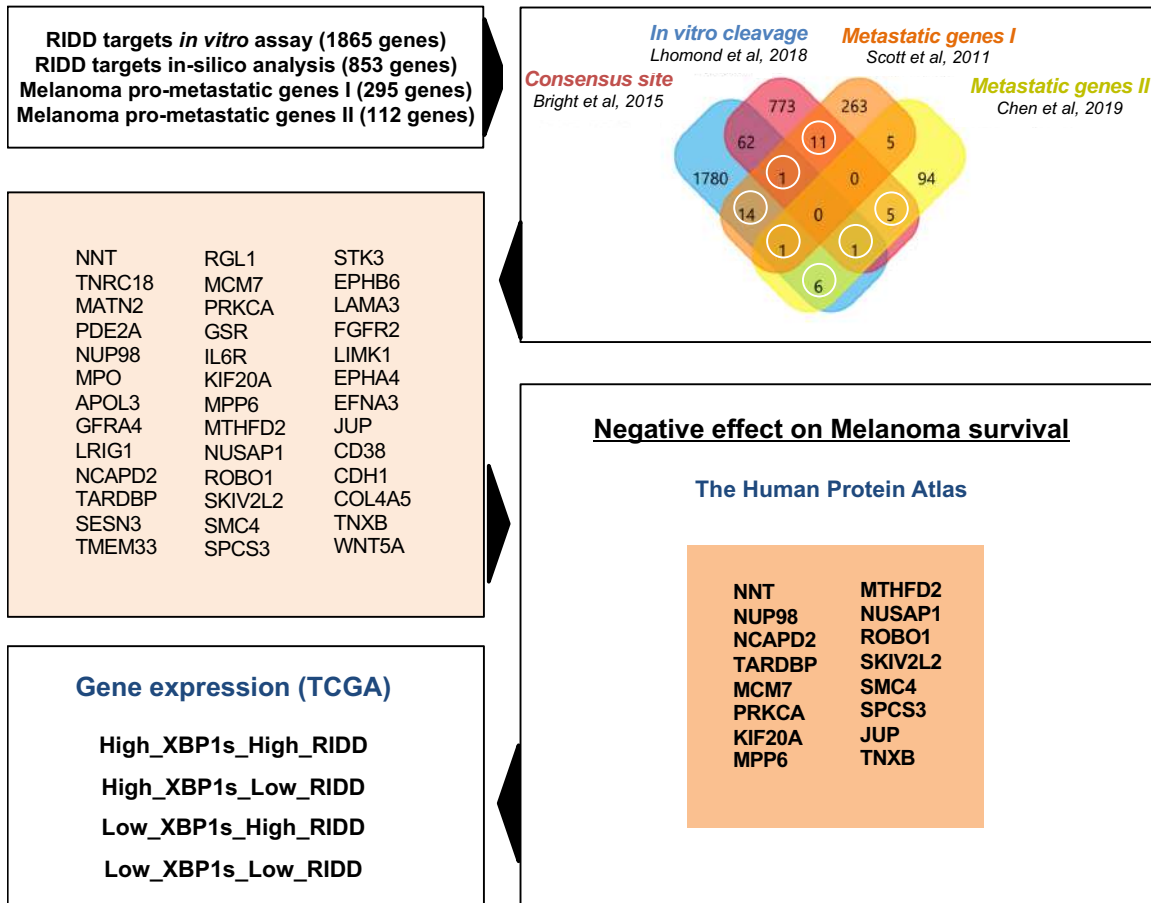


**Figure 29. Pipeline of the analysis to identify pro-metastatic genes and putative RIDD-targets in melanoma.**

**(A)** Interception analysis of a list of genes identified as potential RIDD targets, using two datasets and two lists of genes associated pro-metastatic capacities in melanoma (190, 191). was performed. The two datasets describing possible RIDD targets were based in an in-silico searching of the presence of CUGCAG-like sequences (192) and in an in-vitro cleavage assay by IRE1 recombinant protein (139). This analysis revealed 39 putative RIDD targets with potential pro-migratory and invasive roles in melanoma. From these 39 genes, 16 were identified as candidates significantly associated with poor overall survival in melanoma patients. Survival analysis data were obtained using the Protein Atlas website and the database of human skin cutaneous melanoma from the Cancer Genome Atlas (TCGA) project. The hierarchical clustering of patients using the dataset from the TCGA revealed the existence of four populations displaying either high or low RIDD and XBP1s activities. Correlation of gene expression and IRE1 branch activity was performed.

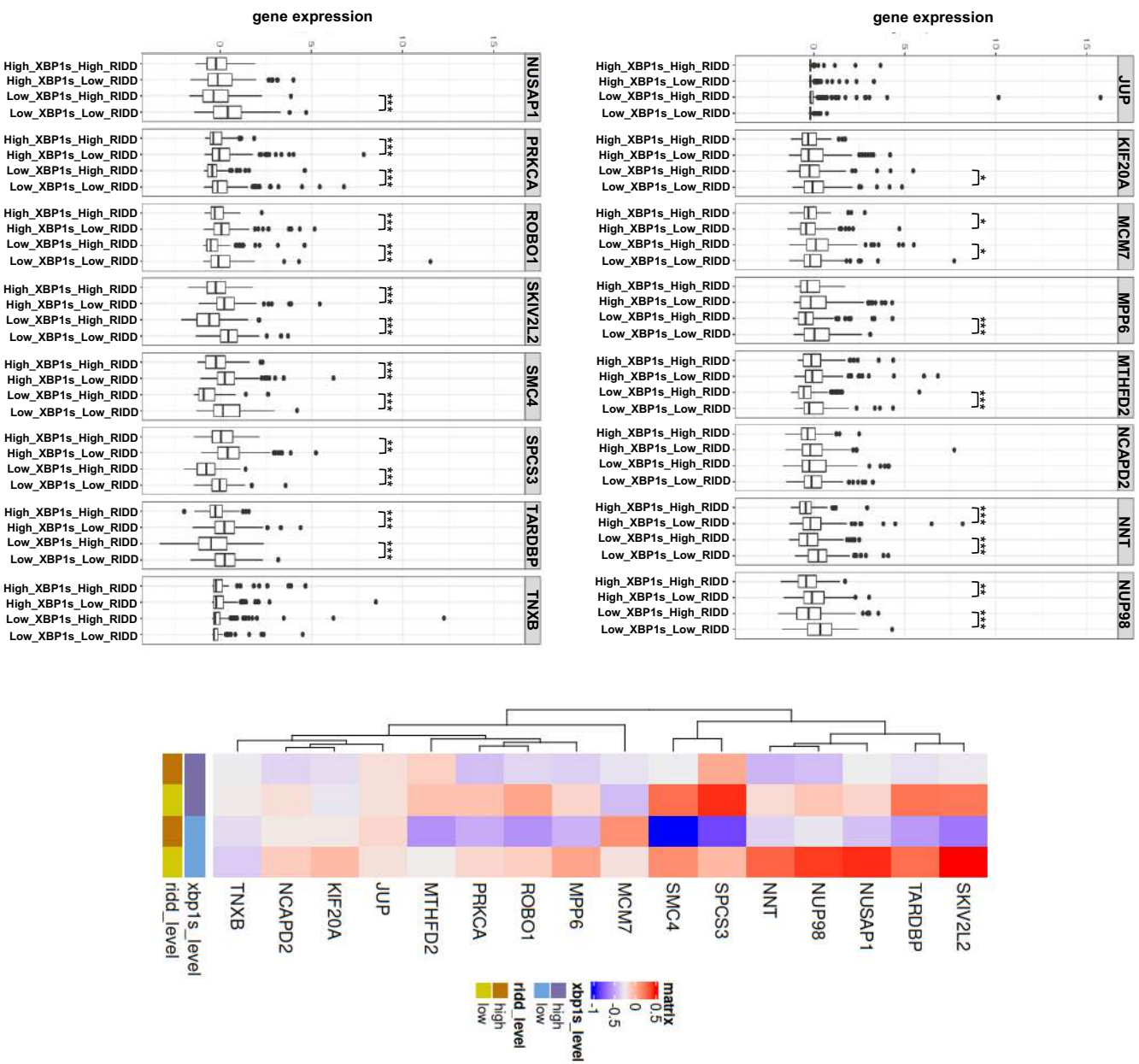


**Figure 30. Pro-metastatic genes and putative RIDD-targets in melanoma.**

Melanoma patients were scored using XBP1s and RIDD signatures. **Left panel:** Signature scores were overlapped to generate 4 cohorts: High\_XBP1s\_High\_RIDD, High\_XBP1s\_Low\_RIDD, Low\_XBP1s\_High\_RIDD, Low\_XBP1s\_Low\_RIDD. The scaled expression of pro-metastatic genes between the four cohorts was compared. **Right panel:** A heatmap was generated to compare the relative expression of the pro-metastatic genes. The genes were clustered using hierarchical clustering. High and Low RIDD groups were statistically compared using a two-tailed t-test. (\*. p < 0.05, \*\*. p < 0.01, \*\*\*. p < 0.001, \*\*\*\*. p < 0.0001).

#### 9.4. ***Correlation of IRE1 activity and metastasis in melanoma in vivo.***

The global analyses of the data obtained in this thesis suggest that IRE1 can suppress cell migration and invasion of metastatic melanoma cells through its RNase activity, probably through RIDD. As shown before, RIDD activity appears to be decreased in metastasis compared with primary tumors (Figure 12B), which supports the hypothesis that this signaling could be acting as a tumor suppressor for melanoma metastasis. Based on this, the next step for our research was to evaluate *in vivo*, in a more complex and complete process, such as metastasis, the observations obtained from the *in vitro* experiments and bioinformatic analysis.

As part of the specific aim 3, we planned an *in vivo* assay to evaluate the generation of lung metastasis using the tail vein injection method in eight-weeks old male NSG mice. NSG mice lack T, B, functional NK cells as well as both alleles of the IL2 receptor common gamma chain, thus lacking cytokine signaling through multiple receptors (167). The severe immunodeficiency of NSG mice allows good engraftment rates of tumors with cells from human origin (167). Thus, the use of this animal strain is the best model to evaluate metastasis of human cell lines.

To set up the number of cells necessary to perform a pulmonary metastasis assay, we injected 25,000, 50,000 and 100,000 parental A375-MA2 cells through the tail vein of immunocompromised mice. The animals were immobilized to proceed with an injection of 200  $\mu$ L of a suspension of tumor cells in PBS in the tail vein. After 28 days of implantation the animals were sacrificed and the lungs were collected, fixed in PFA 4%, and paraffin-embedded for histologic analysis using H&E staining (Figure 8). The number of metastatic nodules was determined through the analysis of the images from serial sections of H&E staining of lungs using the ImageJ

software. We observed metastatic nodules in all conditions, and the number of the nodules was proportional to the number of the cell injected. For further experiments, we decided to use 25,000 cells since we obtained an amount of lung metastasis easier to analyze and to determine differences between conditions (Figure 31).

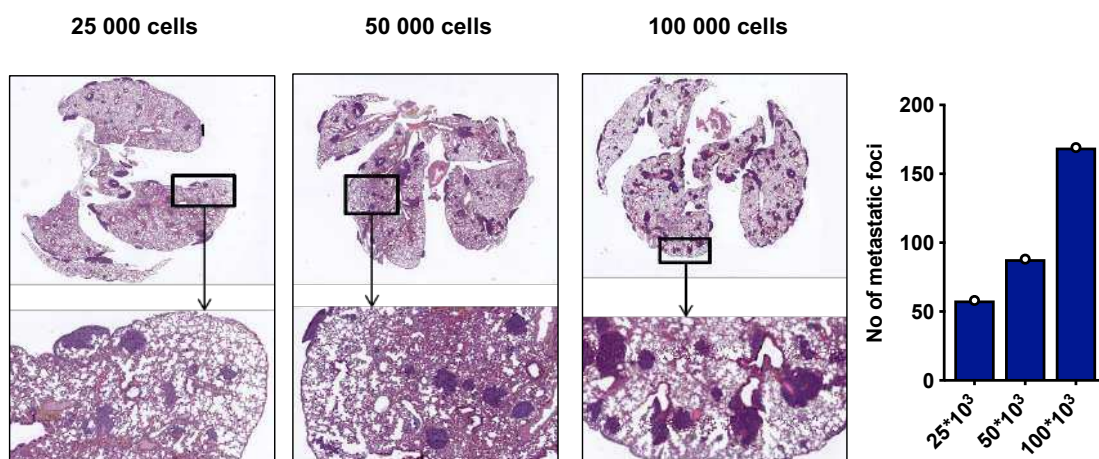


**Figure 31. Standardization of A375-MA2 lung metastatic model by tail vein injection.**

**Left panel:** Different amounts of A375-MA2 parental cells were re-suspended in 500  $\mu$ L saline solution (0.9% NaCl) and injected intravenously into eight-week-old male NSG mice. On day 28 post-inoculation, lungs were collected and fixed with PFA 4% and processed for immunohistochemistry and stained with H&E. **Right panel:** The number of metastatic nodules was quantified using the ImageJ software. Data represents one independent experiment and one mouse per condition.

After we established the metastatic assay, we continued using the IRE1 deficient cells. For this, 25,000 Control or IRE1KO cells were injected in immunocompromised mice, and after 28 days we evaluate the presence of lung metastasis as described previously. Mice weight was weekly monitored and analyzed at the end of the experiment. Interestingly, no changes in the weight of the animals were observed during the experiment (Figure 32A). All the mice injected with the human metastatic cell lines presented metastatic nodules in the lungs (Figure 32B, representative images); however, not statistical differences were obtained between Control and IRE1KO individual clones (Figure 32C, left panel). Of note, the lungs of mice injected with IRE1KO cells analyzed as a group showed an

average of 1.3 times more melanoma nodules compare to the Control group, but still, no significant differences were obtained (Figure 32C, right panel).

The surface area of the metastatic nodules was also determined. When this data is represented as a histogram of frequency, can be seen that tumors from both IRE1KO clones have a lower rate in the range that group the smaller tumors (<52 000  $\mu\text{m}^2$ ), but a higher number of IRE1KO-related metastatic nodules can be observed in most of the ranges sizes over 52 000  $\mu\text{m}^2$  (Figure 33). Based in this result we could conclude that IRE1 expression does not play a major role in the metastatic process in melanoma and that the phenotype observed in cell migration *in vitro*, it is not being reproduced *in vivo*. However, it is important to note that although this assay it is a common way to experimentally evaluate metastasis in a *in vivo* model, is not the best assay since does not reproduce the first stages of the metastatic process, such as cell migration and invasion.

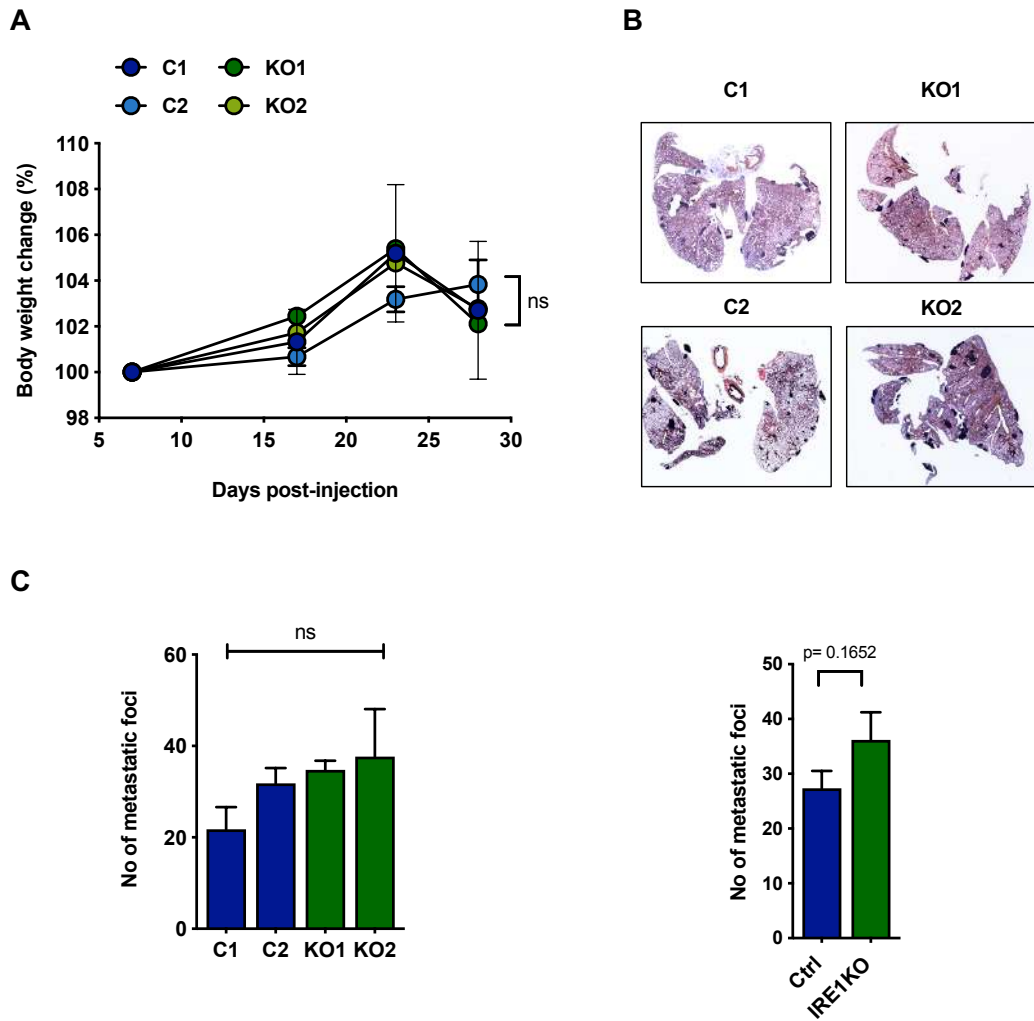


**Figure 32. Lung metastasis is independent of IRE1 expression in an experimental metastatic melanoma model.**

Controls and IRE1KO A375-MA2 cells (25000) were re-suspended in 500  $\mu$ L saline solution and injected intravenously into eight-week-old male NSG mice. **(A)** Mice weight was weakly monitored. **(B)** At day 28 post-inoculation, lungs were collected and fixed with PFA 4% and processed for immunohistochemistry and stained with H&E. Representative images are shown. **(C)** The number of metastatic nodules was quantified using the ImageJ software and represented as individual clones (**Left panel**) or groups (**Right panel**). Data represent the mean  $\pm$  s.e.m of at least 1 independent experiment and at least 6 mice per condition. Results were statistically compared using two-way ANOVA followed by Bonferroni's multiple comparisons test (**A**), one-way ANOVA followed by Dunn's multiple comparison test (**C, Left panel**) or two-tailed t-test (**C, Right panel**). (ns: not statistically significant, p: p value).

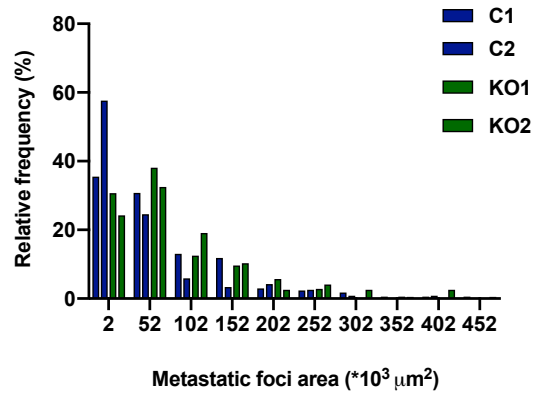


**Figure 33. Frequency distribution of metastatic foci size.**

Controls and IRE1KO A375-MA2 cells (25000) were re-suspended in 500  $\mu$ L saline solution and injected intravenously into eight-week-old male NSG mice. On day 28 post-inoculation, lungs were collected and fixed with PFA 4%, processed for immunohistochemistry, and stained with H&E. The size of metastatic nodules was quantified using the ImageJ software and represented as a relative frequency distribution graph. Data represents 1 independent experiment and at least 6 mice per condition.

The same metastatic assay was used to corroborate the results in a syngeneic model using the mouse cell line B16F10 in C57BL/6 mice. Standardization of the number of cells to inject (50,000, 100,000 and 200,000 cells) into 8-12 weeks old C57BL/6 mice indicates that 100,000 cells is the best amount to visualize tumors (Supplementary Figure 8). Using this approach, we then 100.000 Control and IRE1 KO B16F10 cells, and at day 21 post-inoculation mice were sacrificed, and the number of metastatic nodules was quantified in fixed lungs. We observed a trend to increase the number of metastatic nodules in the mice injected with IRE1KO cells compared to the control, corroborating the result obtained in the metastatic assay with human cells, although significant differences were not found (Supplementary Figure 9).

Altogether, we found that IRE1-deficient cells presented a trend to increase the number of metastatic nodules; however, significant differences were not observed. Interestingly, analyzing the frequency of the nodules in size ranges, IRE1 deficiency appears to increase the growth of these metastatic lesions. Nevertheless, the data is not enough to conclude that IRE1 have a role in the metastatic process of melanoma and further experiments are required. However, these experiments indicate that the effect of IRE1 in melanoma metastasis is not associated with the survival of the tumor cells in the circulation, the extravasation, and colonization in the lungs. Further experiments in models of spontaneous metastasis that include the first stages of metastasis are needed to corroborate the role of IRE1 in melanoma metastasis.



## 10. DISCUSSION.

In the last years, the UPR has emerged as a central factor driving malignant transformation and tumor growth, impacting most hallmarks of cancer (60, 61). IRE1 is the most evolutionary conserved ER stress sensor of the UPR, and its function on carcinogenesis is still not fully understood. Both endoribonuclease activities, XBP1 splicing and RIDD, have been associated with tumor progression; however, the exact impact of each one is still to be uncovered. Also, we recently identified FLNA as a new IRE1 interactor and revealed a new function of this protein in the regulation of actin cytoskeleton dynamics, with a significant impact on cell migration. Despite the growing evidence that indicates that IRE1 is an essential regulator of tumor progression, the role of the IRE1 branch in metastasis is still ambiguous, and most of the evidence available is still correlative.

A few reports correlate IRE1 activity with cell migration, invasion and metastasis. Data from our laboratory indicate that IRE1 can enhance the migratory capacity of normal cells through the specific regulation of the actin cytoskeleton. Moreover, IRE1 acts as a scaffold to promote FLNA phosphorylation in S2152 mediated by PKC $\alpha$  and potentiate cell migration, independent of its RNase activity (93). Nevertheless, some reports indicate that the alternative IRE1 RNase signaling output, RIDD, may exhibit the opposite effect in certain systems. For instance, in GBM the IRE1 signaling negatively regulates cell migration and invasion through a RIDD-mediated mechanism (102, 130, 132, 139). Additionally, it is known that XBP1s can regulate the expression of genes associated with invasion and EMT (125, 126). Thus, the role of IRE1 activity in invasion/metastasis is still controversial and more studies are needed to define its contribution to this process. Altogether

IRE1 might impact in cell movement at three different layers: XBP1s, RIDD and FLNA-dependent mechanisms.

In the initial project, we were particularly interested in elucidating the possible contribution of the newly described IRE1 signaling through FLNA in cell invasion of tumor cells and the corresponding effect on metastasis. Therefore, we aimed to systematically study the role of IRE1 in cell migration and invasion, and the possible regulation of FLNA function, using *in vitro* and *in vivo* approaches. Nevertheless, our initial hypothesis was refuted based on our findings. Our results support a novel function of IRE1 as a suppressor of cell movement of human melanoma cell lines through its RNase activity RIDD.

#### **5.1. *IRE1 pathway is activated in melanoma metastasis.***

Our purpose in this project was to evaluate the contribution of IRE1 signaling, initially the IRE1/FLNA axis, in the development of metastasis in melanoma. Fingerprints of IRE1 branch activation have been found in metastasis of different types of tumors (118-121); but no report has been described in melanoma. Therefore, we proposed to evaluate IRE1 activation status *in vivo* in metastatic melanoma nodules and human patients' database. When we performed the *in vivo* assay by injecting B16F10 cells in the tail vein or subcutaneously in immunocompetent mice we observed an increase in XBP1s expression in the metastatic nodules compared with the adjacent non-tumoral tissue. This is in agreement with the findings that there is basal IRE1 activation in melanoma cells (111, 113, 162). However, a comparison between the primary tumor and the metastatic nodules was not possible since just one primary tumor was obtained. This approach presented several experimental limitations explained previously. The

observed results suggest the possibility that IRE1 activation could be necessary at some stage of the metastatic process; but this phenotype needs to be corroborated by using other experimental approaches. One interesting alternative is to evaluate IRE1 activation status in melanoma DCC. This approach could allow us to study IRE1 branch activation in melanoma cells originated from a primary tumor and that can function as a seed for metastasis (193). This has been already tested in DCC of pancreatic tumors where a downregulation of IRE1 signaling was observed (128).

To go deeper, we next evaluated activation status of the IRE1 branch in human melanoma metastasis. Using gene signatures already described for GBM tumors (139), we compare IRE1 activity in primary and metastatic tumors from 469 patients. Unexpectedly, we observed a significant decrease in IRE1 activity in metastatic samples in comparison with primary tumors (Figure12). This decrease in IRE1 activity in metastasis was correlated with a decrease in the RIDD activity, but not XBP1s activity, suggesting that IRE1/RIDD inhibition could be a necessary process for the development of melanoma metastasis. The finding that IRE1 signaling is inhibited during metastasis opposes to our initial hypothesis, where we propose that IRE1 could act as an enhancer of melanoma metastasis particularly through its interaction with FLNA. This is the first evidence indicating that IRE1, particularly through RIDD, could be acting in melanoma as a suppressor of the metastatic process.

In agreement with our results, it was described that IRE1 pathway was not activated in pancreatic quiescent DCC, but it was activated in cells from the primary tumor (128). These cells presented a phenotype that was linked to a decrease of the proliferation rate and in the expression of MHC I, providing an evasion mechanism to the immune system (128). However, XBP1s over-expression in this

disseminated cancer cells significantly induced the development of hepatic macro-metastasis (128). In melanoma models, is well documented the basal activation of the IRE1 branch and the induction of autophagy in melanoma cells (111, 113, 162). In addition, fingerprints of activation of the three UPR branches have been described in melanoma metastatic cells compared to their non-metastatic counterpart (165). Importantly, regarding IRE1 activity juts downstream targets of the XBP1s axis was evaluated, supporting our findings that the particular branch of XBP1s could be activated in metastasis in comparison with primary tumors. GBM tumors is a particularly interesting example since different axis of IRE1 can actually exert opposite outcome in the same type of tumor (102, 130, 132, 139).

Altogether this evidence suggests that the IRE1 branch could be a relevant pathway during the metastatic process, perhaps exerting opposite roles depending on the stage of the metastatic cascade; however, more experiments are needed to corroborate this hypothesis.

## **5.2. *IRE1 a novel suppressor of melanoma cell migration and invasion.***

Our results involve the comprehensive study of four human cell lines where the non-metastatic cell line A375 was included for comparative purpose. Interestingly, the A375-MA2, one of the three highly metastatic cell lines, is derived from A375 using an *in vivo* selection process in mice.

Boyden chamber assays in cells showed that IRE1 silencing enhanced cell migration in metastatic human cell lines. This result was only observed in the metastatic melanoma cells since no changes were obtained in the non-metastatic melanoma cell line A375, suggesting that IRE1 alone cannot impact in cell migration but requires additional components that are present in metastatic cells. To further

corroborate our results in metastatic melanoma cells, we generated IRE1KO cells by using CRISPR/Cas 9 technology in the metastatic cell line A375-MA2 cells. Under this experimental condition, we observed the same results in Boyden chambers and invasion assays in presence of matrigel. The effect on cell invasion was lower than the one observed in cell migration.

These results suggest that IRE1 may be suppressor of a cell migration/invasion-mechanism relevant only in melanoma metastatic cells. In other types of cancer, IRE1 deficiency exert the opposite effect in cell migration and invasion than the one we obtained. For instance, in colorectal cancer, breast cancer and esophageal squamous cell carcinoma the knockdown of IRE1 or XBP1s impairs cell migration and invasion through a mechanism XBP1-dependent (118-124). Until now, only in GMB-derived cell lines, IRE1 have shown to suppress cell invasion. Importantly, in all this type of tumors high expression or activity of IRE1 correlates with low overall survival and disease-free survival rates (119-124, 139).

Of note, main cause of death in melanoma patients is the spreading of the tumor to different organs (194). In a previous study, comparison between non-metastatic and metastatic patient-derived melanoma cells lines showed an activation of the three UPR branches in metastatic compared to non-metastatic cells; however, only the induction of the ATF6 and PERK branches was associated with poor survival in melanoma patients (165). Interestingly, HERPUD1, a downstream target of the IRE1, showed better prognosis for melanoma patients when it was highly-expressed (165). To determine the relevance of IRE1 expression in melanoma metastasis, we selected an experimental model of metastasis, consisting of the lateral tail vein injection of human metastatic melanoma cells in NSG mice or mouse metastatic melanoma cells in immunocompetent mice.

Although our *in vitro* data support that IRE1 can act in the suppression of cell migration, we did not find significant differences regarding the number of metastatic nodules in the lungs between the IRE1KO and Control metastatic melanoma cells.

The direct role of IRE1 in the generation of metastasis has been poorly characterized and there is not data available in melanoma. Only three studies have demonstrated a correlation between IRE1 activity and metastasis, all of them showing that IRE1 can act as an enhancer of metastasis mediated by XBP1s: (i) in breast cancer cell was observed that orthotopic injection of XBP1 deficient cells decreased the formation of lung metastasis (99), (ii) IRE1 knockdown in colon cancer cells significantly inhibited the generation of spontaneous liver metastases (180) and (iii) overexpression of XBP1s in hepatocellular cancer cells induced an increase in the number of micrometastatic lesions in the lungs after six weeks of tail vein injection of the tumor cells (123). Altogether, these reports indicate that the IRE1/XBP1s branch acts as a promoter of metastasis. Our data suggests that IRE1 could act in melanoma as a suppressor of metastasis, during the first stages of the metastatic cascade and perhaps by a different branch than XBP1s.

An explanation of the low effect of IRE1 deficiency in metastasis in our experiments could be that the chosen *in vivo* model is not adequate to evaluate the mechanism regulated by IRE1 in melanoma. The chosen experimental model of metastasis (direct delivery of tumor cells in the circulation) is an excellent strategy as a first approach, since allows the control of the number of cells delivered, excluding the effect of primary tumor growth. However, this type of experiment has a series of limitations such as (i) due to the artificial route of delivery is possible to evaluate just the capacity of tumor cells to growth in the lungs and (ii) it is not possible to recapitulate the first steps of the metastatic cascade, such as the initial

growth and migration/invasion stages, together with the intravasation into the circulation (195, 196). A new metastatic model has emerged where orthotopic transplantation of tumor cells with primary tumor resection allow the formation of spontaneous metastasis and recapitulate all the steps in the metastatic process. Nevertheless, the main issue about this new model is that requires a longer time for the metastatic disease to become evident. For instance, subcutaneous injection of a melanoma cell line, WM239 require 4-6 month for the formation of visible metastatic nodules after tumor resection (197). We consider that besides the complexity of this experimental model, the evaluation of the effect of IRE1 depletion in a spontaneous metastatic could be relevant to test our hypothesis.

In contrast to most of the literature in several types of tumors where IRE1 acts as an enhancer of metastasis, our results shown that IRE1 can acts as a suppressor of cell migration and invasion at least in metastatic melanoma cell lines. Also, we observed that IRE1 RNase activity, particularly RIDD, is decreased in metastasis compared with primary tumors. However, further experiments to fully uncover the role of IRE1 in melanoma metastasis are needed.

### **5.3. *The suppressor effect of IRE1 in cell migration is independent of Filamin A.***

IRE1 has two main mechanisms to control migration/invasion, the control of gene expression through its RNase activity (XBP1/RIDD), and the modulation of signaling pathways through direct binding with proteins, like FLNA. As we mentioned before, we recently described in non-tumor cells that IRE1 acts as a scaffold protein to recruit FLNA and increases its phosphorylation at serine 2152 mediated by PKC $\alpha$ , enhancing cell migration (93). FLNA is an actin crosslinking

protein, and its function is mainly regulated at the S2152 phosphorylation level (142). Remarkably, FLNA phosphorylation is mediated and regulated by different protein kinases (144-146). FLNA is also regulated through the cleavage by calpains generating a 200 kDa N-terminal and a 90 kDa C-terminal fragments (147). Importantly, this cleavage is inhibited by the serine 2152 phosphorylation (148). The 90kDa fragment translocate to the nucleus and interacts with transcription factors, such as the androgen receptor, and has been recently associated with novel functions like the regulation of gene expression (148).

FLNA has been related to tumor progression, particularly to the enhancement of tumor cell migration capacity and metastasis (198-200). However, this protein can also act as a tumor suppressor, depending on its subcellular localization and its binding partners. Some controversial results suggest that proteolytic regulation of FLNA by calpains and generation of the 90 kDa fragment might suppress metastasis (reviewed in (150)). Recent findings indicate that FLNA negatively regulates cancer cell invasion promoting MMP9 degradation (158, 159) and decrease cell invasion and migration through the regulation of focal adhesions via calpain-dependent mechanism in breast cancer models (160). Based on this evidence, some authors hypothesize that proteolysis and nuclear fragment of FLNA suppress cell migration, while S2152 phosphorylation and cytoplasmic localization of full length FLNA promotes cancer metastasis.

To rule out the possibility that IRE1 could be suppressing cell migration through a mechanism FLNA-dependent, we evaluated the effect of FLNA expression on cell migration in metastatic melanoma cells. Depletion of FLNA by siRNA showed a non-significant increase of cell migration of parental A375-MA2 cells. In melanoma models, FLNA have been mainly correlated with migration and



invasive properties. On one side, depletion of FLNA in melanoma cell lines significantly reduces migration and invasion *in vitro* (198-200). On the other side, using genetic and pharmacological approaches was demonstrated that in melanoma cells FLNA can mediate transcriptional downregulation of MMP9 by suppressing constitutive activation of RAS/MAPK signaling pathways (201). Thus, further experiments are needed in our cellular model to corroborate the role of FLNA in cell invasion. All this evidence shown that the role of FLNA in cell migration and invasion in melanoma is still controversial.

In our experimental model we were not able to demonstrate the interaction of IRE1 and FLNA at basal conditions in human or mouse melanoma cells, nevertheless additional experiments are required to discard this interaction. In addition, we also evaluated if FLNA phosphorylation mediated by IRE1 could suppress cell migration and could be a potential mechanism to explain our phenotype. To this aim, we evaluated the induction of FLNA phosphorylation in the presence or absence of IRE1 and pro-migratory stimuli such as FBS or NIH-CM. In our model, the induction of FLNA phosphorylation by FBS was independent of IRE1 expression. Treatments with NIH-CM and TM failed to induce FLNA phosphorylation in A375-MA2 cells. Therefore, FLNA phosphorylation at S2152 in melanoma cells seems to be independent of IRE1 expression. This suggests that the modulation of FLNA signaling through IRE1 might not be relevant in melanoma cells.

Despite these findings, we decided to evaluate other cellular processes regulated by FLNA, like actin cytoskeleton dynamics and cell adhesion. Our results suggest that deficiency of IRE1 did not induce changes in the actin cytoskeleton or cell adhesion of human metastatic melanoma cells. Of note, our experiments were

performed in absence of ECM or any migratory stimulation, thus further experiments or approaches might be required to really prove this issue.

Altogether our results showed a trend of increased cell migration in FLNA-deficient cell; however, non-significant differences were observed. Also, we were not able to demonstrate an interaction between the two proteins and S2152 FLNA phosphorylation was independent of IRE1 expression that correlates with no changes in actin cytoskeleton and cell adhesion. Nevertheless, based on the previous data FLNA appears to be an enhancer of cell migration in melanoma. In conclusion, our findings in human melanoma cell lines indicate that suppression of cell migration/invasion by IRE1 happens by a mechanism independent of FLNA.

#### ***5.4. The RNase activity is required for IRE1-dependent suppression of cell migration.***

Since IRE1 was not regulating melanoma cell migration through the FLNA axis, we evaluated if the RNase activity of IRE1 was responsible for the phenotype observed in our model. Using the potent and selective IRE1 RNase inhibitor, MKC-8866, a significant increase in migration of A375-M2 cells was observed upon full inhibition of IRE1 RNase activity. These results suggested that IRE1 RNase activity was responsible for the suppression of metastatic melanoma cell migration.

As mentioned before, both IRE1 RNase activities have been linked to cell migration and invasion of tumor cell (Reviewed in (117)). This scenario in melanoma cells open several possibilities. On one side, a role for the IRE1/XBP1s axis as an enhancer of metastasis has been proposed. XBP1s has been mainly associated with the induction of the expression of several EMT transcription factors in colorectal, oral, hepatocellular and breast tumors (118, 119, 121, 123-126). Also,

elevated levels of XBP1 at primary tumors correlates with the presence of distant metastasis in patients with different types of cancer like esophageal carcinoma, hepatocellular carcinoma, and oral squamous cell carcinoma (122-124). Basal XBP1s expression has been described in TNBCs and has a key role on tumorigenicity and tumor dissemination through a heterodimer formed by XBP1s and HIF1 $\alpha$  that promote HIF1 $\alpha$ -regulated genes expression by the recruitment of RNA polymerase II (99). Importantly, it is well documented that HIF1 $\alpha$  transcriptional program play a key role in the metastatic cascade regulating process like EMT, extravasation and metastatic niche formation (202). In melanoma cells, it was found that XBP1s acts as a transcription factor that robustly enhances IL-6 expression, a cytokine that drives melanoma cell motility through p38 $\alpha$ -MAPK-dependent mechanism (203, 204). Supporting this evidence found in other types of cancer, our results showed that cell migration in human metastatic melanoma cells is independent of XBP1s expression, thus another mechanism derived by the RNase domain of IRE1 is responsible for the suppression of cell migration/invasion.

#### ***11.4.1 RIDD as a possible mechanism for the increased migration/invasion in IRE1-deficient melanoma cells.***

In contrast with what has been described in most types of tumors, IRE1 negatively modulates cell migration and invasion in GBM, similar to what we observed in metastatic melanoma cells (98, 102, 129-132). In glioma cells, gene expression profile revealed that loss of IRE1 activity resulted in the up-regulation of extracellular matrix proteins (98, 130). One of these proteins was SPARC, a non-structural glycoprotein present in the extracellular matrix that is associated with changes in cell shape, synthesis of ECM and cell migration and whose mRNA is a direct target of RIDD activity (130). Similar to glioblastoma, the degradation of an

mRNA that encodes for a cell migration/invasion-enhancer could explain the mechanism through which IRE1 suppresses cell migration/invasion in metastatic melanoma cells.

Based on this, we decided to determine possible mRNAs enhancers of cell migration/invasion and metastasis in melanoma that could be regulated by RIDD in our model. To this aim, we used a list intersection-base strategy to detect genes that have been identified as potential RIDD targets and that have been associated with pro-metastatic capacities in melanoma using different published datasets (139, 192). This analysis identified 39 putative RIDD targets with potential pro-invasive role in melanoma, but only 16 of them were identified with a negative impact in survival in patients with melanoma. When we classified the group of patients with melanoma tumors in different populations displaying either High or Low RIDD and XBP1s activity we observed interesting findings. A strong correlation between the low expression levels of these genes in melanoma tumors and a high RIDD activity was observed, suggesting the possibility that these mRNAs could be RIDD targets. Tumors exhibiting high RIDD activity correlated with lower expression levels of at least nine genes associated with melanoma metastasis.

Interestingly, one of these genes was PRKCA that codifies for PKC $\alpha$ . As we mentioned before, IRE1-dependent FLNA phosphorylation is mediated by PKC $\alpha$  (93). Thus, the possibility that in metastatic melanoma cells PKC $\alpha$  is degraded by IRE1/RIDD activity could explain why in our metastatic cell lines we do not observe an induction of FLNA phosphorylation in S2152 dependent of IRE1 and we have an increase in cell migration and invasion with IRE1 depletion. Supporting this, another member of the PKC $\alpha$  family has already been identified as a RIDD target. Oikawa et al., combining an *in vitro* cleavage assay with microarray analysis, identified a

consensus sequence accompanied by a stem-loop structure present in 13 novel targets, between them PKC $\delta$  (205).

Since the 1980s, PKC $\alpha$  was identified as a protein involved in the carcinogenesis of skin tumors (206), a connection that has been studied deeply in the last years. The evidence available indicates that in melanoma progression, PKC $\alpha$  is mainly implicated with an increase of cell migration, invasiveness, and a de-differentiation (191, 207-211). For instance, data obtained in melanoma cells showed that cell motility is derived by a PKC $\alpha$ /JNK-dependent mechanism (207). Importantly, in another study where PKC $\alpha$  was found as a protein involved in melanoma metastasis, expression levels of this protein were significantly higher in metastatic melanoma compared with primary melanoma tumors. The dependence of PKC $\alpha$  for cell migration/invasion in metastatic melanoma cells could be higher than in non-metastatic cells (191). These results support our new hypothesis since, in our model, IRE1 regulates cell migration/invasion only in the metastatic cell lines.

Another interesting target gene that was found in our analysis was ROBO1 that codes for the transmembrane receptor Roundabout receptor (Robo1). Activated signaling of slit glycoprotein (Slit)/Robo1 plays an important role in angiogenesis and cell migration, and have been described to be involved in physiological and pathological processes, including cancer (reviewed in (212)). Robo1 is highly expressed in tumor cells, and its role in metastasis have been documented in different types of cancer such as colorectal carcinoma, glioblastoma and hepatocellular carcinoma (213-215). Importantly, analysis of the expression profile of melanoma tumors identified Robo1 as a marker that predict progression to metastasis (216).

In addition, between the possible RIDD targets we found the TARDBP gene, that codes for the transactive response DNA-binding protein-43 (TDP-43), a ribonucleoprotein able to bind DNA and RNA molecules. This protein has been proposed as a therapeutic target for cancer, since regulates cell proliferation, migration and invasion of tumor cells (217, 218). Also, TDP-43 have been identified as an oncogene in melanoma, regulating proliferation and metastasis potentially through modulation of glucose metabolism (219). Interestingly, mutation of TDP-43 have been associated with alteration in the UPR machinery in affected neurons (220).

In summary, **IRE1, possibly mediated by RIDD, may be an important suppressor of cell migration and invasion in melanoma cells**, and exerts this effect through a mechanism only relevant in cells with high metastatic potential. Importantly, the IRE1-dependent suppression of cell migration, and possibly also invasion, could be mediated by RIDD activity through the degradation of mRNAs of oncogenes associated with the metastatic process in melanoma, such as PKC $\alpha$ , Robo1 and TDP-43. However, future experiments are needed to confirm our candidates.

Our results indicate that IRE1 RNase activity inhibition by specific drugs increase cell migration. Several reports indicate that targeting IRE1 activity affects cancer progression in different models of multiple myeloma, breast and ovarian cancer, and glioblastoma (107, 108, 139, 221-223). This suggests that IRE1 inhibition might be a suitable target for these types of tumors. The first model where IRE1 activity inhibition was evaluated was multiple myeloma. It is known that malignant plasma cells depend on IRE1/XBP1 signaling to cope with the high demand in protein secretion, and treatment with RNase inhibitors like 4 $\mu$ 8C and

MKC-2946 have shown to significantly inhibit tumor growth (107, 108). Also, in a xenograft mouse model of TNBC, inhibition of IRE1 activity by MKC- increased paclitaxel and tamoxifen-mediated tumor suppression (221, 222). Nevertheless, based in our results targeting IRE1 RNase activity might not be the best option in melanoma since it might have adverse effects by promoting migration/invasion and perhaps metastasis.

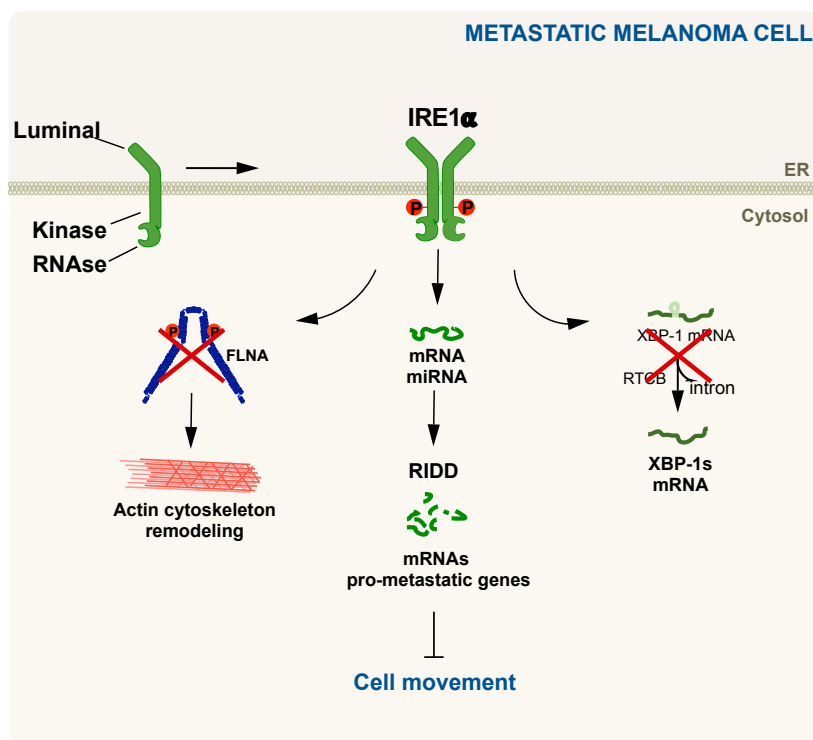


**Figure 34. Regulation of melanoma cell movement by the IRE1 and RIDD axis: Proposed model.**

Tumor cells are exposed to several intrinsic and extrinsic perturbations that can alter the proper functioning of the endoplasmic reticulum (ER), altering protein homeostasis, and engages unfolded protein response (UPR). IRE1 signaling, the most evolutionary conserved sensor from the UPR, presents a basal activation in melanoma cells favoring autophagy and cell death resistance (111, 113). Our results showed that in metastatic melanoma cells, the IRE1 branch, particularly mediated by the RIDD activity, degrade mRNAs that code for oncogenes associated with pro-migratory and pro-invasive properties in melanoma, inhibiting cell movement. However, the role of the IRE1/RIDD axis in the metastatic process in melanoma is still unknown and needs to be evaluated deeper.

## 11. CONCLUSIONS.

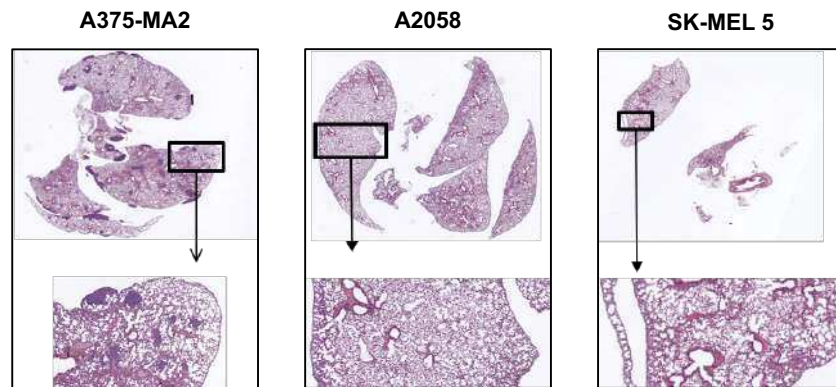
This thesis uncovered a novel function of IRE1 in the regulation of human metastatic melanoma cell migration through an RNase activity-dependent mechanism. The results obtained are the first evidence showing a role of IRE1 in metastasis-related processes in melanoma cells, such as cell migration and invasion. The most relevant results obtained lead us to conclude that:

- By using genetic approaches, we found that deficiency of IRE1 expression enhances cell migration and invasion of human metastatic melanoma cell lines, indicating that the IRE1 branch could be acting as a suppressor of cell migration and invasion in metastatic melanoma cells.
- Opposite to what we initially proposed, our results indicate that regulation of cell migration and invasion by IRE1 in melanoma cells is a FLNA-independent process.
- Specific pharmacological inhibition of the IRE1 RNase activity showed that the RNase activity is required for IRE1-dependent suppression of cell migration in metastatic melanoma cells. Since overexpression of XBP1s does not affect cell migration, we postulate RIDD as the major mechanism involved in the suppressor function of IRE1. We identified several pro-metastatic mRNAs that could be target of RIDD as a possible mechanism for the regulation of migration and invasion in metastatic melanoma cells.

In summary, this Ph.D. thesis has uncovered a novel role of IRE1 as a suppressor of cell movement in human metastatic melanoma cells, *in vitro*, where the RNase activity mediated by RIDD operates a mechanism that degrades pro-metastatic genes in melanoma.

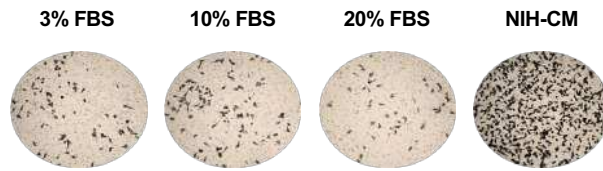


## 12. SUPPLEMENTARY FIGURES.



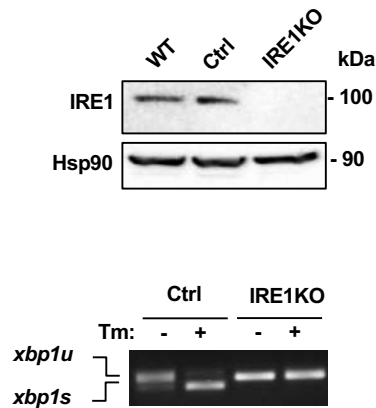
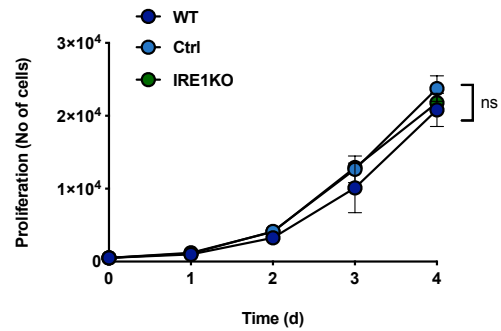
**Supplementary Figure 1. Standardization of metastatic lung model by tail vein injection using human metastatic cell lines.**

Twenty-five thousand cells of A375-MA2, A2058, or SK-MEL 5 were re-suspended in 500  $\mu$ L saline solution (0.9% NaCl) and injected intravenously into eight-weeks old male NSG mice. At day 28 post-inoculation, lungs were collected and fixed with PFA 4% and processed for immunohistochemistry and stained with H&E. Pictures represents 1 independent experiment and 1 mouse per condition.



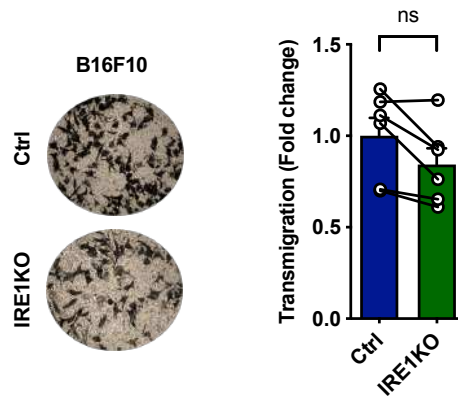
**Supplementary Figure 2. Standardization of the transmigration assay.**

B16F10 mouse melanoma cells ( $2 \times 10^4$ ) were plated on Fibronectin-coated transwell plates. Transmigration was assessed in the presence of FBS, or NIH 3T3 conditioned medium (NIH-CM). After 6h, cells that migrated to the lower side were stained with crystal violet. Images of the lower side of the transwell were taken. Data represent 1 experiment.

**A****B**

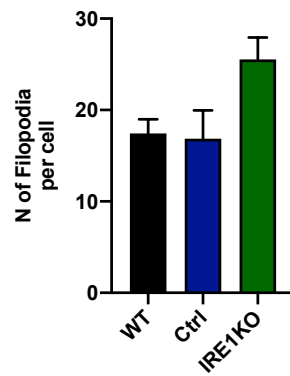
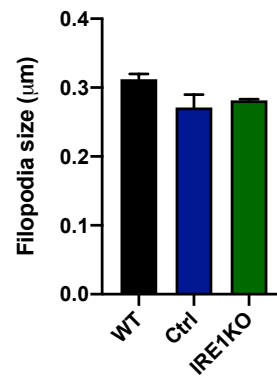
### Supplementary Figure 3. Characterization of IRE1KO B16F10 cells.

IRE1KO B16F10 cells were generated using CRISPR/Cas9 technology. **(A) Top panel:** The levels of IRE1 in the WT, Control, and IRE1KO B16F10 were evaluated by western blot using a specific antibody against IRE1 and HSP90. **Bottom panel:** WT, Control, and IRE1 KO B16F10 cells were treated with 500 ng/mL of Tm for 8h, and then XBP1 mRNA splicing was evaluated by RT-PCR. PCR fragments corresponding to the XBP1u or XBP1s forms of XBP1 mRNA are indicated. **(B)** Viable WT, Control, and IRE1KO B16F10 were counted for four days to generate the growth curves. The cells were stained with 200 ng/mL of Hoechst and counted on an ArrayScan XTI Live High Content Platform. Results were statistically compared using two-way ANOVA followed by Bonferroni's multiple comparisons test. (ns: not statistically significant).

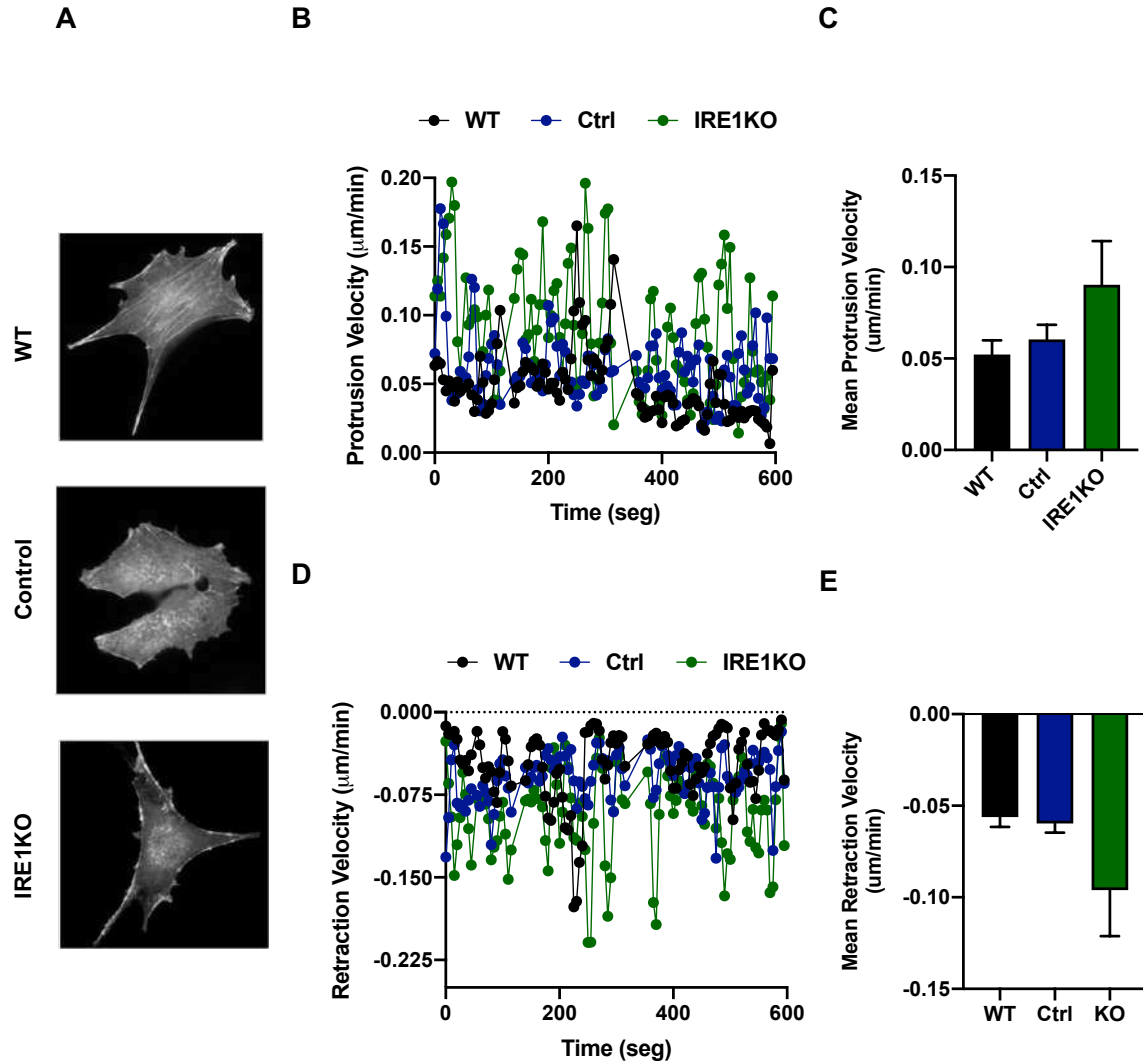


**Supplementary Figure 4. IRE1 deficiency do not affect cell migration in a mouse metastatic melanoma cell line.**

**Left panel:** Control and IRE1KO B16F10 cells were seeded on fibronectin-coated transwell plates, and transmigration was assessed. The conditioned medium from NIH 3T3 was used as a chemoattractant. After 6h, cells that migrated to the lower side were stained with crystal violet. Images of the lower side of the transwell were taken. **Right panel:** The number of cells that invaded was counted using the ImageJ software. Data represent the mean  $\pm$  s.e.m of 6 independent experiments. Results were statistically compared using a two-tailed t-test. (ns: not statistically significant).

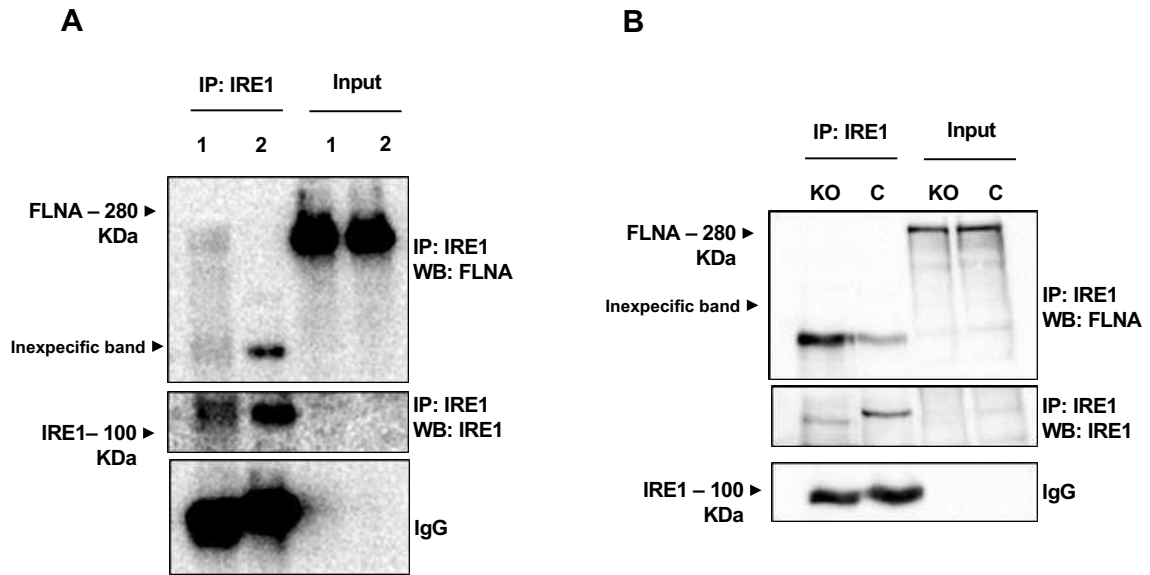
**A****B****Supplementary Figure 5. IRE1 deficiency increase filopodia formation.**

WT, Control and IRE1KO B16F10 cells were transiently transfected with a plasmid coding for the fluorescent protein Life-Act. Cells were plated onto fibronectin coated plates and recorded by time-lapse confocal microscopy every 30 s for 5 min. **(A)** The number of filopodia per cell **(B)** and the filopodia size **(C)** was determined using ADAPT software. Data represents the mean  $\pm$  s.e.m of 2 independent experiments.



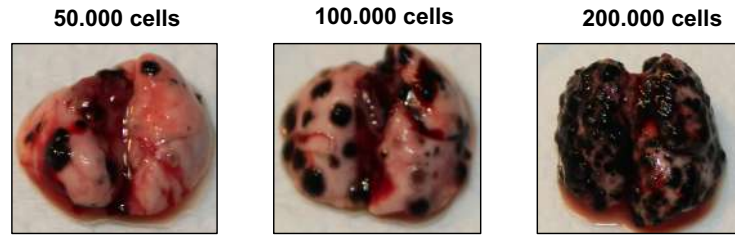
**Supplementary Figure 6. IRE1 deficiency increase actin cytoskeleton dynamics in mouse metastatic melanoma cells.**

(A) WT, Control, and IRE1KO B16F10 cells were transiently transfected with a plasmid coding for the fluorescent protein Life-Act. Cells were plated onto fibronectin-coated plates and recorded by time-lapse confocal microscopy every 30 s for 5 min. Representative images are shown. Segmentation was used to obtain protruding areas and retracting areas. The velocity of protrusions (B) and retractions (C) and the average signal overtime of the protruding cell area (D) or the retracting cell area (E) were determined. Data represent the mean  $\pm$  s.e.m of 2 independent experiments



**Supplementary Figure 7. Evaluation of IRE1 and FLNA complexes in melanoma cells.**

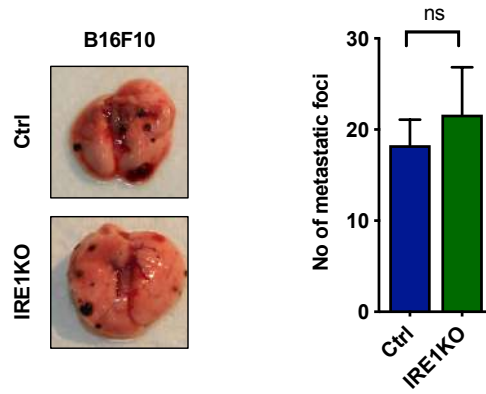
Endogenous interaction between FLNA and IRE1 was analyzed after IRE1 immunoprecipitation in SK-MEL5 (**A**) and B16F10 (**B**) cells. A Rabbit heavy chain Ac (**A**) or IRE1KO cells (**B**) were used as controls. IgG is shown as a control for the IP. Data represents the analysis of one independent experiment for each cell line. (A) 1: Rabbit Ac Control; 2: Rabbit Ac anti IRE1. (B) KO: IRE1KO cells; C: IRE1 expressing cells, control.



**Supplementary Figure 8. Standardization of B16F10 metastatic lung model by tail vein injection.**

Different amounts of B16F10 parental cells were re-suspended in 500  $\mu$ L saline solution (0.9% NaCl) and injected intravenously into 8-12 weeks old C57BL/6 mice. At day 21, post-inoculation, lungs were collected and fixed with Fekete's solution. Pictures of the lungs were taken, and representative images are shown. Data represents 1 independent experiment and 1 mouse per condition.





**Supplementary Figure 9. The formation of lung metastasis in a metastatic melanoma model is independent of IRE1 expression.**

**Left panel:** Control and IRE1KO B16F10 cells ( $1 \times 10^5$ ) were re-suspended in 500  $\mu$ l saline solution (0.9% NaCl) and injected intravenously in 8-12 weeks old C57BL/6 mice. At day 21, post-inoculation, lungs were collected and fixed with Fekete's solution. Pictures of the lungs were taken, and representative images are shown. **Right panel:** The number of metastatic nodules was quantified using the ImageJ software. Data represent the mean  $\pm$  s.e.m of at least 1 independent experiment and at least 7 mice per condition. Results were statistically compared using a two-tailed t-test. (ns: not statistically significant).

## 13. PUBLICATIONS

### 13.1. *IRE1 $\alpha$ controls cytoskeleton remodeling and cell migration through a direct interaction with Filamin A.*

*Nat Cell Biol. 2018 Aug;20(8):942-953.*

#### 13.1.1. **Foreword**

In this paper, we characterized a novel mechanism underlying IRE1 function, where this protein acts as a scaffold to recruit FLNA and increases its phosphorylation at serine 2152, enhancing cell migration. We have used an interactome screening to identify FLNA as a major IRE1-binding partner. FLNA is an actin-crosslinking protein involved in cytoskeleton remodeling and cell migration. The activity of FLNA in cytoskeleton dynamics depends on its phosphorylation at serine 2152, and our results indicate that IRE1 facilitates FLNA phosphorylation to control actin cytoskeleton and cell migration through PKC $\alpha$ . Remarkably, this new IRE1-function in cell migration was independent of IRE1 enzymatic activities but required its dimerization. Besides fibroblasts, this was also observed in various *in vivo* models such as zebrafish, drosophila, and mouse models, suggesting a conserved mechanism in evolution.

#### 13.1.2. **Contribution**

The author of this thesis participated in the experimental design, conducted experiments, and analyzed the data of a siRNA screening that suggested a possible role of IRE1 in tumor cell migration. This experiment was performed with six cell lines originated from different types of tumors and cell migration was analyzed by performing transmigration assays. She also evaluated the contribution of PERK in

cell migration by inhibiting its activity with GSK2606414. The results obtained from this experiment suggested that the effects of IRE1 in cell migration were independent of PERK signaling. She also collaborated in the execution of other experiments and the final revision of the manuscript.

# IRE1 $\alpha$ governs cytoskeleton remodelling and cell migration through a direct interaction with filamin A

Hery Urra<sup>1,2,3</sup>, Daniel R. Henriquez<sup>2,4</sup>, José Cánovas<sup>1</sup>, David Villarroel-Campos<sup>2,4</sup>, Amado Carreras-Sureda<sup>1,2,3</sup>, Eduardo Pulgar<sup>1,5</sup>, Emiliano Molina<sup>4,6</sup>, Younis M. Hazari<sup>1,2,3</sup>, Celia M. Limia<sup>1,2,3</sup>, Sebastián Alvarez-Rojas<sup>2,4</sup>, Ricardo Figueroa<sup>1,3</sup>, Rene L. Vidal<sup>1,2,7</sup>, Diego A. Rodriguez<sup>3</sup>, Claudia A. Rivera<sup>1,2,7</sup>, Felipe A. Court<sup>2,7</sup>, Andrés Couve<sup>1,8</sup>, Ling Qi<sup>9</sup>, Eric Chevet<sup>10,11</sup>, Ryoko Akai<sup>12</sup>, Takao Iwawaki<sup>12</sup>, Miguel L. Concha<sup>1,2,5</sup>, Álvaro Glavic<sup>4,6</sup>, Christian Gonzalez-Billault<sup>2,4</sup> and Claudio Hetz<sup>1,2,3,13,14\*</sup>

**Maintenance of endoplasmic reticulum (ER) proteostasis is controlled by a signalling network known as the unfolded protein response (UPR). Here, we identified filamin A as a major binding partner of the ER stress transducer IRE1 $\alpha$ . Filamin A is an actin crosslinking factor involved in cytoskeleton remodelling. We show that IRE1 $\alpha$  controls actin cytoskeleton dynamics and affects cell migration upstream of filamin A. The regulation of cytoskeleton dynamics by IRE1 $\alpha$  is independent of its canonical role as a UPR mediator, serving instead as a scaffold that recruits and regulates filamin A. Targeting IRE1 $\alpha$  expression in mice affected normal brain development, generating a phenotype resembling periventricular heterotopia, a disease linked to the loss of function of filamin A. IRE1 $\alpha$  also modulated cell movement and cytoskeleton dynamics in fly and zebrafish models. This study unveils an unanticipated biological function of IRE1 $\alpha$  in cell migration, whereby filamin A operates as an interphase between the UPR and the actin cytoskeleton.**

The ER is the largest intracellular organelle and is involved in protein synthesis, folding and secretion. A series of physiological and pathological conditions favour the accumulation of misfolded proteins at the ER lumen, resulting in a cellular state known as ER stress<sup>1</sup>. To cope with misfolded proteins, cells engage a dynamic signalling pathway known as the UPR<sup>2</sup>. In vertebrates, the UPR has evolved towards the establishment of a network of interconnected signalling cascades initiated by three types of transducers known as inositol-requiring enzyme 1 (IRE1) alpha and beta, activating transcription factor-6 (ATF6) alpha and beta, and protein kinase RNA (PKR)-like ER kinase (PERK). The UPR controls specific transcription factors that feedback to restore proteostasis<sup>1</sup> or activate apoptotic programmes<sup>3</sup>. ER stress is also emerging as a relevant factor driving diverse pathological conditions, including cancer, diabetes, inflammatory diseases and neurodegeneration<sup>4,5</sup>.

IRE1 $\alpha$  is a serine/threonine protein kinase and endoribonuclease that catalyses the unconventional processing of the messenger RNA encoding X-box binding protein 1 (XBP1), resulting in the expression of an active transcription factor (XBP1s) that enforces adaptation programmes<sup>6,7</sup>. In addition to the classical role of IRE1 $\alpha$  as

an ER stress mediator, a series of novel physiological outputs of the pathway have been reported that are dependent on XBP1s and affect cell differentiation, angiogenesis and energy metabolism<sup>2</sup>. IRE1 $\alpha$  signalling is tightly regulated by the assembly of protein complexes that fine-tune its activity, a platform referred to as the UPRosome<sup>8</sup>. Thus, defining the IRE1 $\alpha$  interactome may reveal unexpected functions to delineate the significance of the UPR in cell physiology.

Here, we performed a protein–protein interaction screen and identified filamin A as a major IRE1 $\alpha$  binding partner. Filamin A is involved in crosslinking polymerized actin and has a crucial role in adhesion, cell morphology and migration<sup>9</sup>. We demonstrate that the IRE1 $\alpha$ –filamin A axis regulates actin cytoskeleton dynamics and cell movement. Unexpectedly, this function of IRE1 $\alpha$  is controlled by its dimerization, independent of its canonical signalling as a UPR mediator. We also provide evidence indicating that the regulation of cell migration by IRE1 $\alpha$  is disease relevant and evolutionarily conserved. Overall, our results reveal an unanticipated site of control of actin cytoskeleton dynamics from the ER, where IRE1 $\alpha$  serves as a scaffold to engage filamin A signalling and modulate cell movement.

<sup>1</sup>Biomedical Neuroscience Institute, Faculty of Medicine, University of Chile, Santiago, Chile. <sup>2</sup>Center for Geroscience, Brain Health and Metabolism (GERO), Santiago, Chile. <sup>3</sup>Program of Cellular and Molecular Biology, Institute of Biomedical Sciences, University of Chile, Santiago, Chile. <sup>4</sup>Department of Biology, Faculty of Sciences, University of Chile, Santiago, Chile. <sup>5</sup>Program of Anatomy and Developmental Biology, Institute of Biomedical Sciences, University of Chile, Santiago, Chile. <sup>6</sup>Center for Genome Regulation, Faculty of Sciences, University of Chile, Santiago, Chile. <sup>7</sup>Center for Integrative Biology, Faculty of Sciences, Universidad Mayor, Santiago, Chile. <sup>8</sup>Department of Neuroscience, Faculty of Medicine, University of Chile, Santiago, Chile. <sup>9</sup>Department of Molecular and Integrative Physiology, Division of Metabolism, Endocrinology and Diabetes, The University of Michigan Medical School, Ann Arbor, MI, USA. <sup>10</sup>INSERM U1242 Chemistry, Oncogenesis, Stress and Signaling, University of Rennes 1, Rennes, France. <sup>11</sup>Centre de Lutte contre le Cancer Eugène Marquis, Rennes, France. <sup>12</sup>Division of Cell Medicine, Department of Life Science, Medical Research Institute, Kanazawa Medical University, Uchinada, Japan. <sup>13</sup>The Buck Institute for Research in Aging, Novato, CA, USA. <sup>14</sup>Department of Immunology and Infectious Diseases, Harvard School of Public Health, Boston, MA, USA. \*e-mail: [chetz@med.uchile.cl](mailto:chetz@med.uchile.cl)

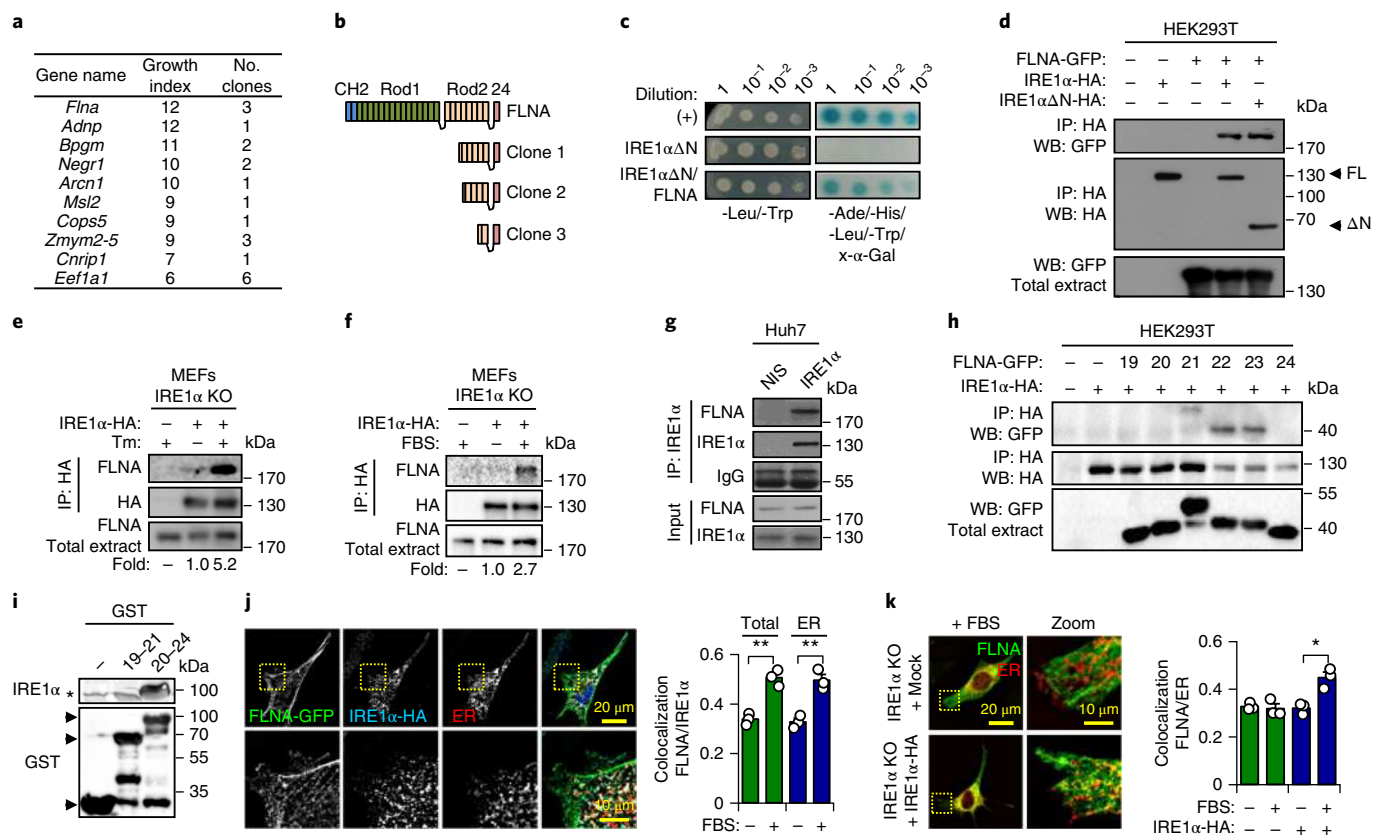


**Fig. 1 | IRE1 $\alpha$  physically interacts with filamin A.** **a**, Results of the yeast two-hybrid screen of the cytosolic domain of IRE1 $\alpha$  and the Matchmaker pretransformed cDNA library from adult mouse brain. The yeast growth index and the number of clones obtained are indicated. **b**, Representation of the primary structure of filamin A (FLNA) and the clones obtained in **a**. The CH2, Rod1, Rod2 and the IgG 24 domains are shown. **c**, Validation of the yeast two-hybrid assay using IRE1 $\alpha$ - $\Delta$ N and wild-type filamin A. (+), positive control for the assay. Data show one out of three experiments, with similar results obtained. **d**, Co-immunoprecipitation (IP) of HA-tagged IRE1 $\alpha$  full length (FL) or the cytosolic portion of IRE1 $\alpha$  ( $\Delta$ N) and GFP-tagged filamin A was assessed by western blotting (WB) using HEK293T cells. **e**, Co-immunoprecipitation of HA-tagged IRE1 $\alpha$  and endogenous filamin A in IRE1 $\alpha$  knockout (KO) MEFs reconstituted with an IRE1 $\alpha$ -HA expression vector in cells treated with 500 ng ml<sup>-1</sup> of tunicamycin (Tm) for 2 h. **f**, Co-immunoprecipitation of starved cells described in **e** treated with 3% FBS for 30 min. **g**, Co-immunoprecipitation of endogenous filamin A and IRE1 $\alpha$  in Huh7 cells. A non-immune serum (NIS) was used as a control. **h**, Co-immunoprecipitation of HA-tagged IRE1 $\alpha$  and individual domains of GFP-tagged filamin A in HEK293T cells. **i**, In vitro pull-down of recombinant GST-fused domains of filamin A (19-21 and 21-24) and recombinant cytosolic IRE1 $\alpha$  portion (IRE1 $\alpha$ - $\Delta$ N) (asterisk indicates nonspecific band). **j**, Left, immunofluorescence images of MEFs expressing filamin A-GFP, IRE1 $\alpha$ -HA and KDEL-RFP stimulated with 3% FBS for 30 min. Right, colocalization results of IRE1 $\alpha$ -HA and filamin A-GFP restricted to the ER or total area ( $n=3$  independent experiments, 50 cells in total). **k**, Left, confocal images of CRISPR-Cas9 IRE1 $\alpha$  KO cells or reconstituted with IRE1 $\alpha$ -HA expressing filamin A-GFP and KDEL-RFP, stimulated with 3% FBS for 60 min. Right, colocalization results of filamin A-GFP and KDEL-RFP ( $n=3$  independent experiments, 50 cells in total). In panels **j** and **k** the area with higher magnification is shown (yellow squares). In all panels, data are shown as the mean  $\pm$  s.e.m.; one-way ANOVA followed by Tukey's test. \* $P < 0.05$  and \*\* $P < 0.01$ . Blots represent one out of two (**f**), three (**d, e, g, i**) or four (**h**) experiments, with similar results obtained.

## Results

**Direct interaction between filamin A and IRE1 $\alpha$ .** To identify new IRE1 $\alpha$ -interacting proteins we performed a yeast two-hybrid screen using the Matchmaker pretransformed complementary DNA library together with the cytosolic domain of IRE1 $\alpha$  (IRE1 $\alpha$ - $\Delta$ N) as bait. Multiple candidates were found (Supplementary Table 1) to be involved in different biological processes (Supplementary Fig. 1A,B), including COPS5, a known IRE1 $\alpha$  binding partner<sup>10</sup>. Among the top ten candidates selected on the basis of the growth index, filamin A presented the strongest interaction (Fig. 1a). Filamin A is an actin-binding protein involved in the orthogonal crosslinking of polymerized actin<sup>9</sup>. It is composed of 24 IgG-like repeats, containing several domains including the CH2 domain, Rod1 and Rod2, and an IgG-like 24 repeat involved in filamin A dimerization<sup>11</sup>. All clones selected corresponded to the carboxy-terminal portion of filamin A (Fig. 1b,c).

To validate our findings, we transfected HEK293T cells with expression vectors for full-length HA (human influenza hemagglutinin)-tagged IRE1 $\alpha$  (IRE1 $\alpha$ -HA) and a filamin A construct fused to green fluorescent protein (GFP) at the C-terminal region (filamin A-GFP). Immunoprecipitation of IRE1 $\alpha$ -HA revealed a clear association of filamin A with the cytosolic domain of IRE1 $\alpha$  (Fig. 1d). Additionally, we detected an association between IRE1 $\alpha$ -HA and endogenous filamin A in IRE1 $\alpha$  knockout mouse embryonic fibroblasts (MEFs) reconstituted with physiological levels of IRE1 $\alpha$ <sup>12</sup> (Fig. 1e; see controls in Supplementary Fig. 1C). Interestingly, this interaction was enhanced under ER stress induced by tunicamycin, a pharmacological inhibitor of N-linked glycosylation (Fig. 1e), or with fetal bovine serum (FBS), a pro-migratory stimulus (Fig. 1f). We also corroborated the existence of an endogenous protein complex in Huh7 cells (Fig. 1g). Using individual IgG-like repeats of filamin A, we demonstrated that domains 22–23

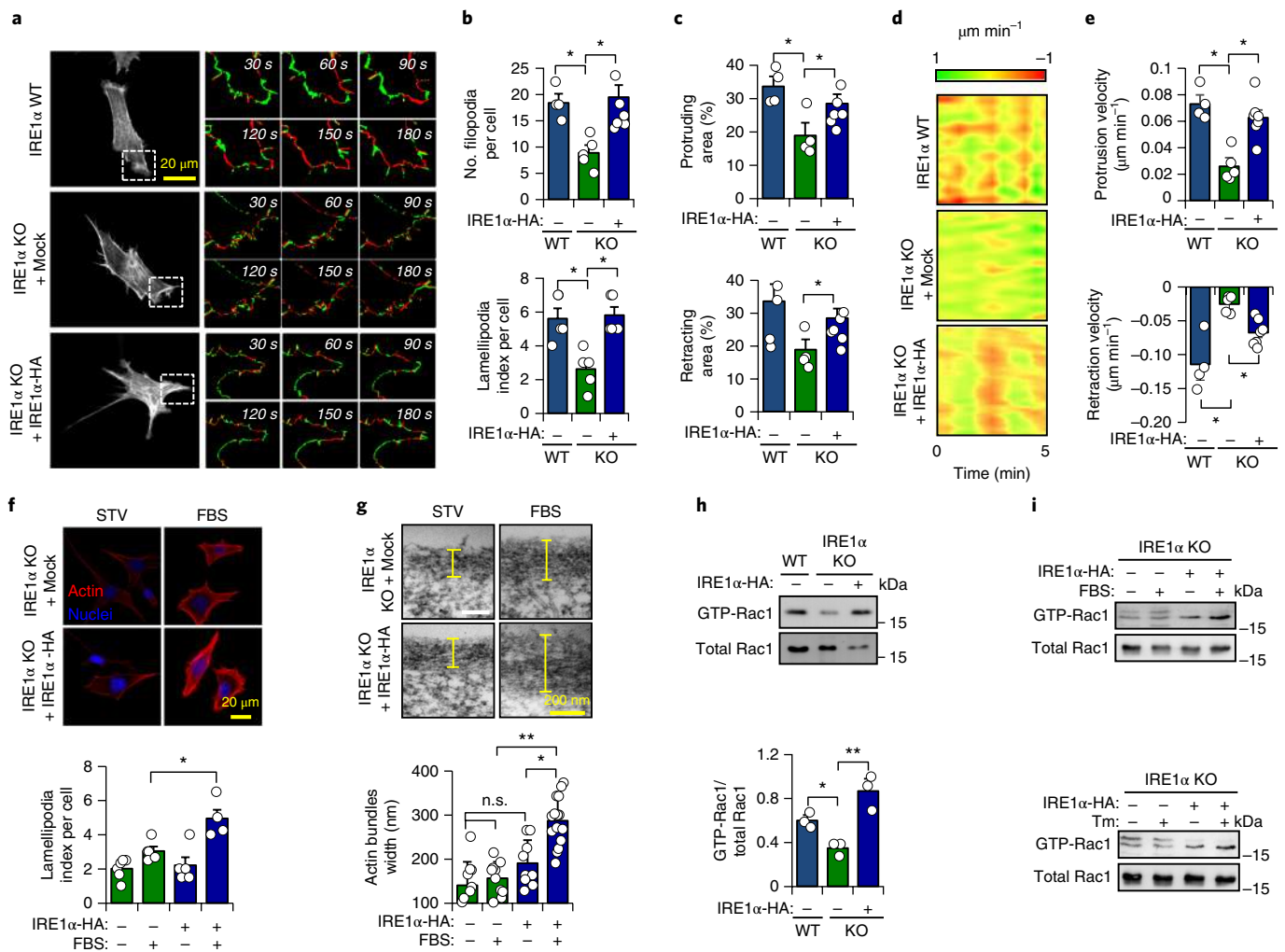


**Fig. 2 | IRE1 $\alpha$  regulates actin cytoskeleton dynamics and Rac1 activation.** **a**, WT, IRE1 $\alpha$  KO or IRE1 $\alpha$ -HA-reconstituted cells were transfected with LifeAct and time-lapse confocal microscopy recordings were made every 30 s for 5 min. Segmentation was used to obtain protruding area (green) and retracting areas (red). Regions in dotted white squares are magnified in time-lapse images on the right. **b**, Top, the number of filopodia per cell was determined using ADAPT software. Bottom, the number of octants showing lamellipodia was evaluated per cell. **c**, The average signal over time of the protruding cell area or the retracting cell area was quantified from experiments presented in **a**. **d**, Heatmaps of LifeAct signal distribution along the cell determined by ADAPT software. **e**, The velocity of protrusions and retractions. For **b–e**,  $n=5$ ,  $n=5$  and  $n=7$  independent experiments were determined for WT, IRE1 $\alpha$  KO and IRE1 $\alpha$ -HA, respectively. **f**, Top, IRE1 $\alpha$  KO and IRE1 $\alpha$ -HA-reconstituted cells were starved (STV) and then stimulated with 3% FBS for 30 min and stained with phalloidin-coupled to rodamine. Bottom, quantification of lamellipodia index per cell as described in **b** ( $n=3$  independent experiments). **g**, Top, electron microscopy sections of cortical actin (bundles) in IRE1 $\alpha$  KO and IRE1 $\alpha$ -HA-reconstituted cells treated with 3% FBS for 30 min ( $\times 67,000$  magnification). Bottom, quantification of width (yellow bars above) of actin bundles ( $n=3$ , 10 cells in total). **h**, Top, pull-down assay using GST-CRIB domain followed by western blot analysis to evaluate Rac1 activation of WT, IRE1 $\alpha$  KO and IRE1 $\alpha$ -HA-reconstituted cells. Bottom, Rac1-GTP levels were quantified and normalized to total Rac1 ( $n=4$  independent experiments). **i**, IRE1 $\alpha$  KO and IRE1 $\alpha$ -HA-reconstituted cells were treated with 3% FBS for 1 h (top) or 100 ng ml $^{-1}$  of Tm for 2 h (bottom). Rac1-GTP levels were evaluated by a pull-down assay using GST-CRIB domain followed by western blot analysis (data represent one out of three experiments, with similar results obtained). In all panels, data are shown as the mean  $\pm$  s.e.m.; one-way ANOVA followed by Tukey's test. n.s., not significant, \* $P < 0.05$  and \*\* $P < 0.01$ .

account for the interaction with IRE1 $\alpha$  (Fig. 1h). These domains are central to the interaction with several signalling proteins, but they are unrelated to its ability to associate with polymerized actin<sup>9</sup>. Finally, using recombinant proteins, we replicated the direct binding of IRE1 $\alpha$  to a fragment of filamin A spanning the 20–24 IgG-like repeat region, but not to the adjacent domain (Fig. 1i).

Quantification of colocalization using the Manders coefficient between IRE1 $\alpha$ -HA and filamin A-GFP showed an enhanced association after stimulation of cells with FBS. Similar results were obtained when the analysis was confined to the ER (KDEL-RFP signal) (Fig. 1j), suggesting that filamin A relocates to the ER in close proximity to IRE1 $\alpha$ . Importantly, the redistribution of filamin A to

the ER was dependent on the expression of IRE1 $\alpha$  (Fig. 1k). Taken together, these results indicate that filamin A interacts directly with IRE1 $\alpha$  at the ER in multiple cellular systems.

**IRE1 $\alpha$  controls the dynamics of the actin cytoskeleton.** Since filamin A has an active role in modulating morphological changes through local actin cytoskeleton remodelling<sup>13</sup>, we tested the contribution of IRE1 $\alpha$  to this process. We monitored actin cytoskeleton dynamics using LifeAct<sup>14</sup>. Time-lapse confocal microscopy of IRE1 $\alpha$ -deficient cells revealed a reduced number of filopodia and lamellipodial protrusions (lamellipodia index) per cell (Fig. 2a,b; Supplementary Movie 1). In addition, the temporal dynamics



of cortical filamentous actin (F-actin), measured by the total area showing protrusions and retractions over time, presented a marked decrease in IRE1 $\alpha$ -deficient cells (Fig. 2a–c; Supplementary Fig. 2A). This observation correlated with an altered distribution of polymerized actin across the cell upon targeting IRE1 $\alpha$  expression (Fig. 2d; Supplementary Fig. 2B). Furthermore, the velocity of protrusions and retractions was dramatically reduced in IRE1 $\alpha$ -null cells (Fig. 2e). For comparison, we also analysed filamin A-deficient cells (Supplementary Fig. 2C). Similar results were obtained when the lamellipodia index was evaluated in fixed cells (Fig. 2f). In addition, electron microscopy analysis of the distribution of cortical actin bundles, a structure highly concentrated in crosslinked actin<sup>13</sup>, indicated a narrower area of actin bundles in IRE1 $\alpha$ -deficient cells (Fig. 2g).

Actin cytoskeleton dynamics is dependent on the activity of small GTPases from the RhoA family<sup>15</sup>. Therefore, we evaluated the activity of Rac1, a RhoA GTPase that mediates the formation of actin protrusions in different cell types<sup>15</sup> and is regulated by filamin A<sup>16</sup>. The amount of active Rac1 coupled to GTP was decreased in IRE1 $\alpha$ -null cells as determined using pull-down assays with the recombinant CRIB1 domain (amino acids 67–150) of p21-activated kinase (PAK1) as bait (Fig. 2h). Remarkably, stimulation with FBS or ER stress enhanced the activation of Rac1 in an IRE1 $\alpha$ -dependent manner (Fig. 2i). These results indicate that IRE1 $\alpha$  expression modulates actin cytoskeleton dynamics and Rac1 activation.

**IRE1 $\alpha$  deficiency impairs cell migration.** We then determined whether IRE1 $\alpha$  regulates cell movement as a readout of cytoskeleton alterations. Stimulation of IRE1 $\alpha$  knockout cells with FBS revealed a significant decrease in cell migration in wound-healing assays compared to control cells (Fig. 3a). Similar results were obtained when transmigration was evaluated using the Boyden chamber assay (Fig. 3b). As a control, we measured cell proliferation, a parameter that was not modified in IRE1 $\alpha$ -null cells (Supplementary Fig. 3A). Importantly, filamin A (*Flna*) knockout MEFs presented a similar extent of cell movement impairment as IRE1 $\alpha$ -deficient cells (Fig. 3b; Supplementary Fig. 3B). Targeting IRE1 $\alpha$  expression using short hairpin RNAs (shRNAs) or via clustered regularly interspaced short palindromic repeats (CRISPR)–Cas9 also led to a significant attenuation of cell migration in MEFs (Fig. 3c,d). Notably, targeting IRE1 $\alpha$  expression affected cell movement in different cell lines (Fig. 3e; Supplementary Figs. 3C, and 8A). Finally, transient overexpression of IRE1 $\alpha$ -HA in wild-type MEFs also enhanced cell migration (Supplementary Fig. 3D).

We next investigated whether filamin A is involved in the regulation of cell movement by IRE1 $\alpha$ . Remarkably, the impairment of cell movement generated by knocking down IRE1 $\alpha$  was reversed by the overexpression of filamin A (Fig. 3f; Supplementary Fig. 3E). In sharp contrast, overexpression of IRE1 $\alpha$  failed to enhance cell migration in filamin A-null cells (Fig. 3g; Supplementary Fig. 3F). Thus, IRE1 $\alpha$  requires filamin A to regulate cell migration. In addition, as reported in filamin A-null cells<sup>17,18</sup>, IRE1 $\alpha$  deficiency led to decreased ER and cell spreading upon attachment (Fig. 3h) and reduced cell adhesion (Fig. 3i).

Recently, it was described that PERK interacts with filamin A, affecting actin localization and the formation of ER–plasma membrane contact sites<sup>19</sup>. Thus, we determined the contribution of other UPR signalling branches to cell movement. Knocking down PERK or inhibiting it with GSK2606414 reduced cell migration with a similar ratio in both IRE1 $\alpha$ -null and control cells (Supplementary Fig. 3G,H). This result suggests that the effects of IRE1 $\alpha$  in cell migration are independent of PERK signalling. In contrast, knocking down ATF6 did not affect cell migration in MEFs (Supplementary Fig. 3I).

**IRE1 $\alpha$  regulates cell migration by interacting with filamin A.** An analysis of the primary sequence of IRE1 $\alpha$  indicated the presence of

a proline-rich domain at the distal C-terminal region that is similar to a SH3-binding domain (XXPXXP or PXXPX) but of unknown function and structure<sup>20</sup> (Fig. 4a). Although filamin A does not contain an SH3 domain, it associates with several proteins containing proline-rich sequences<sup>11</sup>. We performed a pull-down assay using a region containing the proline-rich portion of IRE1 $\alpha$  (previously named F11<sup>21</sup>) and observed a positive interaction with endogenous filamin A (Fig. 4b) but not with a different IRE1 $\alpha$  region (F6 peptide; Fig. 4c). We repeated the pull-down assay and then performed Coomassie Blue staining and a mass spectrometry analysis to identify the most abundant proteins. Remarkably, filamin A was one of the major F11-binding partners found in this screen (Fig. 4d).

We then tested the contribution of the proline-rich domain of IRE1 $\alpha$  to cell movement. Deletion of the complete F11 sequence abrogated the ability of IRE1 $\alpha$  to enhance cell migration (Fig. 4e). Mutagenesis of the proline-rich domain by deleting the fragment spanning amino acids 965–977 of IRE1 $\alpha$  (IRE1 $\alpha$  $\Delta$ <sup>965</sup>) or by replacing all three proline residues to alanine (IRE1 $\alpha$ <sup>AAAA</sup>) (Fig. 4a) did not affect the RNase activity of IRE1 $\alpha$  (Fig. 4f, bottom panel), but fully blocked the ability of IRE1 $\alpha$  to regulate cell migration (Fig. 4g) and actin cytoskeleton remodelling (Fig. 4h; Supplementary Fig. 4). These experiments fully dissected the activity of IRE1 $\alpha$  on UPR and cell migration. In agreement with these findings, a reduction in the binding between IRE1 $\alpha$  and filamin A was observed when IRE1 $\alpha$  $\Delta$ <sup>965</sup> and IRE1 $\alpha$ <sup>AAAA</sup> mutants were tested (Fig. 4i). We also performed competition experiments using different F11 peptide mutants. The expression of the F11 peptide disrupted the interaction between the filamin A-22 domain and IRE1 $\alpha$ -HA in co-immunoprecipitation experiments, whereas this effect was attenuated by mutations in the proline-rich region (Fig. 4j,k). Overall, our results suggest that the physical interaction between filamin A and IRE1 $\alpha$  is required to enhance cell migration.

**IRE1 $\alpha$  is an upstream regulator of filamin A phosphorylation.**

The activity of filamin A in cytoskeleton dynamics and cell migration depends on the phosphorylation of serine 2,152 (S2152)<sup>11,22</sup>. A robust enhancement of filamin A phosphorylation was detected in cells stimulated with serum in IRE1 $\alpha$ -expressing MEFs compared with knockout cells (Fig. 5a,b). Similarly, stimulation of cells with tunicamycin showed significantly higher filamin A phosphorylation in IRE1 $\alpha$ -expressing cells (Fig. 5a,c). The remaining phosphorylation observed in IRE1 $\alpha$ -deficient cells was independent of PERK, as demonstrated by transfecting cells with small interfering (siRNAs) or by treating cells with GSK2606414 (Supplementary Fig. 5A). We also determined that the fraction of filamin A bound to IRE1 $\alpha$  is phosphorylated in cells stimulated with FBS (Fig. 5d) or tunicamycin (Fig. 5e).

We then determined whether filamin A phosphorylation is required for the modulation of actin cytoskeleton dynamics downstream of IRE1 $\alpha$ . Transient transfection of wild-type filamin A, and not a S2152A mutant, restored the normal levels of actin cytoskeleton dynamics and cell migration observed when IRE1 $\alpha$  was targeted (Fig. 5f,g; Supplementary Fig. 5B–E). In addition, simple overexpression of filamin A resulted in its phosphorylation (Supplementary Fig. 5F), which may explain the ability of this strategy to bypass IRE1 $\alpha$  deficiency. Importantly, deletion of the filamin A-binding domain in IRE1 $\alpha$  led to reduced filamin A phosphorylation (Fig. 5h).

Based on our results, we hypothesized that IRE1 $\alpha$  serves as a scaffold to recruit the kinases involved in filamin A phosphorylation. The most relevant regulators of filamin A are PAK1<sup>16</sup>, CDK4<sup>23</sup>, PKC $\alpha$ <sup>24</sup> and MEKK4<sup>22,25</sup>. A pharmacological screen indicated that PAK1 and PKC $\alpha$  mediated filamin A phosphorylation (Supplementary Fig. 5G). These results were then validated using siRNAs. Knocking down PKC $\alpha$  reduced filamin A phosphorylation under ER stress (Fig. 5i; Supplementary Fig. 5H) and FBS stimulation (Supplementary Fig. 5I). In addition, IRE1 $\alpha$  deficiency

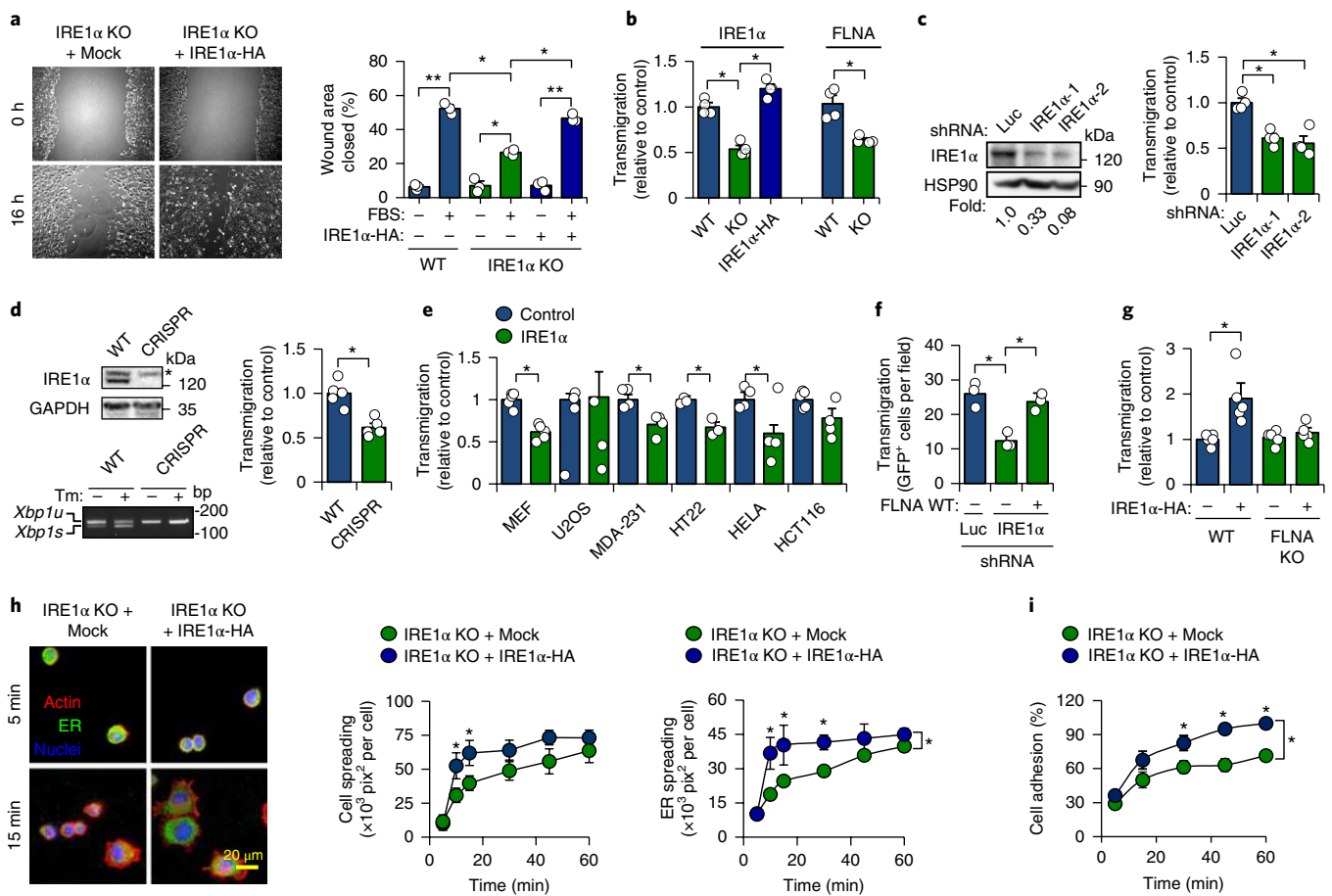


**Fig. 3 | IRE1 $\alpha$  expression enhances cell migration upstream of filamin A.** **a**, Wound-healing assay results of confluent monolayers of WT, IRE1 $\alpha$  KO and IRE1 $\alpha$ -HA-reconstituted cells stimulated with 3% FBS and recorded at 0 and 16 h post-wounding (left) and quantified (right) ( $n=5$  independent experiments). **b**, Transmigration of cells described in **a**, in addition to filamin A WT and KO MEFs using the Boyden chamber assay. After 4 h, cells were stained and counted ( $n=4$  independent experiments). **c**, Knockdown was confirmed by western blotting in MEFs stably expressing two independent IRE1 $\alpha$  shRNAs constructs or control (Luc). The percentage of IRE1 $\alpha$  silencing is indicated. Right, Boyden chamber assay was performed in these cells using fibronectin-coated plates ( $n=3$  independent experiments). **d**, Left, IRE1 $\alpha$  KO MEF cells were generated using CRISPR-Cas9, followed by confirmation using western blotting (asterisk indicates nonspecific band) and *Xbp1* mRNA splicing assays (PCR fragments corresponding to the *Xbp1u* or *Xbp1s* forms are indicated). Right, Boyden chamber assay of control and IRE1 $\alpha$  CRISPR KO cells (two-tailed *t*-test,  $n=3$  independent experiments). **e**, Boyden chamber assay of indicated cell lines transfected with siRNA against IRE1 $\alpha$  or a control siRNA for 48 h (two-tailed *t*-test,  $n=4$ ). **f**, Boyden chamber assay of MEFs expressing control or IRE1 $\alpha$  shRNA transiently transfected with a Myc-tagged filamin A vector or an empty vector followed by quantification of the number of GFP-positive cells in the lower chamber ( $n=3$  independent experiments). **g**, Boyden chamber assay of FLNA WT and KO transiently transfected with pEGFP together with an expression vector for IRE1 $\alpha$ -HA followed by quantification of number of GFP-positive cells in the lower chamber ( $n=4$  independent experiments). **h**, Indirect immunofluorescence of IRE1 $\alpha$  KO and IRE1 $\alpha$ -HA-reconstituted cells stained with anti-KDEL antibody and phalloidin at different time points after seeding. Actin and ER total area was quantified as a measure of spreading ( $n=3$  independent experiments, 50 cells in total). **i**, Cell adhesion assay in fibronectin-coated plates. Cells were stained with crystal violet and the total absorbance was measured ( $n=3$  independent experiments). In all panels, data are shown as the mean  $\pm$  s.e.m of the indicated number of independent experiments; one-way ANOVA followed by Tukey's test. \* $P < 0.05$  and \*\* $P < 0.01$ .

rendered cells less sensitive to the inhibition of migration by the PKC $\alpha$  inhibitor Gö6976 (Fig. 5j). In agreement with this result, PKC $\alpha$  activation was decreased in IRE1 $\alpha$ -deficient cells upon FBS stimulation (Supplementary Fig. 5J,K). We also detected an interaction between IRE1 $\alpha$ , filamin A and PKC $\alpha$  in immunoprecipitation experiments (Fig. 5k). Using cellular fractionation and colocalization experiments, we observed a relocalization of PKC $\alpha$  to the ER in an IRE1 $\alpha$ -dependent manner (Fig. 5L,m; see controls in Supplementary Fig. 5L). Taken together, these data indicate that IRE1 $\alpha$  facilitates filamin A phosphorylation, which is mediated by PKC $\alpha$ , to induce actin cytoskeleton remodelling and cell migration.

**IRE1 $\alpha$  acts as a scaffold to regulate cell migration and filamin A phosphorylation.** Since IRE1 $\alpha$  is required for cell migration, we explored the contribution of XBP1 to this biological function.

Remarkably, XBP1 deficiency or inhibition of the RNase activity of IRE1 $\alpha$  had no impact on cell migration (Fig. 6a; Supplementary Fig. 6A). We also expressed IRE1 $\alpha$  carrying different mutations that impair its kinase activity (K599A), kinase and endoribonuclease activity (P830L) or its ability to dimerize (D123P)<sup>26</sup>. Although all three IRE1 $\alpha$  mutants lost their ability to catalyse *Xbp1* mRNA splicing under ER stress (Fig. 6b; Supplementary Fig. 6B), only the D123P variant impaired the pro-migratory activity of IRE1 $\alpha$  (Fig. 6c; Supplementary Fig. 6C). Consistent with these results, the expression of the D123P mutant did not restore actin dynamics in IRE1 $\alpha$ -null cells (Fig. 6d; Supplementary Fig. 6D). These findings indicate that IRE1 $\alpha$  facilitates cell migration independent of its canonical signalling but requires its dimerization.

We studied IRE1 $\alpha$  oligomerization using an IRE1 $\alpha$ -GFP construct (IRE1-3F6H-GFP) to visualize IRE1 $\alpha$  clustering<sup>27</sup>.



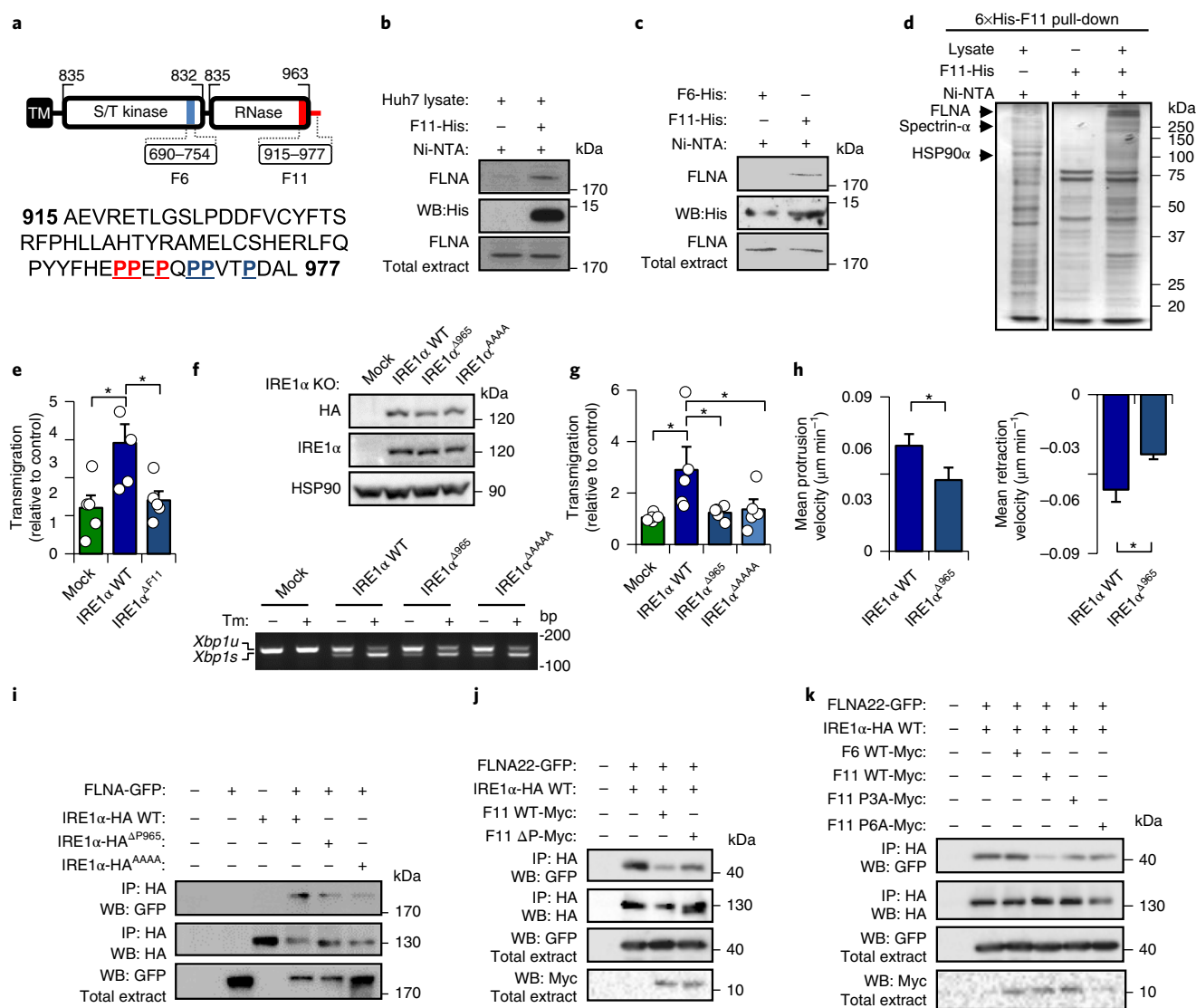


**Fig. 4 | A physical interaction between IRE1α and filamin A is required for cell migration.** **a**, Schematic representation of the C terminus of IRE1α divided into different fragments. The domains serine/threonine protein kinase (S/T kinase) and endoribonuclease (RNase) are shown. A putative SH3-binding domain (PPXP) is shown in red and all prolines are highlighted in blue. **b**, Pull down of purified 6xHis-F11 using Huh7 cell extracts and Ni-NTA (nickel-nitrilotriacetic acid) columns followed by western blotting. **c**, Pull down of purified 6xHis-F11 or F6. **d**, Pull down of 6xHis-F11 analysed by SDS-PAGE and Coomassie staining. Bands were analysed by mass spectrometry to identify the proteins. Images from the same gel were spliced together as indicated (see unprocessed gel scans). **e**, Boyden chamber assay of MEFs transfected with IRE1α WT or a deletion mutant of the F11 domain (ΔF11) ( $n = 5$  independent experiments). **f**, Top, western blot of IRE1α knockout MEFs stably expressing IRE1α-HA WT, a deletion from amino acid P975 (Δ965), or a point mutant replacing PPEP for AAAA. Bottom, *Xbp1* mRNA splicing assay (RT-PCR) of indicated cells were treated with 100 ng ml<sup>-1</sup> of Tm for 8 h. PCR fragments corresponding to the *Xbp1u* or *Xbp1s* forms are indicated. **g**, Boyden chamber assay of cells described in **f** seeded on fibronectin-coated transwell plates ( $n = 5$  independent experiments). **h**, IRE1α KO cells reconstituted with WT or IRE1α Δ965 mutant were transfected with LifeAct and time-lapse confocal microscopy recordings were made. Protrusion and retraction velocity were determined using ADAPT software (two-tailed *t*-test; WT,  $n = 20$  and IRE1α<sup>Δ965</sup>  $n = 14$  independent experiments). **i**, Co-immunoprecipitation of IRE1α-HA (WT, Δ965 and AAAA mutants) and GFP-tagged filamin A was assessed by western blotting using HEK293T cells. **j**, Co-immunoprecipitation of IRE1α-HA and GFP-tagged-filamin A-22 domain in cells expressing F11 WT or a deleted peptide in the proline-rich sequence (F11ΔP) using HEK293T cells. **k**, Similar experiments were performed as in **j** using F11 WT or F11 P3A (proline substitution by alanine in three proline residues), F11 P6A (proline substitution by alanine in all six proline residues) or control F6 peptide. In all panels, data are shown as the mean ± s.e.m. of the indicated number of independent experiments; one-way ANOVA followed by Tukey's test was used unless otherwise indicated. \* $P < 0.05$ . Blots represent one out of two (**d,i**), or three (**b,c,j,k**) experiments, with similar results obtained.

IRE1-3F6H-GFP cells were tested in transmigration assays to monitor cells in the upper chamber (non-migrating) and cells in the lower chamber (migrating). An analysis of Z-stacks of cells in the lower chamber showed the presence of IRE1α-GFP clusters in ~22% of migrating cells (Fig. 6e). As a control, a D123P mutant was used

in the same experiment to confirm that the signal was due to IRE1α oligomerization.

We then tested whether IRE1α dimerization is needed to interact and regulate filamin A. Immunoprecipitation experiments using the K599A, P830L and D123P mutants showed similar

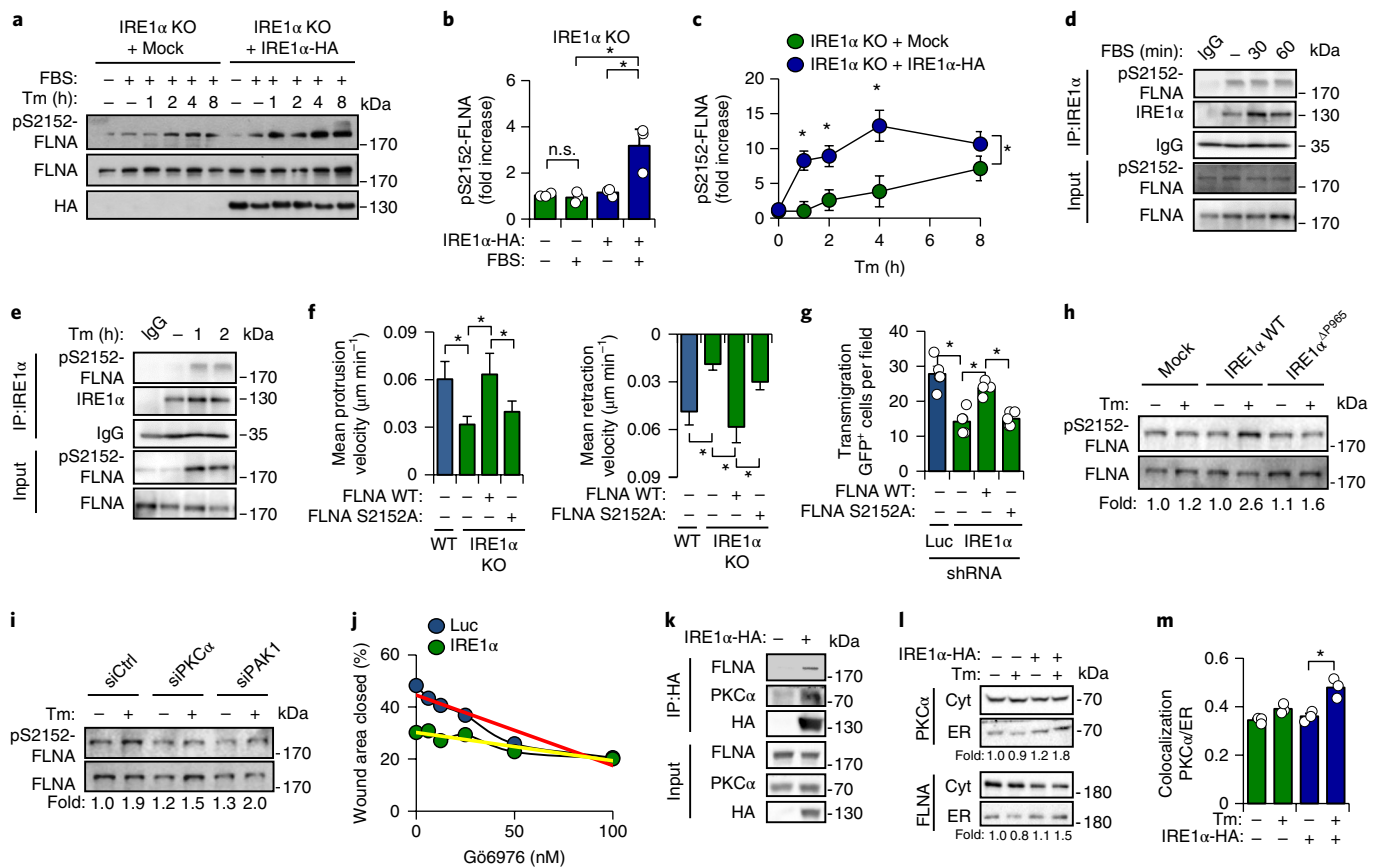


**Fig. 5 | IRE1 $\alpha$  regulates filamin A phosphorylation.** **a–c**, Filamin A phosphorylation at S2152 was measured by western blotting in IRE1 $\alpha$  KO and IRE1 $\alpha$ -HA-reconstituted MEFs treated with FBS or Tm (**a**) followed by quantification (**b,c**) ( $n=3$  independent experiments). **d,e**, Co-immunoprecipitation of endogenous IRE1 $\alpha$  and filamin A in cells treated with 3% FBS (**d**) for 30–60 min or Tm (**e**) for 1–2 h. **f**, WT and IRE1 $\alpha$  KO cells transfected with LifeAct and filamin A WT (FLNA-WT) or S2152A mutant filamin A (FLNA S2152A) were recorded by time-lapse confocal microscopy every 30 s for 5 min. Protrusion and retraction velocity was determined using ADAPT software (WT,  $n=20$ ; KO  $n=11$ ; KO + filamin A,  $n=12$ ; KO + filamin A S2152A,  $n=14$ ). **g**, Boyden chamber assay of shLuc or shIRE1 $\alpha$  MEFs transiently transfected with pEGFP and expression vectors for FLNA-Myc or FLNA S2152A-Myc. Transmigration was evaluated by quantifying the number of GFP-positive cells in the lower chamber ( $n=4$  independent experiments). **h**, Western blot of total protein extracts of IRE1 $\alpha$  KO MEFs reconstituted with IRE1 $\alpha$ -HA WT or IRE1 $\alpha^{\Delta P965}$  mutant treated with Tm for 2 h. **i**, Western blot of MEFs transfected with siRNAs against PKC $\alpha$  (siPKC $\alpha$ ) and PAK1 (siPAK1) for 48 h followed by Tm treatment. **j**, Wound-healing assay of MEFs transfected with shRNA against Luc or IRE1 $\alpha$  and treated with different concentrations of G66976 for 8 h. Slopes are indicated in red and yellow ( $n=2$  independent experiments). **k**, Co-immunoprecipitation of IRE1 $\alpha$ -HA with endogenous PKC $\alpha$  and filamin A. **l**, Subcellular fractionation was performed on IRE1 $\alpha$ -deficient or reconstituted cells treated with Tm for 2 h. Pure microsomal (ER) and cytosolic (Cyt) fractions were analysed by western blotting. **m**, Colocalization of PKC $\alpha$ -FLAG and KDEL-RFP in transfected cells treated with Tm for 2 h (two-tailed  $t$ -test,  $n=3$ , 20 cells in total). In all panels, data represent the mean  $\pm$  s.e.m. of the indicated number of independent experiments; one-way ANOVA followed by Tukey's test. \* $P < 0.05$ . n.s. not significant. Blots represent one out of two (**i,k**), or three (**d,h,i,l**) experiments, with similar results obtained.

associations with filamin A compared with wild-type IRE1 $\alpha$  (Fig. 6f). However, interaction studies using the D123P mutant with the filamin A-22 domain alone indicated reduced binding under resting and ER stress conditions (Fig. 6g,h). Similar results were observed when IRE1 $\alpha^{\Delta 965}$  and IRE1 $\alpha^{\text{AAAA}}$  mutants were tested (Fig. 6g). In addition, IRE1 $\alpha$  expression favours the formation of dimers and larger order oligomers of filamin A (Fig. 6i). Remarkably, filamin A phosphorylation was abolished in IRE1 $\alpha$  knockout cells expressing the D123P dimerization mutant (Fig. 6j). Taken together, these results suggest that IRE1 $\alpha$  acts as a scaffold to recruit filamin A at resting conditions, inducing its phosphorylation upon IRE1 $\alpha$  dimerization.

**IRE1 $\alpha$  regulates actin dynamics and cell migration in multiple model systems.** To explore the physiological relevance of our findings, we used two *in vivo* models of cell migration coupled with genetic manipulation. We studied *Drosophila melanogaster*

plasmatocytes (haemocytes), which are motile cells with functions and features similar to that of vertebrate macrophages<sup>28</sup>. Knocking down fly IRE1 $\alpha$  (Ire1) by RNA interference resulted in reduced distance and velocity of movement (Fig. 7a; Supplementary Movie 2). Under these conditions, haemocytes exhibited an elongated morphology with reduced lamellipodia (Fig. 7b). Remarkably, overexpression of Cheerio (the filamin A form in *D. melanogaster*) fully rescued the migratory impairment triggered by knocking down fly IRE1 $\alpha$  (Fig. 7a). To further examine the role of IRE1 $\alpha$  in cell migration, we used an insertional Ire1 mutant coupled with a mosaic analysis, whereby only IRE1 $\alpha$ -deficient cells are labelled with GFP<sup>29</sup> (scheme shown in Supplementary Fig. 7A). Primary cultures from Ire1 $\alpha$  mutant cells were smaller in size area and showed reduced number of lamellar extensions (Fig. 7c). Remarkably, knocking down IRE1 $\alpha$  led to a reduction of the retrograde flow of actin, reflected in a lower frequency in the velocity maps using the LifeAct reporter (Fig. 7d; Supplementary Movie 3). Taken together, these

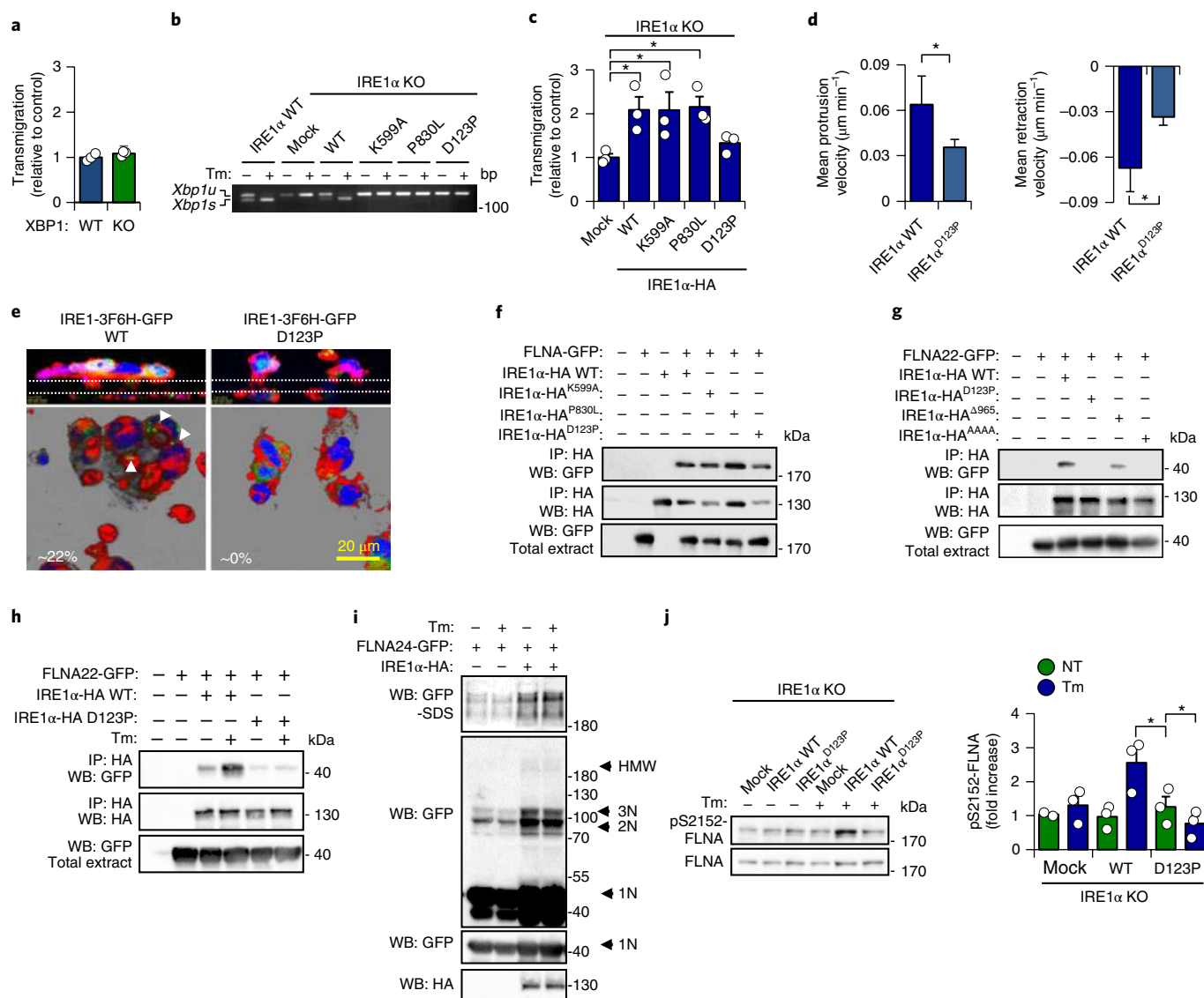


**Fig. 6 | IRE1 $\alpha$  dimerization, but not its enzymatic activities, controls cell migration and filamin A phosphorylation.** **a**, Boyden chamber assay of XBP1-deficient or control MEFs. Transmigration was evaluated as described previously (two-tailed *t*-test,  $n=3$ ) **b**, *Xbp1* mRNA splicing assay of indicated cells treated with Tm (K599A: kinase dead; P830L: kinase and RNase dead; D123P: non-dimerizing). **c**, Boyden chamber assay of IRE1 $\alpha$  KO cells stably expressing IRE1 $\alpha$ -HA WT, K599A, P830L or D123P mutants ( $n=3$  independent experiments). **d**, Retractions and protrusions of IRE1 $\alpha$  KO MEFs reconstituted with IRE1 $\alpha$  WT or D123P mutant transfected with LifeAct were recorded by time-lapse confocal microscopy. The protrusion and retraction velocity were determined using ADAPT software (two-tailed *t*-test, IRE1 $\alpha$  WT  $n=20$ , IRE1 $\alpha$ <sup>D123P</sup>  $n=15$  independent experiments) **e**, Top, Z-stacks of TREX cells expressing IRE1-3F6H-GFP WT or IRE1-3F6H-GFP D123P mutant plated on transwell plates for 6 h and stained with phalloidin coupled to rhodamine. Lower panel: maximal projection of Z-stacks of cells in the lower chamber of a transwell. Arrowheads indicate IRE1 $\alpha$ -GFP-positive foci. **f**, Co-immunoprecipitation of IRE1 $\alpha$ -HA (WT, K599A, P830L and D123P) and GFP-tagged filamin A in HEK293T cells was assessed by western blotting. **g**, Co-immunoprecipitation of IRE1 $\alpha$ -HA (WT, D123P,  $\Delta$ 965 and AAAA) and GFP-tagged filamin A-22 domain in HEK293T cells was analysed by western blotting. **h**, Co-immunoprecipitation of HA-tagged IRE1 $\alpha$  (WT and D123P) and GFP-tagged filamin A-22 domain treated with Tm for 2 h was analysed by western blotting. **i**, Native-PAGE and western blot of HEK293T cells transfected with HA-tagged IRE1 $\alpha$  and GFP-tagged filamin A-24 dimerization domain treated with Tm for 2 h. GFP-tagged filamin A-24 domain monomer (1N), dimer (2N), trimer (3N) and high molecular weight species (HMW) are indicated. **j**, Left, filamin A phosphorylation was assessed by western blotting of protein extracts from IRE1 $\alpha$  KO cells expressing IRE1 $\alpha$ -HA (WT, D123P or Mock) treated or not treated (NT) with with Tm. Right, quantification of the levels of filamin A phosphorylation in cells stimulated with FBS ( $n=3$  independent experiments). In all panels, data represent the mean  $\pm$  s.e.m. of the indicated number of independent experiments; one-way ANOVA followed by Tukey's test was used unless otherwise indicated. \* $P < 0.05$ . Blots represent one out of two (**g,h**), or three (**f,i,j**) experiments, with similar results obtained.

results demonstrate a functional role of the IRE1 $\alpha$ -filamin A axis in cell migration and actin dynamics in vivo in an invertebrate model.

We then assessed cell migration in zebrafish embryos, which show a well-characterized pattern of morphogenetic cell movements that are dependent on the actin cytoskeleton during gastrulation<sup>30</sup>.

Three major stereotyped cell movements have been described: epiboly, convergence and extension (scheme shown in Fig. 7e). We blocked the activity of IRE1 $\alpha$  during zebrafish development using a dominant-negative form (IRE1 $\alpha$ -DN)<sup>31,32</sup> (Supplementary Fig. 7B) that also reduced filamin A phosphorylation in vitro

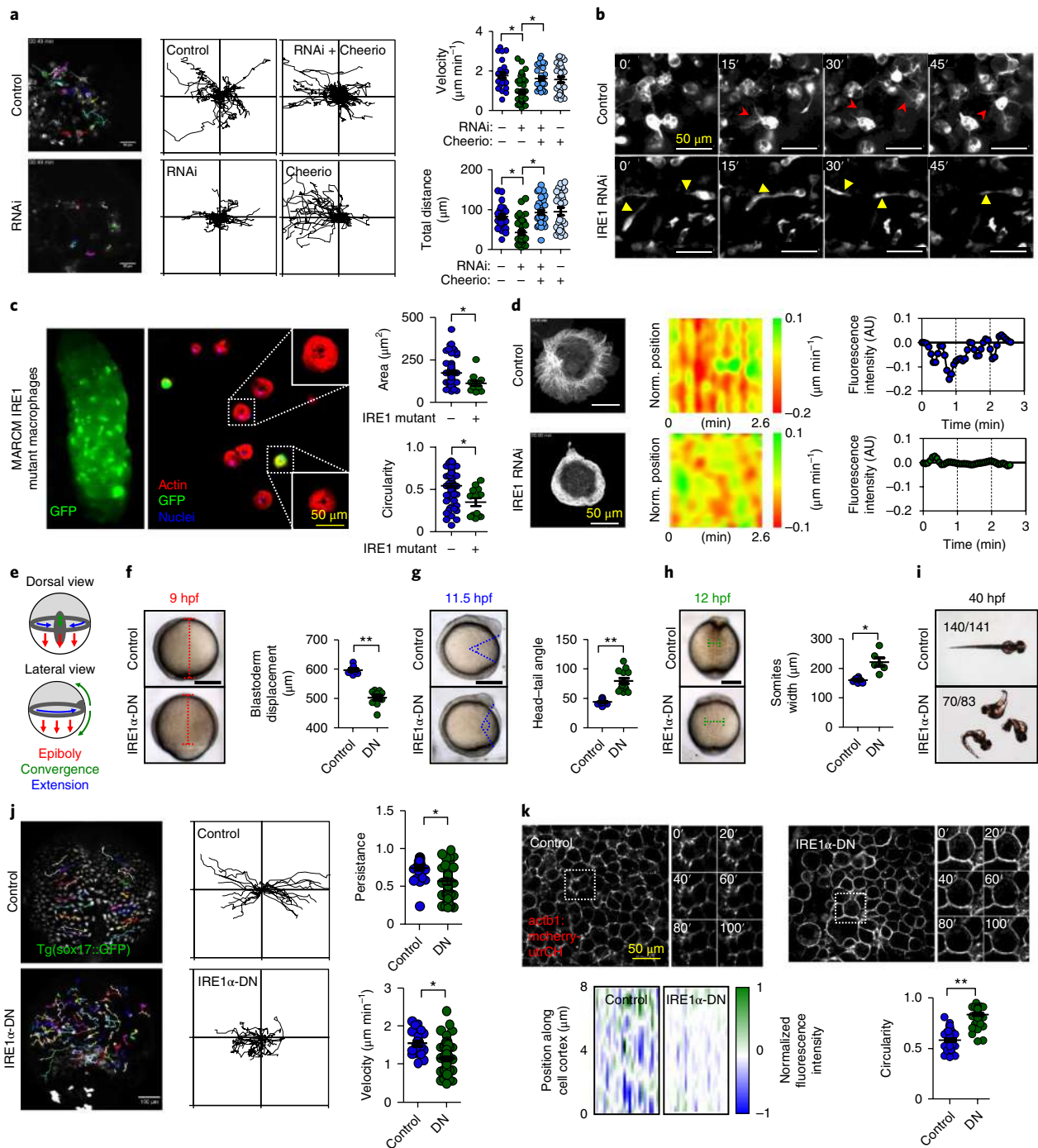


**Fig. 7 | The activity of IRE1 $\alpha$  in cell migration and actin dynamics is evolutionarily conserved.** **a**, Cell movement trajectories of *D. melanogaster* macrophages expressing control or an IRE1 $\alpha$  RNAi under the control of the Hml $\Delta$ -Gal4 driver. For rescue experiments, IRE1 $\alpha$  RNAi and Cheerio P(EP) cheer<sup>G9093</sup> were co-expressed. Tracks were plotted (x and y axes correspond from -150 to 150  $\mu\text{m}$ ) (one-way ANOVA followed by Tukey's test; Control,  $n=3$ ; IRE1 $\alpha$  RNAi,  $n=4$ ; and Cheerio,  $n=3$  independent experiments). **b**, Time-lapse images of macrophages from **a**. Lamellipodia (red arrows) and filopodia (yellow arrows) are indicated. **c**, Images of macrophages from MARCM mutant animals (see Methods). GFP-positive cells (IRE1 $\alpha$  mutant) or negative (control) were stained for F-actin (red) and DNA (blue) ( $n=3$ ). **d**, Actin dynamics were recorded in time-lapse images of macrophages co-expressing LifeAct-GFP and IRE1 $\alpha$  RNAi using the Cg-Gal4 driver (Control,  $n=12$  and IRE1 $\alpha$  RNAi,  $n=9$ ). Velocity maps of representative cells for each condition were generated using the ADAPT tool. **e**, Schematic representation of the three morphogenetic movements during zebrafish gastrulation. **f**, Blastoderm displacement at 9 hpf was determined (broken red bracket). **g**, The angle formed between the radial lines that intersect the tip of the head and tail at 11.5 hpf was plotted. **h**, The width of the first three somites at 12 hpf was calculated (broken green bracket) ( $n$  for controls = 9 (**f**), 19 (**g**) or 8 (**h**);  $n$  for IRE1 $\alpha$ -DN = 10 (**f**), 14 (**g**) or 6 (**h**)). **i**, Global phenotypes of embryos at 40 hpf are presented and quantified. **j**, Cell movement trajectories are shown of control and IRE1 $\alpha$ -DN injected Tg(sox17::GFP) embryos at 7 hpf. The persistence and cell velocity of migrating cells was determined. **k**, Top, maximum projections of time-lapse confocal microscopy images of control and IRE1 $\alpha$ -DN-injected Tg(actb1::mcherry-utrCH) embryos at 7 hpf. Time-lapse images of higher magnification area is indicated (white square). Bottom, heatmap of normalized fluorescence intensity along the cell cortex of individual cells and cell circularity ( $n=47$  for control;  $n=61$  for IRE1 $\alpha$ -DN). In all panels, data represent the mean  $\pm$  s.e.m. of the indicated number of independent experiments; two-tailed  $t$ -test was used unless otherwise indicated. \* $P < 0.05$  and \*\* $P < 0.01$ . Scale bars, 50  $\mu\text{m}$  (**a**, **j**); 250  $\mu\text{m}$  (**f**, **h**).



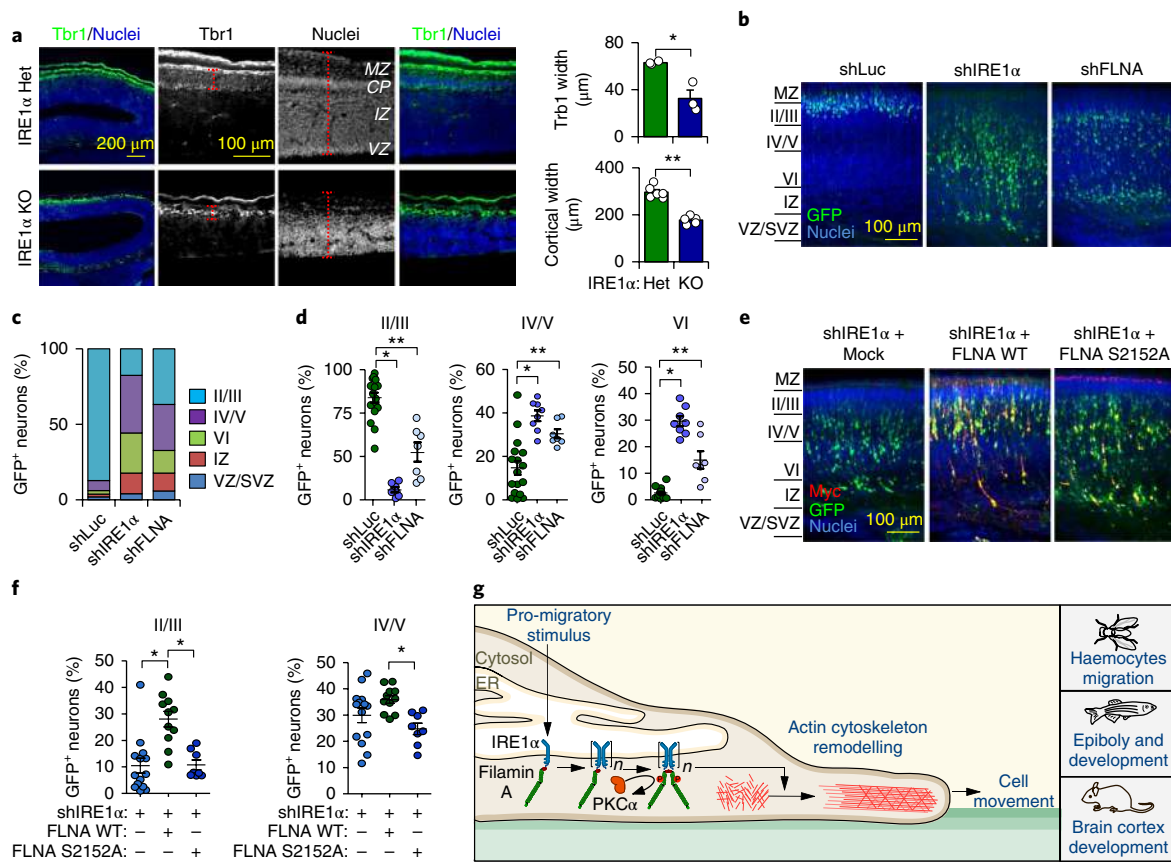


**Fig. 8 | IRE1 $\alpha$  is required for neuronal migration during brain cortex development.** **a**, Left, IRE1 $\alpha$  heterozygous (Het) or KO embryos were collected at E14.5 and brain tissue analysed by Trb1 and nuclei staining. MZ, marginal zone, CP, cortical plate; IZ, intermediate zone; VZ, ventricular zone. Global image is shown on the left, three magnified images are shown on the right. The dotted red lines indicate the area used for quantification. Right, quantification of Trb1 (two-tailed *t*-test, *n* = 3) or cortical thickness (two-tailed *t*-test, *n* = 5) (red dotted line). **b**, Coronal sections were visualized for transfected neurons (green) and cell nuclei using DAPI (blue). Merged images are shown. **c**, The percentage of GFP-positive cells was determined in different cortical brain layers for each mouse (shRNA Luc, *n* = 19; shRNA IRE1 $\alpha$ , *n* = 9; and shRNA filamin A, *n* = 7). VZ/subventricular zone (SVZ), IZ, layer VI (VI), layers IV/V (IV/V) and layers II/III (II/III) are shown. **d**, Individual dot plots of the analysis by cortical layer are shown for all groups. **e**, In utero co-electroporation was performed using shRNA to target IRE1 $\alpha$  together with constructs expressing filamin A WT-Myc, filamin A S2152A-Myc or empty vector. Sections were stained for Myc using specific antibodies and visualized by fluorescence microscopy. **f**, The percentage of transfected GFP-positive cells was determined in indicated cortical layers in animals electroporated with shRNA IRE1 $\alpha$  (Mock, *n* = 14; filamin A WT-Myc, *n* = 11; and filamin A S2152A-Myc, *n* = 7). In all panels, the data are shown as the mean  $\pm$  s.e.m. of the indicated number of independent experiments; one-way ANOVA followed by Tukey's test was used unless otherwise indicated. \**P* < 0.05 and \*\**P* < 0.01. **g**, Working model. The UPR transducer IRE1 $\alpha$  signals through an unconventional mechanism that is independent of its enzymatic activities to control actin cytoskeleton dynamics. Monomeric IRE1 $\alpha$  physically interacts with filamin A through a novel domain located at the distal C-terminal region. A pro-migratory stimulus triggers IRE1 $\alpha$  dimerization, increasing the binding of filamin A and the recruitment of PKC $\alpha$ . Phosphorylation of filamin A at S2152 by PKC $\alpha$  increases actin cytoskeleton remodelling and cell migration in various animal species.

(Supplementary Fig. 7C). Remarkably, the vegetal progression of epiboly was delayed in IRE1 $\alpha$ -DN embryos compared with control animals (Fig. 7f). Furthermore, this phenotype was associated with an increased head-to-tail angular separation (Fig. 7g) that is indicative of reduced anterior-posterior axial movements<sup>33</sup>. Finally, the width of the first somites at 12 h post fertilization was increased by ~40 % in IRE1 $\alpha$ -DN embryos compared with controls (Fig. 7h), suggesting that the paraxial mesoderm suffered defective convergence. These alterations resulted in embryos with a shortened anterior-posterior axis at 24 h post fertilization (Fig. 7i), a phenotype that is suggestive of defective early gastrulation movements<sup>34</sup>. Importantly, none of these phenotypes were observed in embryos overexpressing wild-type IRE1 $\alpha$  (Supplementary Fig. 7D).

We also observed reduced cell movement with single-cell tracking during the epiboly process (Fig. 7j; Supplementary Movie 4). In addition, using an actin reporter<sup>35</sup>, we observed that epiblast cells of embryos injected with IRE1 $\alpha$ -DN became rounded and

less cohesive during gastrulation, showing reduced filopodial-like activity and increased formation of blebs compared with controls (Fig. 7k; Supplementary Movie 5). Moreover, the cortical distribution of F-actin appeared more homogeneous and less dynamic in IRE1 $\alpha$ -DN embryos compared with controls (Fig. 7k; Supplementary Fig. 7E). Together, these experiments indicate that IRE1 $\alpha$  expression has a fundamental and evolutionarily conserved activity in controlling actin cytoskeleton function and cell movement in vivo.

**IRE1 $\alpha$  deficiency alters radial migration of cortical neurons mimicking periventricular nodular heterotopia.** Filamin A expression is essential for neuronal migration during brain cortex development, and mutations in the *FLNA* gene are the main cause of periventricular nodular heterotopia, a syndrome characterized by the abnormal localization of neurons along the walls of the lateral ventricle<sup>36,37</sup>. Full IRE1 $\alpha$  deficiency is embryonic lethal, and the reported characterization did not include the study of brain

structures<sup>38</sup>. Therefore, we generated *IRE1α* (*Ern1*)-null animals and examined brain tissue at embryonic day 14.5 (E14.5). An analysis of post-mitotic cells of layer VI of the brain cortex after Tbr1 staining revealed a delay in the formation of this layer in *IRE1α* knockout animals compared with heterozygous mice (Fig. 8a). Similar observations were obtained when the width of the cortex was quantified (Fig. 8a).

We defined whether the morphological alterations observed during brain development in *IRE1α*-deficient animals were due to altered radial cell migration *in vivo*. We studied animals at E14.5 because high levels of filamin A and *IRE1α* were detected at that developmental stage (E12.5–14.5) (Supplementary Fig. 8C,D). We then performed *in utero* brain electroporation to knock down *IRE1α* in the developing cortex together with GFP at E14.5 to target cortical neural progenitors (strategy in Supplementary Fig. 8B). Normal development of neurons in layers II/III at birth was observed in control brains electroporated with a construct expressing a shRNA against luciferase mRNA (control). In contrast, brains electroporated with a shRNA to target *IRE1α* showed delayed migration (Fig. 8b). Quantification of neuronal distribution in cortical layers demonstrated that knocking down *IRE1α* resulted in a significant delay of neuronal migration, with cells accumulating at inferior cortical layers (Fig. 8c,d; Supplementary Fig. 8E). For comparison, we also knocked down filamin A, which also resulted in altered neuronal migration (Fig. 8b–d). Remarkably, electroporation of wild-type filamin A together with the shRNA targeting *IRE1α*, but not the filamin A S2152 mutant, rescued the detrimental effects of *IRE1α* deficiency in cortical neuronal migration, leading to a recovery in the percentage of cells reaching layer II/III and IV/V (Fig. 8e,f; Supplementary Fig. 8E,G). Overall, these results demonstrate that the regulation of filamin A by *IRE1α* plays an essential role in neuronal migration during brain cortex development.

## Discussion

Although *IRE1α* represents the most conserved UPR signal transducer, its physiological function is still poorly understood. Most studies addressing the biological relevance of *IRE1α* in tissue homeostasis have been developed in artificial models of ER stress, and only a few reports support the existence of alternative activities of the pathway beyond protein-folding stress. Here, we identified filamin A as a major *IRE1α* interactor and uncovered a previously unanticipated function of this protein in the regulation of actin cytoskeleton dynamics, with a significant impact on cell migration in various model systems. Remarkably, although many interactome studies have been performed to identify novel *IRE1α* binding partners<sup>2</sup>, no direct connections between *IRE1α* and cytoskeleton dynamics have been reported.

We characterized an unconventional signalling mechanism underlying *IRE1α* function, whereby it serves as a scaffold to recruit filamin A and potentiate the migratory capacity of the cell. We fully dissected the impact of *IRE1α* in cell migration, which is distinct from its classical role in the UPR and mediated by a previously uncharacterized proline-rich domain. We propose a two-step model whereby filamin A is associated to the ER through direct binding to *IRE1α*. Then, after stimulation with a pro-migratory stimulus, *IRE1α* dimerization and oligomerization induces a further recruitment of filamin A, scaffolding to PKC $\alpha$ , to increase filamin A dimerization and phosphorylation. This mechanism results in increased cytoskeleton dynamics (Fig. 8g). At the molecular level, we provide evidence to indicate that *IRE1α* increases filamin A phosphorylation at S2152, a specific regulatory event controlling cytoskeleton dynamics. One main question that remains to be addressed is the nature of the signals promoting *IRE1α* oligomerization during cell migration.

Alterations of filamin A are the underlying cause of periventricular nodular heterotopia, a human condition affecting brain

development and is associated with mental retardation and cognitive impairment<sup>36,37</sup>. Our study demonstrates that targeting *IRE1α* phenocopies the consequences of filamin A deficiency in the developing brain. At least ten different regulators of filamin A are able to modulate neuronal migration<sup>39</sup>, suggesting that a tight regulatory network that fine-tunes filamin A function is fundamental for brain development. Fingerprints of UPR activation were reported during the brain development in mouse, *Caenorhabditis elegans* and *D. melanogaster* models (reviewed previously<sup>40</sup>). Interestingly, PERK expression also affects brain development at the level of neurogenesis and the generation of intermediate progenitors and projection neurons of the brain cortex<sup>41</sup>. Moreover, the alternative activity of *IRE1α* described here may be relevant in the context of other diseases. Filamin A has been proposed to contribute to the metastatic potential of cancer<sup>42</sup>. Thus, the *IRE1α*–filamin A axis may also enhance the occurrence of metastasis, an activity that may be insensitive to chemotherapy based on *IRE1α* RNase inhibitors. Overall, our study demonstrates a conserved function of *IRE1α* in actin cytoskeleton dynamics that is independent of its well-known role as an ER stress transducer, acting as a scaffold that recruits and potentiates filamin A function. Our findings illuminate how fundamental processes surveilling ER homeostasis are interconnected with the global machinery controlling cell movement.

## Methods

Methods, including statements of data availability and any associated accession codes and references, are available at <https://doi.org/10.1038/s41556-018-0141-0>.

Received: 21 June 2017; Accepted: 13 June 2018;

Published online: 16 July 2018

## References

- Walter, P. & Ron, D. The unfolded protein response: from stress pathway to homeostatic regulation. *Science* **334**, 1081–1086 (2011).
- Hetz, C., Chevet, E. & Oakes, S. A. Proteostasis control by the unfolded protein response. *Nat. Cell Biol.* **17**, 829–838 (2015).
- Úrra, H., Dufey, E., Lisbona, F. & Rojas-Rivera, D. When ER stress reaches a dead end. *Biochim. Biophys. Acta* **1833**, 3507–3517 (2013).
- Oakes, S. A. & Papa, F. R. The role of endoplasmic reticulum stress in human pathology. *Annu. Rev. Pathol.* **10**, 173–194 (2015).
- Wang, M. & Kaufman, R. J. Protein misfolding in the endoplasmic reticulum as a conduit to human disease. *Nature* **529**, 326–335 (2016).
- Calfon, M. et al. *IRE1* couples endoplasmic reticulum load to secretory capacity by processing the XBP-1 mRNA. *Nature* **415**, 92–96 (2002).
- Lee, K. et al. *IRE1*-mediated unconventional mRNA splicing and S2P-mediated ATF6 cleavage merge to regulate XBP1 in signaling the unfolded protein response. *Genes Dev.* **16**, 452–466 (2002).
- Hetz, C. & Glimcher, L. H. Fine-tuning of the unfolded protein response: Assembling the *IRE1α* interactome. *Mol. Cell* **35**, 551–561 (2009).
- Feng, Y. & Walsh, C. A. The many faces of filamin: a versatile molecular scaffold for cell motility and signalling. *Nat. Cell Biol.* **6**, 1034–1038 (2004).
- Oono, K. et al. JAB1 participates in unfolded protein responses by association and dissociation with *IRE1*. *Neurochem. Int.* **45**, 765–772 (2004).
- Nakamura, F., Stosel, T. P. & Hartwig, J. H. The filamins: organizers of cell structure and function. *Cell Adhes. Migr.* **5**, 160–169 (2011).
- Sepulveda, D. et al. Interactome screening identifies the ER luminal chaperone Hsp47 as a regulator of the unfolded protein response transducer *IRE1α*. *Mol. Cell* **69**, 238–252 (2018).
- Nakamura, F., Osborn, T. M., Hartemink, C. A., Hartwig, J. H. & Stosel, T. P. Structural basis of filamin A functions. *J. Cell Biol.* **179**, 1011–1025 (2007).
- Riedl, J. et al. Lifeact: a versatile marker to visualize F-actin. *Nat. Methods* **5**, 605–607 (2008).
- Ridley, A. J. Rho GTPases and cell migration. *J. Cell Sci.* **114**, 2713–2722 (2001).
- Vadlamudi, R. K. et al. Filamin is essential in actin cytoskeletal assembly mediated by p21-activated kinase 1. *Nat. Cell Biol.* **4**, 681–690 (2002).
- Baldassarre, M. et al. Filamins regulate cell spreading and initiation of cell migration. *PLoS ONE* **4**, e7830 (2009).
- Lynch, C. D. et al. Filamin depletion blocks endoplasmic spreading and destabilizes force-bearing adhesions. *Mol. Biol. Cell* **22**, 1263–1273 (2011).
- van Vliet, A. R. et al. The ER stress sensor PERK coordinates ER-plasma membrane contact site formation through interaction with filamin-A and F-actin remodeling. *Mol. Cell* **65**, 885–899 (2017).

20. Ali, M. M. et al. Structure of the Ire1 autophosphorylation complex and implications for the unfolded protein response. *EMBO J.* **30**, 894–905 (2011).
21. Bouchecareilh, M., Higa, A., Fribourg, S., Moenner, M. & Chevet, E. Peptides derived from the bifunctional kinase/RNase enzyme IRE1 $\alpha$  modulate IRE1 $\alpha$  activity and protect cells from endoplasmic reticulum stress. *FASEB J.* **25**, 3115–3129 (2011).
22. Zhou, A.-X., Hartwig, J. H. & Akyurek, L. M. Filamins in cell signaling, transcription and organ development. *Trends Cell Biol.* **20**, 113–123 (2010).
23. Zhong, Z. et al. Cyclin D1/cyclin-dependent kinase 4 interacts with filamin A and affects the migration and invasion potential of breast cancer cells. *Cancer Res.* **70**, 2105–2114 (2010).
24. Tigges, U., Koch, B., Wissing, J., Jockusch, B. M. & Ziegler, W. H. The F-actin cross-linking and focal adhesion protein filamin A is a ligand and in vivo substrate for protein kinase C alpha. *J. Biol. Chem.* **278**, 23561–23569 (2003).
25. Sarkisian, M. R. et al. MEKK4 signaling regulates filamin expression and neuronal migration. *Neuron* **52**, 789–801 (2006).
26. Xue, Z. et al. A conserved structural determinant located at the interdomain region of mammalian inositol-requiring enzyme 1 $\alpha$ . *J. Biol. Chem.* **286**, 30859–30866 (2011).
27. Li, H., Korennykh, A. V., Behrman, S. L. & Walter, P. Mammalian endoplasmic reticulum stress sensor IRE1 signals by dynamic clustering. *Proc. Natl Acad. Sci. USA* **107**, 16113–16118 (2010).
28. Wood, W. & Jacinto, A. Drosophila melanogaster embryonic haemocytes: masters of multitasking. *Nat. Rev. Mol. Cell Biol.* **8**, 542–551 (2007).
29. Lee, T. & Luo, L. Mosaic analysis with a repressible cell marker (MARCM) for Drosophila neural development. *Trends Neurosci.* **24**, 251–254 (2001).
30. Solnica-Krezel, L. & Sepich, D. S. Gastrulation: making and shaping germ layers. *Annu. Rev. Cell Dev. Biol.* **28**, 687–717 (2012).
31. Auf, G. et al. Inositol-requiring enzyme 1 $\alpha$  is a key regulator of angiogenesis and invasion in malignant glioma. *Proc. Natl Acad. Sci. USA* **107**, 15553–15558 (2010).
32. Nguyen, D. T. et al. Nck-dependent activation of extracellular signal-regulated kinase-1 and regulation of cell survival during endoplasmic reticulum stress. *Mol. Biol. Cell* **15**, 4248–4260 (2004).
33. Hammerschmidt, M. et al. Mutations affecting morphogenesis during gastrulation and tail formation in the zebrafish, *Danio rerio*. *Development* **123**, 143–151 (1996).
34. Waxman, J. S., Hocking, A. M., Stoick, C. L. & Moon, R. T. Zebrafish Dapper1 and Dapper2 play distinct roles in Wnt-mediated developmental processes. *Development* **131**, 5909–5921 (2004).
35. Behrndt, M. et al. Forces driving epithelial spreading in zebrafish gastrulation. *Science* **338**, 257–260 (2012).
36. Fox, J. W. et al. Mutations in filamin 1 prevent migration of cerebral cortical neurons in human periventricular heterotopia. *Neuron* **21**, 1315–1325 (1998).
37. Sheen, V. L. et al. Mutations in the X-linked filamin 1 gene cause periventricular nodular heterotopia in males as well as in females. *Hum. Mol. Genet.* **10**, 1775–1783 (2001).
38. Iwakaki, T., Akai, R., Yamanaka, S. & Kohno, K. Function of IRE1 alpha in the placenta is essential for placental development and embryonic viability. *Proc. Natl Acad. Sci. USA* **106**, 16657–16662 (2009).
39. Sarkisian, M. R., Bartley, C. M. & Rakic, P. Trouble making the first move: interpreting arrested neuronal migration in the cerebral cortex. *Trends Neurosci.* **31**, 54–61 (2008).
40. Martinez, G., Khatiwada, S., Costa-Mattioli, M. & Hetz, C. ER proteostasis control of neuronal physiology and synaptic function. *Trends Neurosci.* <https://doi.org/10.1016/j.tins.2018.05.009> (2018).
41. Laguesse, S. et al. A dynamic unfolded protein response contributes to the control of cortical neurogenesis. *Dev. Cell* **35**, 553–567 (2015).
42. Savoy, R. M. & Ghosh, P. M. The dual role of filamin A in cancer: can't live with (too much of) it, can't live without it. *Endocr. Relat. Cancer* **20**, R341–R356 (2013).

## Acknowledgements

We thank P. Walter for providing IRE1-3F6H-GFP cells and M. P. Sheetz for providing filamin A-deficient cells and expression vectors. In addition, we thank D. Calderwood and D. Iwamoto for providing IgG-like filamin A individual plasmids tagged with GFP or GST. We thank L. Leyton for providing phospho-specific anti-PKC antibodies. This work was funded by the following bodies: FONDECYT no. 3160461 (to H.U.), no. 1140549 and 1180993 (to C.H.), no. 1140325 (to C.G.-B.), no. 1150608 (to R.L.V.); no. 1150766 (to F.C.); no. 3160478 (to E.P.); no. 3150113 (to A.C.-S.) and no. 1140522 (to Á.G.); Millennium Institute No. P09-015-F (to C.H., A.C. and M.L.C.); FONDAP 15150012 (to C.H., F.C., C.G.-B. and M.L.C.); FONDAP 15090007 (to Á.G.); ECOS-CONICYT 170032 (to C.H.); PIA-CONICYT ACT1401 (to Á.G.); NIH R01 Gm113188 (L.Q.) and CONICYT ACT1402 (to M.L.C.). We also thank the following organizations: the European Commission R&D MSCA-RISE #734749; The Michael J Fox Foundation for Parkinson's Research—Target Validation grant No 9277; FONDEF ID16110223; FONDEF D11E1007; the US Office of Naval Research-Global (ONR-G) N62909-16-1-2003; the US Air Force Office of Scientific Research FA9550-16-1-0384; ALSRP Therapeutic Idea Award AL150111; Muscular Dystrophy Association 382453; and CONICYT-Brazil 441921/2016-7 (to C.H.). T.I. is supported by the Toray Science Foundation. J.C., C.M.L. (no. 21160967) and D.R.H. are doctoral fellows supported by a CONICYT fellowship and by a CONICYT research grant.

## Author contributions

H.U. and C.H. designed the study. H.U., D.R.H., J.C., D.V.-C., A.C.-S., E.C., E.P., E.M., Y.M.H., C.M.L., S.A.-R., R.F., R.L.V., R.A., D.A.R. and C.A.R. participated in experimental designs, performed experiments and analysed the data. R.L.V., F.C., A.C., L.Q., E.C., T.I., M.L.C., Á.G. and C.G.-B. supervised the experiments and participated in the designs. H.U. and C.H. wrote or contributed to writing the manuscript. All authors read and approved the final version of the manuscript.

## Competing interests

The authors declare no competing interests.

## Additional information

**Supplementary information** is available for this paper at <https://doi.org/10.1038/s41556-018-0141-0>.

**Reprints and permissions information** is available at [www.nature.com/reprints](http://www.nature.com/reprints).

**Correspondence and requests for materials** should be addressed to C.H.

**Publisher's note:** Springer Nature remains neutral with regard to jurisdictional claims in published maps and institutional affiliations.



## Methods

**Reagents.** Tunicamycin was purchased from Calbiochem EMB Bioscience. Cell culture media, fetal calf serum and antibiotics were obtained from Life Technologies. Fluorescent probes and secondary antibodies coupled to fluorescent markers were purchased from Molecular Probes, Invitrogen. All other reagents used were from Sigma or of the highest grade available.

**Cell culture and DNA constructs.** All MEFs and HEK cells were maintained in Dulbecco's modified Eagle's medium (DMEM) supplemented with 5% FBS, non-essential amino acids and grown at 37 °C and 5% CO<sub>2</sub>. IRE1 $\alpha$ -deficient cells were produced as previously described<sup>6</sup>. Briefly, retroviral plasmids were transfected using Effectene (Qiagen) into HEK293GPG cells in order to prepare IRE1 $\alpha$ -HA expressing retroviruses were generated, as previously described<sup>13</sup>, in the pMSCV-Hygro vector, whereby the IRE1 $\alpha$  contains two tandem HA sequences at the C-terminal domain and a precision enzyme site before the HA tag. pRK5-F6 or F11 plasmids were generated as previously described<sup>21</sup>. Constructs of pEGFP expressing filamin A were generated as previously described<sup>18</sup>. Wild-type filamin A or S2152A mutants in pcDNA3.1 plasmids were a gift from J. Blenis (Addgene plasmid # 8982 and # 8983) (Weill Cornell Medicine, New York, NY). Wild-type filamin A or S2152A mutants in pcDNA3.1 plasmids were subcloned into the pCAGIG vector for in utero electroporation experiments<sup>44</sup>.

**Yeast-two hybrid assays.** The interaction between the IRE1 $\alpha$  $\Delta$ N protein and a library of adult mouse cDNA was performed using a Matchmaker Gold Yeast Two-Hybrid System (Clontech) according to the manufacturer's protocols. Briefly, AH109 yeast cells were transformed with plasmid pGADT7 (bait) encoding the cytoplasmic domain of IRE1 $\alpha$  (IRE1 $\alpha$  $\Delta$ N). The Y187 yeast strain contains the plasmid pGBKT7 (prey) encoding for a Normalized Yeast Two-Hybrid cDNA Library derived from adult mouse brain. Both plasmids encode for four different reporters: HIS3, ADE2, MEL1 and LacZ. AH109 and Y187 were mated for 24 h at 30 °C in YPDA media (common media containing yeast extract, peptone, dextrose and adenine). Mated yeasts were plated in synthetic defined medium SD-Leu/-Trp (DDO), SD-Leu/-Trp/-His (TDO) or SD-Leu/-Trp/-His/-Ade (QDO) for 3–7 days at 30 °C. The positive interactions were re-tested by re-streaking on TDO and QDO media after 3–7 days at 30 °C. Media lacking amino acids were also supplemented with X- $\alpha$ -galactoside (40  $\mu$ g ml<sup>-1</sup>), which changes the colonies that exhibit a positive interaction blue in colour. A growth index was calculated by visual observation (0 to 3 score) of the size and blue colouration of the selected colonies in TDO and QDO media. We used the interaction between pGBKT7-p53 and pGADT7-T as a positive control (Clontech). Plasmids of yeast colonies that showed positive interactions were rescued and transformed into *Escherichia coli* and then purified. Purified clones were then sequenced, and bioinformatics analysis was performed to identify target sequences.

To validate the interaction between IRE1 $\alpha$  and filamin A, AH109 yeast cells were co-transformed with plasmid pGADT7-IRE1 $\alpha$  $\Delta$ N and pGBKT7-filamin A. Eight microlitres of each suspension and three subsequent tenfold serial dilutions were individually spotted onto a medium SD-Leu/-Trp, SD-Leu/-Trp/-His and SD (-Leu/-Trp/-His/X- $\alpha$ -Gal) plates for selection. Cells were incubated at 30 °C for 2 days.

**RNA isolation, RT-PCR and real-time PCR.** PCR primers and methods for the *Xbp1* mRNA splicing assay have been previously described<sup>45</sup>. *Xbp1s* mRNA was monitored by semi-quantitative PCR using the following primers: 5'-AAGAACACGCTTGGGAATGG-3' and 5'-CTGCACCTGCTGCGGAC-3'. For the analysis of transcription targets and mRNA decay, real-time PCR assays were performed as described previously<sup>46</sup> using the following primers: Erdj4: 5'-CCCCAGTGTCAAACCTGTACCAG-3' and 5'-AGCGTTTCCAATTTTCCATAAATT-3';  $\beta$ -actin: 5'-TACCACCATGTACCCAGGCA-3' and 5'-CTCAGGAGGCAATGATCTTGAT-3'; Blos1: 5'-TCCCGCCTGCTCAAAGAAC-3' and 5'-GAGGTGATCCACCAACGCTT-3'; and Rpl19: 5'-CTGATCAAGGATGGGCTGAT-3' and 5'-GCCGCTATGTA CAGACAGCA-3'.

For mRNA analysis of cortex samples, real-time PCR assays were performed using the following primers: IRE1 $\alpha$ : 5'-CTCAGGATAATGGTAGCCATGTC-3' and 5'-ACACCGACCACCGTATCTCA-3', filamin A: 5'-TGGGATGCTAGTAAGCCTGTG-3' and 5'-CTGGGGTAATCACCTGAGGAAT-3' and  $\beta$ -actin: 5'-CTCAGGAGGAGCAATGATCTTGAT-3' and 5'-TACCACCATGTACCCAGGCA-3'.

**Immunoprecipitation assays.** HEK cells were co-transfected with different DNA constructs. After 48 h, protein extracts were prepared in lysis buffer (0.5% NP-40, 150–350 mM NaCl, 150 mM KCl, 50 mM Tris pH 7.6, 5% glycerol, 50 mM NaF, 1 mM Na<sub>3</sub>VO<sub>4</sub>, 250 mM PMSE, and protease inhibitors). Immunoprecipitation assays were performed as previously described<sup>46</sup>. In brief, to immunoprecipitate HA-tagged IRE1 $\alpha$ , protein extracts were incubated with anti-HA antibody-agarose complexes (Roche) for 4 h at 4 °C, and then washed 3 times with lysis buffer (1 ml) and then once in lysis buffer with 500 mM NaCl. Protein complexes were eluted by heating at 95 °C for 5 min in loading buffer.

IRE1 $\alpha$ -deficient MEFs cells stably transduced with retroviral expression vectors for IRE1 $\alpha$ -HA or empty vector were incubated in the presence or absence of tunicamycin (500 ng ml<sup>-1</sup>). Cell lysates were prepared for immunoprecipitation as described above for HEK cells. As a control, to eliminate nonspecific background binding, experiments were performed in parallel in IRE1 $\alpha$  knockout cells. Protein complexes were eluted by heating at 95 °C for 5 min in loading buffer. Huh7 cells grown to subconfluency were lysed using 0.5% NP-40, 30 mM Tris-HCl pH 7.5, 150 mM NaCl, and proteases and phosphatases inhibitors (Complete, Phostop; Lysis Buffer) for 20 min at 4 °C, and lysates were clarified by centrifugation at 13,200 r.p.m. for 15 min. Clarified lysates were precleared with Protein A Sepharose beads (or magnetic beads) for 30 min at 4 °C. Precleared lysates were then incubated overnight with 5  $\mu$ l ml<sup>-1</sup> of lysate of anti-IRE1 $\alpha$  antibodies (Santa Cruz Biotechnologies) at 4 °C followed by incubation with Protein A for 30 min at 4 °C. Beads were collected by centrifugation (30 s, 13,200 r.p.m. (rotor FA-45-18-11)) and washed 5 times with Lysis Buffer. Beads were dried and resuspended in sample buffer 2 $\times$ . Samples were heated for 5 min at 95 °C and resolved by SDS-PAGE 8% followed by western blot analysis.

**Expression of recombinant proteins.** Expression and purification of the CRIB domain of PAK1 or the FLNA-19–21 and FLNA-21–24 IgG repeats were performed as described previously<sup>17</sup>. BL21 (DE3) *E. coli* strains carrying pGEX-glutathione S-transferase (GST)-CRIB were grown overnight at 37 °C in Luria broth media containing ampicillin. Cultures were diluted 1:100 and grown in fresh medium at 37 °C to an optical density at 600 nm of 0.7. Next, IPTG (isopropyl  $\beta$ -D-1-thiogalactopyranoside) was added to a final concentration of 1 mM. The cultures were grown for an additional 2 h and then samples were collected and sonicated in lysis buffer A (50 mM Tris-HCl pH 8.0, 1% Triton X-100, 1 mM EDTA, 150 mM NaCl, 25 mM NaF, 0.5 mM PMSF and protease inhibitor complex (Roche)). Cleared lysates were affinity purified with glutathione-Sepharose beads (Amersham). Loaded beads were washed ten times with lysis buffer B (lysis buffer A with 300 mM NaCl) at 4 °C. GST fusion protein was quantified and visualized in SDS-polyacrylamide gels stained with Coomassie brilliant blue.

**Pull-down assays.** FLNA-19–21 and FLNA-21–24 GST filamin domains bound to Sepharose-glutathione resin were incubated with 4  $\mu$ g of the cytoplasmic domain of GST-tagged IRE1 $\alpha$  for 6 h at 4 °C on an end-to-end rotor. After incubation, the mixture was centrifuged at 2,000 r.p.m. for 4 min and the supernatant was discarded. The resin was washed with 400  $\mu$ l of lysis buffer at 4 °C for 10 min and subsequently centrifuged. This process was repeated five times. The bound proteins were eluted by boiling in SDS sample buffer at 95 °C for 5 min and analysed by western blotting.

**Western blot analysis.** Cells were collected and homogenized in RIPA buffer (20 mM Tris pH 8.0, 150 mM NaCl, 0.1% SDS, 0.5% Triton X-100) containing a protease inhibitor cocktail (Roche) in presence of 50 mM NaF and 1 mM Na<sub>3</sub>VO<sub>4</sub>. Protein concentrations were determined in all experiments by micro-BCA assay (Pierce), and 20–40  $\mu$ g of total protein was loaded onto 8–12% SDS-PAGE minigels (Bio-Rad Laboratories) before transfer onto polyvinylidene fluoride membranes. Membranes were blocked using PBS, 0.1% Tween20 (PBST) containing 5% milk for 60 min at room temperature then probed overnight with primary antibodies. The following antibodies diluted in blocking solution were used: anti-HSP90 (1:5000); anti-HA (1:1000; Roche); anti-GFP (1:3000; Sigma); anti-filamin A (1:1000); anti-phospho S2152 filamin A (1:1000); and anti-IRE1 $\alpha$  (1:1000; Cell Signaling Technology). Bound antibodies were detected with peroxidase-coupled secondary antibodies (incubated for 1 h at room temperature) and an ECL system.

**ER fractionation.** Subcellular fractionation was performed following a previously described protocol<sup>48</sup>. In brief, cells were washed and ground in a stainless-steel dounce dura-grind tissue grinder (Wheaton). Cellular integrity was evaluated every five strokes with trypan blue staining. Homogenate was centrifuged 2 times at 640  $\times$ g to remove unbroken cells and nuclei. Supernatant was centrifuged twice at 9,000  $\times$ g to pellet crude mitochondria. The supernatant was further spun at 20,000  $\times$ g for 30 min to obtain a pellet of lysosomes and plasma membrane and a supernatant that, upon further 100,000  $\times$ g centrifugation, gave a supernatant (cytosol) and a pellet (ER). Western blot analyses were used to validate each fraction with different antibodies.

**Indirect immunofluorescence analysis.** IRE1 $\alpha$ -HA, PKC $\alpha$ -Flag and KDEL proteins were visualized by immunofluorescence. Cells were fixed for 30 min with 4% paraformaldehyde and permeabilized with 0.5% NP-40 in PBS containing 0.5% bovine serum albumin (BSA) for 10 min. After blocking for 1 h with 10% FBS in PBS containing 0.5% BSA, cells were incubated with anti-HA, anti-Flag or anti-KDEL antibodies overnight at 4 °C. Cells were washed three times in PBS containing 0.5% BSA, and incubated with Alexa-conjugated secondary antibodies (Molecular Probes) for 1 h at 37 °C. Nuclei were stained with Hoechst dye. Coverslips were mounted with Fluoromount G onto slides and visualized by confocal microscopy (Fluoview FV1000).

We used a sensitive method based on a confined displacement analysis algorithm to calculate colocalization coefficients between IRE1 $\alpha$ -HA and filamin A-GFP<sup>49</sup>.



The colocalization of images was performed as previously described<sup>49</sup>. Briefly, images obtained by confocal microscopy using a  $\times 60$  oil objective lens (NA: 1.35) were subjected to Huygens deconvolution software. Each channel used for filamin A-GFP, IRE1 $\alpha$ -HA and KDEL RFP (or Flag) was then segmented using a series of filters using IDL software to obtain masked images of each channel. These masked images were used to determine Manders colocalization coefficients and to quantify true and random colocalization between channels. In addition, a specific mask was applied to evaluate colocalization in the ER region (KDEL-RFP) or total cellular area (filamin A-GFP).

**Targeting IRE1 $\alpha$  in MEFs.** We generated stable MEFs with reduced levels of IRE1 $\alpha$  using previously described methods<sup>50</sup> by targeting IRE1 $\alpha$  mRNA with two different shRNAs using the lentiviral expression vector pLKO.1 and puromycin selection. As a control, a shRNA against the luciferase gene was used. Constructs were obtained from The Broad Institute. Targeting sequences used for mouse IRE1 $\alpha$  were as follows: GGAATCCTCTACATGGGTAAA and GCTGAACACTTGGAGGAATTA. To generate lentiviruses, HEK cells were transfected using the calcium phosphate protocol with 1  $\mu$ g of VSV-G vector, 1  $\mu$ g of  $\Delta 8.9$  vector and 1  $\mu$ g of shRNA vector. After 48 h of transfection, the supernatant was collected and filtered through a 0.45  $\mu$ m filter. MEF cells were transduced with a 1:1 dilution of viral supernatant containing 8  $\mu$ g ml<sup>-1</sup> of polybrene. After 24 h of infection, cells were washed and incubated with 2  $\mu$ g ml<sup>-1</sup> of puromycin until selection was obtained. The CRISPR line IRE1 $\alpha$ <sup>CRISPR</sup> was generated using the mouse IRE1 $\alpha$  Double Nickase system (Santa Cruz Biotechnology) as indicated by the manufacturer.

**Cell migration assays.** Confluent monolayers of MEF cells were wounded with a 20–200  $\mu$ l pipette tip. Cells were washed twice with PBS and DMEM with 3% FBS was added as stimuli. Images were acquired using a  $\times 10$  objective lens and an inverted microscope at 0 and 16 h of migration. The wounded area was calculated using ImageJ software as previously described<sup>51</sup>. Transwell assays were performed in Boyden chambers (Transwell Costar, 6.5 mm diameter, 8  $\mu$ m pore size) according to the manufacturer's instructions. Briefly, the bottom of the inserts were coated with 2  $\mu$ g ml<sup>-1</sup> fibronectin. Cells ( $3 \times 10^4$ ) re-suspended in serum-free medium were plated onto the top of each chamber insert and serum-free medium was added to the bottom chamber. After 4–6 h, inserts were removed, washed and cells that migrated to the bottom portion of the inserts were stained with 0.1% crystal violet in 2% ethanol and counted using an inverted microscope. In addition, cell-bound dye was eluted with methanol, and the absorbance was measured at 600 nm. For cell adhesion experiments, cells were plated on fibronectin-coated coverslips for different times. Cells were fixed with 4% paraformaldehyde and stained with 0.1% crystal violet in 2% ethanol to evaluate cell adhesion or processed for immunofluorescence to evaluate cell and ER spreading.

In addition, MEFs were co-transfected with different plasmids and pEGFP. Cells were re-seeded onto the top of each chamber insert coated with 2  $\mu$ g ml<sup>-1</sup> fibronectin and allowed to migrate for 4–6 h. Then, inserts were removed, washed and the number of GFP-positive cells was counted in 8 different fields using a fluorescent inverted microscope and a  $\times 20$  objective lens.

**Actin cytoskeleton dynamics.** MEF cells were seeded onto fibronectin-coated 25-mm coverslips, transfected with EGFP-Lifeact using Lipofectamine 2000 Transfection Reagent and imaged in HBSS medium supplemented with HEPES using a confocal microscope (Zeiss LSM 710) with a  $\times 63/1.4$  NA oil-immersion objective lens at 37 °C. Images were acquired every 30 s for 5 min, and the number of lamellipodia per cell was determined manually, as previously described<sup>52</sup>. In addition, to perform a protrusion and retraction analysis, images were segmented using maximum threshold<sup>53</sup>. Then, subsequent images were merged assigning the first image as green and the second image as red. The total area of green (protrusions) and red (retractions) colour of merged images was obtained using ImageJ software. In addition, cells were fixed and stained with phalloidin coupled to rodamine and visualized by confocal microscopy. The number of lamellipodia per cell was determined manually as described previously<sup>52</sup>.

**Rac1 activation assays.** Purified loaded beads containing the CRIB domain were incubated for 70 min at 4 °C with 1 mg of either MEF lysates using fishing buffer (50 mM Tris-HCl pH 7.5, 10% glycerol, 1% Triton X-100, 200 mM NaCl, 10 mM MgCl<sub>2</sub>, 25 mM NaF and protease inhibitor complex). The beads were washed three times with washing buffer (50 mM Tris-HCl pH 7.5, 30 mM MgCl<sub>2</sub> and 40 mM NaCl) and then re-suspended in SDS-PAGE sample buffer. Bound Rac1-GTP was subjected to immunoblot analysis and quantified with respect to total Rac1 using ImageJ.

**IRE1 $\alpha$  oligomerization assay.** TREX cells expressing IRE1-3F6H-GFP wild-type or D123P were obtained from Cornell University and were generated as previously described<sup>27</sup>. TREX cells plated and treated with doxycycline (500 ng ml<sup>-1</sup>) for 48 h. Cells were treated with tunicamycin (1  $\mu$ g ml<sup>-1</sup>) for different time points and fixed with 4% paraformaldehyde for 30 min. Nuclei were stained with Hoechst dye. Coverslips were mounted with Fluoromount G onto slides and visualized by

confocal microscopy (Fluoview FV1000). The number and size of IRE1 $\alpha$  clusters were quantified using segmentation and particle analysis in ImageJ software.

**Brain analysis of IRE1 $\alpha$  knockout animals.** Female and male IRE1 $\alpha$  heterozygous mice were mated to obtain IRE1 $\alpha$  heterozygous and knockout embryos. Both IRE1 $\alpha$  knockout and control embryos at E14.5 were surgically collected from the pregnant IRE1 $\alpha$  heterozygous mice. Each tail tip was immediately cut off from the embryonic body and was used for genotyping as previously described<sup>54</sup>. Then, each embryonic body was rinsed in PBS and then fixed in 4% paraformaldehyde phosphate buffer solution on a reciprocal shaker (50 osc. per min) for 24 h at room temperature. After fixation, each embryonic body was cryoprotected in 30% sucrose PBS on a reciprocal shaker (50 osc. per min) for 24 h at room temperature. Brains were collected and coronal sections were obtained for histological analyses, using anti-Trb1-specific antibodies and nuclei staining with DAPI. Images were obtained using an epifluorescence inverted microscope at  $\times 10$  and  $\times 20$  magnification. The width of the cortex and layer IV (Trb1 staining) was measured using ImageJ software. The experimental protocol (#2017-51) was approved by the Animal Studies Committees at Kanazawa Medical University and was compliant with all relevant ethical regulations regarding animal research.

**In utero electroporation.** In utero electroporation was performed as described previously<sup>54,55</sup>. Uterine horns of timed-pregnant dams were exposed by midline laparotomy after anaesthetization with isoflurane inhalation. A 2- $\mu$ l solution containing 4  $\mu$ g of DNA plasmid (shRNAs for IRE1 $\alpha$  or a luciferase control co-expressed with a GFP-encoding vector at a 1:5 ratio) mixed with 0.02% fast green dye were injected into the lateral ventricles of E14.5 brains and then introduced into ventricular zone cells by delivering five electric pulses at 45 V for 50 ms, with 950 ms intervals, through the uterine wall using a Gene Pulser Xcell (Bio-Rad). After electroporation of all embryos, the uterus was replaced within the abdomen, the cavity was filled with warm sterile saline, and the abdominal muscle and skin incisions were closed with silk sutures. Animals were left to recover in a warm clean cage. Pups were harvested 5 days later (P0), and the position of transfected neurons in coronal sections was analysed by fluorescence microscopy. Cortex layers were identified via the nuclei density among the analysed section. The number of GFP-positive cells and total fluorescence intensity by layer was quantified using ImageJ software in all brain sections. All experiments were performed in accordance with the appropriate institutional guidelines of the Faculty of Medicine of the University of Chile and compliant with all relevant ethical regulations regarding animal research.

**D. melanogaster strains and in vivo imaging.** The following strains were obtained from the Bloomington Stock Center: Cg-Gal4; Hml $\Delta$ -Gal4, 2xEGFP; UAS-mCDS8-GFP; Iref02170/TM6B; hsFLP; Tub-Gal4, UAS-GFP/CyO, Act-GFP; Tub-Gal80TS, FRT82B P{EP}cher<sup>G093</sup>; UAS-Ire1-IR (v39562) was obtained from the Vienna Drosophila Research Center. All crosses were made at 25 °C. Pupae at 20  $\pm$  2 h after puparium formation were mounted as described previously<sup>56</sup>. The migration of GFP-labelled macrophages was recorded using a Carl Zeiss LSM710 microscope with a  $\times 40$  objective. Movies are Z-projections of 12 1- $\mu$ m slices acquired every 60 s for 50 min. Cells trajectories were recorded using the ImageJ Manual Tracking plugin, and their speed calculated using the Chemotaxis Tool plugin. The LifeAct-GFP reporter was expressed in macrophages using the Cg-Gal4 driver (Cg-Gal4 > LifeAct-GFP). After 75 min of culture, movies were recorded every 4 s for ~3 min using a Carl Zeiss LSM710 with a  $\times 63$  objective. Individual macrophages were recorded in the plane in which the largest membrane extension was observed. Velocity maps were generated using the ADAPT tool for imageJ as indicated previously<sup>57</sup>. For mosaic analysis, the following lines were crossed and grown at 25 °C: hsFLP; Tub-Gal4, UAS-GFP/CyO, Act-GFP; Tub-Gal80TS, FRT82B and Iref02170, FRT82B/TM6B. Progeny were subjected to a heat-shock of 1 h at 37 °C at 48, 72 and 96 h. After egg laying<sup>58</sup> third-instar larvae containing GFP-expressing macrophages were selected, and macrophage primary cultures were made.

To prepare primary culture coverslips, four third-instar larvae were washed in PBS then rinsed in 70% ethanol and washed once in PBS. Larvae were placed on coverslips with 120  $\mu$ l Schneider's Insect Medium (Sigma-Aldrich), and immediately, a small incision was made in the posterior section of the cuticle using dissecting forceps. The haemolymph was collected for 1 min. Macrophages were allowed to adhere for 1 h and 15 min at 25 °C in a humidity chamber. The coverslip was then transferred to a 12-well plate, medium was removed and washed with PBS. For F-actin staining, cells were fixed in 4% paraformaldehyde for 10 min, permeabilized with PBS-0.1% Triton for 10 min and incubated for 2 h at room temperature with Phalloidin-FITC (50  $\mu$ M, Sigma) in PBS-BSA 1%. TO-PRO-3 (10  $\mu$ M; Invitrogen) was added in the last 20 min of incubation. Finally, cells were washed three times with PBS for 15 min each and mounted on Vectashield (Vector Laboratories). Imaging of cells was conducted using a Zeiss LSM710 microscope with  $\times 63$  objective. The images were processed using the software PHOTOSHOP CS4. All experiments were performed in accordance with the appropriate institutional guidelines of the Faculty of Medicine of the University of Chile and compliant with all relevant ethical regulations regarding animal research.

**Zebrafish studies.** Wild-type TAB5 and Tg(actb1:mCherry-utrCH) fish lines were used. Embryos were raised in E3 medium, kept at 28°C and staged according to age (hours post fertilization; hpf). Sixty picograms of capped IRE1 $\alpha$ -DN mRNA synthesized using a T7 mMessage mMachine Kit (Ambion) from the pcDNA-IRE1 $\alpha$ -DN-DN<sup>31,32</sup>, was injected into one-cell stage embryos as previously described<sup>58</sup>. To calculate the extent of cell movements during gastrulation, embryos were imaged using a stereoscope and the progression of the blastoderm, the head-to-tail angle and width of the first three somites were measured as previously described using Fiji free software at 9, 11.5 and 12 hpf<sup>59</sup>. For confocal imaging, Tg(actb1:mCherry-utrCH) embryos were placed in custom-made chambers and imaged on a Volocity ViewVox spinning disc (Perkin Elmer) coupled to a Zeiss Axiovert 200 confocal microscope using a Pan-Apochromatic X 40/1.2W objective. Images were deconvolved using Huygens software (Scientific Volume Imaging). To measure circularity and pixel signal intensity, cells were segmented manually using Fiji free software. All experiments were performed in accordance with the appropriate institutional guidelines of the Faculty of Medicine of the University of Chile and compliant with all relevant ethical regulations regarding animal research.

**Statistics and reproducibility.** For all experiments in cell lines, at least three independent biological experiments were performed. For all colocalization and electron microscopy experiments, we performed three independent biological experiments; however, since analysis was performed in individual cells, data analysis of all cells analysed are indicated in the legends. Results were statistically compared using one-way analysis of variance (ANOVA) for unpaired groups followed by multiple comparison post-tests (Tukey's multiple comparison test). When pertinent, two-tailed Student's *t*-test was performed for unpaired or paired groups. In all plots, *P* values are shown as indicated: \**P* < 0.05, \*\**P* < 0.01 and \*\*\**P* < 0.001 and were considered significant. All results are presented as the mean  $\pm$  s.e.m. Analyses were performed using PRISM software.

**Reporting Summary.** Further information on experimental design is available in the Nature Research Reporting Summary linked to this article.

**Data availability.** All data supporting the findings of this study are available from the corresponding author on reasonable request.

## References

43. Hetz, C. et al. Proapoptotic BAX and BAK modulate the unfolded protein response by a direct interaction with IRE1 $\alpha$ . *Science* **312**, 572–576 (2006).
44. Matsuda, T. & Cepko, C. L. Electroporation and RNA interference in the rodent retina in vivo and in vitro. *Proc. Natl Acad. Sci. USA* **101**, 16–22 (2004).
45. Lisbona, F. et al. BAX inhibitor-1 is a negative regulator of the ER stress sensor IRE1 $\alpha$ . *Mol. Cell* **33**, 679–691 (2009).
46. Rodriguez, D. A. et al. BH3-only proteins are part of a regulatory network that control the sustained signalling of the unfolded protein response sensor IRE1 $\alpha$ . *EMBO J.* **31**, 2322–2335 (2012).
47. Henriquez, D. R., Bodaleo, F. J., Montenegro-Venegas, C. & Gonzalez-Billault, C. The light chain 1 subunit of the microtubule-associated protein 1B (MAP1B) is responsible for Tiam1 binding and Rac1 activation in neuronal cells. *PLoS ONE* **7**, e53123 (2012).
48. Wieckowski, M. R., Giorgi, C., Lebedzinska, M., Duszynski, J. & Pinton, P. Isolation of mitochondria-associated membranes and mitochondria from animal tissues and cells. *Nat. Protoc.* **4**, 1582–1590 (2009).
49. Ramirez, O., Garcia, A., Rojas, R., Couve, A. & Hartel, S. Confined displacement algorithm determines true and random colocalization in fluorescence microscopy. *J. Microsc.* **239**, 173–183 (2010).
50. Hetz, C. et al. The proapoptotic BCL-2 family member BIM mediates motoneuron loss in a model of amyotrophic lateral sclerosis. *Cell Death Differ.* **14**, 1386–1389 (2007).
51. Urra, H. et al. Caveolin-1-enhanced motility and focal adhesion turnover require tyrosine-14 but not accumulation to the rear in metastatic cancer cells. *PLoS ONE* **7**, e33085 (2012).
52. Lim, K. B. et al. The Cdc42 effector IRSp53 generates filopodia by coupling membrane protrusion with actin dynamics. *J. Biol. Chem.* **283**, 20454–20472 (2008).
53. Grande-Garcia, A. et al. Caveolin-1 regulates cell polarization and directional migration through Src kinase and Rho GTPases. *J. Cell Biol.* **177**, 683–694 (2007).
54. Fuentes, P., Canovas, J., Berndt, F. A., Noctor, S. C. & Kukuljan, M. CoREST/ LSD1 control the development of pyramidal cortical neurons. *Cereb. Cortex* **22**, 1431–1441 (2012).
55. LoTurco, J., Manent, J. B., Sidiqi, F. New and improved tools for in utero electroporation studies of developing cerebral cortex. *Cereb. Cortex* **19**, 20–25 (2009).
56. Moreira, C. G., Regan, J. C., Zaidman-Remy, A., Jacinto, A. & Prag, S. *Drosophila* hemocyte migration: an in vivo assay for directional cell migration. *Methods Mol. Biol.* **769**, 249–260 (2011).
57. Barry, D.J., Durkin, C.H., Abella, J.V. & Way, M. Open source software for quantification of cell migration, protrusions, and fluorescence intensities. *J. Cell Biol.* **209**, 163–180 (2015).
58. Barth, K. A. & Wilson, S. W. Expression of zebrafish nk2.2 is influenced by sonic hedgehog/vertebrate hedgehog-1 and demarcates a zone of neuronal differentiation in the embryonic forebrain. *Development* **121**, 1755–1768 (1995).
59. Yeh, C.-M. et al. Ptenb mediates gastrulation cell movements via Cdc42/AKT1 in zebrafish. *PLoS ONE* **6**, e18702 (2011).

## Reporting Summary

Nature Research wishes to improve the reproducibility of the work that we publish. This form provides structure for consistency and transparency in reporting. For further information on Nature Research policies, see [Authors & Referees](#) and the [Editorial Policy Checklist](#).

### Statistical parameters

When statistical analyses are reported, confirm that the following items are present in the relevant location (e.g. figure legend, table legend, main text, or Methods section).

n/a Confirmed

- The exact sample size ( $n$ ) for each experimental group/condition, given as a discrete number and unit of measurement
- An indication of whether measurements were taken from distinct samples or whether the same sample was measured repeatedly
- The statistical test(s) used AND whether they are one- or two-sided  
*Only common tests should be described solely by name; describe more complex techniques in the Methods section.*
- A description of all covariates tested
- A description of any assumptions or corrections, such as tests of normality and adjustment for multiple comparisons
- A full description of the statistics including central tendency (e.g. means) or other basic estimates (e.g. regression coefficient) AND variation (e.g. standard deviation) or associated estimates of uncertainty (e.g. confidence intervals)
- For null hypothesis testing, the test statistic (e.g.  $F$ ,  $t$ ,  $r$ ) with confidence intervals, effect sizes, degrees of freedom and  $P$  value noted  
*Give  $P$  values as exact values whenever suitable.*
- For Bayesian analysis, information on the choice of priors and Markov chain Monte Carlo settings
- For hierarchical and complex designs, identification of the appropriate level for tests and full reporting of outcomes
- Estimates of effect sizes (e.g. Cohen's  $d$ , Pearson's  $r$ ), indicating how they were calculated
- Clearly defined error bars  
*State explicitly what error bars represent (e.g. SD, SE, CI)*

*Our web collection on [statistics for biologists](#) may be useful.*

### Software and code

Policy information about [availability of computer code](#)

#### Data collection

For co-localization a three step processes was done. First deconvolution of images were done using Huygens Professional software. Second, segmentation and total and endoplasmic reticulum (ER) masks were done using IDL 7.0. Finally, colocalization between IRE1a/ Filamin A, Filamin A/ER and PKCa/ER was done using Colocalization displacement analysis available in IDL7.0 or Image J software.

All quantifications of number of cell of transmigration assays, area of wound in healing assays, total and ER area of adhesion assays and width measurement were done using Image J software.

Gene Ontology analysis of proteins obtained in the Yeast-two hybrid screen was done using Toppgene analysis available online

#### Data analysis

Data acquisition and graphs were done in excel files and statistical analysis were done using GraphPad Prism 5 software.

For manuscripts utilizing custom algorithms or software that are central to the research but not yet described in published literature, software must be made available to editors/reviewers upon request. We strongly encourage code deposition in a community repository (e.g. GitHub). See the Nature Research [guidelines for submitting code & software](#) for further information.

## Data

Policy information about [availability of data](#)

All manuscripts must include a [data availability statement](#). This statement should provide the following information, where applicable:

- Accession codes, unique identifiers, or web links for publicly available datasets
- A list of figures that have associated raw data
- A description of any restrictions on data availability

All data and materials along with detailed instructions on their use are available from the authors upon request. No raw data have been linked in the manuscript.

## Field-specific reporting

Please select the best fit for your research. If you are not sure, read the appropriate sections before making your selection.

Life sciences       Behavioural & social sciences       Ecological, evolutionary & environmental sciences

For a reference copy of the document with all sections, see [nature.com/authors/policies/ReportingSummary-flat.pdf](https://www.nature.com/authors/policies/ReportingSummary-flat.pdf)

## Life sciences study design

All studies must disclose on these points even when the disclosure is negative.

Sample size	<p>All experiments performed in this work were repeated at least three times, unless indicated otherwise in individual figure legends. All repeats performed resulted in exact agreement or similar results.</p> <p>No sample size calculation were performed for in vitro experiments and sample sizes were chosen for individual experiments according to previous expertise.</p> <p>For cellular based-assays we repeat a minimum of 4 experiments in order to perform statistical analysis.</p> <p>For in vivo experiments using in utero electroporation we define a minimum of experimental animals based on the indications suggested in "Guidelines for the Care and Use of Mammals in Neuroscience and Behavioral Research" using the following model <math>n=1+2C(s/d)^2</math> (n is the number of animals; C is a constant that depend on the power and statistical differences; s is the standard deviation of the measurement and d is the differences expected in each condition)</p>
Data exclusions	No data was excluded from the analysis.
Replication	<p>For immunoprecipitation experiments every time we prepared freshly made lysis buffer we stock solutions. For endogenous IP we always used a 10 cm plate containing around <math>7 \times 10^6</math> cells. For IP using over expression of proteins we transfected 2 well of 6-well plates. Transfection efficiency was observed every time to be sure to have enough material. Although initial experiments were hard to observe the co-IP, once we setup the right buffer we always observed the co-IP of Filamin A and IRE1a.</p> <p>For cell culture experiments, we track the passage of cells in order to used cells in similar passages and used new batch after 10 passages. Selection of cells was done every two week to always work with cells expressing WT and mutant IRE1a. Wound healing assays, transmigration and actin cytoskeleton dynamics were done almost at same days or weeks to ensure reproducibility.</p> <p>Since working with tunicamycin is complicated since freezing cycles affects the stability of the molecule we always used small aliquots that only have been thawed once in order to ensure reproducibility.</p>
Randomization	<p>For in utero electroporation samples were divided in control and the experimental condition based in the position in the uterine horns. Left side of the uterine horns were injected with control conditions always. The experimental condition was injected in pups in the right side of the horns.</p> <p>No randomization was done</p>
Blinding	Quantification of actin bundles by EM and the GFP% neurons in the in utero electroporation experiments were done blinded.

## Reporting for specific materials, systems and methods

## Materials &amp; experimental systems

n/a	Involvement	Involved in the study
<input type="checkbox"/>	<input checked="" type="checkbox"/>	Unique biological materials
<input type="checkbox"/>	<input checked="" type="checkbox"/>	Antibodies
<input type="checkbox"/>	<input checked="" type="checkbox"/>	Eukaryotic cell lines
<input checked="" type="checkbox"/>	<input type="checkbox"/>	Palaeontology
<input type="checkbox"/>	<input checked="" type="checkbox"/>	Animals and other organisms
<input checked="" type="checkbox"/>	<input type="checkbox"/>	Human research participants

## Methods

n/a	Involvement	Involved in the study
<input checked="" type="checkbox"/>	<input type="checkbox"/>	ChIP-seq
<input checked="" type="checkbox"/>	<input type="checkbox"/>	Flow cytometry
<input checked="" type="checkbox"/>	<input type="checkbox"/>	MRI-based neuroimaging

## Unique biological materials

Policy information about [availability of materials](#)

Obtaining unique materials

## Antibodies

## Antibodies used

Antibody Anti-HA High Affinity 3F10  
 Supplier name: Roche  
 Catalog number 11867423001  
 Dilution 1:3000  
 Used as recommended by manufacturer

Antibody Anti-GFP (B-2)  
 Supplier name: Santa cruz biotechnology  
 Catalog number SC-9996  
 Dilution 1:3000  
 Used as recommended by manufacturer

Antibody Anti-Filamin A  
 Supplier name: Cell Signaling Technology  
 Catalog number 4762  
 Dilution 1:1000  
 Used as recommended by manufacturer

3  
 nature research | reporting summary March 2018

Antibody Anti-pS2152-Filamin A  
 Supplier name: Cell Signaling Technology  
 Catalog number 4761  
 Dilution 1:1000  
 Used as recommended by manufacturer

Antibody Anti-Filamin A  
 Supplier name: ABCAM  
 Catalog number ab76289  
 Dilution 1:5000  
 Used as recommended by manufacturer

Antibody Anti-pS2152-Filamin A  
 Supplier name: ABCAM  
 Catalog number ab51229  
 Dilution 1:1000  
 Used as recommended by manufacturer

Antibody Anti-Glutathione-S-Transferase (GST) antibody produced in rabbit  
 Supplier name: Santa cruz biotechnology  
 Catalog number sc-53909  
 Dilution 1:1000  
 Used as recommended by manufacturer

Antibody Anti-IRE1a  
 Supplier name: Cell Signaling Technology  
 Catalog number 32945  
 Dilution 1:1000  
 Used as recommended by manufacturer

Antibody Anti-Rac1 Clone 102  
 Supplier name: BD Transduction Laboratories  
 Catalog number 610650  
 Dilution 1:5000  
 Used as recommended by manufacturer

Antibody Anti-HSP90  
 Supplier name: Santa cruz biotechnology  
 Catalog number SC-7947  
 Dilution 1:5000  
 Used as recommended by manufacturer

Antibody Anti-KDEL  
 Supplier name: Enzo Life Sciences  
 Catalog number SPA-827  
 Dilution 1:200 (IFi)  
 Used as recommended by manufacturer

Antibody Anti-HIS  
 Supplier name: Santa cruz biotechnology  
 Catalog number sc-803  
 Dilution 1:1000  
 Used as recommended by manufacturer

Antibody Anti-Trb1  
 Supplier name: Abcam  
 Catalog number ab31940  
 Dilution 1:200 (IFi)  
 Used as recommended by manufacturer

Antibody Anti-Myc  
 Supplier name: Santa cruz biotechnology  
 Catalog number sc-40  
 Dilution 1:1000  
 Used as recommended by manufacturer

#### Validation

For most of endogenous proteins tested we validated the antibody using the WT and Knockout proteins. For the antibodies used for IP, the antibody was tested using the over expression of tagged proteins. All antibodies used for indirect immunofluorescence we performed primary and secondary antibodies control in addition to used en knockout cells.

## Eukaryotic cell lines

Policy information about [cell lines](#)

#### Cell line source(s)

MEF IRE1 WT and knockout cells were provided David Ron. From this cell lines we reconstitute with IRE1a WT and the different mutants tested in the manuscript. All other cells used including HEK-293 (ATCC), MDA-231, HT22, HELA and HCT116 were obtained from the University of Chile. The cell line U2OS was obtained from Guido Kroemer laboratory.

#### Authentication

Since cell lines were obtained from animals in a previously described publication and their are not commercially available we did not performed any cell line authentication. We surely perform validation of knockout cells by PCR and western blot of selected proteins. To evaluate the activity of IRE1a mutants we performed XBP1 mRNA splicing assay as described in methods.

#### Mycoplasma contamination

All cells were negative for mycoplasma contamination. All cells were routinely tested for mycoplasma contamination using the EZ-PCR Mycoplasma Test Kit (Biological Industries). In case of any contamination, the cell line was eliminated inmediately and a new batch was thawed.

#### Commonly misidentified lines (See [ICLAC](#) register)

No common misidentified cell lines were used

## Animals and other organisms

Policy information about [studies involving animals](#); [ARRIVE guidelines](#) recommended for reporting animal research

#### Laboratory animals

For in utero electroporation experiments we used pregnant female mice and intervned at E14.5 and at P0.

For the embryo analysis of IRE1 Knockout animals we used Female and male IRE1 $\alpha$  Heterozygous (Het) C57BL6 mice mated to obtain IRE1 $\alpha$  Het and KO embryos. Both IRE1 $\alpha$  KO and control embryos were surgically collected from the pregnant IRE1 $\alpha$  Het mice at 14.5.

For D. Melanogaster experiments we used several strains obtained from Bloomington stock center: Cg-Gal4; Hml $\Delta$ -Gal4, 2xEGFP; UAS-mCD8-GFP; Iref02170/TM6B; hsFLP; Tub-Gal4, UAS-GFP/CyO, Act-GFP; Tub-Gal80TS. FRT82B P{EP}cherG9093 are from the Vienna Drosophila Research Center: UAS-Ire1-IR (v39562). For all experiments we used pupae at 20  $\pm$  2 h APF (After Puparium Formation)

For Zebrafish experiments we used several strains available in Miguel Concha's Laboratory including Wild-type TAB5, Tg(actb1:mCherry-utrCH) and Tg(sox17::GFP). Embryos were used at 1-cell stage embryos to inject mRNAs and then analyzed at

7, 9, 11.5 and 12 hpf depending on the experiment.

Wild animals

The study did not involve wild animals, no animals in the study were collected from the field

Field-collected samples

The study did not involve wild animals, no animals in the study were collected from the field

## 13.2. *Emerging Roles of the Endoplasmic Reticulum Associated Unfolded Protein Response in Cancer Cell Migration and Invasion.*

*Cancers (Basel). 2019 May 6;11(5).*

### 13.2.1. *Foreword*

Tumor cells develop a highly efficient secretory pathway since there is a group of stressful factors responsible for alterations in the secretory machinery. These factors can cause the loss of protein homeostasis in the ER by the accumulation of misfolded proteins, generating a cellular condition known as ER stress. The stress of ER triggers an adaptive response called unfolded protein response (UPR). The activation of the UPR has been described in different tumors and multiple cellular and animal models of cancer. The three pathways of the UPR have been related to cancer progression and are directly connected to different hallmarks of cancer. In this review, we covered relevant aspects of the cell migration and invasion processes. Next, we discuss and summarize state of the art on the roles of the UPR in the regulation of cell migration, invasion, and metastasis. A discussion about the therapeutic potential of targeting the different UPR branches is also included.

### 13.2.2. *Contribution*



The author of the present thesis wrote section number 3 that contains a brief overview of the UPR and discusses the role of UPR in cancer and the connections with metastasis.



She was in constant communication with Tony Avril, who supervised the construction of the review. She additionally participated in the revision of the figures and the manuscript on its final form.

Review

# Emerging Roles of the Endoplasmic Reticulum Associated Unfolded Protein Response in Cancer Cell Migration and Invasion

Celia Maria Limia <sup>1,2,3,4,5,†</sup>, Chloé Sauzay <sup>1,2,†</sup>, Hery Urra <sup>3,4</sup> , Claudio Hetz <sup>3,4,5,6,7</sup>, Eric Chevet <sup>1,2,8</sup> and Tony Avril <sup>1,2,8,\*</sup> 

<sup>1</sup> Proteostasis & Cancer Team, Institut National de la Santé Et la Recherche Médicale U1242 Chemistry, Oncogenesis, Stress and Signaling, Université de Rennes, 35042 Rennes, France; cema201089@gmail.com (C.M.L.); Sauzay.Chloe@chu-amiens.fr (C.S.); eric.chevet@inserm.fr (E.C.)

<sup>2</sup> Centre Eugène Marquis, 35042 Rennes, France

<sup>3</sup> Biomedical Neuroscience Institute, University of Chile, 8380453 Santiago, Chile; hery.urr@gmail.com (H.U.); claudio.hetz@gmail.com (C.H.)

<sup>4</sup> Center for Geroscience, Brain Health and Metabolism (GERO), 8380453 Santiago, Chile

<sup>5</sup> Institute of Biomedical Sciences (ICBM), Faculty of Medicine, University of Chile, 8380453 Santiago, Chile

<sup>6</sup> The Buck Institute for Research in Aging, Novato, CA 94945, USA

<sup>7</sup> Department of Immunology and Infectious Diseases, Harvard School of Public Health, Boston, MA 02115, USA

<sup>8</sup> Rennes Brain Cancer Team (REACT), 35042 Rennes, France

\* Correspondence: t.avril@rennes.unicancer.fr

† Co-first authors.

Received: 9 April 2019; Accepted: 1 May 2019; Published: 6 May 2019



**Abstract:** Endoplasmic reticulum (ER) proteostasis is often altered in tumor cells due to intrinsic (oncogene expression, aneuploidy) and extrinsic (environmental) challenges. ER stress triggers the activation of an adaptive response named the Unfolded Protein Response (UPR), leading to protein translation repression, and to the improvement of ER protein folding and clearance capacity. The UPR is emerging as a key player in malignant transformation and tumor growth, impacting on most hallmarks of cancer. As such, the UPR can influence cancer cells' migration and invasion properties. In this review, we overview the involvement of the UPR in cancer progression. We discuss its cross-talks with the cell migration and invasion machinery. Specific aspects will be covered including extracellular matrix (ECM) remodeling, modification of cell adhesion, chemo-attraction, epithelial-mesenchymal transition (EMT), modulation of signaling pathways associated with cell mobility, and cytoskeleton remodeling. The therapeutic potential of targeting the UPR to treat cancer will also be considered with specific emphasis in the impact on metastasis and tissue invasion.

**Keywords:** cancer; cell invasion; cell migration; ER stress; IRE1; PERK; ATF6

## 1. Introduction

Cell migration/invasion is one of the cancer hallmarks that drives cancer progression leading to tumor expansion of the adjacent tissues and/or to tumor dissemination through metastasis. These properties compromise the efficacy of the anti-cancer therapeutic approaches such as surgery or irradiation that rely on the existence of defined and limited zones within the tumor site. For instance, in glioblastoma (GBM), the diffuse infiltration of tumor cells into the cerebral neighboring parenchyma renders the complete and safe tumor resection as almost impossible. In turn, this leads to the recurrence of GBM [1,2]. Metastases observed in many tumor types, in concert with anti-cancer drugs tumor resistance, also largely contribute to most of the curative failures in cancers and in cancer-related

mortality [3,4]. Therefore, in recent years, targeting tumor invasion/migration has become an attractive approach for the development of new types of anti-cancer treatments [2,5].

Cancer cells can adapt to restrictive microenvironmental conditions associated with nutrient and oxygen deprivation. This occurs by triggering a series of adaptive stress responses that include the Unfolded Protein Response (UPR). The activation of the UPR allows tumor cells to restore Endoplasmic Reticulum (ER) proteostasis [6–8]. In the past couple of years, increasing evidence has linked the UPR to cancer progression due to the ability to regulate many cancer cell functions. However, the link between the UPR and the ability of cancer cells to migrate and invade has not been addressed in depth, and only a few examples have been described so far. In this review, after a brief overview of ER stress signaling, we describe the cellular and molecular aspects of the cell migration and their relevance to cancer cell migration/invasion, mainly focusing on brain and skin tumors, and how this can be connected to UPR signaling. Moreover, we discuss the therapeutic perspectives targeting the UPR/cancer cell migration/invasion links to limit the tumor dissemination.

## 2. Mechanisms and Molecular Actors of Tumor Cell Migration and Invasion

Increased tumor cell migration/invasion capacity is one of the hallmarks of cancer [9,10] and leads to tumor dissemination and aggressiveness [11]. To spread within the tissues, tumor cells use migration mechanisms that are similar to those occurring in physiological processes such as embryonic development (Figure 1) [12]. Tumor cell invasion/migration involves diverse patterns of interconvertible strategies including mesenchymal, amoeboid single migration or collective movements (Figure 2).

### 2.1. Different Steps of the Migration Process at the Cellular and Molecular Levels

#### 2.1.1. Polarization of the Migrating Cell

Cell migration can be described as a five-step process [11,12]. In the first step, the moving cell becomes polarized and elongated due to the generation of a protrusion at the leading edge (Figure 1, (1)). These protrusions, composed of parallel and crosslinked actin filaments, take several forms such as broad lamellipodia, or spike-like filopodia [11,13]. This step is initiated spontaneously or by different stimuli including chemokines and growth factors leading to the activation of RHO family GTPases such as RAC1, RHOA and CDC42 [11,12]. RAC1 is a key regulator of migration and localizes to the leading edge of moving cells [14,15]; together with CDC42, these GTPases are involved in the formation of filopodia and lamellipodia whereas RHOA is involved in the formation of stress fibers [16].

#### 2.1.2. Dynamic Interactions of the Migrating Cell with ECM

In the second step, the elongated protrusions form focal contacts with adjacent extracellular matrix (ECM) components which then mature into focal adhesions (Figure 1, (2)). These stable cell-ECM interactions comprise adhesion molecules, most notably transmembrane receptors of the integrin family, and other receptors such as CD44 and syndecans [17]. Intracellularly, focal adhesions are composed by integrin clusters that recruit signaling proteins such as the non-receptor protein tyrosine kinase named focal adhesion kinase (FAK, also known as PTK2 for protein tyrosine kinase 2) that acts a major player in the positive regulation of cell migration. Upon integrin-mediated cell adhesion formation, FAK becomes auto-phosphorylated on Y397 residue leading to its association with SRC and resulting in activation of both kinases. Through carboxy-terminal proline-rich regions, FAK binds CAS (for Crk-associated substrate), a scaffold molecule important for regulating cell migration; and paxillin (PXN), another important molecule for cell spreading and migration events, resulting into more stable and mature focal adhesions [18–20]. In a third step, specific surface proteins are recruited near substrate attachment sites leading to the cleavage of ECM components, such as collagen, fibronectin and laminins (Figure 1, (3)). These proteins involved in ECM degradation comprise secreted metalloproteinases such as MT1-MMP, MMP1 and MMP2 (Figure 1, (3)) [11,21]. In this step, one of the major driver of tumor cell invasion through ECM is the invadopodium. Invadopodia are  $\beta$ -actin rich invasive protrusions that degrade the cross-linked networks of EMC which

restrict tumor cell motility to cross the epithelia and endothelia cell layers. The capacity of these structures to degrade ECM is attributed to the presence of membrane-bound MMPs such as MT1-MMP and to the release of others MMPs, like MMP2 and MMP9 [22,23].

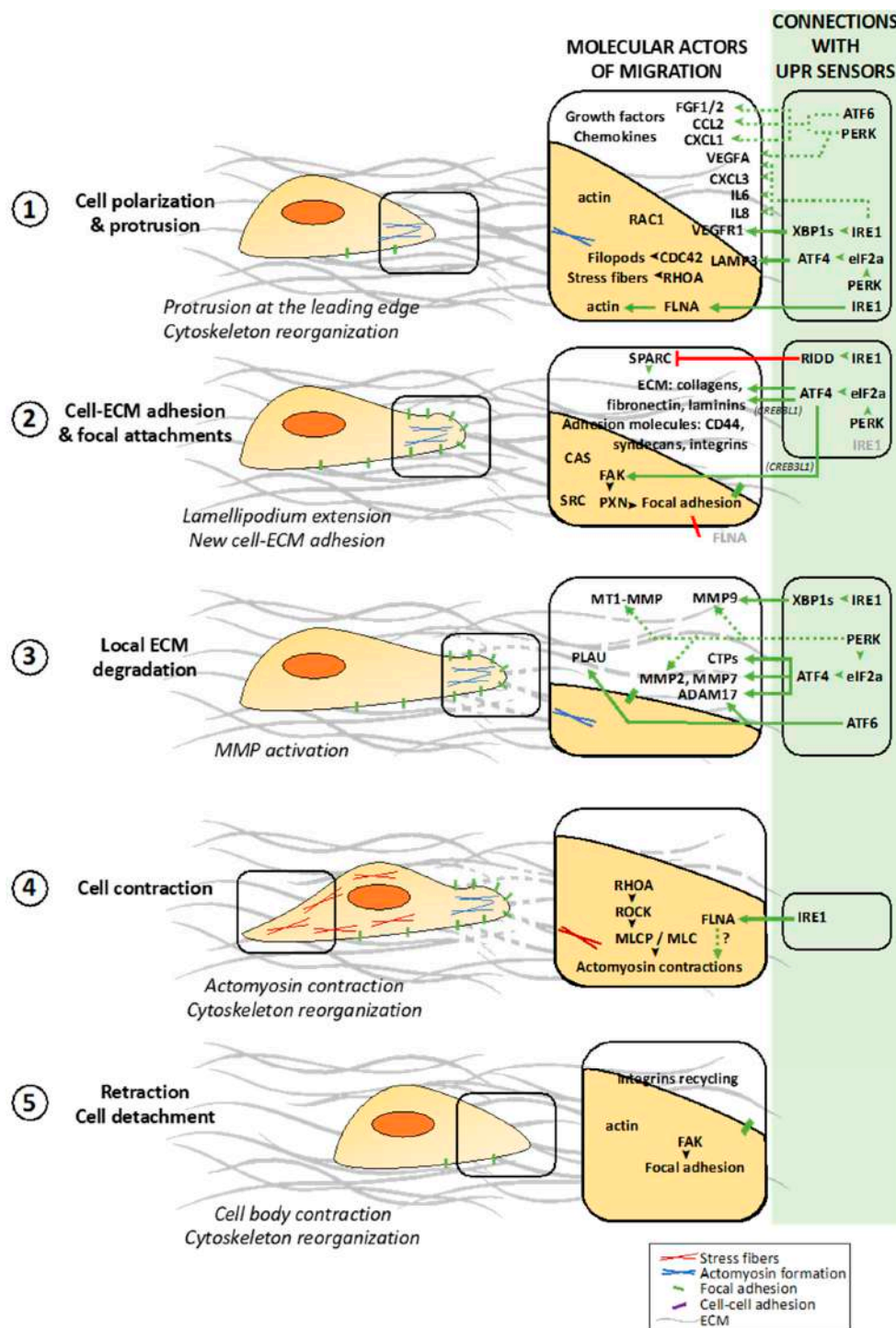


**Figure 1.** The cellular processes and molecular actors involved in cancer cell migration/invasion and their links to the Unfolded Protein Response (UPR) sensors. Cancer cells start to polarize via cytoskeleton reorganization at the leading edge (1) and generate new cell-matrix contacts (2). The proximal extracellular matrix (ECM) surrounding the leading edge is degraded by metalloproteinases (MMPs) activation to

allow cell movement (3). Finally, cell contractions (4) and retractions allowed by cytoskeleton reorganizations, synchronized with cell-matrix detachments (5), lead the movement of the cell body. The molecular partners involved in the different cancer cell migration steps are presented in the associated boxes. The UPR sensors and their down-stream pathways that control the migration associated molecules are indicated in the green boxes (i.e., direct (solid lines) or indirect (dotted lines) links).

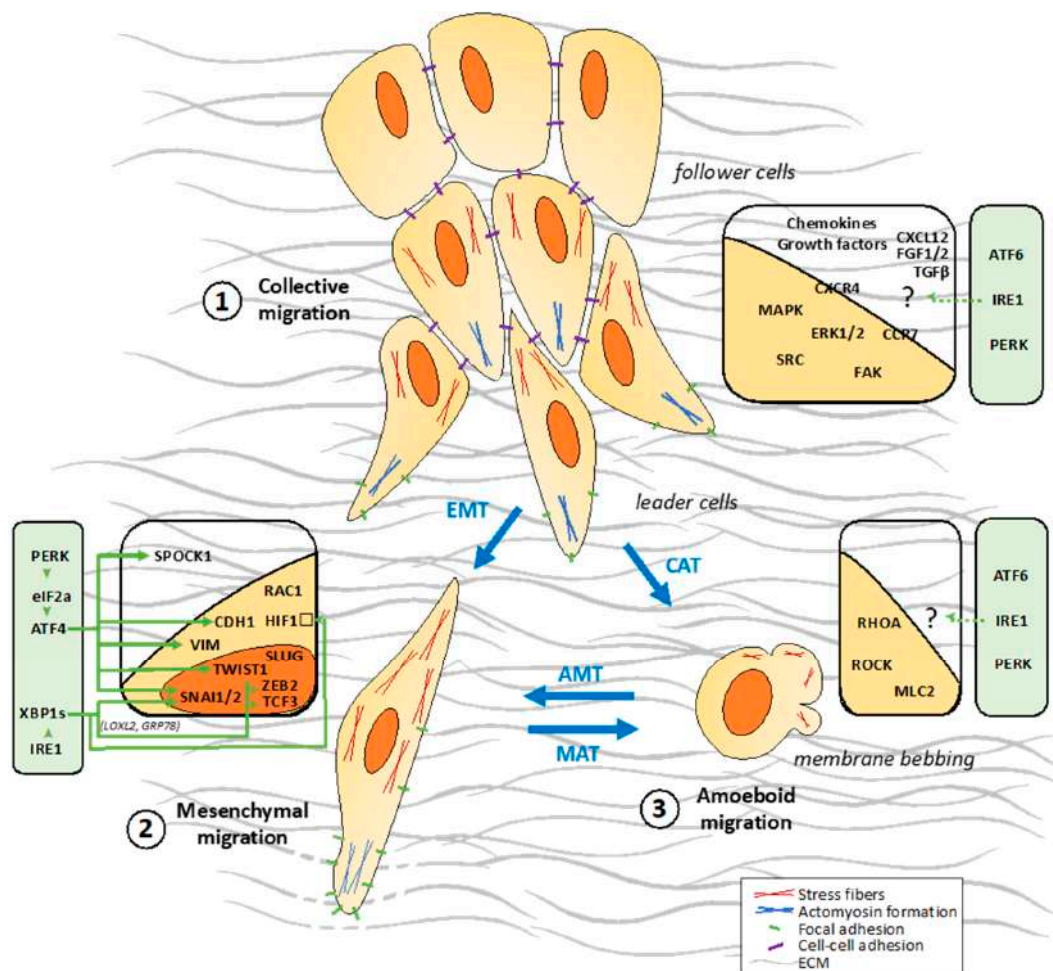


**Figure 2.** The migration modes used in cancer cell migration/invasion and their links to the UPR sensors. Cancer cells migrate either collectively (1) or individually according to the mesenchymal (2) or amoeboid (3) modes. The latter modes involve cell reprogramming processes including epithelial-to-mesenchymal (EMT), mesenchymal-to-amoeboid (MAT) and amoeboid-to-mesenchymal (AMT) transitions. Although less characterized, a collective-to-amoeboid transition (CAT) has been also documented. The molecules involved in these different cancer cell migration modes are presented in the associated boxes. The UPR sensors and their down-stream pathways that control the migration associated molecular partners are indicated in the green boxes.

### 2.1.3. Cell Contraction and Detachment to ECM Allowing Cell Movement

In the fourth step, intracellular myosin II binds to actin filaments to form actomyosin, thus allowing cell contraction due to a reorganization of the actin cytoskeleton (Figure 1, (4)). The calcium/calmodulin dependent enzyme myosin light chain kinase (MLCK) phosphorylates myosin light chains (MLC) to activate myosin II and generate actomyosin contraction [24]. Dephosphorylation of the myosin light chain by the MLC phosphatase (MLCP) results in myosin II inactivation. RHOA regulates actomyosin contraction predominantly through its effector, ROCK (for RHO-associated protein kinase), which



phosphorylates and inhibits MLCP [25,26]. In the last, the detachment of the tail occurs through different actin binding proteins cause actin filament strand breakage thereby promoting filament turnover. FAK causes focal contact disassembly once phosphorylated by AKT1 [27]. Following this focal contact disassembly, integrins detach from the substrate and become internalized through endocytosis for further recycling towards the leading edge (Figure 1, (5)) [11]. Integrin endocytosis is mediated by clathrin, and its adaptor molecules ARH (for autosomal recessive hypercholesterolemia) and DAG2 (for Disabled-2) [28]. All these steps are sequential and polarized through the cell in order to induce a positive force that allow cell to move in a specific direction.

## 2.2. Different Cellular Patterns of Migration

### 2.2.1. Collective Migration

Collective cell migration is a fundamental process that enables the coordinated movement of groups of cells that remain connected via cell-cell junctions (Figure 2, (1)) [29]. In this migration mode, cells remain physically and functionally connected, preserving the integrity of cell-cell junctions during movement. The connected cells require multicellular polarity and “supra-cellular” organization of the actin cytoskeleton generating traction and protrusion force for migration and maintaining cell-cell junctions (Figure 2, (1)). Migrating groups of cells structurally modify the tissue along the migration path, which may result in the deposition of a basement membrane. All of these processes are guided by chemical and physical cues including chemokines, such as stromal cell-derived factor 1 (SDF1; also known as CXCL12), and members of the fibroblast growth factor (FGF) and transforming growth factor- $\beta$  (TGF $\beta$ ) families [30]. Cell-cell adhesion is mediated by adherens junction proteins, including cadherins, other immunoglobulin superfamily members and integrins, all of which directly or indirectly connect intracellularly to the actin and/or intermediate filament cytoskeleton. Several mechanisms polarize the cell group into “leader” cells that guide “follower” cells. Leader cells localize at the front of a moving group, where they receive guidance signals and instruct follower cells, at the rear, into directional migration through chemical and/or mechanical signaling [31]. This polarity of a group of cells is probably cell type and tissue/context specific and might result from the differential expression of surface receptors, extracellular inputs and downstream intracellular signals that define and maintain leader cells. The key components that induce and regulate collective migration include the chemokine receptors CXCR4 and CCR7, mitogen-activated protein kinase (MAPK)/extracellular signal-regulated kinase (ERK), focal adhesion kinase FAK, phosphoinositide-3-kinase (PI3K)/AKT, SRC kinases, NOTCH and RHO GTPases [29,30,32]. The key point of a collective migration is that moving cells influence each other bidirectionally between leading cells and follower cells. Follower cells can also influence the behavior of the leaders to modulate the collective movement. Follower cells can also engage in cell-substrate traction forces, and transmit forces across a longer distance and multiple cell bodies within moving cell sheets [29].

### 2.2.2. Single Cell Migration/Invasion through a Mesenchymal Mode

Mesenchymal cells move via the five-step migration cycle presented above. Mesenchymal migration can be compared to fibroblast-like motility. Apart from fibroblasts, keratinocytes and endothelial cells, some tumor cells also use this mode of migration. In mesenchymal migration, cells adopt an elongated, spindle-like shape and exert traction on their substrates via focal adhesions associated with actin rich protrusions at the leading edge, such as lamellipodia or filopodia (Figure 2, (2)) [11,33], where RHO-family small GTPases RAC1 and CDC42 are key players [11,33,34].

RAC1 is activated by DOCK3 (for Dedicated Of Cytokinesis 3) and its adaptor molecule NEDD9 to drive mesenchymal migration [34]. Active RAC1 negatively regulates RHO/ROCK signaling, inhibiting cell rounding and promoting mesenchymal movement. The mesenchymal mode requires ECM proteolysis to allow RAC1-dependent actin protrusions to pass through the ECM mesh [34]. Integrins, membrane-type MMPs and other proteases co-localize at fiber binding sites to contribute to

ECM degradation. The activation of MMPs and uPA (for urokinase-type plasminogen activator) is required for maintenance of the phenotype and mesenchymal migration [11].

### 2.2.3. Single Cell Migration/Invasion through an Amoeboid Mode

Amoeboid-like movement has been described in leukocytes and certain types of tumor cells. In amoeboid migration, cells adopt round or irregular shapes (Figure 2, (3)). During locomotion these cells constantly change shape by rapidly protruding and retracting extensions, which allow them to squeeze through gaps in the ECM [33,35]. These cells are highly deformable, due to their lack of focal contacts, allowing them to move at 10- to 30-fold higher velocities than cells that use mesenchymal migration mechanisms [11]. Amoeboid migration involves a range of different sub-modes, such as bleb-based migration or gliding. Bleb expansion is driven by hydrostatic pressure generated in the cytoplasm by the contractile actomyosin cortex [36]. In contrast to the mesenchymal mode of invasion, in the amoeboid-like migration, the contractile polarized actomyosin cytoskeleton is crucial for the generation of the motive force, promoted by the RHO/ROCK signaling pathway [37]. This underlines a mutual antagonistic role between RHO-family GTPases RAC1 and RHO/ROCK that display exclusive functions in mesenchymal and amoeboid-like migration respectively [38–40]. By modulating these RHO GTPases, several molecules as such FILGAPP and ARHGAP22 control the mesenchymal/amoeboid switch in cancer cells [34,40,41]. Importantly, the key marker of the amoeboid invasiveness is its independence from ECM proteolytic degradation [35,36].

## 2.3. Migration Strategies Used by Tumor Cells at the Cellular and Molecular Levels

The ability of cancer cells to invade adjacent tissues or to form distant metastases is one of the most life-threatening aspects of cancer. Most solid cancers progress to disseminated metastatic disease, leading to secondary tumors arising in sites distal to the primary tumor [42]. The local invasion of tumor cells to tissues adjacent to the primary tumor site is one of the early steps in the metastatic process and one of the key determinants of the metastatic potential of tumor cells. In order to overcome the ECM barriers and surrounding cells, tumor cells develop abilities to use and switch between different migration modes, i.e., collective, mesenchymal and amoeboid (see above) resulting in the high plasticity of cancer cells. The conversion from epithelial cells to motile individually migrating cells is an intensively studied phenomenon known as epithelial-mesenchymal transition (EMT) [42]. The amoeboid and mesenchymal types of migration/invasion are mutually interchangeable in processes named mesenchymal-to-amoeboid transition (MAT) or amoeboid-to-mesenchymal transition (AMT), respectively (Figure 2) [33]. In the following sections, we describe the tumor migration processes by mainly focusing on two well characterized tumor types (i.e., melanoma and GBM) known to exhibit high migration/invasion properties through a metastatic or a tissue infiltration process.

### 2.3.1. The Metastatic Process in Melanoma

Cutaneous melanoma is a skin cancer derived from melanocytes is considered as one of the most aggressive malignancies with one of the worst prognoses. The aggressiveness of this malignancy is due to the complexity and dissemination potential of this disease. Metastatic melanoma accounts for approximately 80% of skin cancer-related deaths [43]. Malignant melanoma represents a very relevant model for studying tumor invasion because of its highly metastatic behavior. Melanoma progression involved radial and vertical growth phases. The radial growth phase (RGP) represents early-stage disease and encompasses horizontal growth within the epidermis. When the tumor lesion enters the vertical growth phase (VGP), the repertoire of adhesion molecules changes, the tumor enters the dermis and acquires the capacity to metastasize [44]. At the cellular level, melanoma cells invasion results from a combination of several mechanisms: (i) the epithelial-to-mesenchymal transition, (ii) the loss of cell-to-cell adhesion, (iii) the loss of cell-matrix adhesion, (iv) matrix degradation, (v) chemo-attraction/repulsion and (vi) migration. At the molecular level, all these cellular events are closely regulated and tightly interconnected through the activation of select signaling

pathways including MAPK, PI3K and WNT/ $\beta$ -catenin [43,45]. Somatic mutations in the *BRAF* or *NRAS* oncogenes are present in the majority of melanoma cells and lead to the spontaneous activation of the MAPK pathway, promoting cell proliferation, migration and survival [46]. One of the best described phenomena of cell-cell interactions responsible for melanoma progression is the “cadherin switch” [47] by replacing E-cadherin to N-cadherin. This switch is mainly regulated by the PI3K/PTEN pathway through the transcription factors TWIST and SNAI1, two major players of EMT [48]. Loss of E-cadherin may affect the  $\beta$ -catenin/WNT signaling pathway, resulting in upregulation of genes involved in growth and metastasis [44]. Moreover, in malignant melanoma,  $\alpha 4/\beta 1$  and  $\alpha v/\beta 3$  integrins play a major role in metastasis dissemination. Indeed the expression of integrin  $\alpha 4/\beta 1$  correlates with the development of metastases and is negatively associated with disease-free and overall survival [49]. Moreover, the  $\alpha v/\beta 3$  integrin is highly expressed during the transition from RGP to VGP, suggesting a specific role in melanoma invasion. Indeed, the silencing of integrin  $\alpha v/\beta 3$  in B16 melanoma cells reduces their migratory capacity in vitro and metastatic potential in vivo [50]. Other important players involved in melanoma invasion are metalloproteinases. Protein and activation levels of MMP1, 2, 9 and 13 are upregulated in malignant melanoma [51]. As such, MMP2 cleaves fibronectin into small fragments to enhance the adhesion and migration of human melanoma cells mediated by  $\alpha v/\beta 3$  integrin [52]. In addition to mesenchymal movement, melanoma cells can also adopt amoeboid motility through specific effectors of RHOA, namely ROCK and MLC2 [43], stimulated by the TGF $\beta$ /SMAD pathway [53]. RAC1 is involved in mesenchymal migration of melanoma cells, through the adaptor protein NEDD9. *NEDD9* gene is amplified in approximately 50% of melanomas [54]. NEDD9 is a member of the CAS family of proteins that interacts with the guanine nucleotide exchange factor DOCK3 to promote RAC1 activation [55]. Besides, NEDD9 overexpression leads to increased phosphorylation of  $\beta 3$ -integrin on Tyr785 in the cytoplasmic domain promoting the assembly of a signaling complex containing  $\beta 3$ -integrin, SRC, FAK and NEDD9. Altogether, this leads to an increased activation of RAC1, SRC and FAK and a decreased ROCK signaling that drive an elongated, mesenchymal type invasion [54]. Malignant melanoma represents a very relevant model for studying tumor invasion because of its highly metastatic behavior.

### 2.3.2. Tumor Migration in Glioblastoma

If most solid tumors spread by metastasis like melanoma, there are exceptions such as glioblastoma (GBM) which is characterized by a diffuse invasion of tumor cells within the surrounding brain parenchyma (referred to as diffuse infiltration hereafter). GBM is the most common primary malignant brain tumors. Despite the aggressive standard of care currently used, including surgery, chemo- and radiotherapy, the prognosis remains very poor. One of the central hallmarks of GBM is the diffuse infiltration of tumor cells throughout the neighboring normal tissues, rendering complete and safe resection almost impossible [56]. GBM cells mainly appear to invade the surrounding brain parenchyma using the mesenchymal form of motility in vivo, in contrast, amoeboid invasion of GBM cells has been only described in vitro [56–58]. GBM cells move along myelinated axon tracks and disseminate into healthy brain regions along the vascular basement membrane and the glia limitans externa where fibrous proteins such as collagens, fibronectin, laminins and vitronectin are expressed [56]. GBM cells secrete ECM proteins into the microenvironment and release MMPs for ECM remodeling and to promote their own infiltration. In GBM, matrix metalloproteinases are particularly involved in aggressive tumor cell infiltration [59]. MMP2, MT1-MMP and MT2-MMP activities are highly increased in GBM tumors compared to normal [60–62]. MMP2 expression levels correlate with malignant progression in vivo [60,63]. Concomitant with the upregulation of pro-migratory ECM proteins, elevated expression cell adhesion molecules such as integrins receptors and ICAM1 (for intercellular adhesion molecule) has been detected in GBM samples. Integrin receptors reported to be upregulated on glioma cells include  $\alpha 2\beta 1$ ,  $\alpha 5\beta 1$ ,  $\alpha 6\beta 1$  and  $\alpha v\beta 3$ . ICAM1 and LFA3 (for lymphocyte function-associated antigen 3) were distinctive markers of GBM [2,64]. A recent study showed that  $\beta 1$  and  $\alpha v$  integrins represent the primary adhesion systems for glioma cell migration in different



migration models [65]. Interestingly, SRC, FYN, and c-YES kinases belonging to the SRC-family kinase (SFK) are involved in glioma proliferation and motility in vitro [66]. Conversely, LYN, another kinase of this family, shows anti-tumor effect in a glioma orthotopic xenograft model [66]. Components of the FAK/SRC tyrosine kinase migration signaling network are upregulated and activated in GBM suggesting a role of this pathway in tumor invasion [67,68]. The IL6/STAT3 signaling axis is also involved in GBM cell migration by modulating the expression of metalloproteinases MMP2 and MMP9 [69,70], as well as GRP1 (for Glioma Pathogenesis-Related 1) that contributes to GBM stem cell migration [71]. STAT3 is also implicated in mesenchymal GBM progression by modulating the mucin-type protein podoplanin and the EMT-related transcription factors SNAIL and TWIST [72]. Recently we showed that CD90 (THY1) expression controls tumor cell migration/adhesion mainly through SRC signaling. In addition, we show that CD90 expression regulates tumor invasive characteristics in a mouse model and in human tumors [73]. CD90 is a glycosphosphatidylinositol anchored glycoprotein considered as a marker for mesenchymal stromal/stem cells that has been earlier described in glioma/GBM specimens and immortalized glioma/GBM cell lines [73].

In the past few years, pharmacological approaches aiming at dampening GBM invasiveness showed promising results in vitro, in mouse models or in clinical trials and targeted metalloproteinases [74–76], integrins [77], cytoskeleton reorganization [78], or signaling molecules such as FAK [79–81] and SRC [82–85]. Despite intensive efforts, there has been little improvement in the ability to treat GBM. Hence, understanding cell migration is a necessary first step in developing new “anti-migration” therapies.

### 3. Brief Overview of the Unfolded Protein Response and of the ER Stress Sensors

Cells depend on the production of membrane and secretory proteins to maintain their survival. The production of these proteins is ensured in part by the early secretory pathway comprising the ER and the Golgi apparatus [8]. To adapt to the cellular demand and to the challenges imposed by the surrounding environment, the secretory pathway needs to adjust the associated molecular network involved in protein biogenesis including chaperones, foldases, glycosylation enzymes, oxidoreductases and molecules involved in protein quality control [8]. Despite this elaborate system, a proportion of newly synthesized proteins does not reach the quality criteria and is targeted to the ER Associated Degradation (ERAD) system. When the protein folding demand outweighs the ER folding capacity, improperly folded proteins accumulate in the ER lumen resulting in a condition named ER stress. To combat ER stress and return to a homeostatic situation, an adaptive cellular stress response named UPR is triggered [6,86]. The UPR is exacerbated in the course of tumor development, when cancer cells are exposed to intrinsic and extrinsic challenges, i.e., activation of their oncogenic program or nutrient and oxygen deprivation [6,7].

#### 3.1. UPR Signaling Pathways

The UPR activation is controlled by three ER resident transmembrane proteins that act as molecular ER stress sensors: the activating transcription factor 6 alpha (ATF6 $\alpha$ , referred to as ATF6), the inositol-requiring enzyme 1 alpha (IRE1 $\alpha$ , referred to as IRE1 hereafter) and the protein kinase RNA-like ER kinase (PERK) [6–8,87]. Herein, we will provide a brief overview of the UPR signaling pathways and invite the readers to refer to the following reviews on UPR for more details [6–8,86–96].

##### 3.1.1. Activation Mechanisms of the ER Stress Sensors

The current dogma reports that activation of these three sensors is regulated by the ER resident chaperone GRP78/BiP. Under basal conditions, GRP78 constitutively associates with the luminal domains of the 3 sensors, thus repressing their activation [7,8,97]. The fine tuning of the ER stress sensors activation has been more precisely described by different mechanisms but a consensus about IRE1 and PERK activation is missing. For instance, several key players have been described such as the importance of the ATPase domain of GRP78 for the interaction with IRE1 [98]; and the involvement of

other molecular partners such as the co-chaperone ERDJ4 and the protein disulfide isomerase PDIA6 that participate in the stabilization of the GRP78 and IRE1 interaction [99,100]; and also facilitates IRE1 dimerization during ER stress induced after disruption of ER calcium homeostasis [100]; the heat shock protein HSP47 that favors GRP78 release and stabilizes IRE1 dimerization [101]; or misfolded proteins that can directly interact with IRE1 to trigger IRE1 dimerization/oligomerization [102]. Upon accumulation of misfolded proteins in the ER lumen, GRP78 is released from the ER stress sensors which leads to their activation by allowing IRE1 and PERK dimerization/oligomerization and ATF6 export to the Golgi apparatus [87,97]. ATF6, IRE1 and PERK then trigger downstream signaling pathways to reprogram cells to cope with the stress or to die if the stress cannot be resolved.

### 3.1.2. ATF6

ATF6 is an ER-localized protein that exists in two isoforms  $\alpha$  and  $\beta$  forming homo- and heterodimers [103,104]. Compared to the isoform ATF6 $\beta$ , ATF6 $\alpha$  appears to be a very potent transcription factor [105]. ATF6 is considered as a natively unstable protein [106]. Under ER stress, GRP78 dissociation and disulfide bond modification mediated by the protein disulfide isomerase PDIA5 [107,108] stabilize ATF6 and promotes its export to the Golgi apparatus. In the Golgi apparatus, ATF6 is activated by its cleavage mediated by the S1P and S2P proteases [109–111]. This releases an active membrane-free transcription factor, ATF6f, that translocates to the nucleus and induces the transcription of genes mainly involved in protein folding and ERAD such as calreticulin, GRP78, HERPUD1 and SEL1L [7,89,112,113].

### 3.1.3. IRE1

The cytoplasmic region of IRE1 is composed of two domains with distinct enzymatic functions including a serine/threonine kinase and an endoribonuclease (RNase). During ER stress, IRE1 dimerization/oligomerization leads its trans-autophosphorylation that prompts a conformation change, resulting in the activation of its RNase domain [7]. This RNase has the unique ability to proceed with the excision of 26 nucleotides of a short intronic region of the mRNA of the X-box binding protein XBP1. Together with the tRNA ligase RTCB, IRE1 catalyzes the unconventional splicing of XBP1 to generate a new mRNA with a novel open-reading frame encoding for the transcription factor XBP1s. XBP1s activates expression of genes involved in protein folding, secretion, ERAD and lipid synthesis [7]. When ER stress cannot be resolved, IRE1 RNase also catalyzes the degradation of ER localized mRNA, ribosomal RNA and microRNAs through a process called Regulated IRE1 Dependent Decay of RNA (RIDD), participating to the attenuation of the global mRNA translation. The dual IRE1 RNase activity (XBP1 splicing vs. RIDD) is dependent on IRE1 dimerization/oligomerization state with still debated models [7,86,87]. On the other hand, once IRE1 is activated, IRE1 kinase domain interacts with the adaptor protein TRAF2, and triggers a phosphorylation cascade leading to c-Jun N-terminal protein kinase (JNK) and NF $\kappa$ B activation [114,115]. Upon sustained ER stress, IRE1 activation favors the activation of cell apoptosis through terminal RIDD that cleaves mRNAs non-specifically.

### 3.1.4. PERK

Upon ER stress, PERK trans-autophosphorylation leads to its activation and phosphorylation of the eukaryotic translation initiation factor 2 alpha (eIF2 $\alpha$ ) and the transcription factor NRF2 [7,8,92,95]. Phosphorylation of eIF2 $\alpha$  leads to the attenuation of the global translation, reducing the folding demand on the ER [7,89,116,117]. Phosphorylation of eIF2 $\alpha$  also prompts the translation of the transcription factor ATF4 through a uORF-dependent mechanism [118,119]. Phosphorylation of cytoplasmic NRF2 leads to its dissociation from KEAP1 and its nuclear import [120]. The transcription factors ATF4 and NRF2 induce expression of genes involved in protein folding (via HSF1 that regulates HSP genes), amino-acid metabolism (PHGDH, PSAT1, SHMT2 and SLC genes), antioxidant response (NQO1), autophagy (ATG genes) and apoptosis (CHOP) [7,8,121,122]. Translation restoration is induced by eIF2 $\alpha$  dephosphorylation which is catalyzed by the GADD34/PP1c complex [123]. GADD34 is

activated downstream of CHOP and its expression results in a negative feedback loop for PERK signaling pathway. If the stress of the ER is maintained, sustained ATF4/CHOP activation leads to the apoptosis of the cell through induction of pro-apoptotic genes related to BCL2 family such as BIM and PUMA [124,125].

### 3.2. Roles of the ER Stress Sensors in Cancer

During tumor development, cancer cells are exposed to several challenges such as acute demands of protein synthesis due to oncogene expression and drastic extracellular conditions linked to hypoxia or low nutrient availability. These challenges require efficient UPR allowing the cancer cells to cope and adapt [88,92,95]. Thus, fingerprints of UPR activation have been found in several types of primary and metastatic tumors including brain, breast, colon, liver, lung, hepatocellular carcinoma and skin (reviewed in reference [126]). For instance, GRP78 and ATF6 mRNAs are up-regulated as the histological grade increases in hepatocellular carcinoma tissues [127]. In human breast carcinomas, high GRP78 and XBP1 protein levels are found in comparison with normal tissue [128]. High GRP78 expression is associated with metastasis and poor prognosis in breast, colon, esophageal, lung and skin cancers [129–133]. Moreover, ablation of the UPR sensors leads to a significant reduction in tumor growth in different types of cancers like colon, pancreatic, breast cancer and GBM [134–137]. In addition to restoring ER proteostasis, a number of studies have demonstrated that tumor cells hijack the UPR machinery to provide new molecular pathways for supporting tumor development and aggressiveness associated with microenvironment remodeling of the stroma and resistance to anti-cancer treatments [88,92,95]. For instance angiogenesis, another important cancer hallmark, is modulated after hypoxia-induced UPR activation by modulating expression of several proangiogenic mediators as such VEGF and angiogenic inhibitors including THBS1, CXCL14 and CXCL10 [88,138]. Moreover, UPR activation is also observed in tumor associated cells such as endothelial cells and infiltrating macrophages, lymphocytes and dendritic cells to increase their ability to support tumor growth by promoting neo-angiogenesis and by providing important secreted growth factors [90,93]. Currently, many studies are further documenting the involvement of ER stress in cancer hallmarks [9,10]. The following section of this review will be mainly focused on the links between UPR and tumor migration/invasion.

## 4. Connections between UPR Signaling and Tumor Cell Migration

Growing evidence suggests that the UPR is an important regulator of different steps of the tumor migration and metastasis. The three sensors of the UPR have been recently linked to tumor cell migration/invasion processes such as ECM and actin cytoskeleton remodeling and cytoskeleton reorganization, modification of cellular adhesion, activation of signaling pathways associated with cell mobility, and EMT [7,91,94,95].

### 4.1. Links between UPR Sensors Activation and Cancer Metastasis

The IRE1/XBP1 axis has been the most extensively correlated with cancer progression and metastasis. Importantly, studies with tumor samples from patients with colorectal carcinoma, breast cancer and oral squamous cell carcinoma, described the overexpression of IRE1 or XBP1 in metastatic samples compared to the primary tumors [139–142]. In addition, elevated levels of XBP1 at primary tumors are statistically associated to the presence of distant metastasis in patients with esophageal carcinoma, hepatocellular carcinoma and oral squamous cell carcinoma [143–145]. XBP1s overexpression at the primary tumor was correlated with intrahepatic invasion and distant metastasis in hepatocellular carcinoma [144]. In pancreatic cancers, latent liver metastases are developing from quiescent single disseminated cancer cells (DCCs) that evade to the anti-tumor immune response [146]. Intriguingly, these DCCs shut down IRE1 activity leading to escape from CD8 T cell cytotoxicity by down-regulating MHC class I molecules expression. Restoration of IRE1 signaling branch by overexpressing XBP1s in DCCs leads to the outgrowth of liver macro-metastatic lesions [146]. These

findings suggest that IRE1 activation might be important for the initial and final steps in metastasis, like tumor cell dissemination and the formation of macro-metastasis, with a temporary downregulation for avoiding anti-tumor immune response. Besides IRE1, PERK activation has been also linked to tumor invasiveness. In triple negative breast cancers (TNBC), PERK activation characterized by a cancer-specific PERK signaling gene set is associated with distant metastasis [147]. Also, overexpression of ATF4, a component of PERK pathway, is associated with lymph node metastasis in esophageal squamous cell carcinoma [148]. In vivo experiments demonstrated that ATF4 induce cell invasion and metastasis stimulating MMP2 and MMP7 expression [148]. Although more accurate experiments are required, this evidence shows that UPR activation might be relevant for the development of metastatic lesions.

#### 4.2. UPR-Dependent Control of ECM Protein Production and ECM Remodeling

ECM remodeling is an important step to allow tumor migration/invasion. ECM degradation is a key phenomenon in tumor cells migration through the adjacent tissues. In addition, the regulation of cell/ECM interactions determines the cell ability to migrate, i.e., strong cell adhesion to the ECM will limit cell invasion [30]. UPR-regulated molecules such as ECM components, i.e., collagens and fibronectin, enzymes that cleave ECM, i.e., cathepsin and MMPs and adhesion molecules, i.e., integrins, are involved in this process.

##### 4.2.1. ECM Remodeling by the IRE1/XBP1s Signaling Axis

One important process in metastasis is the invasion allowed by the degradation of the ECM through the expression of MMPs [149]. In esophageal squamous cell carcinomas, XBP1s overexpression promotes cell invasion and metastasis through the upregulation of MMP9, one of the MMPs most widely associated with cancer progression [143]. Similarly, XBP1 deficiency in oral squamous cell carcinoma cells impairs cell invasion and leads to a decrease in the expression of invasion-associated genes including MMP1, MMP3 and PLAUR [141]. Intriguingly, in GBM, IRE1 signaling is found to negatively modulate cell migration and invasion [137,150–153]. Gene expression profiling reveals that loss of enzymatic IRE1 activity results in an upregulation of ECM proteins, by negatively regulating the expression of SPARC through the RIDD-mediated degradation of its mRNA, a protein associated with changes in cell shape, synthesis of ECM and cell migration [151]. In addition, the expression of genes involved in cancer cell migration including ECM components (i.e., collagens), MMPs and chemokines is under the control of IRE1 activation in GBM cells [152].

##### 4.2.2. PERK-Dependent Regulation of MMPs in Cancers

As described above for IRE1, PERK is also found to contribute to ECM reorganization in cancer cells. For instance, in esophageal squamous carcinoma cells, ATF4 directly controls tumor migration in vitro and in vivo by regulating the expression of the metalloproteinases MMP2 and MMP7 that, in turn, facilitate this process via the ECM remodeling [148]. Interestingly, ATF4 has been described as a potential poor prognostic biomarker in this cancer type [148]. In chronic myeloid leukemia, eIF2 $\alpha$  is constitutively phosphorylated and enhances invasive ability of tumor cells but also tumor associated stromal fibroblasts by modulating ECM remodeling through cathepsin and MMPs expression via the induction of ATF4 [154]. Interestingly, TRAM2 (for translocation associated membrane protein 2), a component of the SEC61 translocation channel located at ER, is highly expressed in oral squamous cell carcinoma and has a main role in metastasis by controlling PERK activation and the expression of MT1-MMP, MMP2, and MMP9 [155]. Breast cancer cell lines exhibit increased secretion of ECM proteins that perturbs ER morphology due to the overload in secretory proteins and show a constitutively activated PERK/eIF2 $\alpha$ /ATF4 axis [156].

#### 4.2.3. ECM Remodeling upon ATF6 Activation

Little has been described so far on the potential role of ATF6 in modulating tumor cell migration/invasion. One recent study reports that ATF6 activation, upon ER stress induced by gemcitabine, leads to the increased expression of PLAU, a serine protease involved in the degradation of the ECM. Its activation is, in turn, associated with enhanced migration properties of pancreatic cancer stem cells [157]. Also, ADAM17, a member of the disintegrins and metalloproteases family that promotes tumor invasiveness and is found to be up-regulated in breast, gastric ovary and prostatic cancers and is induced by ATF6 in breast cancer cells [158]. Interestingly, PERK/eIF2 $\alpha$ /ATF4 UPR arm also regulates ADAM17 expression as ATF4 binding sites are present in the ADAM17 promoter and PERK activation induces the ADAM17 protein release [158].

#### 4.3. Involvement of the UPR-Dependent Secretome in Tumor Migration

Tumor cell migration depends on the interaction with the microenvironment, extracellular matrix adhesion, cell-cell contacts and matrix remodeling. Cytokines and growth factors that are secreted in the tumor microenvironment regulate all of these processes and therefore control the invasion capacity of tumor cells. These molecules can be secreted by both the tumor cells (autocrine signals) and by the surrounding non-tumor cells (paracrine signals), controlling the initial steps for the metastatic cascade and allowing tumor cell adaptation to environmental changes. The different UPR sensors have been involved in the production of pro-migratory cytokines and chemokines. IRE1 has been described to regulate the secretion of several factors that control tumor angiogenesis that can also affect tumor cell migration. For instance, in GBM, the inhibition of IRE1 decreases the expression of proangiogenic factors such as VEGFA, IL1 $\beta$ , IL6, and CXCL8 (also named IL8) and leads to a reduction of angiogenesis [150,151]. Moreover, IRE1 activity affects the adhesion, migration and invasion properties of GBM tumor cells [150–152] by controlling the production of the chemokines/cytokines IL6, CXCL8, and CXCL3, all involved in these processes [150,152]. Selective impairment of IRE1 RNase increase invasion, vessel co-option capacity and mesenchymal features in U87 glioma cells [153]. Interestingly, in colorectal cancers high XBP1s expression is associated with metastatic tumors in patients and with cancer cell invasion in vitro by controlling VEGFR2 expression [139]. In intestinal cancer cells, early growth response protein 1 (EGR1), an important transcription factor that controls the expression of chemokines/cytokines involved in tumor metastasis such as CCL2 and CXCL1, is positively regulated upon activation of PERK and ATF6 [159]. Suppression of PERK or targeting ATF6 decreased EGR1 expression levels as well as EGR1-associated chemokine expression. Interestingly, ATF3 through a direct interaction with histone deacetylase 1 (HDAC1) mediate EGR1 suppression [159]. PERK activation also increases VEGFA expression in medulloblastoma, which favors tumor migration through an autocrine manner by interacting with its receptor VEGFR2 [160]. In melanoma, both ATF6 and PERK branches of the UPR are involved in the induction of the fibroblast growth factors FGF1/2 increasing cancer cell migration in vitro [161].

#### 4.4. UPR-Mediated Regulation of EMT in Cancers

In recent years, the EMT and UPR activation mainly through IRE1 and PERK signaling pathways have been closely linked to cancer progression in many models [7,91,94,156,162]. EMT-like phenotypes are induced upon UPR activation including cellular morphological changes and modulation of EMT markers, i.e., E-cadherin and vimentin [140,156,163]. Importantly, the common chemotherapeutic drugs used in cancers induce ER-stress mediated EMT, independent of the cancer type [164]. PERK activation is mandatory for tumor cells to invade and metastasize [147]. Furthermore, EMT gene expression signature has been correlated with ECM protein secretion and ATF4 expression (but not XBP1) in various cancers including breast and colon [156]. Inhibition of the PERK/eIF2 $\alpha$ /ATF4 signaling axis with acriflavine (an antiseptic agent that also targets HIF1 pathway) prevents EMT at the cellular and molecular levels (i.e., no change in cellular morphology and no induction of EMT markers as such



E-cadherin, vimentin, SNAI1, SPOCK1 and TWIST1); and inhibits the tumor cell migration (Figure 2, (2)) [165]. However, other studies indicate that XBP1s increases the metastatic potential of tumor cells by the induction of the expression of several EMT transcription factors, including SNAI1, SNAI2, ZEB2 and TCF3 [140,144,163,166]. The induction of these transcription factors for the IRE1/XBP1s signaling is dependent of lysyl oxidase-like 2 (LOXL2). Overexpression of LOXL2 induces its accumulation in the ER and its interaction with GRP78 inducing IRE1/XBP1s branch activation [163]. The inhibition of the RNase activity of IRE1 using small molecules reduced EMT markers expression patterns in breast cancer cells [140].

#### 4.5. UPR-Dependent Regulation of Other Molecular Actors of Tumor Cell Migration

##### 4.5.1. Direct Interaction between IRE1 and Filamin A

We have recently uncovered a novel mechanism of cell migration regulation underlying IRE1 function. Using an interactome screening, FLNA is identified as a major IRE1-binding partner in non-cancer mouse and human cells [167]. FLNA is a 280 kDa actin crosslinking protein involved in the regulation of cytoskeleton remodeling through a direct phosphorylation at serine 2152 [168]. Remarkably, the regulation of cytoskeleton dynamics by IRE1 is independent of its canonical RNase activity, but instead IRE1 serves as a scaffold that recruits FLNA, scaffolding to PKC $\alpha$ , to increase FLNA phosphorylation. Using genetic manipulation, it was determined that deletion of IRE1 impaired actin cytoskeleton dynamics at the protruding and retracting areas. These findings were corroborated in zebra fish, drosophila and mouse models. In addition, using a panel of tumor cell lines, IRE1 silencing decreased tumor cell migration [151,169]. This discovery unveils the possibility of direct interaction between IRE1 and the cytoskeleton network which could also take place in cancer cells (Figure 1, (1) and (4)) [167].

##### 4.5.2. HIF1 $\alpha$ Regulation by XBP1s

Basal XBP1s expression has been described in TNBCs and has a key role on tumorigenicity and tumor dissemination [170]. According to genome-wide mapping to determine XBP1s regulatory network, XBP1s interacts with HIF1 $\alpha$  forming a transcriptional complex that enhances the expression of HIF1 $\alpha$ -regulated genes by promoting the recruitment of RNA polymerase II [170]. It is well documented that the HIF1 $\alpha$  transcriptional program plays a key role in critical steps of metastasis like EMT, extravasation and metastatic niche formation [171]. Furthermore, silencing of XBP1 decreased the formation of lung metastases in an orthotopic TNBC xenograft mouse model (Figure 2, (2)) [170].

##### 4.5.3. Dual Functions of CREB3L1 Induced by ER Stress on Tumor Migration

CREB3L1 (so called OASIS) is a transcription factor initially described in human astrocytes [172] and later considered as an ER stress sensor [173]. This protein is located at the ER membrane and under ER stress, CREB3L1, like ATF6, is exported to the Golgi apparatus and cleaved by S1P and S2P proteases. The membrane-free cytosolic domain is released and translocates to the nucleus to act as a transcription factor regulating the expression of several genes including ER chaperones such as GRP78, and CREB3L1 itself [173]. Using a bioinformatic approach that integrates gene mutations and DNA methylation changes, CREB3L1 was identified as an important regulatory driver in prostate cancer [174,175]. In glioma cells, ER stress induces CREB3L1 that, in turn, negatively modulates the expression of chondroitin sulfate proteoglycan and is associated with increased ability of tumor cell migration/invasion [176]. Surprisingly, CREB3L1 is lost in metastatic cells from breast and bladder tumors due to the methylation of its gene (in the promoter region and the first intronic region) leading to an epigenetic silencing [175,177]. Restoration of CREB3L1 expression in metastatic cells dramatically reduces their migration/invasion ability [175,177]. Importantly, CREB3L1 is transcriptionally regulated downstream of PERK via ATF4 induction but this also requires additional signaling molecules from the EMT pathway such as COL1A1, COL1A2, and FN1 [147]. Remarkably, CREB3L1 expression is

a predictive marker for distant metastasis in the mesenchymal subtype of TNBCs [147]. CREB3L1 increases breast tumor migration capacities through ECM production and remodeling, i.e., COL1A2 and FN1. CREB3L1 inhibition also reduces FAK activation, an important kinase that regulates cell/ECM interaction via its impact on ECM (Figure 1, (2)) [147].

#### 4.5.4. LAMP3 Regulation by PERK Signaling in Cancers

Under hypoxic conditions, the PERK/ATF4 axis is activated and promotes breast tumor cell migration/invasion through the up-regulation and activation of LAMP3, a lysosomal-associated membrane protein [178]. PERK-mediated eIF2 $\alpha$  phosphorylation also induces LAMP3-dependent cervix cancer cell migration under hypoxia [179]. Importantly, LAMP3 expression is also associated with metastasis and poor prognostic in breast, cervix and colorectal cancers and head and neck squamous carcinomas [178–182]. Although the LAMP family members are described as lysosomal membrane proteins, their cell surface expression is often observed in cancer cells. The biologic function of LAMP3 in tumor migration and metastasis needs therefore to be further characterized. As described with LAMP1, LAMP3 might participate to the membrane ruffles and filopodia in migrating tumor cells (Figure 1, (1)) [183].

### 5. Conclusions: UPR Signaling and Cell Migration as Future Targets in Cancer Therapy

Cancer cell migration/invasion has appeared as an important axis to target in the perspectives of anti-cancer therapies development [2,5]. As described above, tumor cell migration is linked to UPR signaling, thereby opening new therapeutic avenues. Interestingly, several inhibitors of the ER stress sensors have been reported to affect tumor migration. For instance, ATF6 inhibitors of the flavonoid family extracted from plants, i.e., apigenin, baicalein, kaempferol; display a strong effect on inhibiting tumor migration of the large range of cancer types including brain, breast, liver, lung, pancreas and skin, however this might be due to off target effects [184–195]. They mainly modulate MMP2 and MMP9 metalloproteinases expression [184,188,190–192], interfere with the EMT process through the regulation of SNAI1 and SLUG [187,189,194] and affect the AKT and MAPK signaling pathways [186,190–192,194,195]. Like flavonoid molecules, another ATF6 inhibitor melatonin modulates important kinases FAK, SRC and ROCK1 involved in tumor migration [195–197]. IRE1 inhibitors such as quercetin and sunitinib also inhibit tumor migration by modulating the same molecular actors of the ECM remodeling and intracellular signaling pathways, i.e., metalloproteinases and kinases, but again, these effects were not yet proven to occur through the inhibition of IRE1 [198–201]. More specific molecules that inhibit the PERK/eIF2 $\alpha$  branch also affect tumor migration. The PERK inhibitor GSK2606414 blocks brain tumor cell migration [160], but this inhibitor is also known to target RIPK1 and c-KIT [202,203]. Subtoxic doses of eIF2 $\alpha$  phosphatase GADD34/PP1c inhibitors guanabenz or salubrinal reduce breast and bone cancer cell migration/invasion through the reduction of SRC [204] and RAC1 [204,205] activity and through the modulation of MMP13 expression (for salubrinal) [204]. Altogether, although none of the UPR inhibitors are currently tested on clinical trials for cancer patients, these findings highlight the need for clarifying the molecular mechanisms occurring under UPR that control tumor migration/invasion. Better understanding of these mechanisms will allow to more specifically target the relevant actors to prevent tumor invasion and metastasis; and therefore, improve current therapeutic approaches for patients with cancer diseases.

**Funding:** This work was funded by a CONICYT fellowship (21160967) and an ARED international fellowship from the Region Bretagne to C.M.L.; by a post-doctoral fellowship from the Plan Cancer to C.S.; by grants from MSCA RISE-734749 (INSPIRED) to E.C. and C.H.; by FONDECYT Iniciación 11180825 to H.U.; and FONDECYT 1140549, FONDAF program 15150012, Millennium Institute P09-015-F, Michael J Fox Foundation for Parkinson's Research, Target Validation grant 9277, FONDEF ID16I10223, FONDEF D11E1007, US Office of Naval Research-Global N62909-16-1-2003, US Air Force Office of Scientific Research FA9550-16-1-0384, ALSRP Therapeutic Idea Award AL150111, Muscular Dystrophy Association 382453, Seed grant Leading House for the Latin American Region, Switzerland, and CONICYT-Brazil 441921/2016-7 to C.H.; by grants from INSERM, Institut National du Cancer (INCa), Région Bretagne, Rennes Métropole, Fondation pour la Recherche Médicale (FRM), EU H2020 MSCA ITN-675448 (TRAINERS) to E.C.; by la Ligue contre le Cancer (Comités 35, 56 et 37) to T.A.

**Conflicts of Interest:** The authors declare no conflict of interest. The funders had no role in the design of the study; in the collection, analyses, or interpretation of data; in the writing of the manuscript, or in the decision to publish the results.

## References

1. Louis, D.N.; Ohgaki, H.; Wiestler, O.D.; Cavenee, W.K.; Burger, P.C.; Jouvett, A.; Scheithauer, B.W.; Kleihues, P. The 2007 WHO classification of tumours of the central nervous system. *Acta Neuropathol.* **2007**, *114*, 97–109. [[CrossRef](#)] [[PubMed](#)]
2. Vehlow, A.; Cordes, N. Invasion as target for therapy of glioblastoma multiforme. *Biochim. Biophys. Acta* **2013**, *1836*, 236–244. [[CrossRef](#)]
3. Cheung, K.J.; Ewald, A.J. A collective route to metastasis: Seeding by tumor cell clusters. *Science* **2016**, *352*, 167–169. [[CrossRef](#)]
4. Lawson, D.A.; Kessenbrock, K.; Davis, R.T.; Pervolarakis, N.; Werb, Z. Tumour heterogeneity and metastasis at single-cell resolution. *Nat. Cell Biol.* **2018**, *20*, 1349–1360. [[CrossRef](#)]
5. Luo, X.; Zhao, X.; Cheng, C.; Li, N.; Liu, Y.; Cao, Y. The implications of signaling lipids in cancer metastasis. *Exp. Mol. Med.* **2018**, *50*, 127. [[CrossRef](#)] [[PubMed](#)]
6. Almanza, A.; Carlesso, A.; Chinthath, C.; Creedican, S.; Doultinos, D.; Leuzzi, B.; Luis, A.; McCarthy, N.; Montibeller, L.; More, S.; et al. Endoplasmic reticulum stress signaling—From basic mechanisms to clinical applications. *FEBS J.* **2018**, *286*, 241–278. [[CrossRef](#)] [[PubMed](#)]
7. Chevet, E.; Hetz, C.; Samali, A. Endoplasmic reticulum stress-activated cell reprogramming in oncogenesis. *Cancer Discov.* **2015**, *5*, 586–597. [[CrossRef](#)]
8. Hetz, C.; Chevet, E.; Oakes, S.A. Proteostasis control by the unfolded protein response. *Nat. Cell Rev.* **2015**, *17*, 829–838. [[CrossRef](#)] [[PubMed](#)]
9. Hanahan, D.; Weinberg, R.A. Hallmarks of cancer: The next generation. *Cell* **2011**, *144*, 646–674. [[CrossRef](#)]
10. Hanahan, D.; Weinberg, R.A. The hallmarks of cancer. *Cell* **2000**, *100*, 57–70. [[CrossRef](#)]
11. Friedl, P.; Wolf, K. Tumour-cell invasion and migration: Diversity and escape mechanisms. *Nat. Rev. Cancer* **2003**, *3*, 362–374. [[CrossRef](#)]
12. Friedl, P.; Wolf, K. Proteolytic interstitial cell migration: A five-step process. *Cancer Metastasis Rev.* **2009**, *28*, 129–135. [[CrossRef](#)] [[PubMed](#)]
13. Ridley, A.J.; Schwartz, M.A.; Burridge, K.; Firtel, R.A.; Ginsberg, M.H.; Borisy, G.; Parsons, J.T.; Horwitz, A.R. Cell migration: Integrating signals from front to back. *Science* **2003**, *302*, 1704–1709. [[CrossRef](#)] [[PubMed](#)]
14. Kraynov, V.S.; Chamberlain, C.; Bokoch, G.M.; Schwartz, M.A.; Slabaugh, S.; Hahn, K.M. Localized Rac activation dynamics visualized in living cells. *Science* **2000**, *290*, 333–337. [[CrossRef](#)]
15. Ridley, A.J. Rho GTPase signalling in cell migration. *Curr. Opin. Cell Biol.* **2015**, *36*, 103–112. [[CrossRef](#)]
16. Nobes, C.D.; Hall, A. Rho, rac, and cdc42 GTPases regulate the assembly of multimolecular focal complexes associated with actin stress fibers, lamellipodia, and filopodia. *Cell* **1995**, *81*, 53–62. [[CrossRef](#)]
17. Roper, J.A.; Williamson, R.C.; Bass, M.D. Syndecan and integrin interactomes: Large complexes in small spaces. *Curr. Opin. Struct. Biol.* **2012**, *22*, 583–590. [[CrossRef](#)]
18. Sieg, D.J.; Hauck, C.R.; Schlaepfer, D.D. Required role of focal adhesion kinase (FAK) for integrin-stimulated cell migration. *J. Cell Sci.* **1999**, *112*, 2677–2691. [[PubMed](#)]
19. Cary, L.A.; Klinghoffer, R.A.; Sachsenmaier, C.; Cooper, J.A. SRC catalytic but not scaffolding function is needed for integrin-regulated tyrosine phosphorylation, cell migration, and cell spreading. *Mol. Cell. Biol.* **2002**, *22*, 2427–2440. [[CrossRef](#)]
20. Zaidel-Bar, R.; Milo, R.; Kam, Z.; Geiger, B. A paxillin tyrosine phosphorylation switch regulates the assembly and form of cell-matrix adhesions. *J. Cell Sci.* **2007**, *120*, 137–148. [[CrossRef](#)] [[PubMed](#)]
21. Bauvois, B. New facets of matrix metalloproteinases MMP-2 and MMP-9 as cell surface transducers: Outside-in signaling and relationship to tumor progression. *Biochim. Biophys. Acta* **2012**, *1825*, 29–36. [[CrossRef](#)]
22. Eddy, R.J.; Weidmann, M.D.; Sharma, V.P.; Condeelis, J.S. Tumor cell invadopodia: Invasive protrusions that orchestrate metastasis. *Trends Cell Biol.* **2017**, *27*, 595–607. [[CrossRef](#)]
23. Jacob, A.; Prekeris, R. The regulation of MMP targeting to invadopodia during cancer metastasis. *Front. Cell Dev. Biol.* **2015**, *3*, 4. [[CrossRef](#)]



24. Kamm, K.E.; Stull, J.T. Dedicated myosin light chain kinases with diverse cellular functions. *J. Biol. Chem.* **2001**, *276*, 4527–4530. [[CrossRef](#)]
25. Katoh, K.; Kano, Y.; Amano, M.; Onishi, H.; Kaibuchi, K.; Fujiwara, K. Rho-kinase-mediated contraction of isolated stress fibers. *J. Cell Biol.* **2001**, *153*, 569–584. [[CrossRef](#)]
26. Fukata, Y.; Amano, M.; Kaibuchi, K. Rho-Rho-kinase pathway in smooth muscle contraction and cytoskeletal reorganization of non-muscle cells. *Trends Pharmacol. Sci.* **2001**, *22*, 32–39. [[CrossRef](#)]
27. Higuchi, M.; Kihara, R.; Okazaki, T.; Aoki, I.; Suetsugu, S.; Gotoh, Y. Akt1 promotes focal adhesion disassembly and cell motility through phosphorylation of FAK in growth factor-stimulated cells. *J. Cell Sci.* **2013**, *126*, 745–755. [[CrossRef](#)]
28. Ezratty, E.J.; Bertaux, C.; Marcantonio, E.E.; Gundersen, G.G. Clathrin mediates integrin endocytosis for focal adhesion disassembly in migrating cells. *J. Cell Biol.* **2009**, *187*, 733–747. [[CrossRef](#)] [[PubMed](#)]
29. Haeger, A.; Wolf, K.; Zegers, M.M.; Friedl, P. Collective cell migration: Guidance principles and hierarchies. *Trends Cell Biol.* **2015**, *25*, 556–566. [[CrossRef](#)] [[PubMed](#)]
30. Friedl, P.; Gilmour, D. Collective cell migration in morphogenesis, regeneration and cancer. *Nat. Rev. Mol. Cell Biol.* **2009**, *10*, 445–457. [[CrossRef](#)] [[PubMed](#)]
31. Khalil, A.A.; Friedl, P. Determinants of leader cells in collective cell migration. *Integr. Biol. (Camb)*. **2010**, *2*, 568–574. [[CrossRef](#)] [[PubMed](#)]
32. Legler, D.F.; Uetz-von Allmen, E.; Hauser, M.A. CCR7: Roles in cancer cell dissemination, migration and metastasis formation. *Int. J. Biochem. Cell Biol.* **2014**, *54*, 78–82. [[CrossRef](#)] [[PubMed](#)]
33. Pankova, K.; Rosel, D.; Novotny, M.; Brabek, J. The molecular mechanisms of transition between mesenchymal and amoeboid invasiveness in tumor cells. *Cell. Mol. Life Sci.* **2010**, *67*, 63–71. [[CrossRef](#)]
34. Sanz-Moreno, V.; Gadea, G.; Ahn, J.; Paterson, H.; Marra, P.; Pinner, S.; Sahai, E.; Marshall, C.J. Rac activation and inactivation control plasticity of tumor cell movement. *Cell* **2008**, *135*, 510–523. [[CrossRef](#)]
35. Lammermann, T.; Sixt, M. Mechanical modes of ‘amoeboid’ cell migration. *Curr. Opin. Cell Biol.* **2009**, *21*, 636–644. [[CrossRef](#)] [[PubMed](#)]
36. Paluch, E.K.; Raz, E. The role and regulation of blebs in cell migration. *Curr. Opin. Cell Biol.* **2013**, *25*, 582–590. [[CrossRef](#)]
37. Sahai, E.; Marshall, C.J. Differing modes of tumour cell invasion have distinct requirements for Rho/ROCK signalling and extracellular proteolysis. *Nat. Cell Rev.* **2003**, *5*, 711–719. [[CrossRef](#)]
38. Symons, M.; Segall, J.E. Rac and Rho driving tumor invasion: who’s at the wheel? *Genome Biol.* **2009**, *10*, 213. [[CrossRef](#)]
39. Parri, M.; Chiarugi, P. Rac and Rho GTPases in cancer cell motility control. *Cell Commun. Signal.* **2010**, *8*, 23. [[CrossRef](#)]
40. Lawson, C.D.; Ridley, A.J. Rho GTPase signaling complexes in cell migration and invasion. *J. Cell Biol.* **2018**, *217*, 447–457. [[CrossRef](#)]
41. Saito, K.; Ozawa, Y.; Hibino, K.; Ohta, Y. FilGAP, a Rho/Rho-associated protein kinase-regulated GTPase-activating protein for Rac, controls tumor cell migration. *Mol. Biol. Cell.* **2012**, *23*, 4739–4750. [[CrossRef](#)] [[PubMed](#)]
42. Kopfstein, L.; Christofori, G. Metastasis: Cell-autonomous mechanisms versus contributions by the tumor microenvironment. *Cell. Mol. Life Sci.* **2006**, *63*, 449–468. [[CrossRef](#)] [[PubMed](#)]
43. Aladowicz, E.; Ferro, L.; Vitali, G.C.; Venditti, E.; Fornasari, L.; Lanfrancone, L. Molecular networks in melanoma invasion and metastasis. *Future Oncol.* **2013**, *9*, 713–726. [[CrossRef](#)] [[PubMed](#)]
44. McGary, E.C.; Lev, D.C.; Bar-Eli, M. Cellular adhesion pathways and metastatic potential of human melanoma. *Cancer Biol. Ther.* **2002**, *1*, 459–465. [[CrossRef](#)]
45. Bonaventure, J.; Domingues, M.J.; Larue, L. Cellular and molecular mechanisms controlling the migration of melanocytes and melanoma cells. *Pigment Cell Melanoma Res.* **2013**, *26*, 316–325. [[CrossRef](#)] [[PubMed](#)]
46. Omholt, K.; Platz, A.; Kanter, L.; Ringborg, U.; Hansson, J. NRAS and BRAF mutations arise early during melanoma pathogenesis and are preserved throughout tumor progression. *Clin. Cancer Res.* **2003**, *9*, 6483–6488.
47. Wheelock, M.J.; Shintani, Y.; Maeda, M.; Fukumoto, Y.; Johnson, K.R. Cadherin switching. *J. Cell Sci.* **2008**, *121*, 727–735. [[CrossRef](#)]

48. Hao, L.; Ha, J.R.; Kuzel, P.; Garcia, E.; Persad, S. Cadherin switch from E- to N-cadherin in melanoma progression is regulated by the PI3K/PTEN pathway through twist and snail. *Br. J. Dermatol.* **2012**, *166*, 1184–1197. [[CrossRef](#)] [[PubMed](#)]
49. Schadendorf, D.; Gawlik, C.; Haney, U.; Ostmeier, H.; Suter, L.; Czarnetzki, B.M. Tumour progression and metastatic behaviour in vivo correlates with integrin expression on melanocytic tumours. *J. Pathol.* **1993**, *170*, 429–434. [[CrossRef](#)]
50. Nasulewicz-Goldeman, A.; Uszczyńska, B.; Szczauńska-Nowak, K.; Wietrzyk, J. siRNA-mediated silencing of integrin beta3 expression inhibits the metastatic potential of B16 melanoma cells. *Oncol. Rep.* **2012**, *28*, 1567–1573. [[CrossRef](#)]
51. Nikkola, J.; Vihinen, P.; Vuoristo, M.S.; Kellokumpu-Lehtinen, P.; Kahari, V.M.; Pyrhonen, S. High serum levels of matrix metalloproteinase-9 and matrix metalloproteinase-1 are associated with rapid progression in patients with metastatic melanoma. *Clin. Cancer Res.* **2005**, *11*, 5158–5166. [[CrossRef](#)]
52. Jiao, Y.; Feng, X.; Zhan, Y.; Wang, R.; Zheng, S.; Liu, W.; Zeng, X. Matrix metalloproteinase-2 promotes alphavbeta3 integrin-mediated adhesion and migration of human melanoma cells by cleaving fibronectin. *PLoS ONE* **2012**, *7*, e41591. [[CrossRef](#)] [[PubMed](#)]
53. Cantelli, G.; Orgaz, J.L.; Rodriguez-Hernandez, I.; Karagiannis, P.; Maiques, O.; Matias-Guiu, X.; Nestle, F.O.; Marti, R.M.; Karagiannis, S.N.; Sanz-Moreno, V. TGF-beta-induced transcription sustains amoeboid melanoma migration and dissemination. *Curr. Biol.* **2015**, *25*, 2899–2914. [[CrossRef](#)]
54. Ahn, J.; Sanz-Moreno, V.; Marshall, C.J. The metastasis gene NEDD9 product acts through integrin beta3 and Src to promote mesenchymal motility and inhibit amoeboid motility. *J. Cell Sci.* **2012**, *125*, 1814–1826. [[CrossRef](#)]
55. Guerrero, M.S.; Parsons, J.T.; Bouton, A.H. Cas and NEDD9 contribute to tumor progression through dynamic regulation of the cytoskeleton. *Genes Cancer* **2012**, *3*, 371–381. [[CrossRef](#)] [[PubMed](#)]
56. Zhong, J.; Paul, A.; Kellie, S.J.; O'Neill, G.M. Mesenchymal migration as a therapeutic target in glioblastoma. *J. Oncol.* **2010**, *2010*, 430142. [[CrossRef](#)]
57. Beadle, C.; Assanah, M.C.; Monzo, P.; Vallee, R.; Rosenfeld, S.S.; Canoll, P. The role of myosin II in glioma invasion of the brain. *Mol. Biol. Cell.* **2008**, *19*, 3357–3368. [[CrossRef](#)] [[PubMed](#)]
58. Caspani, E.M.; Echevarria, D.; Rottner, K.; Small, J.V. Live imaging of glioblastoma cells in brain tissue shows requirement of actin bundles for migration. *Neuron Glia Biol.* **2006**, *2*, 105–114. [[CrossRef](#)]
59. Rao, J.S. Molecular mechanisms of glioma invasiveness: The role of proteases. *Nat. Rev. Cancer* **2003**, *3*, 489–501. [[CrossRef](#)] [[PubMed](#)]
60. Deryugina, E.I.; Bourdon, M.A.; Luo, G.X.; Reisfeld, R.A.; Strongin, A. Matrix metalloproteinase-2 activation modulates glioma cell migration. *J. Cell Sci.* **1997**, *110*, 2473–2482. [[PubMed](#)]
61. Nakada, M.; Nakamura, H.; Ikeda, E.; Fujimoto, N.; Yamashita, J.; Sato, H.; Seiki, M.; Okada, Y. Expression and tissue localization of membrane-type 1, 2, and 3 matrix metalloproteinases in human astrocytic tumors. *Am. J. Pathol.* **1999**, *154*, 417–428. [[CrossRef](#)]
62. Yamamoto, M.; Mohanam, S.; Sawaya, R.; Fuller, G.N.; Seiki, M.; Sato, H.; Gokaslan, Z.L.; Liotta, L.A.; Nicolson, G.L.; Rao, J.S. Differential expression of membrane-type matrix metalloproteinase and its correlation with gelatinase A activation in human malignant brain tumors in vivo and in vitro. *Cancer Res.* **1996**, *56*, 384–392. [[PubMed](#)]
63. Lampert, K.; Machein, U.; Machein, M.R.; Conca, W.; Peter, H.H.; Volk, B. Expression of matrix metalloproteinases and their tissue inhibitors in human brain tumors. *Am. J. Pathol.* **1998**, *153*, 429–437. [[CrossRef](#)]
64. Gingras, M.C.; Roussel, E.; Bruner, J.M.; Branch, C.D.; Moser, R.P. Comparison of cell adhesion molecule expression between glioblastoma multiforme and autologous normal brain tissue. *J. Neuroimmunol.* **1995**, *57*, 143–153. [[CrossRef](#)]
65. Gritsenko, P.G.; Friedl, P. Adaptive adhesion systems mediate glioma cell invasion in complex environments. *J. Cell Sci.* **2018**, *131*, jcs216382. [[CrossRef](#)] [[PubMed](#)]
66. Lewis-Tuffin, L.J.; Feathers, R.; Hari, P.; Durand, N.; Li, Z.; Rodriguez, F.J.; Bakken, K.; Carlson, B.; Schroeder, M.; Sarkaria, J.N.; et al. Src family kinases differentially influence glioma growth and motility. *Mol. Oncol.* **2015**, *9*, 1783–1798. [[CrossRef](#)] [[PubMed](#)]
67. Natarajan, M.; Hecker, T.P.; Gladson, C.L. FAK signaling in anaplastic astrocytoma and glioblastoma tumors. *Cancer J.* **2003**, *9*, 126–133. [[CrossRef](#)] [[PubMed](#)]

68. Natarajan, M.; Stewart, J.E.; Golemis, E.A.; Pugacheva, E.N.; Alexandropoulos, K.; Cox, B.D.; Wang, W.; Grammer, J.R.; Gladson, C.L. HGF1 is a necessary and specific downstream effector of FAK that promotes the migration of glioblastoma cells. *Oncogene* **2006**, *25*, 1721–1732. [[CrossRef](#)]
69. Liu, Q.; Li, G.; Li, R.; Shen, J.; He, Q.; Deng, L.; Zhang, C.; Zhang, J. IL-6 promotion of glioblastoma cell invasion and angiogenesis in U251 and T98G cell lines. *J. Neuro-Oncol.* **2010**, *100*, 165–176. [[CrossRef](#)]
70. Li, R.; Li, G.; Deng, L.; Liu, Q.; Dai, J.; Shen, J.; Zhang, J. IL-6 augments the invasiveness of U87MG human glioblastoma multiforme cells via up-regulation of MMP-2 and fascin-1. *Oncol. rep.* **2010**, *23*, 1553–1559. [[CrossRef](#)]
71. Li, G.H.; Wei, H.; Lv, S.Q.; Ji, H.; Wang, D.L. Knockdown of STAT3 expression by RNAi suppresses growth and induces apoptosis and differentiation in glioblastoma stem cells. *Int. J. Oncol.* **2010**, *37*, 103–110.
72. Priester, M.; Copanaki, E.; Vafaizadeh, V.; Hensel, S.; Bernreuther, C.; Glatzel, M.; Seifert, V.; Groner, B.; Kogel, D.; Weissenberger, J. STAT3 silencing inhibits glioma single cell infiltration and tumor growth. *Neuro-Oncology* **2013**, *15*, 840–852. [[CrossRef](#)]
73. Avril, T.; Etcheverry, A.; Pineau, R.; Obacz, J.; Jegou, G.; Jouan, F.; Le Reste, P.J.; Hatami, M.; Colen, R.R.; Brett, L.; et al. CD90 expression controls migration and predicts dasatinib response in glioblastoma. *Clin. Cancer Res.* **2017**, *23*, 7360–7374. [[CrossRef](#)]
74. Noha, M.; Yoshida, D.; Watanabe, K.; Teramoto, A. Suppression of cell invasion on human malignant glioma cell lines by a novel matrix-metalloproteinase inhibitor SI-27: In vitro study. *J. Neuro-Oncol.* **2000**, *48*, 217–223. [[CrossRef](#)]
75. Tonn, J.C.; Kerkau, S.; Hanke, A.; Bouterfa, H.; Mueller, J.G.; Wagner, S.; Vince, G.H.; Roosen, K. Effect of synthetic matrix-metalloproteinase inhibitors on invasive capacity and proliferation of human malignant gliomas in vitro. *Int. J. Cancer* **1999**, *80*, 764–772. [[CrossRef](#)]
76. Price, A.; Shi, Q.; Morris, D.; Wilcox, M.E.; Brasher, P.M.; Rewcastle, N.B.; Shalinsky, D.; Zou, H.; Appelt, K.; Johnston, R.N.; et al. Marked inhibition of tumor growth in a malignant glioma tumor model by a novel synthetic matrix metalloproteinase inhibitor AG3340. *Clin. Cancer Res.* **1999**, *5*, 845–854.
77. Yamada, S.; Bu, X.Y.; Khankaldyyan, V.; Gonzales-Gomez, I.; McComb, J.G.; Laug, W.E. Effect of the angiogenesis inhibitor Cilengitide (EMD 121974) on glioblastoma growth in nude mice. *Neurosurgery* **2006**, *59*, 1304–1312. [[CrossRef](#)]
78. Yap, C.T.; Simpson, T.I.; Pratt, T.; Price, D.J.; Maciver, S.K. The motility of glioblastoma tumour cells is modulated by intracellular cofilin expression in a concentration-dependent manner. *Cell Motil. Cytoskelet.* **2005**, *60*, 153–165. [[CrossRef](#)]
79. Shi, Q.; Hjelmeland, A.B.; Keir, S.T.; Song, L.; Wickman, S.; Jackson, D.; Ohmori, O.; Bigner, D.D.; Friedman, H.S.; Rich, J.N. A novel low-molecular weight inhibitor of focal adhesion kinase, TAE226, inhibits glioma growth. *Mol. Carcinog.* **2007**, *46*, 488–496. [[CrossRef](#)]
80. Golubovskaya, V.M.; Huang, G.; Ho, B.; Yemma, M.; Morrison, C.D.; Lee, J.; Eliceiri, B.P.; Cance, W.G. Pharmacologic blockade of FAK autophosphorylation decreases human glioblastoma tumor growth and synergizes with temozolomide. *Mol. Cancer Ther.* **2013**, *12*, 162–172. [[CrossRef](#)]
81. Schultze, A.; Decker, S.; Otten, J.; Horst, A.K.; Vohwinkel, G.; Schuch, G.; Bokemeyer, C.; Loges, S.; Fiedler, W. TAE226-mediated inhibition of focal adhesion kinase interferes with tumor angiogenesis and vasculogenesis. *Investig. New Drugs* **2010**, *28*, 825–833. [[CrossRef](#)]
82. Lu, K.V.; Zhu, S.; Cvrljevic, A.; Huang, T.T.; Sarkaria, S.; Ahkavan, D.; Dang, J.; Dinca, E.B.; Plaisier, S.B.; Oderberg, I.; et al. Fyn and SRC are effectors of oncogenic epidermal growth factor receptor signaling in glioblastoma patients. *Cancer Res.* **2009**, *69*, 6889–6898. [[CrossRef](#)]
83. Angers-Loustau, A.; Hering, R.; Werbowetski, T.E.; Kaplan, D.R.; Del Maestro, R.F. SRC regulates actin dynamics and invasion of malignant glial cells in three dimensions. *Mol. Cancer Res.* **2004**, *2*, 595–605.
84. Milano, V.; Piao, Y.; LaFortune, T.; de Groot, J. Dasatinib-induced autophagy is enhanced in combination with temozolomide in glioma. *Mol. Cancer Ther.* **2009**, *8*, 394–406. [[CrossRef](#)]
85. Huvelde, D.; Lewis-Tuffin, L.J.; Carlson, B.L.; Schroeder, M.A.; Rodriguez, F.; Giannini, C.; Galanis, E.; Sarkaria, J.N.; Anastasiadis, P.Z. Targeting Src family kinases inhibits bevacizumab-induced glioma cell invasion. *PLoS ONE* **2013**, *8*, e56505. [[CrossRef](#)]
86. Rojas-Rivera, D.; Rodriguez, D.A.; Sepulveda, D.; Hetz, C. ER stress sensing mechanism: Putting off the brake on UPR transducers. *Oncotarget* **2018**, *9*, 19461–19462. [[CrossRef](#)]

87. Hetz, C.; Papa, F.R. The unfolded protein response and cell fate control. *Mol. Cell.* **2018**, *69*, 169–181. [[CrossRef](#)]
88. Avril, T.; Vauleon, E.; Chevet, E. Endoplasmic reticulum stress signaling and chemotherapy resistance in solid cancers. *Oncogenesis* **2017**, *6*, e373. [[CrossRef](#)] [[PubMed](#)]
89. Dejeans, N.; Barroso, K.; Fernandez-Zapico, M.E.; Samali, A.; Chevet, E. Novel roles of the unfolded protein response in the control of tumor development and aggressiveness. *Sem. Cancer Biol.* **2015**, *33*, 67–73. [[CrossRef](#)]
90. Galmiche, A.; Sauzay, C.; Chevet, E.; Pluquet, O. Role of the unfolded protein response in tumor cell characteristics and cancer outcome. *Curr. Opin. Oncol.* **2017**, *29*, 41–47. [[CrossRef](#)]
91. Madden, E.; Logue, S.E.; Healy, S.J.; Manie, S.; Samali, A. The role of the unfolded protein response in cancer progression: From oncogenesis to chemoresistance. *Biol. Cell.* **2019**, *111*, 1–17. [[CrossRef](#)]
92. Obacz, J.; Avril, T.; Le Reste, P.J.; Urra, H.; Quillien, V.; Hetz, C.; Chevet, E. Endoplasmic reticulum proteostasis in glioblastoma—From molecular mechanisms to therapeutic perspectives. *Sci. Signal.* **2017**, *10*, eal2323. [[CrossRef](#)] [[PubMed](#)]
93. Obacz, J.; Avril, T.; Rubio-Patino, C.; Bossowski, J.P.; Igarria, A.; Ricci, J.E.; Chevet, E. Regulation of tumor-stroma interactions by the unfolded protein response. *FEBS J.* **2017**, *286*, 279–296. [[CrossRef](#)] [[PubMed](#)]
94. Papaioannou, A.; Chevet, E. Driving cancer tumorigenesis and metastasis through UPR signaling. *Curr. Top. Microbiol. Immunol.* **2018**, *414*, 159–192. [[PubMed](#)]
95. Urra, H.; Dufey, E.; Avril, T.; Chevet, E.; Hetz, C. Endoplasmic reticulum stress and the hallmarks of cancer. *Trends Cancer* **2016**, *2*, 252–262. [[CrossRef](#)] [[PubMed](#)]
96. Walter, P.; Ron, D. The unfolded protein response: From stress pathway to homeostatic regulation. *Science* **2011**, *334*, 1081–1086. [[CrossRef](#)] [[PubMed](#)]
97. Bertolotti, A.; Zhang, Y.; Hendershot, L.M.; Harding, H.P.; Ron, D. Dynamic interaction of BiP and ER stress transducers in the unfolded-protein response. *Nat. Cell Rev.* **2000**, *2*, 326–332. [[CrossRef](#)]
98. Carrara, M.; Prischi, F.; Nowak, P.R.; Kopp, M.C.; Ali, M.M. Noncanonical binding of BiP ATPase domain to Ire1 and Perk is dissociated by unfolded protein CH1 to initiate ER stress signaling. *eLife* **2015**, *4*, e03522. [[CrossRef](#)]
99. Amin-Wetzel, N.; Saunders, R.A.; Kamphuis, M.J.; Rato, C.; Preissler, S.; Harding, H.P.; Ron, D. A J-protein co-chaperone recruits BiP to monomerize IRE1 and repress the unfolded protein response. *Cell* **2017**, *171*, 1625–1637. [[CrossRef](#)]
100. Groenendyk, J.; Peng, Z.; Dudek, E.; Fan, X.; Mizianty, M.J.; Dufey, E.; Urra, H.; Sepulveda, D.; Rojas-Rivera, D.; Lim, Y.; et al. Interplay between the oxidoreductase PDIA6 and microRNA-322 controls the response to disrupted endoplasmic reticulum calcium homeostasis. *Sci. Signal.* **2014**, *7*, ra54. [[CrossRef](#)]
101. Sepulveda, D.; Rojas-Rivera, D.; Rodriguez, D.A.; Groenendyk, J.; Kohler, A.; Lebeaupin, C.; Ito, S.; Urra, H.; Carreras-Sureda, A.; Hazari, Y.; et al. Interactome screening identifies the ER luminal chaperone Hsp47 as a regulator of the unfolded protein response transducer IRE1alpha. *Mol. Cell* **2018**, *69*, 238–252. [[CrossRef](#)] [[PubMed](#)]
102. Karagoz, G.E.; Acosta-Alvear, D.; Nguyen, H.T.; Lee, C.P.; Chu, F.; Walter, P. An unfolded protein-induced conformational switch activates mammalian IRE1. *eLife* **2017**, *6*, e30700. [[CrossRef](#)]
103. Haze, K.; Yoshida, H.; Yanagi, H.; Yura, T.; Mori, K. Mammalian transcription factor ATF6 is synthesized as a transmembrane protein and activated by proteolysis in response to endoplasmic reticulum stress. *Mol. Biol. Cell.* **1999**, *10*, 3787–3799. [[CrossRef](#)] [[PubMed](#)]
104. Haze, K.; Okada, T.; Yoshida, H.; Yanagi, H.; Yura, T.; Negishi, M.; Mori, K. Identification of the G13 (cAMP-response-element-binding protein-related protein) gene product related to activating transcription factor 6 as a transcriptional activator of the mammalian unfolded protein response. *Biochem. J.* **2001**, *355*, 19–28. [[CrossRef](#)] [[PubMed](#)]
105. Thuerauf, D.J.; Marcinko, M.; Belmont, P.J.; Glembotski, C.C. Effects of the isoform-specific characteristics of ATF6 alpha and ATF6 beta on endoplasmic reticulum stress response gene expression and cell viability. *J. Biol. Chem.* **2007**, *282*, 22865–22878. [[CrossRef](#)] [[PubMed](#)]
106. Shen, J.; Snapp, E.L.; Lippincott-Schwartz, J.; Prywes, R. Stable binding of ATF6 to BiP in the endoplasmic reticulum stress response. *Mol. Cell. Biol.* **2005**, *25*, 921–932. [[CrossRef](#)]



107. Higa, A.; Taouji, S.; Lhomond, S.; Jensen, D.; Fernandez-Zapico, M.E.; Simpson, J.C.; Pasquet, J.M.; Schekman, R.; Chevet, E. Endoplasmic reticulum stress-activated transcription factor ATF6alpha requires the disulfide isomerase PDIA5 to modulate chemoresistance. *Mol. Cell. Biol.* **2014**, *34*, 1839–1849. [[CrossRef](#)]
108. Nadanaka, S.; Okada, T.; Yoshida, H.; Mori, K. Role of disulfide bridges formed in the luminal domain of ATF6 in sensing endoplasmic reticulum stress. *Mol. Cell. Biol.* **2007**, *27*, 1027–1043. [[CrossRef](#)]
109. Shen, J.; Chen, X.; Hendershot, L.; Prywes, R. ER stress regulation of ATF6 localization by dissociation of BiP/GRP78 binding and unmasking of Golgi localization signals. *Dev. Cell* **2002**, *3*, 99–111. [[CrossRef](#)]
110. Lu, Y.; Liang, F.X.; Wang, X. A synthetic biology approach identifies the mammalian UPR RNA ligase RtcB. *Mol. Cell* **2014**, *55*, 758–770. [[CrossRef](#)]
111. Ye, J.; Rawson, R.B.; Komuro, R.; Chen, X.; Dave, U.P.; Prywes, R.; Brown, M.S.; Goldstein, J.L. ER stress induces cleavage of membrane-bound ATF6 by the same proteases that process SREBPs. *Mol. Cell* **2000**, *6*, 1355–1364. [[CrossRef](#)]
112. Yamamoto, K.; Sato, T.; Matsui, T.; Sato, M.; Okada, T.; Yoshida, H.; Harada, A.; Mori, K. Transcriptional induction of mammalian ER quality control proteins is mediated by single or combined action of ATF6alpha and XBP1. *Dev. Cell* **2007**, *13*, 365–376. [[CrossRef](#)] [[PubMed](#)]
113. Yoshida, H.; Matsui, T.; Yamamoto, A.; Okada, T.; Mori, K. XBP1 mRNA is induced by ATF6 and spliced by IRE1 in response to ER stress to produce a highly active transcription factor. *Cell* **2001**, *107*, 881–891. [[CrossRef](#)]
114. Urano, F.; Wang, X.; Bertolotti, A.; Zhang, Y.; Chung, P.; Harding, H.P.; Ron, D. Coupling of stress in the ER to activation of JNK protein kinases by transmembrane protein kinase IRE1. *Science* **2000**, *287*, 664–666. [[CrossRef](#)]
115. Tam, A.B.; Mercado, E.L.; Hoffmann, A.; Niwa, M. ER stress activates NF-kappaB by integrating functions of basal IKK activity, IRE1 and PERK. *PLoS ONE* **2012**, *7*, e45078. [[CrossRef](#)] [[PubMed](#)]
116. Scheuner, D.; Song, B.; McEwen, E.; Liu, C.; Laybutt, R.; Gillespie, P.; Saunders, T.; Bonner-Weir, S.; Kaufman, R.J. Translational control is required for the unfolded protein response and in vivo glucose homeostasis. *Mol. Cell* **2001**, *7*, 1165–1176. [[CrossRef](#)]
117. Harding, H.P.; Zhang, Y.; Bertolotti, A.; Zeng, H.; Ron, D. Perk is essential for translational regulation and cell survival during the unfolded protein response. *Mol. Cell* **2000**, *5*, 897–904. [[CrossRef](#)]
118. Lu, P.D.; Harding, H.P.; Ron, D. Translation reinitiation at alternative open reading frames regulates gene expression in an integrated stress response. *J. Cell Biol.* **2004**, *167*, 27–33. [[CrossRef](#)]
119. Vattam, K.M.; Wek, R.C. Reinitiation involving upstream ORFs regulates ATF4 mRNA translation in mammalian cells. *Proc. Natl. Acad. Sci. USA* **2004**, *101*, 11269–11274. [[CrossRef](#)]
120. Cullinan, S.B.; Zhang, D.; Hannink, M.; Arvisais, E.; Kaufman, R.J.; Diehl, J.A. Nrf2 is a direct PERK substrate and effector of PERK-dependent cell survival. *Mol. Cell. Biol.* **2003**, *23*, 7198–7209. [[CrossRef](#)]
121. Harding, H.P.; Zhang, Y.; Zeng, H.; Novoa, I.; Lu, P.D.; Calton, M.; Sadri, N.; Yun, C.; Popko, B.; Paules, R.; et al. An integrated stress response regulates amino acid metabolism and resistance to oxidative stress. *Mol. Cell* **2003**, *11*, 619–633. [[CrossRef](#)]
122. Ye, J.; Koumenis, C. ATF4, an ER stress and hypoxia-inducible transcription factor and its potential role in hypoxia tolerance and tumorigenesis. *Curr. Mol. Med.* **2009**, *9*, 411–416. [[CrossRef](#)]
123. Tsaytler, P.; Harding, H.P.; Ron, D.; Bertolotti, A. Selective inhibition of a regulatory subunit of protein phosphatase 1 restores proteostasis. *Science* **2011**, *332*, 91–94. [[CrossRef](#)]
124. Puthalakath, H.; O'Reilly, L.A.; Gunn, P.; Lee, L.; Kelly, P.N.; Huntington, N.D.; Hughes, P.D.; Michalak, E.M.; McKimm-Breschkin, J.; Motoyama, N.; et al. ER stress triggers apoptosis by activating BH3-only protein Bim. *Cell* **2007**, *129*, 1337–1349. [[CrossRef](#)]
125. Galehdar, Z.; Swan, P.; Fuerth, B.; Callaghan, S.M.; Park, D.S.; Cregan, S.P. Neuronal apoptosis induced by endoplasmic reticulum stress is regulated by ATF4-CHOP-mediated induction of the Bcl-2 homology 3-only member PUMA. *J. Neurosci.* **2010**, *30*, 16938–16948. [[CrossRef](#)]
126. Wang, M.; Kaufman, R.J. The impact of the endoplasmic reticulum protein-folding environment on cancer development. *Nat. Rev. Cancer* **2014**, *14*, 581–597. [[CrossRef](#)]
127. Shuda, M.; Kondoh, N.; Imazeki, N.; Tanaka, K.; Okada, T.; Mori, K.; Hada, A.; Arai, M.; Wakatsuki, T.; Matsubara, O. Activation of the ATF6, XBP1 and grp78 genes in human hepatocellular carcinoma: A possible involvement of the ER stress pathway in hepatocarcinogenesis. *J. Hepatol.* **2003**, *38*, 605–614. [[CrossRef](#)]

128. Scriven, P.; Coulson, S.; Haines, R.; Balasubramanian, S.; Cross, S.; Wyld, L. Activation and clinical significance of the unfolded protein response in breast cancer. *Br. J. Cancer* **2009**, *101*, 1692–1698. [[CrossRef](#)]
129. Lizardo, M.M.; Morrow, J.J.; Miller, T.E.; Hong, E.S.; Ren, L.; Mendoza, A.; Halsey, C.H.; Scacheri, P.C.; Helman, L.J.; Khanna, C. Upregulation of glucose-regulated protein 78 in metastatic cancer cells is necessary for lung metastasis progression. *Neoplasia* **2016**, *18*, 699–710. [[CrossRef](#)]
130. Miao, Y.R.; Eckhardt, B.L.; Cao, Y.; Pasqualini, R.; Argani, P.; Arap, W.; Ramsay, R.G.; Anderson, R.L. Inhibition of established micrometastases by targeted drug delivery via cell surface-associated GRP78. *Clin. Cancer Res.* **2013**, *19*, 2107–2116. [[CrossRef](#)]
131. Chang, Y.J.; Chen, W.Y.; Huang, C.Y.; Liu, H.H.; Wei, P.L. Glucose-regulated protein 78 (GRP78) regulates colon cancer metastasis through EMT biomarkers and the NRF-2/HO-1 pathway. *Tumour Biol.* **2015**, *36*, 1859–1869. [[CrossRef](#)] [[PubMed](#)]
132. Ren, P.; Chen, C.; Yue, J.; Zhang, J.; Yu, Z. High expression of glucose-regulated protein 78 (GRP78) is associated with metastasis and poor prognosis in patients with esophageal squamous cell carcinoma. *OncoTargets Ther.* **2017**, *10*, 617–625. [[CrossRef](#)]
133. Guan, M.; Chen, X.; Ma, Y.; Tang, L.; Guan, L.; Ren, X.; Yu, B.; Zhang, W.; Su, B. MDA-9 and GRP78 as potential diagnostic biomarkers for early detection of melanoma metastasis. *Tumour Biol.* **2015**, *36*, 2973–2982. [[CrossRef](#)] [[PubMed](#)]
134. Li, X.X.; Zhang, H.S.; Xu, Y.M.; Zhang, R.J.; Chen, Y.; Fan, L.; Qin, Y.Q.; Liu, Y.; Li, M.; Fang, J. Knockdown of IRE1alpha inhibits colonic tumorigenesis through decreasing beta-catenin and IRE1alpha targeting suppresses colon cancer cells. *Oncogene* **2017**, *36*, 6738–6746. [[CrossRef](#)]
135. Atkins, C.; Liu, Q.; Minthorn, E.; Zhang, S.Y.; Figueroa, D.J.; Moss, K.; Stanley, T.B.; Sanders, B.; Goetz, A.; Gaul, N.; et al. Characterization of a novel PERK kinase inhibitor with antitumor and antiangiogenic activity. *Cancer Res.* **2013**, *73*, 1993–2002. [[CrossRef](#)]
136. Bobrovnikova-Marjon, E.; Grigoriadou, C.; Pytel, D.; Zhang, F.; Ye, J.; Koumenis, C.; Cavener, D.; Diehl, J.A. PERK promotes cancer cell proliferation and tumor growth by limiting oxidative DNA damage. *Oncogene* **2010**, *29*, 3881–3895. [[CrossRef](#)]
137. Drogat, B.; Auguste, P.; Nguyen, D.T.; Bouchecareilh, M.; Pineau, R.; Nalbantoglu, J.; Kaufman, R.J.; Chevet, E.; Bikfalvi, A.; Moenner, M. IRE1 signaling is essential for ischemia-induced vascular endothelial growth factor-A expression and contributes to angiogenesis and tumor growth in vivo. *Cancer Res.* **2007**, *67*, 6700–6707. [[CrossRef](#)]
138. Wang, Y.; Alam, G.N.; Ning, Y.; Visioli, F.; Dong, Z.; Nor, J.E.; Polverini, P.J. The unfolded protein response induces the angiogenic switch in human tumor cells through the PERK/ATF4 pathway. *Cancer Res.* **2012**, *72*, 5396–5406. [[CrossRef](#)]
139. Mhaidat, N.M.; Alzoubi, K.H.; Abushbak, A. X-box binding protein 1 (XBP-1) enhances colorectal cancer cell invasion. *J. Chemother.* **2015**, *27*, 167–173. [[CrossRef](#)]
140. Li, H.; Chen, X.; Gao, Y.; Wu, J.; Zeng, F.; Song, F. XBP1 induces snail expression to promote epithelial-to-mesenchymal transition and invasion of breast cancer cells. *Cell. Signal.* **2015**, *27*, 82–89. [[CrossRef](#)]
141. Sun, Y.; Jiang, F.; Pan, Y.; Chen, X.; Chen, J.; Wang, Y.; Zheng, X.; Zhang, J. XBP1 promotes tumor invasion and is associated with poor prognosis in oral squamous cell carcinoma. *Oncol. Rep.* **2018**, *40*, 988–998. [[CrossRef](#)] [[PubMed](#)]
142. Jin, C.; Jin, Z.; Chen, N.Z.; Lu, M.; Liu, C.B.; Hu, W.L.; Zheng, C.G. Activation of IRE1alpha-XBP1 pathway induces cell proliferation and invasion in colorectal carcinoma. *Biochem. Biophys. Res. Commun.* **2016**, *470*, 75–81. [[CrossRef](#)] [[PubMed](#)]
143. Xia, T.; Tong, S.; Fan, K.; Zhai, W.; Fang, B.; Wang, S.H.; Wang, J.J. XBP1 induces MMP-9 expression to promote proliferation and invasion in human esophageal squamous cell carcinoma. *Am. J. Cancer Res.* **2016**, *6*, 2031–2040.
144. Wu, S.; Du, R.; Gao, C.; Kang, J.; Wen, J.; Sun, T. The role of XBPs in the metastasis and prognosis of hepatocellular carcinoma. *Biochem. Biophys. Res. Commun.* **2018**, *500*, 530–537. [[CrossRef](#)]
145. Hsu, H.T.; Hsing, M.T.; Yeh, C.M.; Chen, C.J.; Yang, J.S.; Yeh, K.T. Decreased cytoplasmic X-box binding protein-1 expression is associated with poor prognosis and overall survival in patients with oral squamous cell carcinoma. *Clin. Chim. Acta* **2018**, *479*, 66–71. [[CrossRef](#)]

146. Pommier, A.; Anaparthi, N.; Memos, N.; Kelley, Z.L.; Gouronnet, A.; Yan, R.; Auffray, C.; Albregues, J.; Egeblad, M.; Lacobuzio-Donahue, C.A.; et al. Unresolved endoplasmic reticulum stress engenders immune-resistant, latent pancreatic cancer metastases. *Science* **2018**, *360*, eaao4908. [[CrossRef](#)] [[PubMed](#)]
147. Feng, Y.X.; Jin, D.X.; Sokol, E.S.; Reinhardt, F.; Miller, D.H.; Gupta, P.B. Cancer-specific PERK signaling drives invasion and metastasis through CREB3L1. *Nat. Commun.* **2017**, *8*, 1079. [[CrossRef](#)]
148. Zhu, H.; Chen, X.; Chen, B.; Chen, B.; Song, W.; Sun, D.; Zhao, Y. Activating transcription factor 4 promotes esophageal squamous cell carcinoma invasion and metastasis in mice and is associated with poor prognosis in human patients. *PLoS ONE* **2014**, *9*, e103882. [[CrossRef](#)]
149. Kessenbrock, K.; Plaks, V.; Werb, Z. Matrix metalloproteinases: Regulators of the tumor microenvironment. *Cell* **2010**, *141*, 52–67. [[CrossRef](#)]
150. Auf, G.; Jabouille, A.; Guerit, S.; Pineau, R.; Delugin, M.; Bouche-careilh, M.; Meynard-Cadars, M.; Bidaud-Meynard, A.; Gentil, C.; Moreau, V.; et al. Inositol-requiring enzyme 1alpha is a key regulator of angiogenesis and invasion in malignant glioma. *Proc. Natl. Acad. Sci. USA* **2010**, *107*, 15553–15558. [[CrossRef](#)]
151. Dejeans, N.; Pluquet, O.; Lhomond, S.; Grise, F.; Bouche-careilh, M.; Juin, A.; Meynard-Cadars, M.; Bidaud-Meynard, A.; Gentil, C.; Moreau, V.; et al. Autocrine control of glioma cells adhesion and migration through IRE1alpha-mediated cleavage of SPARC mRNA. *J. Cell Sci.* **2012**, *125*, 4278–4287. [[CrossRef](#)]
152. Pluquet, O.; Dejeans, N.; Bouche-careilh, M.; Lhomond, S.; Pineau, R.; Higa, A.; Delugin, M.; Combe, C.; Lorient, S.; Cubel, G.; et al. Posttranscriptional regulation of PER1 underlies the oncogenic function of IRE1alpha. *Cancer Res.* **2013**, *73*, 4732–4743. [[CrossRef](#)]
153. Jabouille, A.; Delugin, M.; Pineau, R.; Dubrac, A.; Soulet, F.; Lhomond, S.; Pallares-Lupon, N.; Prats, H.; Bikfalvi, A.; Chevet, E.; et al. Glioblastoma invasion and cooption depend on IRE1alpha endoribonuclease activity. *Oncotarget* **2015**, *6*, 24922–24934. [[CrossRef](#)]
154. Podrzywalow-Bartnicka, P.; Cmoch, A.; Wolczyk, M.; Bugajski, L.; Tkaczyk, M.; Dadlez, M.; Nieborowska-Skorska, M.; Koromilas, A.E.; Skorski, T.; Piwocka, K. Increased phosphorylation of eIF2alpha in chronic myeloid leukemia cells stimulates secretion of matrix modifying enzymes. *Oncotarget* **2016**, *7*, 79706–79721. [[CrossRef](#)]
155. Fukushima, R.; Kasamatsu, A.; Nakashima, D.; Higo, M.; Fushimi, K.; Kasama, H.; Endo-Sakamoto, Y.; Shiiba, M.; Tanzawa, H.; Uzawa, K. Overexpression of translocation associated membrane protein 2 leading to cancer-associated matrix metalloproteinase activation as a putative metastatic factor for human oral cancer. *J. Cancer* **2018**, *9*, 3326–3333. [[CrossRef](#)]
156. Feng, Y.X.; Sokol, E.S.; Del Vecchio, C.A.; Sanduja, S.; Claessen, J.H.; Proia, T.A.; Jin, D.X.; Reinhardt, F.; Ploegh, H.L.; Wang, Q.; et al. Epithelial-to-mesenchymal transition activates PERK-eIF2alpha and sensitizes cells to endoplasmic reticulum stress. *Cancer Discov.* **2014**, *4*, 702–715. [[CrossRef](#)]
157. Wang, L.; Zhang, Y.; Wang, W.; Zhu, Y.; Chen, Y.; Tian, B. Gemcitabine treatment induces endoplasmic reticular (ER) stress and subsequently upregulates urokinase plasminogen activator (uPA) to block mitochondrial-dependent apoptosis in Panc-1 cancer stem-like cells (CSCs). *PLoS ONE* **2017**, *12*, e0184110. [[CrossRef](#)]
158. Rzymiski, T.; Petry, A.; Kracun, D.; Riess, F.; Pike, L.; Harris, A.L.; Gorch, A. The unfolded protein response controls induction and activation of ADAM17/TACE by severe hypoxia and ER stress. *Oncogene* **2012**, *31*, 3621–3634. [[CrossRef](#)]
159. Park, S.H.; Kim, J.; Do, K.H.; Park, J.; Oh, C.G.; Choi, H.J.; Song, B.G.; Lee, S.J.; Kim, Y.S.; Moon, Y. Activating transcription factor 3-mediated chemo-intervention with cancer chemokines in a noncanonical pathway under endoplasmic reticulum stress. *J. Biol. Chem.* **2014**, *289*, 27118–27133. [[CrossRef](#)]
160. Jamison, S.; Lin, Y.; Lin, W. Pancreatic endoplasmic reticulum kinase activation promotes medulloblastoma cell migration and invasion through induction of vascular endothelial growth factor A. *PLoS ONE* **2015**, *10*, e0120252. [[CrossRef](#)]
161. Eigner, K.; Filik, Y.; Mark, F.; Schutz, B.; Klambauer, G.; Moriggl, R.; Hengstschlager, M.; Stangl, H.; Mikula, M.; Rohrl, C. The unfolded protein response impacts melanoma progression by enhancing FGF expression and can be antagonized by a chemical chaperone. *Sci. Rep.* **2017**, *7*, 17498. [[CrossRef](#)]
162. Zeindl-Eberhart, E.; Brandl, L.; Liebmann, S.; Ormanns, S.; Scheel, S.K.; Brabletz, T.; Kirchner, T.; Jung, A. Epithelial-mesenchymal transition induces endoplasmic-reticulum-stress response in human colorectal tumor cells. *PLoS ONE* **2014**, *9*, e87386. [[CrossRef](#)]

163. Cuevas, E.P.; Eraso, P.; Mazon, M.J.; Santos, V.; Moreno-Bueno, G.; Cano, A.; Portillo, F. LOXL2 drives epithelial-mesenchymal transition via activation of IRE1-XBP1 signalling pathway. *Sci. Rep.* **2017**, *7*, 44988. [[CrossRef](#)] [[PubMed](#)]
164. Shah, P.P.; Dupre, T.V.; Siskind, L.J.; Beverly, L.J. Common cytotoxic chemotherapeutics induce epithelial-mesenchymal transition (EMT) downstream of ER stress. *Oncotarget* **2017**, *8*, 22625–22639. [[CrossRef](#)]
165. Dekervel, J.; Bulle, A.; Windmolders, P.; Lambrechts, D.; Van Cutsem, E.; Verslype, C.; van Pelt, J. Acriflavine inhibits acquired drug resistance by blocking the epithelial-to-mesenchymal transition and the unfolded protein response. *Translat. Oncol.* **2017**, *10*, 59–69. [[CrossRef](#)]
166. Mo, X.T.; Zhou, W.C.; Cui, W.H.; Li, D.L.; Li, L.C.; Xu, L.; Zhao, P.; Gao, J. Inositol-requiring protein 1—X-box-binding protein 1 pathway promotes epithelial-mesenchymal transition via mediating snail expression in pulmonary fibrosis. *Int. J. Biochem. Cell Biol.* **2015**, *65*, 230–238. [[CrossRef](#)]
167. Urra, H.; Henriquez, D.R.; Canovas, J.; Villarroel-Campos, D.; Carreras-Sureda, A.; Pulgar, E.; Molina, E.; Hazari, Y.M.; Limia, C.M.; Alvarez-Rojas, S.; et al. IRE1alpha governs cytoskeleton remodelling and cell migration through a direct interaction with filamin A. *Nat. Cell Rev.* **2018**, *20*, 942–953.
168. Li, L.; Lu, Y.; Stemmer, P.M.; Chen, F. Filamin A phosphorylation by Akt promotes cell migration in response to arsenic. *Oncotarget* **2015**, *6*, 12009–12019. [[CrossRef](#)]
169. Lhomond, S.; Avril, T.; Dejeans, N.; Voutetakis, K.; Doultsinos, D.; McMahon, M.; Pineau, R.; Obacz, J.; Papadodima, O.; Jouan, F.; et al. Dual IRE1 RNase functions dictate glioblastoma development. *EMBO Mol. Med.* **2018**, *10*, e7929. [[CrossRef](#)]
170. Chen, X.; Iliopoulos, D.; Zhang, Q.; Tang, Q.; Greenblatt, M.B.; Hatziapostolou, M.; Lim, E.; Tam, W.L.; Ni, M.; Chen, Y.; et al. XBP1 promotes triple-negative breast cancer by controlling the HIF1alpha pathway. *Nature* **2014**, *508*, 103–107. [[CrossRef](#)] [[PubMed](#)]
171. Liu, Z.J.; Semenza, G.L.; Zhang, H.F. Hypoxia-inducible factor 1 and breast cancer metastasis. *J. Zhejiang Univ. Sci. B* **2015**, *16*, 32–43. [[CrossRef](#)] [[PubMed](#)]
172. Honma, Y.; Kanazawa, K.; Mori, T.; Tanno, Y.; Tojo, M.; Kiyosawa, H.; Takeda, J.; Nikaido, T.; Tsukamoto, T.; Yokoya, S.; et al. Identification of a novel gene, OASIS, which encodes for a putative CREB/ATF family transcription factor in the long-term cultured astrocytes and gliotic tissue. *Brain Res. Mol. Brain Res.* **1999**, *69*, 93–103. [[CrossRef](#)]
173. Murakami, T.; Kondo, S.; Ogata, M.; Kanemoto, S.; Saito, A.; Wanaka, A.; Imaizumi, K. Cleavage of the membrane-bound transcription factor OASIS in response to endoplasmic reticulum stress. *J. Neurochem.* **2006**, *96*, 1090–1100. [[CrossRef](#)] [[PubMed](#)]
174. Dhingra, P.; Martinez-Fundichely, A.; Berger, A.; Huang, F.W.; Forbes, A.N.; Liu, E.M.; Sboner, A.; Tamayo, P.; Rickman, D.S.; Rubin, M.A.; et al. Identification of novel prostate cancer drivers using RegNetDriver: A framework for integration of genetic and epigenetic alterations with tissue-specific regulatory network. *Genome Biol.* **2017**, *18*, 141. [[CrossRef](#)]
175. Rose, M.; Schubert, C.; Dierichs, L.; Gaisa, N.T.; Heer, M.; Heidenreich, A.; Knuchel, R.; Dahl, E. OASIS/CREB3L1 is epigenetically silenced in human bladder cancer facilitating tumor cell spreading and migration in vitro. *Epigenetics* **2014**, *9*, 1626–1640. [[CrossRef](#)] [[PubMed](#)]
176. Vellanki, R.N.; Zhang, L.; Volchuk, A. OASIS/CREB3L1 is induced by endoplasmic reticulum stress in human glioma cell lines and contributes to the unfolded protein response, extracellular matrix production and cell migration. *PLoS ONE* **2013**, *8*, e54060. [[CrossRef](#)] [[PubMed](#)]
177. Ward, A.K.; Mellor, P.; Smith, S.E.; Kendall, S.; Just, N.A.; Vizeacoumar, F.S.; Sarker, S.; Phillips, Z.; Alvi, R.; Saxena, A.; et al. Epigenetic silencing of CREB3L1 by DNA methylation is associated with high-grade metastatic breast cancers with poor prognosis and is prevalent in triple negative breast cancers. *Breast Cancer Res.* **2016**, *18*, 12. [[CrossRef](#)] [[PubMed](#)]
178. Nagelkerke, A.; Bussink, J.; Mujcic, H.; Wouters, B.G.; Lehmann, S.; Sweep, F.C.; Span, P.N. Hypoxia stimulates migration of breast cancer cells via the PERK/ATF4/LAMP3-arm of the unfolded protein response. *Breast Cancer Res.* **2013**, *15*, R2. [[CrossRef](#)]
179. Mujcic, H.; Nagelkerke, A.; Rouschop, K.M.; Chung, S.; Chaudary, N.; Span, P.N.; Clarke, B.; Milosevic, M.; Sykes, J.; Hill, R.P.; et al. Hypoxic activation of the PERK/eIF2alpha arm of the unfolded protein response promotes metastasis through induction of LAMP3. *Clin. Cancer Res.* **2013**, *19*, 6126–6137. [[CrossRef](#)] [[PubMed](#)]



180. Nagelkerke, A.; Mujcic, H.; Bussink, J.; Wouters, B.G.; van Laarhoven, H.W.; Sweep, F.C.; Span, P.N. Hypoxic regulation and prognostic value of LAMP3 expression in breast cancer. *Cancer* **2011**, *117*, 3670–3681. [[CrossRef](#)] [[PubMed](#)]
181. Kanao, H.; Enomoto, T.; Kimura, T.; Fujita, M.; Nakashima, R.; Ueda, Y.; Miyatake, T.; Yoshizaki, T.; Buzard, G.S.; Tanigami, A.; et al. Overexpression of LAMP3/TSC403/DC-LAMP promotes metastasis in uterine cervical cancer. *Cancer Res.* **2005**, *65*, 8640–8645. [[CrossRef](#)]
182. Nagelkerke, A.; Sweep, F.C.; Stegeman, H.; Grenman, R.; Kaanders, J.H.; Bussink, J.; Span, P.N. Hypoxic regulation of the PERK/ATF4/LAMP3-arm of the unfolded protein response in head and neck squamous cell carcinoma. *Head Neck* **2015**, *37*, 896–905. [[CrossRef](#)]
183. Garrigues, J.; Anderson, J.; Hellstrom, K.E.; Hellstrom, I. Anti-tumor antibody BR96 blocks cell migration and binds to a lysosomal membrane glycoprotein on cell surface microspikes and ruffled membranes. *J. Cell Biol.* **1994**, *125*, 129–142. [[CrossRef](#)] [[PubMed](#)]
184. Santos, B.L.; Oliveira, M.N.; Coelho, P.L.; Pitanga, B.P.; da Silva, A.B.; Adelita, T.; Silva, V.D.; Costa Mde, F.; El-Bacha, R.S.; Tardy, M.; et al. Flavonoids suppress human glioblastoma cell growth by inhibiting cell metabolism, migration, and by regulating extracellular matrix proteins and metalloproteinases expression. *Chem. Biol. Interact.* **2015**, *242*, 123–138. [[CrossRef](#)]
185. Bauer, D.; Redmon, N.; Mazziro, E.; Soliman, K.F. Apigenin inhibits TNFalpha/IL-1alpha-induced CCL2 release through IKK-epsilon signaling in MDA-MB-231 human breast cancer cells. *PLoS ONE* **2017**, *12*, e0175558. [[CrossRef](#)] [[PubMed](#)]
186. Lin, C.H.; Chang, C.Y.; Lee, K.R.; Lin, H.J.; Chen, T.H.; Wan, L. Flavones inhibit breast cancer proliferation through the Akt/FOXO3a signaling pathway. *BMC Cancer* **2015**, *15*, 958. [[CrossRef](#)] [[PubMed](#)]
187. Qin, Y.; Zhao, D.; Zhou, H.G.; Wang, X.H.; Zhong, W.L.; Chen, S.; Gu, W.G.; Wang, W.; Zhang, C.H.; Liu, Y.R.; et al. Apigenin inhibits NF-kappaB and snail signaling, EMT and metastasis in human hepatocellular carcinoma. *Oncotarget* **2016**, *7*, 41421–41431. [[CrossRef](#)] [[PubMed](#)]
188. Cao, H.H.; Chu, J.H.; Kwan, H.Y.; Su, T.; Yu, H.; Cheng, C.Y.; Fu, X.Q.; Guo, H.; Li, T.; Tse, A.K.; et al. Inhibition of the STAT3 signaling pathway contributes to apigenin-mediated anti-metastatic effect in melanoma. *Sci. Rep.* **2016**, *6*, 21731. [[CrossRef](#)]
189. Chung, H.; Choi, H.S.; Seo, E.K.; Kang, D.H.; Oh, E.S. Baicalin and baicalein inhibit transforming growth factor-beta1-mediated epithelial-mesenchymal transition in human breast epithelial cells. *Biochem. Biophys. Res. Commun.* **2015**, *458*, 707–713. [[CrossRef](#)]
190. Wang, L.; Ling, Y.; Chen, Y.; Li, C.L.; Feng, F.; You, Q.D.; Lu, N.; Guo, Q.L. Flavonoid baicalein suppresses adhesion, migration and invasion of MDA-MB-231 human breast cancer cells. *Cancer Lett.* **2010**, *297*, 42–48. [[CrossRef](#)]
191. Lin, C.W.; Chen, P.N.; Chen, M.K.; Yang, W.E.; Tang, C.H.; Yang, S.F.; Hsieh, Y.S. Kaempferol reduces matrix metalloproteinase-2 expression by down-regulating ERK1/2 and the activator protein-1 signaling pathways in oral cancer cells. *PLoS ONE* **2013**, *8*, e80883. [[CrossRef](#)] [[PubMed](#)]
192. Chen, K.; Zhang, S.; Ji, Y.; Li, J.; An, P.; Ren, H.; Liang, R.; Yang, J.; Li, Z. Baicalein inhibits the invasion and metastatic capabilities of hepatocellular carcinoma cells via down-regulation of the ERK pathway. *PLoS ONE* **2013**, *8*, e72927. [[CrossRef](#)] [[PubMed](#)]
193. Wu, B.; Li, J.; Huang, D.; Wang, W.; Chen, Y.; Liao, Y.; Tang, X.; Xie, H.; Tang, F. Baicalein mediates inhibition of migration and invasiveness of skin carcinoma through Ezrin in A431 cells. *BMC Cancer* **2011**, *11*, 527. [[CrossRef](#)]
194. Jo, E.; Park, S.J.; Choi, Y.S.; Jeon, W.K.; Kim, B.C. Kaempferol suppresses transforming growth factor-beta1-induced epithelial-to-mesenchymal transition and migration of A549 lung cancer cells by inhibiting Akt1-mediated phosphorylation of Smad3 at Threonine-179. *Neoplasia* **2015**, *17*, 525–537. [[CrossRef](#)] [[PubMed](#)]
195. Lee, J.; Kim, J.H. Kaempferol inhibits pancreatic cancer cell growth and migration through the blockade of EGFR-related pathway in vitro. *PLoS ONE* **2016**, *11*, e0155264. [[CrossRef](#)]
196. Xu, C.S.; Wang, Z.F.; Huang, X.D.; Dai, L.M.; Cao, C.J.; Li, Z.Q. Involvement of ROS-alpha v beta 3 integrin-FAK/Pyk2 in the inhibitory effect of melatonin on U251 glioma cell migration and invasion under hypoxia. *J. Transl. Med.* **2015**, *13*, 95. [[CrossRef](#)] [[PubMed](#)]

197. Borin, T.F.; Arbab, A.S.; Gelaleti, G.B.; Ferreira, L.C.; Moschetta, M.G.; Jardim-Perassi, B.V.; Iskander, A.S.; Varma, N.R.; Shankar, A.; Coimbra, V.B.; et al. Melatonin decreases breast cancer metastasis by modulating Rho-associated kinase protein-1 expression. *J. Pineal. Res.* **2016**, *60*, 3–15. [[CrossRef](#)] [[PubMed](#)]
198. Zhang, N.; Ying, M.D.; Wu, Y.P.; Zhou, Z.H.; Ye, Z.M.; Li, H.; Lin, D.S. Hyperoside, a flavonoid compound, inhibits proliferation and stimulates osteogenic differentiation of human osteosarcoma cells. *PLoS ONE* **2014**, *9*, e98973. [[CrossRef](#)]
199. Lin, C.W.; Hou, W.C.; Shen, S.C.; Juan, S.H.; Ko, C.H.; Wang, L.M.; Chen, Y.C. Quercetin inhibition of tumor invasion via suppressing PKC delta/ERK/AP-1-dependent matrix metalloproteinase-9 activation in breast carcinoma cells. *Carcinogenesis* **2008**, *29*, 1807–1815. [[CrossRef](#)]
200. Zhao, J.; Fang, Z.; Zha, Z.; Sun, Q.; Wang, H.; Sun, M.; Qiao, B. Quercetin inhibits cell viability, migration and invasion by regulating miR-16/HOXA10 axis in oral cancer. *Eur. J. Pharmacol.* **2019**, *847*, 11–18. [[CrossRef](#)]
201. Cao, H.H.; Cheng, C.Y.; Su, T.; Fu, X.Q.; Guo, H.; Li, T.; Tse, A.K.; Kwan, H.Y.; Yu, H.; Yu, Z.L. Quercetin inhibits HGF/c-Met signaling and HGF-stimulated melanoma cell migration and invasion. *Mol. Cancer* **2015**, *14*, 103. [[CrossRef](#)] [[PubMed](#)]
202. Rojas-Rivera, D.; Delvaeye, T.; Roelandt, R.; Nerinckx, W.; Augustyns, K.; Vandenabeele, P.; Bertrand, M.J.M. When PERK inhibitors turn out to be new potent RIPK1 inhibitors: Critical issues on the specificity and use of GSK2606414 and GSK2656157. *Cell Death Differ.* **2017**, *24*, 1100–1110. [[CrossRef](#)]
203. Mahameed, M.; Wilhelm, T.; Darawshi, O.; Obiedat, A.; Tommy, W.S.; Chintha, C.; Schubert, T.; Samali, A.; Chevet, E.; Eriksson, L.A.; et al. The unfolded protein response modulators GSK2606414 and KIRA6 are potent KIT inhibitors. *Cell Death Dis.* **2019**, *10*, 300. [[CrossRef](#)]
204. Xu, W.; Wan, Q.; Na, S.; Yokota, H.; Yan, J.L.; Hamamura, K. Suppressed invasive and migratory behaviors of SW1353 chondrosarcoma cells through the regulation of Src, Rac1 GTPase, and MMP13. *Cell. Signal.* **2015**, *27*, 2332–2342. [[CrossRef](#)]
205. Hamamura, K.; Minami, K.; Tanjung, N.; Wan, Q.; Koizumi, M.; Matsuura, N.; Na, S.; Yokota, H. Attenuation of malignant phenotypes of breast cancer cells through eIF2alpha-mediated downregulation of Rac1 signaling. *Int. J. Oncol.* **2014**, *44*, 1980–1988. [[CrossRef](#)] [[PubMed](#)]



© 2019 by the authors. Licensee MDPI, Basel, Switzerland. This article is an open access article distributed under the terms and conditions of the Creative Commons Attribution (CC BY) license (<http://creativecommons.org/licenses/by/4.0/>).

## 14. CONGRESSES AND FUNDING

### 14.1. *Congresses*

- Annual meeting Cell Biology Society of Chile. 22-26 October, 2018. Puerto Varas. Chile. (author). **Novel function of the ER stress transducer IRE1 $\alpha$  in cell invasion and metastasis.**
- Endoplasmic Reticulum\_2019 From basic cell biology to translational approaches: a path to the clinic. Paris, 9-11 October 2019. (author). **Novel function of the ER stress transducer IRE1 $\alpha$  in cell migration and invasion of melanoma cells.**

### 14.2. *Funding*

This work was funded by CONICYT fellowship 21160967 (C.M.L), ARED international fellowship from the Region Bretagne (C.M.L), Fondo Nacional de Desarrollo Científico y Tecnológico (FONDECYT) 11180825 (H.U.), FONDECYT 1180186 (C.H.), FONDECYT 3200716 (P.P.) ANID/FONDAP/15150012 (C.H.), ECOS Comisión Nacional de Investigación Científica y Tecnológica (CONICYT) Cooperation grant Chile-France ECOS170032 (H.U., C.H.), Millennium Institute P09-015-F (C.H.) and European Commission R&D MSCA-RISE 734749 (C.H., E.C).

## 15. REFERENCES.

1. Sanchez-Tapia C, Wan FY. Fastest time to cancer by loss of tumor suppressor genes. *Bull Math Biol.* 2014;76(11):2737-84.
2. Global Burden of Disease Cancer C, Fitzmaurice C, Dicker D, Pain A, Hamavid H, Moradi-Lakeh M, et al. The Global Burden of Cancer 2013. *JAMA Oncol.* 2015;1(4):505-27.
3. Health Mo. National Cancer Strategy. Chile 2016 2016 [
4. Goss PE, Lee BL, Badovinac-Crnjevic T, Strasser-Weippl K, Chavarri-Guerra Y, St Louis J, et al. Planning cancer control in Latin America and the Caribbean. *Lancet Oncol.* 2013;14(5):391-436.
5. Ministerio de Salud GdC. Plan Nacional de Cáncer 2018-2020 2018 [Available from: [https://www.minsal.cl/wp-content/uploads/2019/01/2019.01.23\\_PLAN-NACIONAL-DE-CANCER\\_web.pdf](https://www.minsal.cl/wp-content/uploads/2019/01/2019.01.23_PLAN-NACIONAL-DE-CANCER_web.pdf).
6. Global Cancer Observatory [Internet]. 2020. Available from: <https://gco.iarc.fr/today/data/factsheets/populations/250-france-fact-sheets.pdf>.
7. Sung H, Ferlay J, Siegel RL, Laversanne M, Soerjomataram I, Jemal A, et al. Global cancer statistics 2020: GLOBOCAN estimates of incidence and mortality worldwide for 36 cancers in 185 countries. *CA Cancer J Clin.* 2021.
8. Liu Q, Zhang H, Jiang X, Qian C, Liu Z, Luo D. Factors involved in cancer metastasis: a better understanding to "seed and soil" hypothesis. *Molecular cancer.* 2017;16(1):176.
9. Zemelman VB, Valenzuela CY, Sazunic I, Araya I. Malignant melanoma in Chile: different site distribution between private and state patients. *Biol Res.* 2014;47:34.
10. Society AC. Cancer Fact and Figures 2016 2016 [
11. Bedrosian I, Faries MB, Guerry Dt, Elenitsas R, Schuchter L, Mick R, et al. Incidence of sentinel node metastasis in patients with thin primary melanoma (< or = 1 mm) with vertical growth phase. *Ann Surg Oncol.* 2000;7(4):262-7.
12. Hanahan D, Weinberg RA. Hallmarks of cancer: the next generation. *Cell.* 2011;144(5):646-74.
13. Friedl P, Alexander S. Cancer invasion and the microenvironment: plasticity and reciprocity. *Cell.* 2011;147(5):992-1009.
14. Witsch E, Sela M, Yarden Y. Roles for growth factors in cancer progression. *Physiology (Bethesda).* 2010;25(2):85-101.
15. Cheng N, Chytil A, Shyr Y, Joly A, Moses HL. Transforming growth factor-beta signaling-deficient fibroblasts enhance hepatocyte growth factor signaling in

mammary carcinoma cells to promote scattering and invasion. *Molecular cancer research : MCR*. 2008;6(10):1521-33.

16. Burkhart DL, Sage J. Cellular mechanisms of tumour suppression by the retinoblastoma gene. *Nature reviews Cancer*. 2008;8(9):671-82.

17. Sherr CJ, McCormick F. The RB and p53 pathways in cancer. *Cancer cell*. 2002;2(2):103-12.

18. Junttila MR, Evan GI. p53--a Jack of all trades but master of none. *Nature reviews Cancer*. 2009;9(11):821-9.

19. Hanahan D, Folkman J. Patterns and emerging mechanisms of the angiogenic switch during tumorigenesis. *Cell*. 1996;86(3):353-64.

20. Carmeliet P. VEGF as a key mediator of angiogenesis in cancer. *Oncology*. 2005;69 Suppl 3:4-10.

21. Kazerounian S, Yee KO, Lawler J. Thrombospondins in cancer. *Cellular and molecular life sciences : CMLS*. 2008;65(5):700-12.

22. Senft D, Ronai ZE. Adaptive Stress Responses During Tumor Metastasis and Dormancy. *Trends in cancer*. 2016;2(8):429-42.

23. Talmadge JE, Fidler IJ. AACR centennial series: the biology of cancer metastasis: historical perspective. *Cancer Res*. 2010;70(14):5649-69.

24. Chaffer CL, Weinberg RA. A perspective on cancer cell metastasis. *Science*. 2011;331(6024):1559-64.

25. Steeg PS. Targeting metastasis. *Nat Rev Cancer*. 2016;16(4):201-18.

26. Kopfstein L, Christofori G. Metastasis: cell-autonomous mechanisms versus contributions by the tumor microenvironment. *Cellular and molecular life sciences : CMLS*. 2006;63(4):449-68.

27. Aladowicz E, Ferro L, Vitali GC, Venditti E, Fornasari L, Lanfrancione L. Molecular networks in melanoma invasion and metastasis. *Future oncology*. 2013;9(5):713-26.

28. Clark WH, Jr., Elder DE, Guerry Dt, Braitman LE, Trock BJ, Schultz D, et al. Model predicting survival in stage I melanoma based on tumor progression. *Journal of the National Cancer Institute*. 1989;81(24):1893-904.

29. Damsky WE, Theodosakis N, Bosenberg M. Melanoma metastasis: new concepts and evolving paradigms. *Oncogene*. 2014;33(19):2413-22.

30. Fife CM, McCarroll JA, Kavallaris M. Movers and shakers: cell cytoskeleton in cancer metastasis. *British journal of pharmacology*. 2014;171(24):5507-23.

31. Jiang WG, Sanders AJ, Katoh M, Ungefroren H, Gieseler F, Prince M, et al. Tissue invasion and metastasis: Molecular, biological and clinical perspectives. *Seminars in cancer biology*. 2015;35 Suppl:S244-75.
32. Mehlen P, Puisieux A. Metastasis: a question of life or death. *Nature reviews Cancer*. 2006;6(6):449-58.
33. Webb DJ, Horwitz AF. New dimensions in cell migration. *Nature cell biology*. 2003;5(8):690-2.
34. Trepap X, Chen Z, Jacobson K. Cell migration. *Compr Physiol*. 2012;2(4):2369-92.
35. Ridley AJ, Schwartz MA, Burridge K, Firtel RA, Ginsberg MH, Borisy G, et al. Cell migration: integrating signals from front to back. *Science*. 2003;302(5651):1704-9.
36. De Craene B, Berx G. Regulatory networks defining EMT during cancer initiation and progression. *Nature reviews Cancer*. 2013;13(2):97-110.
37. Hui L, Chen Y. Tumor microenvironment: Sanctuary of the devil. *Cancer letters*. 2015;368(1):7-13.
38. Friedl P, Wolf K. Tumour-cell invasion and migration: diversity and escape mechanisms. *Nature reviews Cancer*. 2003;3(5):362-74.
39. Friedl P, Wolf K. Proteolytic interstitial cell migration: a five-step process. *Cancer Metastasis Rev*. 2009;28(1-2):129-35.
40. Carlson B, Soderling SH. Mechanisms of cellular protrusions branch out. *Dev Cell*. 2009;17(3):307-9.
41. Nobes CD, Hall A. Rho, rac, and cdc42 GTPases regulate the assembly of multimolecular focal complexes associated with actin stress fibers, lamellipodia, and filopodia. *Cell*. 1995;81(1):53-62.
42. Skoble J, Portnoy DA, Welch MD. Three regions within ActA promote Arp2/3 complex-mediated actin nucleation and *Listeria monocytogenes* motility. *The Journal of cell biology*. 2000;150(3):527-38.
43. Sieg DJ, Hauck CR, Schlaepfer DD. Required role of focal adhesion kinase (FAK) for integrin-stimulated cell migration. *Journal of cell science*. 1999;112 ( Pt 16):2677-91.
44. Cary LA, Klinghoffer RA, Sachsenmaier C, Cooper JA. SRC catalytic but not scaffolding function is needed for integrin-regulated tyrosine phosphorylation, cell migration, and cell spreading. *Molecular and cellular biology*. 2002;22(8):2427-40.
45. Zaidel-Bar R, Milo R, Kam Z, Geiger B. A paxillin tyrosine phosphorylation switch regulates the assembly and form of cell-matrix adhesions. *Journal of cell science*. 2007;120(Pt 1):137-48.

46. Bauvois B. New facets of matrix metalloproteinases MMP-2 and MMP-9 as cell surface transducers: outside-in signaling and relationship to tumor progression. *Biochimica et biophysica acta*. 2012;1825(1):29-36.
47. Ferrari R, Martin G, Tagit O, Guichard A, Cambi A, Voituriez R, et al. MT1-MMP directs force-producing proteolytic contacts that drive tumor cell invasion. *Nature communications*. 2019;10(1):4886.
48. Murphy DA, Courtneidge SA. The 'ins' and 'outs' of podosomes and invadopodia: characteristics, formation and function. *Nature reviews Molecular cell biology*. 2011;12(7):413-26.
49. Katoh K, Kano Y, Amano M, Onishi H, Kaibuchi K, Fujiwara K. Rho-kinase--mediated contraction of isolated stress fibers. *The Journal of cell biology*. 2001;153(3):569-84.
50. Totsukawa G, Yamakita Y, Yamashiro S, Hartshorne DJ, Sasaki Y, Matsumura F. Distinct roles of ROCK (Rho-kinase) and MLCK in spatial regulation of MLC phosphorylation for assembly of stress fibers and focal adhesions in 3T3 fibroblasts. *The Journal of cell biology*. 2000;150(4):797-806.
51. Potter DA, Tirnauer JS, Janssen R, Croall DE, Hughes CN, Fiocco KA, et al. Calpain regulates actin remodeling during cell spreading. *The Journal of cell biology*. 1998;141(3):647-62.
52. Higuchi M, Kihara R, Okazaki T, Aoki I, Suetsugu S, Gotoh Y. Akt1 promotes focal adhesion disassembly and cell motility through phosphorylation of FAK in growth factor-stimulated cells. *Journal of cell science*. 2013;126(Pt 3):745-55.
53. Nagano M, Hoshino D, Koshikawa N, Akizawa T, Seiki M. Turnover of focal adhesions and cancer cell migration. *International journal of cell biology*. 2012;2012:310616.
54. Dejeans N, Manie S, Hetz C, Bard F, Hupp T, Agostinis P, et al. Addicted to secrete - novel concepts and targets in cancer therapy. *Trends in molecular medicine*. 2014;20(5):242-50.
55. Hetz C, Chevet E, Oakes SA. Proteostasis control by the unfolded protein response. *Nat Cell Biol*. 2015;17(7):829-38.
56. Wang M, Kaufman RJ. Protein misfolding in the endoplasmic reticulum as a conduit to human disease. *Nature*. 2016;529(7586):326-35.
57. Ron D, Walter P. Signal integration in the endoplasmic reticulum unfolded protein response. *Nature reviews Molecular cell biology*. 2007;8(7):519-29.
58. Urra H, Dufey E, Lisbona F, Rojas-Rivera D, Hetz C. When ER stress reaches a dead end. *Biochimica et biophysica acta*. 2013;1833(12):3507-17.
59. Chevet E, Hetz C, Samali A. Endoplasmic reticulum stress-activated cell reprogramming in oncogenesis. *Cancer discovery*. 2015;5(6):586-97.

60. Urra H, Dufey E, Avril T, Chevet E, Hetz C. Endoplasmic Reticulum Stress and the Hallmarks of Cancer. *Trends Cancer*. 2016;2(5):252-62.
61. Wang M, Kaufman RJ. The impact of the endoplasmic reticulum protein-folding environment on cancer development. *Nature reviews Cancer*. 2014;14(9):581-97.
62. Wang M, Kaufman RJ. The impact of the endoplasmic reticulum protein-folding environment on cancer development. *Nat Rev Cancer*. 2014;14(9):581-97.
63. Schroder M, Kaufman RJ. The mammalian unfolded protein response. *Annu Rev Biochem*. 2005;74:739-89.
64. Almanza A, Carlesso A, Chintla C, Creedican S, Doultzinos D, Leuzzi B, et al. Endoplasmic reticulum stress signalling - from basic mechanisms to clinical applications. *The FEBS journal*. 2018.
65. Hetz C, Papa FR. The Unfolded Protein Response and Cell Fate Control. *Mol Cell*. 2018;69(2):169-81.
66. Walter P, Ron D. The unfolded protein response: from stress pathway to homeostatic regulation. *Science*. 2011;334(6059):1081-6.
67. Lu PD, Harding HP, Ron D. Translation reinitiation at alternative open reading frames regulates gene expression in an integrated stress response. *The Journal of cell biology*. 2004;167(1):27-33.
68. Vatter KM, Wek RC. Reinitiation involving upstream ORFs regulates ATF4 mRNA translation in mammalian cells. *Proc Natl Acad Sci U S A*. 2004;101(31):11269-74.
69. Harding HP, Zhang Y, Zeng H, Novoa I, Lu PD, Calton M, et al. An integrated stress response regulates amino acid metabolism and resistance to oxidative stress. *Mol Cell*. 2003;11(3):619-33.
70. Ye J, Koumenis C. ATF4, an ER stress and hypoxia-inducible transcription factor and its potential role in hypoxia tolerance and tumorigenesis. *Curr Mol Med*. 2009;9(4):411-6.
71. Pihan P, Carreras-Sureda A, Hetz C. BCL-2 family: integrating stress responses at the ER to control cell demise. *Cell death and differentiation*. 2017;24(9):1478-87.
72. Tsaytler P, Harding HP, Ron D, Bertolotti A. Selective inhibition of a regulatory subunit of protein phosphatase 1 restores proteostasis. *Science*. 2011;332(6025):91-4.
73. Haze K, Yoshida H, Yanagi H, Yura T, Mori K. Mammalian transcription factor ATF6 is synthesized as a transmembrane protein and activated by proteolysis in response to endoplasmic reticulum stress. *Mol Biol Cell*. 1999;10(11):3787-99.



74. Haze K, Okada T, Yoshida H, Yanagi H, Yura T, Negishi M, et al. Identification of the G13 (cAMP-response-element-binding protein-related protein) gene product related to activating transcription factor 6 as a transcriptional activator of the mammalian unfolded protein response. *The Biochemical journal*. 2001;355(Pt 1):19-28.
75. Shen J, Chen X, Hendershot L, Prywes R. ER stress regulation of ATF6 localization by dissociation of BiP/GRP78 binding and unmasking of Golgi localization signals. *Dev Cell*. 2002;3(1):99-111.
76. Ye J, Rawson RB, Komuro R, Chen X, Dave UP, Prywes R, et al. ER stress induces cleavage of membrane-bound ATF6 by the same proteases that process SREBPs. *Molecular cell*. 2000;6(6):1355-64.
77. Yamamoto K, Sato T, Matsui T, Sato M, Okada T, Yoshida H, et al. Transcriptional induction of mammalian ER quality control proteins is mediated by single or combined action of ATF6alpha and XBP1. *Dev Cell*. 2007;13(3):365-76.
78. Yoshida H, Matsui T, Yamamoto A, Okada T, Mori K. XBP1 mRNA is induced by ATF6 and spliced by IRE1 in response to ER stress to produce a highly active transcription factor. *Cell*. 2001;107(7):881-91.
79. Cox JS, Shamu CE, Walter P. Transcriptional induction of genes encoding endoplasmic reticulum resident proteins requires a transmembrane protein kinase. *Cell*. 1993;73(6):1197-206.
80. Cox JS, Walter P. A novel mechanism for regulating activity of a transcription factor that controls the unfolded protein response. *Cell*. 1996;87(3):391-404.
81. Zhou J, Liu CY, Back SH, Clark RL, Peisach D, Xu Z, et al. The crystal structure of human IRE1 luminal domain reveals a conserved dimerization interface required for activation of the unfolded protein response. *Proc Natl Acad Sci U S A*. 2006;103(39):14343-8.
82. Calton M, Zeng H, Urano F, Till JH, Hubbard SR, Harding HP, et al. IRE1 couples endoplasmic reticulum load to secretory capacity by processing the XBP-1 mRNA. *Nature*. 2002;415(6867):92-6.
83. Hollien J, Weissman JS. Decay of endoplasmic reticulum-localized mRNAs during the unfolded protein response. *Science*. 2006;313(5783):104-7.
84. Hollien J, Lin JH, Li H, Stevens N, Walter P, Weissman JS. Regulated Ire1-dependent decay of messenger RNAs in mammalian cells. *J Cell Biol*. 2009;186(3):323-31.
85. Urano F, Wang X, Bertolotti A, Zhang Y, Chung P, Harding HP, et al. Coupling of stress in the ER to activation of JNK protein kinases by transmembrane protein kinase IRE1. *Science*. 2000;287(5453):664-6.
86. Tam AB, Mercado EL, Hoffmann A, Niwa M. ER stress activates NF-kappaB by integrating functions of basal IKK activity, IRE1 and PERK. *PLoS one*. 2012;7(10):e45078.

87. Woehlbier U, Hetz C. Modulating stress responses by the UPRosome: a matter of life and death. *Trends in biochemical sciences*. 2011;36(6):329-37.
88. Nguyen DT, Kebache S, Fazel A, Wong HN, Jenna S, Emadali A, et al. Nck-dependent activation of extracellular signal-regulated kinase-1 and regulation of cell survival during endoplasmic reticulum stress. *Mol Biol Cell*. 2004;15(9):4248-60.
89. Brozzi F, Gerlo S, Grieco FA, Nardelli TR, Lievens S, Gysemans C, et al. A combined "omics" approach identifies N-Myc interactor as a novel cytokine-induced regulator of IRE1 protein and c-Jun N-terminal kinase in pancreatic beta cells. *J Biol Chem*. 2014;289(30):20677-93.
90. Castillo K, Rojas-Rivera D, Lisbona F, Caballero B, Nassif M, Court FA, et al. BAX inhibitor-1 regulates autophagy by controlling the IRE1alpha branch of the unfolded protein response. *The EMBO journal*. 2017;36(11):1640.
91. Morita S, Villalta SA, Feldman HC, Register AC, Rosenthal W, Hoffmann-Petersen IT, et al. Targeting ABL-IRE1alpha Signaling Spares ER-Stressed Pancreatic beta Cells to Reverse Autoimmune Diabetes. *Cell Metab*. 2017;25(4):883-97 e8.
92. Carreras-Sureda A, Jana F, Urrea H, Durand S, Mortenson DE, Sagredo A, et al. Non-canonical function of IRE1alpha determines mitochondria-associated endoplasmic reticulum composition to control calcium transfer and bioenergetics. *Nat Cell Biol*. 2019;21(6):755-67.
93. Urrea H, Henriquez DR, Canovas J, Villarroel-Campos D, Carreras-Sureda A, Pulgar E, et al. IRE1alpha governs cytoskeleton remodelling and cell migration through a direct interaction with filamin A. *Nat Cell Biol*. 2018;20(8):942-53.
94. Greenman C, Stephens P, Smith R, Dalgliesh GL, Hunter C, Bignell G, et al. Patterns of somatic mutation in human cancer genomes. *Nature*. 2007;446(7132):153-8.
95. Oakes SA. Endoplasmic Reticulum Proteostasis: A Key Checkpoint in Cancer. *American journal of physiology Cell physiology*. 2016:ajpcell.00266.2016.
96. Romero-Ramirez L, Cao H, Nelson D, Hammond E, Lee AH, Yoshida H, et al. XBP1 is essential for survival under hypoxic conditions and is required for tumor growth. *Cancer research*. 2004;64(17):5943-7.
97. Bujisic B, De Gassart A, Tallant R, Demaria O, Zaffalon L, Chelbi S, et al. Impairment of both IRE1 expression and XBP1 activation is a hallmark of GCB DLBCL and contributes to tumor growth. *Blood*. 2017;129(17):2420-8.
98. Pluquet O, Dejeans N, Bouchecareilh M, Lhomond S, Pineau R, Higa A, et al. Posttranscriptional regulation of PER1 underlies the oncogenic function of IREalpha. *Cancer Res*. 2013;73(15):4732-43.
99. Chen X, Iliopoulos D, Zhang Q, Tang Q, Greenblatt MB, Hatziaepostolou M, et al. XBP1 promotes triple-negative breast cancer by controlling the HIF1alpha pathway. *Nature*. 2014;508(7494):103-7.

100. Carrasco DR, Sukhdeo K, Protopopova M, Sinha R, Enos M, Carrasco DE, et al. The differentiation and stress response factor XBP-1 drives multiple myeloma pathogenesis. *Cancer cell*. 2007;11(4):349-60.
101. Kharabi Masouleh B, Geng H, Hurtz C, Chan LN, Logan AC, Chang MS, et al. Mechanistic rationale for targeting the unfolded protein response in pre-B acute lymphoblastic leukemia. *Proc Natl Acad Sci U S A*. 2014;111(21):E2219-28.
102. Auf G, Jabouille A, Guerit S, Pineau R, Delugin M, Bouchecareilh M, et al. Inositol-requiring enzyme 1alpha is a key regulator of angiogenesis and invasion in malignant glioma. *Proc Natl Acad Sci U S A*. 2010;107(35):15553-8.
103. Dejeans N, Glorieux C, Guenin S, Beck R, Sid B, Rousseau R, et al. Overexpression of GRP94 in breast cancer cells resistant to oxidative stress promotes high levels of cancer cell proliferation and migration: implications for tumor recurrence. *Free radical biology & medicine*. 2012;52(6):993-1002.
104. Cubillos-Ruiz JR, Silberman PC, Rutkowski MR, Chopra S, Perales-Puchalt A, Song M, et al. ER Stress Sensor XBP1 Controls Anti-tumor Immunity by Disrupting Dendritic Cell Homeostasis. *Cell*. 2015;161(7):1527-38.
105. Urra H, Hetz C. A novel ER stress-independent function of the UPR in angiogenesis. *Mol Cell*. 2014;54(4):542-4.
106. Maly DJ, Papa FR. Druggable sensors of the unfolded protein response. *Nat Chem Biol*. 2014;10(11):892-901.
107. Mimura N, Fulciniti M, Gorgun G, Tai YT, Cirstea D, Santo L, et al. Blockade of XBP1 splicing by inhibition of IRE1alpha is a promising therapeutic option in multiple myeloma. *Blood*. 2012;119(24):5772-81.
108. Papandreou I, Denko NC, Olson M, Van Melckebeke H, Lust S, Tam A, et al. Identification of an Ire1alpha endonuclease specific inhibitor with cytotoxic activity against human multiple myeloma. *Blood*. 2011;117(4):1311-4.
109. Ri M, Tashiro E, Oikawa D, Shinjo S, Tokuda M, Yokouchi Y, et al. Identification of Toyocamycin, an agent cytotoxic for multiple myeloma cells, as a potent inhibitor of ER stress-induced XBP1 mRNA splicing. *Blood cancer journal*. 2012;2(7):e79.
110. Sykes EK, Mactier S, Christopherson RI. Melanoma and the Unfolded Protein Response. *Cancers*. 2016;8(3).
111. Tay KH, Luan Q, Croft A, Jiang CC, Jin L, Zhang XD, et al. Sustained IRE1 and ATF6 signaling is important for survival of melanoma cells undergoing ER stress. *Cellular signalling*. 2014;26(2):287-94.
112. Ma XH, Piao SF, Dey S, McAfee Q, Karakousis G, Villanueva J, et al. Targeting ER stress-induced autophagy overcomes BRAF inhibitor resistance in melanoma. *The Journal of clinical investigation*. 2014;124(3):1406-17.

113. Corazzari M, Rapino F, Ciccocanti F, Giglio P, Antonioli M, Conti B, et al. Oncogenic BRAF induces chronic ER stress condition resulting in increased basal autophagy and apoptotic resistance of cutaneous melanoma. *Cell Death Differ.* 2015;22(6):946-58.
114. Chevet E, Hetz C, Samali A. Endoplasmic Reticulum Stress-Activated Cell Reprogramming in Oncogenesis. *Cancer discovery.* 2015;5(6):586-97.
115. Papaioannou A, Chevet E. Driving Cancer Tumorigenesis and Metastasis Through UPR Signaling. *Current topics in microbiology and immunology.* 2018;414:159-92.
116. Madden E, Logue SE, Healy SJ, Manie S, Samali A. The role of the unfolded protein response in cancer progression: From oncogenesis to chemoresistance. *Biol Cell.* 2019;111(1):1-17.
117. Limia CM, Sauzay C, Urra H, Hetz C, Chevet E, Avril T. Emerging Roles of the Endoplasmic Reticulum Associated Unfolded Protein Response in Cancer Cell Migration and Invasion. *Cancers.* 2019;11(5).
118. Mhaidat NM, Alzoubi KH, Abushbak A. X-box binding protein 1 (XBP-1) enhances colorectal cancer cell invasion. *J Chemother.* 2015;27(3):167-73.
119. Li H, Chen X, Gao Y, Wu J, Zeng F, Song F. XBP1 induces snail expression to promote epithelial- to-mesenchymal transition and invasion of breast cancer cells. *Cellular signalling.* 2015;27(1):82-9.
120. Sun Y, Jiang F, Pan Y, Chen X, Chen J, Wang Y, et al. XBP1 promotes tumor invasion and is associated with poor prognosis in oral squamous cell carcinoma. *Oncology reports.* 2018;40(2):988-98.
121. Jin C, Jin Z, Chen NZ, Lu M, Liu CB, Hu WL, et al. Activation of IRE1alpha-XBP1 pathway induces cell proliferation and invasion in colorectal carcinoma. *Biochem Biophys Res Commun.* 2016;470(1):75-81.
122. Xia T, Tong S, Fan K, Zhai W, Fang B, Wang SH, et al. XBP1 induces MMP-9 expression to promote proliferation and invasion in human esophageal squamous cell carcinoma. *American journal of cancer research.* 2016;6(9):2031-40.
123. Wu S, Du R, Gao C, Kang J, Wen J, Sun T. The role of XBP1s in the metastasis and prognosis of hepatocellular carcinoma. *Biochemical and biophysical research communications.* 2018;500(3):530-7.
124. Hsu HT, Hsing MT, Yeh CM, Chen CJ, Yang JS, Yeh KT. Decreased cytoplasmic X-box binding protein-1 expression is associated with poor prognosis and overall survival in patients with oral squamous cell carcinoma. *Clin Chim Acta.* 2018;479:66-71.
125. Mo XT, Zhou WC, Cui WH, Li DL, Li LC, Xu L, et al. Inositol-requiring protein 1 - X-box-binding protein 1 pathway promotes epithelial-mesenchymal transition via mediating snail expression in pulmonary fibrosis. *The international journal of biochemistry & cell biology.* 2015;65:230-8.

126. Cuevas EP, Eraso P, Mazon MJ, Santos V, Moreno-Bueno G, Cano A, et al. LOXL2 drives epithelial-mesenchymal transition via activation of IRE1-XBP1 signalling pathway. *Scientific reports*. 2017;7:44988.
127. Kessenbrock K, Plaks V, Werb Z. Matrix Metalloproteinases: Regulators of the Tumor Microenvironment. *Cell*. 2010;141(1):52-67.
128. Pommier A, Anaparthi N, Memos N, Kelley ZL, Gouronnec A, Yan R, et al. Unresolved endoplasmic reticulum stress engenders immune-resistant, latent pancreatic cancer metastases. *Science*. 2018;360(6394).
129. Drogat B, Auguste P, Nguyen DT, Bouche-careilh M, Pineau R, Nalbantoglu J, et al. IRE1 signaling is essential for ischemia-induced vascular endothelial growth factor-A expression and contributes to angiogenesis and tumor growth in vivo. *Cancer Res*. 2007;67(14):6700-7.
130. Dejeans N, Pluquet O, Lhomond S, Grise F, Bouche-careilh M, Juin A, et al. Autocrine control of glioma cells adhesion and migration through IRE1alpha-mediated cleavage of SPARC mRNA. *J Cell Sci*. 2012;125(Pt 18):4278-87.
131. Jabouille A, Delugin M, Pineau R, Dubrac A, Soulet F, Lhomond S, et al. Glioblastoma invasion and cooption depend on IRE1alpha endoribonuclease activity. *Oncotarget*. 2015;6(28):24922-34.
132. Wirthschaft P, Bode J, Soni H, Dietrich F, Kruwel T, Fischer B, et al. RhoA regulates translation of the Nogo-A decoy SPARC in white matter-invading glioblastomas. *Acta neuropathologica*. 2019;138(2):275-93.
133. Hao L, Ha JR, Kuzel P, Garcia E, Persad S. Cadherin switch from E- to N-cadherin in melanoma progression is regulated by the PI3K/PTEN pathway through Twist and Snail. *Br J Dermatol*. 2012;166(6):1184-97.
134. Robert G, Gaggioli C, Bailet O, Chavey C, Abbe P, Aberdam E, et al. SPARC represses E-cadherin and induces mesenchymal transition during melanoma development. *Cancer research*. 2006;66(15):7516-23.
135. Girotti MR, Fernandez M, Lopez JA, Camafeita E, Fernandez EA, Albar JP, et al. SPARC promotes cathepsin B-mediated melanoma invasiveness through a collagen I/alpha2beta1 integrin axis. *The Journal of investigative dermatology*. 2011;131(12):2438-47.
136. Fenouille N, Tichet M, Dufies M, Pottier A, Mogha A, Soo JK, et al. The epithelial-mesenchymal transition (EMT) regulatory factor SLUG (SNAI2) is a downstream target of SPARC and AKT in promoting melanoma cell invasion. *PLoS one*. 2012;7(7):e40378.
137. Smit DJ, Gardiner BB, Sturm RA. Osteonectin downregulates E-cadherin, induces osteopontin and focal adhesion kinase activity stimulating an invasive melanoma phenotype. *International journal of cancer*. 2007;121(12):2653-60.
138. Botti G, Scognamiglio G, Marra L, Collina F, Di Bonito M, Cerrone M, et al. SPARC/osteonectin is involved in metastatic process to the lung during melanoma

progression. *Virchows Archiv : an international journal of pathology*. 2014;465(3):331-8.

139. Lhomond S, Avril T, Dejeans N, Voutetakis K, Doultinos D, McMahon M, et al. Dual IRE1 RNase functions dictate glioblastoma development. *EMBO molecular medicine*. 2018;10(3).

140. Lynch CD, Sheetz MP. Cellular mechanotransduction: filamin a strains to regulate motility. *Curr Biol*. 2011;21(22):R916-8.

141. Urra H. Role of IRE1 $\alpha$  in cytoskeleton remodeling and cell migration: a new function of IRE1 $\alpha$  beyond ER stress [PhD thesis]. Santiago: University of Chile; 2015.

142. Nakamura F, Stossel TP, Hartwig JH. The filamins: organizers of cell structure and function. *Cell adhesion & migration*. 2011;5(2):160-9.

143. van der Flier A, Sonnenberg A. Structural and functional aspects of filamins. *Biochim Biophys Acta*. 2001;1538(2-3):99-117.

144. Vadlamudi RK, Li F, Adam L, Nguyen D, Ohta Y, Stossel TP, et al. Filamin is essential in actin cytoskeletal assembly mediated by p21-activated kinase 1. *Nature cell biology*. 2002;4(9):681-90.

145. Tigges U, Koch B, Wissing J, Jockusch BM, Ziegler WH. The F-actin cross-linking and focal adhesion protein filamin A is a ligand and in vivo substrate for protein kinase C alpha. *J Biol Chem*. 2003;278(26):23561-9.

146. Ohta Y, Hartwig JH. Phosphorylation of actin-binding protein 280 by growth factors is mediated by p90 ribosomal protein S6 kinase. *The Journal of biological chemistry*. 1996;271(20):11858-64.

147. Fox JE, Goll DE, Reynolds CC, Phillips DR. Identification of two proteins (actin-binding protein and P235) that are hydrolyzed by endogenous Ca<sup>2+</sup>-dependent protease during platelet aggregation. *J Biol Chem*. 1985;260(2):1060-6.

148. Loy CJ, Sim KS, Yong EL. Filamin-A fragment localizes to the nucleus to regulate androgen receptor and coactivator functions. *Proceedings of the National Academy of Sciences of the United States of America*. 2003;100(8):4562-7.

149. Yue J, Huhn S, Shen Z. Complex roles of filamin-A mediated cytoskeleton network in cancer progression. *Cell & bioscience*. 2013;3(1):7.

150. Shao QQ, Zhang TP, Zhao WJ, Liu ZW, You L, Zhou L, et al. Filamin A: Insights into its Exact Role in Cancers. *Pathology oncology research : POR*. 2016;22(2):245-52.

151. Ai J, Huang H, Lv X, Tang Z, Chen M, Chen T, et al. FLNA and PGK1 are two potential markers for progression in hepatocellular carcinoma. *Cellular physiology and biochemistry : international journal of experimental cellular physiology, biochemistry, and pharmacology*. 2011;27(3-4):207-16.

152. Jiang X, Yue J, Lu H, Campbell N, Yang Q, Lan S, et al. Inhibition of filamin-A reduces cancer metastatic potential. *International journal of biological sciences*. 2013;9(1):67-77.
153. Tian HM, Liu XH, Han W, Zhao LL, Yuan B, Yuan CJ. Differential expression of filamin A and its clinical significance in breast cancer. *Oncology letters*. 2013;6(3):681-6.
154. Alper O, Stetler-Stevenson WG, Harris LN, Leitner WW, Ozdemirli M, Hartmann D, et al. Novel anti-filamin-A antibody detects a secreted variant of filamin-A in plasma from patients with breast carcinoma and high-grade astrocytoma. *Cancer science*. 2009;100(9):1748-56.
155. Zhou AX, Toylyu A, Nallapalli RK, Nilsson G, Atabay N, Heldin CH, et al. Filamin a mediates HGF/c-MET signaling in tumor cell migration. *International journal of cancer*. 2011;128(4):839-46.
156. Huang C, Miller RT, Freter CE. Signaling regulation and role of filamin A cleavage in Ca<sup>2+</sup>-stimulated migration of androgen receptor-deficient prostate cancer cells. *Oncotarget*. 2016.
157. Li C, Yu S, Nakamura F, Pentikainen OT, Singh N, Yin S, et al. Pro-prion binds filamin A, facilitating its interaction with integrin beta1, and contributes to melanomagenesis. *J Biol Chem*. 2010;285(39):30328-39.
158. Baldassarre M, Razinia Z, Brahme NN, Buccione R, Calderwood DA. Filamin A controls matrix metalloproteinase activity and regulates cell invasion in human fibrosarcoma cells. *J Cell Sci*. 2012;125(Pt 16):3858-69.
159. Sun GG, Wei CD, Jing SW, Hu WN. Interactions between filamin A and MMP-9 regulate proliferation and invasion in renal cell carcinoma. *Asian Pacific journal of cancer prevention : APJCP*. 2014;15(8):3789-95.
160. Xu Y, Bismar TA, Su J, Xu B, Kristiansen G, Varga Z, et al. Filamin A regulates focal adhesion disassembly and suppresses breast cancer cell migration and invasion. *The Journal of experimental medicine*. 2010;207(11):2421-37.
161. Bonaventure J, Domingues MJ, Larue L. Cellular and molecular mechanisms controlling the migration of melanocytes and melanoma cells. *Pigment Cell Melanoma Res*. 2013;26(3):316-25.
162. Croft A, Tay KH, Boyd SC, Guo ST, Jiang CC, Lai F, et al. Oncogenic activation of MEK/ERK primes melanoma cells for adaptation to endoplasmic reticulum stress. *The Journal of investigative dermatology*. 2014;134(2):488-97.
163. Zhuang L, Scolyer RA, Lee CS, McCarthy SW, Cooper WA, Zhang XD, et al. Expression of glucose-regulated stress protein GRP78 is related to progression of melanoma. *Histopathology*. 2009;54(4):462-70.
164. Guan M, Chen X, Ma Y, Tang L, Guan L, Ren X, et al. MDA-9 and GRP78 as potential diagnostic biomarkers for early detection of melanoma metastasis. *Tumour*

biology : the journal of the International Society for Oncodevelopmental Biology and Medicine. 2015;36(4):2973-82.

165. Eigner K, Filik Y, Mark F, Schutz B, Klambauer G, Moriggl R, et al. The unfolded protein response impacts melanoma progression by enhancing FGF expression and can be antagonized by a chemical chaperone. *Scientific reports*. 2017;7(1):17498.

166. Lisbona F, Rojas-Rivera D, Thielen P, Zamorano S, Todd D, Martinon F, et al. BAX inhibitor-1 is a negative regulator of the ER stress sensor IRE1alpha. *Mol Cell*. 2009;33(6):679-91.

167. Maletzki C, Bock S, Fruh P, Macius K, Witt A, Prall F, et al. NSG mice as hosts for oncological precision medicine. *Lab Invest*. 2020;100(1):27-37.

168. Domingues B, Lopes JM, Soares P, Populo H. Melanoma treatment in review. *Immunotargets Ther*. 2018;7:35-49.

169. Obiedat A, Seidel E, Mahameed M, Berhani O, Tsukerman P, Voutetakis K, et al. Transcription of the NKG2D ligand MICA is suppressed by the IRE1/XBP1 pathway of the unfolded protein response through the regulation of E2F1. *FASEB journal : official publication of the Federation of American Societies for Experimental Biology*. 2018:fj201801350RR.

170. Ma Y, Hendershot LM. The role of the unfolded protein response in tumour development: friend or foe? *Nat Rev Cancer*. 2004;4(12):966-77.

171. Long GV, Menzies AM, Nagrial AM, Haydu LE, Hamilton AL, Mann GJ, et al. Prognostic and clinicopathologic associations of oncogenic BRAF in metastatic melanoma. *J Clin Oncol*. 2011;29(10):1239-46.

172. Ascierto PA, Kirkwood JM, Grob JJ, Simeone E, Grimaldi AM, Maio M, et al. The role of BRAF V600 mutation in melanoma. *Journal of translational medicine*. 2012;10:85.

173. Overwijk WW, Restifo NP. B16 as a Mouse Model for Human Melanoma. *Current protocols in immunology / edited by John E Coligan [et al]*. 2001;CHAPTER:Unit-20.1.

174. Chen HC. Boyden chamber assay. *Methods Mol Biol*. 2005;294:15-22.

175. Justus CR, Leffler N, Ruiz-Echevarria M, Yang LV. In vitro cell migration and invasion assays. *J Vis Exp*. 2014(88).

176. Trimmer C, Whitaker-Menezes D, Bonuccelli G, Milliman JN, Daumer KM, Aplin AE, et al. CAV1 inhibits metastatic potential in melanomas through suppression of the integrin/Src/FAK signaling pathway. *Cancer research*. 2010;70(19):7489-99.

177. Jiang G, Yang CS, Xu D, Sun C, Zheng JN, Lei TC, et al. Potent anti-tumour activity of a novel conditionally replicating adenovirus for melanoma via inhibition of migration and invasion. *British journal of cancer*. 2014;110(10):2496-505.



178. Tiwary S, Preziosi M, Rothberg PG, Zeitouni N, Corson N, Xu L. ERBB3 is required for metastasis formation of melanoma cells. *Oncogenesis*. 2014;3:e110.
179. Berridge MV, Herst PM, Tan AS. Tetrazolium dyes as tools in cell biology: new insights into their cellular reduction. *Biotechnol Annu Rev*. 2005;11:127-52.
180. Xie Y, Liu C, Qin Y, Chen J, Fang J. Knockdown of IRE1a suppresses metastatic potential of colon cancer cells through inhibiting FN1-Src/FAK-GTPases signaling. *The international journal of biochemistry & cell biology*. 2019;114:105572.
181. Ridley AJ. Life at the leading edge. *Cell*. 2011;145(7):1012-22.
182. Burridge K. Focal adhesions: a personal perspective on a half century of progress. *The FEBS journal*. 2017;284(20):3355-61.
183. Rottner K, Schaks M. Assembling actin filaments for protrusion. *Current opinion in cell biology*. 2019;56:53-63.
184. Riedl J, Crevenna AH, Kessenbrock K, Yu JH, Neukirchen D, Bista M, et al. Lifeact: a versatile marker to visualize F-actin. *Nat Methods*. 2008;5(7):605-7.
185. Winklbauer R. Cell adhesion strength from cortical tension - an integration of concepts. *Journal of cell science*. 2015;128(20):3687-93.
186. Janiszewska M, Primi MC, Izard T. Cell adhesion in cancer: Beyond the migration of single cells. *The Journal of biological chemistry*. 2020;295(8):2495-505.
187. Odenthal J, Takes R, Friedl P. Plasticity of tumor cell invasion: governance by growth factors and cytokines. *Carcinogenesis*. 2016;37(12):1117-28.
188. Savoy RM, Ghosh PM. The dual role of filamin A in cancer: can't live with (too much of) it, can't live without it. *Endocrine-related cancer*. 2013;20(6):R341-56.
189. Volkmann K, Lucas JL, Vuga D, Wang X, Brumm D, Stiles C, et al. Potent and Selective Inhibitors of the Inositol-requiring Enzyme 1 Endoribonuclease. *J Biol Chem*. 2011;286(14):12743-55.
190. Scott KL, Nogueira C, Heffernan TP, van Doorn R, Dhakal S, Hanna JA, et al. Proinvasion metastasis drivers in early-stage melanoma are oncogenes. *Cancer cell*. 2011;20(1):92-103.
191. Chen J, Wu F, Shi Y, Yang D, Xu M, Lai Y, et al. Identification of key candidate genes involved in melanoma metastasis. *Molecular medicine reports*. 2019;20(2):903-14.
192. Bright MD, Itzhak DN, Wardell CP, Morgan GJ, Davies FE. Cleavage of BLOC1S1 mRNA by IRE1 Is Sequence Specific, Temporally Separate from XBP1 Splicing, and Dispensable for Cell Viability under Acute Endoplasmic Reticulum Stress. *Mol Cell Biol*. 2015;35(12):2186-202.

193. Yang C, Xia BR, Jin WL, Lou G. Circulating tumor cells in precision oncology: clinical applications in liquid biopsy and 3D organoid model. *Cancer Cell Int.* 2019;19:341.
194. Society AC. Cancer facts and figures 2007 GA, USA2008 [
195. Francia G, Cruz-Munoz W, Man S, Xu P, Kerbel RS. Mouse models of advanced spontaneous metastasis for experimental therapeutics. *Nature reviews Cancer.* 2011;11(2):135-41.
196. Gomez-Cuadrado L, Tracey N, Ma R, Qian B, Brunton VG. Mouse models of metastasis: progress and prospects. *Disease models & mechanisms.* 2017;10(9):1061-74.
197. Cruz-Munoz W, Man S, Xu P, Kerbel RS. Development of a preclinical model of spontaneous human melanoma central nervous system metastasis. *Cancer research.* 2008;68(12):4500-5.
198. Zhang K, Zhu T, Gao D, Zhang Y, Zhao Q, Liu S, et al. Filamin A expression correlates with proliferation and invasive properties of human metastatic melanoma tumors: implications for survival in patients. *Journal of cancer research and clinical oncology.* 2014;140(11):1913-26.
199. Gawecka JE, Griffiths GS, Ek-Rylander B, Ramos JW, Matter ML. R-Ras regulates migration through an interaction with filamin A in melanoma cells. *PLoS one.* 2010;5(6):e11269.
200. O'Connell MP, Fiori JL, Baugher KM, Indig FE, French AD, Camilli TC, et al. Wnt5A activates the calpain-mediated cleavage of filamin A. *The Journal of investigative dermatology.* 2009;129(7):1782-9.
201. Zhu TN, He HJ, Kole S, D'Souza T, Agarwal R, Morin PJ, et al. Filamin A-mediated down-regulation of the exchange factor Ras-GRF1 correlates with decreased matrix metalloproteinase-9 expression in human melanoma cells. *The Journal of biological chemistry.* 2007;282(20):14816-26.
202. Liu ZJ, Semenza GL, Zhang HF. Hypoxia-inducible factor 1 and breast cancer metastasis. *Journal of Zhejiang University Science B.* 2015;16(1):32-43.
203. Chen C, Zhang X. IRE1 $\alpha$ -XBP1 pathway promotes melanoma progression by regulating IL-6/STAT3 signaling. *Journal of translational medicine.* 2017;15(1):42.
204. Linnskog R, Jonsson G, Axelsson L, Prasad CP, Andersson T. Interleukin-6 drives melanoma cell motility through p38 $\alpha$ -MAPK-dependent up-regulation of WNT5A expression. *Molecular oncology.* 2014;8(8):1365-78.
205. Oikawa D, Tokuda M, Hosoda A, Iwawaki T. Identification of a consensus element recognized and cleaved by IRE1  $\alpha$ . *Nucleic acids research.* 2010;38(18):6265-73.

206. Nishizuka Y. The molecular heterogeneity of protein kinase C and its implications for cellular regulation. *Nature*. 1988;334(6184):661-5.
207. Chalkiadaki G, Nikitovic D, Katonis P, Berdiaki A, Tsatsakis A, Kotsikogianni I, et al. Low molecular weight heparin inhibits melanoma cell adhesion and migration through a PKCa/JNK signaling pathway inducing actin cytoskeleton changes. *Cancer letters*. 2011;312(2):235-44.
208. Zhang P, Goodrich C, Fu C, Dong C. Melanoma upregulates ICAM-1 expression on endothelial cells through engagement of tumor CD44 with endothelial E-selectin and activation of a PKCalpha-p38-SP-1 pathway. *FASEB journal : official publication of the Federation of American Societies for Experimental Biology*. 2014;28(11):4591-609.
209. Dissanayake SK, Wade M, Johnson CE, O'Connell MP, Leotlela PD, French AD, et al. The Wnt5A/protein kinase C pathway mediates motility in melanoma cells via the inhibition of metastasis suppressors and initiation of an epithelial to mesenchymal transition. *The Journal of biological chemistry*. 2007;282(23):17259-71.
210. Lahn MM, Sundell KL. The role of protein kinase C-alpha (PKC-alpha) in melanoma. *Melanoma research*. 2004;14(2):85-9.
211. Leotlela PD, Wade MS, Duray PH, Rhode MJ, Brown HF, Rosenthal DT, et al. Claudin-1 overexpression in melanoma is regulated by PKC and contributes to melanoma cell motility. *Oncogene*. 2007;26(26):3846-56.
212. Koohini Z, Teimourian S. Slit/Robo Signaling Pathway in Cancer; a New Stand Point for Cancer Treatment. *Pathol Oncol Res*. 2019;25(4):1285-93.
213. Yao Y, Zhou Z, Li L, Li J, Huang L, Qi C, et al. Activation of Slit2/Robo1 Signaling Promotes Tumor Metastasis in Colorectal Carcinoma through Activation of the TGF- $\beta$ /Smads Pathway. *Cells*. 2019;8(6).
214. Chen W, Ye L, Wen D, Chen F. MiR-490-5p Inhibits Hepatocellular Carcinoma Cell Proliferation, Migration and Invasion by Directly Regulating ROBO1. *Pathol Oncol Res*. 2019;25(1):1-9.
215. Mertsch S, Schmitz N, Jeibmann A, Geng JG, Paulus W, Senner V. Slit2 involvement in glioma cell migration is mediated by Robo1 receptor. *J Neurooncol*. 2008;87(1):1-7.
216. Onken MD, Worley LA, Tuscan MD, Harbour JW. An accurate, clinically feasible multi-gene expression assay for predicting metastasis in uveal melanoma. *J Mol Diagn*. 2010;12(4):461-8.
217. Guo F, Jiao F, Song Z, Li S, Liu B, Yang H, et al. Regulation of MALAT1 expression by TDP43 controls the migration and invasion of non-small cell lung cancer cells in vitro. *Biochem Biophys Res Commun*. 2015;465(2):293-8.

218. Lin TW, Chen MT, Lin LT, Huang PI, Lo WL, Yang YP, et al. TDP-43/HDAC6 axis promoted tumor progression and regulated nutrient deprivation-induced autophagy in glioblastoma. *Oncotarget*. 2017;8(34):56612-25.
219. Zeng Q, Cao K, Liu R, Huang J, Xia K, Tang J, et al. Identification of TDP-43 as an oncogene in melanoma and its function during melanoma pathogenesis. *Cancer Biol Ther*. 2017;18(1):8-15.
220. Tong J, Huang C, Bi F, Wu Q, Huang B, Zhou H. XBP1 depletion precedes ubiquitin aggregation and Golgi fragmentation in TDP-43 transgenic rats. *J Neurochem*. 2012;123(3):406-16.
221. Ming J, Ruan S, Wang M, Ye D, Fan N, Meng Q, et al. A novel chemical, STF-083010, reverses tamoxifen-related drug resistance in breast cancer by inhibiting IRE1/XBP1. *Oncotarget*. 2015;6(38):40692-703.
222. Logue SE, McGrath EP, Cleary P, Greene S, Mnich K, Almanza A, et al. Inhibition of IRE1 RNase activity modulates the tumor cell secretome and enhances response to chemotherapy. *Nature communications*. 2018;9(1):3267.
223. Song M, Sandoval TA, Chae CS, Chopra S, Tan C, Rutkowski MR, et al. IRE1alpha-XBP1 controls T cell function in ovarian cancer by regulating mitochondrial activity. *Nature*. 2018;562(7727):423-8.

## Résumé

Les cellules tumorales sont exposées à plusieurs perturbations intrinsèques et extrinsèques qui peuvent altérer le bon fonctionnement du réticulum endoplasmique (RE), une condition cellulaire connue sous le nom de stress ER. Ce stress engage une réponse adaptative appelée « Unfolded Protein Response » (UPR), une voie de signalisation qui transmet les informations sur l'état de repliement des protéines dans la lumière ER vers le noyau en vue de rétablir l'homéostasie protéique. La signalisation des trois branches de l'UPR a été liée à la progression tumorale. La voie de signalisation transduite par la protéine IRE1 $\alpha$  (appelée ci-après IRE1) est la branche la plus conservée de l'UPR, et son association avec le développement des cancers a été documentée au cours des dernières années. L'activation d'IRE1 induit l'épissage non conventionnel de l'ARNm XBP1 contrôlant l'expression du facteur de transcription XBP1s et simultanément la dégradation d'ARNm et de microARN par un processus appelé RIDD. En outre, nous avons décrit qu'IRE1 interagit directement avec la filamine A (FLNA), une protéine de réticulation de l'actine impliquée dans la migration cellulaire.

Malgré les preuves croissantes suggérant qu'IRE1 est un régulateur important de la progression tumorale et d'autres caractéristiques du cancer, son implication dans l'apparition de métastases et les mécanismes moléculaires sous-jacents restent ambigus. Plusieurs études ont lié l'activité IRE1 à la migration cellulaire, à l'invasion et aux métastases dans différents types de tumeurs. Cependant, la plupart des preuves disponibles sont toujours corrélatives et les mécanismes moléculaires restent à élucider complètement. L'une des tumeurs les plus métastatiques est le mélanome cutané malin, dont l'incidence et la mortalité ont augmenté au cours des dernières

décennies. Aucune preuve concernant le rôle de l'IRE1 dans la migration et l'invasion cellulaires du mélanome n'a été publiée jusqu'ici. Par conséquent, dans cette thèse, je vise à caractériser la contribution de l'IRE1 dans la migration et l'invasion cellulaires dans les cellules de mélanome, son impact sur le processus métastatique et sa relation avec la signalisation de la FLNA.

À cette fin, j'ai sélectionné comme modèle cellulaire quatre lignées cellulaires de mélanome humain, dont une non métastatique et trois métastatiques. J'ai également utilisé la lignée cellulaire B16F10 dérivée de C57BL/6 pour des expériences complémentaires, un modèle hautement métastatique et bien établi pour l'étude des métastases de mélanome. Fait intéressant, l'ablation génétique de l'expression d'IRE1 a conduit à une augmentation de la capacité de migration et d'invasion cellulaire des lignées cellulaires de mélanome métastatique humain. Notamment, je n'ai pas pu corroborer une interaction entre IRE1 et FLNA, ni la phosphorylation IRE1-dépendante de FLNA sur la sérine S2152 avec ce phénomène. Surtout, les processus connus pour être régulés par FLNA, comme le cytosquelette d'actine et l'adhésion cellulaire, ne sont pas affectés par la déplétion de l'IRE1 dans les cellules de mélanome métastatique humain. Ces résultats suggèrent que la régulation de la migration / invasion cellulaire par IRE1 est un mécanisme indépendant de la FLNA. Qui plus est, en utilisant un inhibiteur sélectif de la RNase IRE1 (MKC-8866), une augmentation significative de la migration des cellules de mélanome métastatique a aussi été observée. Ainsi, nous avons évalué l'effet de la surexpression de XBP1 sur la migration cellulaire des cellules de mélanome métastatique humain sur le déficit ou le contrôle pharmacologique de l'activité d'IRE1. En utilisant cette approche expérimentale, nous avons observé que XBP1 n'affecte pas la capacité des cellules de mélanome humain à migrer. Sur cette base, nous avons émis l'hypothèse que

RIDD en aval de l'activité IRE1 RNase pourrait être responsable de l'atténuation de la migration des cellules de mélanome métastatique.

À l'aide d'analyses bioinformatiques, nous avons ensuite évalué l'état d'activation de la branche IRE1 (XBP1 ou RIDD) dans les métastases du mélanome humain. En utilisant les signatures génétiques déjà décrites pour les tumeurs de glioblastomes, nous avons comparé l'activité IRE1 dans les tumeurs primaires et métastatiques de 469 patients. Nous avons observé une diminution significative de l'activité IRE1 dans les échantillons métastatiques par rapport aux tumeurs primaires. Cette diminution de l'activité IRE1 dans les métastases était corrélée à une diminution de l'activité RIDD, mais pas de l'activité XBP1s, ce qui suggère que l'inhibition IRE1 / RIDD pourrait être un processus nécessaire pour développer des métastases de mélanome. En utilisant la même base de données d'expression génique, nous avons constaté que les tumeurs identifiées avec une activité RIDD élevée présentaient une diminution significative de l'expression d'au moins neuf gènes impliqués dans les métastases du mélanome. Un effet totalement indépendant de l'activité XBP1s. Bien que ces cibles RIDD possibles doivent encore être validées in vitro, nos résultats soutiennent fortement l'idée qu'IRE1, à travers l'activité RIDD et la dégradation de multiples ARNm, pourrait agir comme un suppresseur de migration, et peut-être d'invasion, dans les lignées cellulaires de mélanome humain.

Enfin, pour déterminer la pertinence de l'expression d'IRE1 dans les métastases de mélanome in vivo, j'ai sélectionné un modèle expérimental de métastase, consistant en l'injection de veine latérale de la queue de cellules de mélanome métastatique humain chez des souris NSG ou des cellules de mélanome métastatique de souris chez des souris immunocompétentes. Bien que les données obtenues in

in vitro soutiennent qu'IRE1 peut supprimer la migration cellulaire, je n'ai pas trouvé de différence significative concernant le nombre de nodules métastatiques dans les poumons entre les cellules de mélanome métastatique IRE1KO et contrôle. Une explication du faible effet de la déficience IRE1 dans les métastases dans nos expériences pourrait être que le modèle in vivo choisi n'est pas adéquat pour évaluer le mécanisme régulé par IRE1 dans le mélanome. Le modèle expérimental de métastase choisi (injection directe de cellules tumorales dans la circulation) est une excellente stratégie en première approche car il permet le contrôle du nombre de cellules injectées, en excluant l'effet de la croissance tumorale primaire. Cependant, ce type d'expérience a des limites. Je considère qu'outre la complexité de ce modèle, l'évaluation de l'effet de la déplétion IRE1 dans les métastases spontanées pourrait être pertinente pour tester mon hypothèse de travail.

Les résultats obtenus dans cette thèse constituent la première analyse de l'implication d'IRE1 dans les processus liés aux métastases dans le mélanome, comme la migration et l'invasion cellulaires. Surtout, plusieurs résultats indiquent que l'inhibition de l'activité IRE1 RNase altère la progression tumorale dans différents types de cancer. Néanmoins, les résultats obtenus corroborent la complexité et le rôle tumeur-spécifique de la signalisation IRE1. Les données obtenues au cours de ma thèse suggèrent que le ciblage de l'activité IRE1 RNase pourrait ne pas être la meilleure option dans le traitement du mélanome car cela pourrait avoir des effets indésirables sur l'amélioration de la migration / invasion et peut-être des métastases.



**Titre :** Une nouvelle fonction du transducteur de stress ER IRE1 dans la migration cellulaire et l'invasion des cellules de mélanome métastatique.

**Mots clés :** Stress du RE, UPR, IRE1, mélanome, migration cellulaire, métastase.

**Résumé :** Les cellules tumorales sont exposées à des perturbations intrinsèques et extrinsèques qui altèrent le bon fonctionnement du réticulum endoplasmique (RE); une condition cellulaire connue sous le nom de stress du RE. Cette condition engage une réponse adaptative appelée « Unfolded Protein Response » (UPR). IRE1 est le capteur du stress du RE qui est le plus conservé dans l'évolution. L'activation de l'activité RNase d'IRE1 contrôle l'expression du facteur de transcription XBP1s et la dégradation d'ARNm par un processus appelé RIDD. L'activité IRE1 a été liée à la migration et à l'invasion cellulaires dans différents types de tumeurs. Cependant, aucune preuve concernant le rôle de l'IRE1 dans la migration / l'invasion des cellules de mélanome n'a été publiée jusqu'ici. Il est important de noter qu'en 2018, notre groupe a décrit une nouvelle fonction de l'IRE1 indépendante de son activité catalytique, dans laquelle IRE1 agissait comme un échafaudage favorisant la migration cellulaire via la filamin A (FLNA), une protéine de réticulation de l'actine impliquée dans la migration cellulaire. Cela a été démontré dans des cellules non tumorales. Par conséquent, dans cette thèse, mon objectif initial était de tester et caractériser la contribution de la signalisation IRE1/FLNA dans la migration cellulaire et l'invasion dans les cellules de mélanome, son impact sur le processus métastatique.

En utilisant des approches génétiques et pharmacologiques, j'ai constaté que le déficit d'expression d'IRE1 et/ou l'inhibition de son activité RNase augmentent les propriétés de migration et d'invasion des lignées cellulaires de mélanome métastatique humain, indiquant que la branche IRE1 pourrait agir comme un suppresseur de la migration et de l'invasion dans ces cellules. Notamment, nous n'avons pas été en mesure de corroborer la phosphorylation dépendante d'IRE1 de la FLNA. Surtout, les structures et processus connus pour être régulés par la FLNA comme le cytosquelette d'actine et l'adhésion cellulaire ne sont pas affectés par la déplétion de l'IRE1 dans les cellules de mélanome métastatique humain. Ces résultats suggèrent que la régulation de la migration/invasion par IRE1 est un mécanisme indépendant du FLNA. En analysant une base de données d'expression génique de tumeurs de mélanome, nous avons constaté que les tumeurs identifiées avec une activité RIDD élevée présentaient une diminution significative de l'expression des gènes impliqués dans les métastases du mélanome. Nos résultats suggèrent que IRE1 (via le RIDD) pourrait agir comme un suppresseur de la migration et de l'invasion des cellules de mélanome métastatique. Les résultats obtenus dans cette thèse constituent une première étape dans la caractérisation de l'implication d'IRE1 dans les processus liés aux métastases dans le mélanome.

**Title :** Novel function of the ER stress transducer IRE1 in cell migration and invasion of metastatic melanoma cells.

**Keywords :** ER stress, UPR, IRE1, melanoma, cell migration, metastasis.

**Abstract :** Tumor cells are exposed to cell-intrinsic and extrinsic perturbations that alter the proper functioning of the endoplasmic reticulum (ER); a cellular condition known as ER stress. This condition engages an adaptive response termed as unfolded protein response (UPR). IRE1 is the most evolutionary conserved ER stress sensor of the UPR. Activation of the IRE1 RNase activity controls the expression of the transcription factor XBP1s and the degradation of mRNA through a process termed RIDD. IRE1 activity has been linked to cell migration and invasion in different types of tumors. However, no evidence regarding the role of IRE1 in melanoma cell migration/invasion has been published. Importantly in 2018 our group described a novel function of IRE1 independent of its catalytic activity, where IRE1 acted as a scaffold favoring cell migration through FLNA, an actin crosslinking protein involved in cell migration. This was demonstrated in non-tumoral cells. Therefore, in this thesis, we initially aimed to uncover the contribution of IRE1/FLNA signaling in cell migration and invasion in melanoma cells, its impact on the metastatic process.

By using genetic and pharmacologic approaches, we found that deficiency of IRE1 expression or RNase activity inhibition enhances cell migration and invasion of human metastatic melanoma cell lines, indicating that the IRE1 branch could be acting as a suppressor of cell migration and invasion in metastatic melanoma cells. Notably, we were not able to corroborate the IRE1-dependent phosphorylation of FLNA. Importantly, processes that are known to be regulated by FLNA like actin cytoskeleton and cell adhesion were not affected by IRE1 depletion in human metastatic melanoma cells. These findings suggest that the regulation of cell migration/invasion by IRE1 is an FLNA-independent mechanism. Analyzing a gene expression database of melanoma tumors, we found that tumors identified with high RIDD activity presented a significant decrease in the expression of genes involved in melanoma metastasis. Our findings suggest that IRE1 through RIDD acts as a suppressor of metastatic melanoma cell migration and invasion. The results obtained in this thesis constitute the first approximation on the implication of IRE1 in metastasis-related processes in melanoma, such as cell migration and invasion.